University of London

Novel ‘Click’ Generated Sensors and Molecular Machines for Fluorescent Sensing of Zn^{2+}

Jessica Pancholi

Supervisors:

Dr. Stephen M. Goldup

Prof. Michael Watkinson

Submitted in partial fulfilment of the requirements of the Degree of Doctor of Philosophy

Statement of Originality

I, Jessica Pancholi, confirm that the research included within this thesis is my own work or that where it has been carried out in collaboration with, or supported by others, that this is duly acknowledged below and my contribution indicated. Previously published material is also acknowledged below.

I attest that I have exercised reasonable care to ensure that the work is original, and does not to the best of my knowledge break any UK law, infringe any third party's copyright or other Intellectual Property Right, or contain any confidential material.

I accept that the College has the right to use plagiarism detection software to check the electronic version of the thesis.

I confirm that this thesis has not been previously submitted for the award of a degree by this or any other university.

Signature:

Date: 16th October 2015

Details of collaboration and publications:

Collaboration with Professor Guy Rutter and Dr. David Hodson, Imperial College UK

- J. Pancholi, D. J. Hodson, K. Jobe, G. A. Rutter, S. M. Goldup and M. Watkinson, *Chem. Sci.*, 2014, **5**, 3528 - 3535

Abstract

Zinc is now firmly established as an essential trace element in the human body. Whilst it has many key structural and catalytic fixed roles, it is also found in "mobile" pools in many essential organs and organelles that are readily chelatable. The presence and trafficking of these zinc pools are thought to contribute in some form to many human disease states associated with these organs, for example, Type 2 diabetes in the pancreas, some forms of cancer in the prostate, and even ischemic stroke, epilepsy and Alzheimer's disease. The exact role however, remains largely unknown and this is due to our current limitations with the methods in which we monitor the movement of this important element in our body.

This thesis presents our efforts to develop novel Zn^{2+} selective chemosensors that can meet contemporary criteria for successful and simple imaging. Many efforts are being made to develop simple fluorescent molecular probes to monitor the trafficking and progress of Zn^{2+} through these cells and organs in real time via these chelatable "mobile" pools. Chapter 1 will outline some successful efforts towards these and discuss their relevance and mechanisms of action, as well as outlining "click"-chemistry and its' role in chemosensing to date.

Chapter 2 describes a novel "click"-chemistry approach designed to aid with the simple construction of novel zinc-chelating probes in a facile and high yielding manner. This methodology was taken forward to the synthesis of 6 novel Zn^{2+}-selective small molecule fluorescent probes that incorporate a cell organelle targeting motif in their structure. These are described in Chapter 3, and their successful testing both *in-vitro* and *in-cellulo* in murine pancreatic islet cells is presented and discussed.

Finally, Chapter 4 discusses the development of some modified fluorescent [2]rotaxanes as molecularly interlocked architectures capable of binding and sensing metals, and will specifically focus on how small structural changes led to vast differences in their

fluorescence properties, ultimately resulting in a Zn^{2+}-selective [2]rotaxane in organic media.

Table of Contents

List of Abbreviations

δ	Chemical shift
AT-CuAAC	Active Template Cu-catalysed Azide-alkyne Cycloaddition
Bipy	Bipyridine
Boc	*t*-Butyloxycarbonyl
CHEF	Chelation-enhanced fluorescence
CuAAC	Cu(I) Azide-Alkyne Cycloaddition
DEAD	Diethyl azodicarboxylate
DMAP	4-Dimethylaminopyridine
DMF	*N,N'*-Dimethylformamide
DMSO	Dimethylsulfoxide
DPPA	Diphenyl phosphoryl azide
EDTA	Ethylenediamine tetraacetic acid
EPR	Electron Paramagnetic Resonance
Equiv.	Equivalent
ESI	Electrospray Ionization
EtOH	Ethanol
FRET	Forster Resonance Energy Transfer
h	Hours
HRMS	High Resolution Mass Spectrometry
ICT	Intramolecular Charge Transfer
IR	Infrared radiation
J	Coupling constant
LRMS	Low Resolution Mass Spectrometry
M	Molar
min	Minutes

mmol	Millimoles
m.p.	Melting point
MS	Mass Spectrometry
NMR	Nuclear Magnetic Resonance
PET	Photoinduced Electron Transfer
ppm	Parts per million
rt	Room Temperature
sat.	Saturated
THF	Tetrahydrofuran
TFA	Trifluroacetic acid
TLC	Thin Layer Chromatography
UV/Vis	Ultraviolet/visible radiation

Acknowledgements

I want to start with the most important acknowledgement of all; to my PhD supervisors Mike and Steve, for every opportunity and every single piece of guidance and advice. Also for the chance to go to China; I can't put into words what that meant to me. Thank you for having faith in me and my abilities from the very beginning and for being the driving force behind a wonderful and interesting project that I am proud to have been a part of. I am super grateful and honoured to be Team Watkinson and Goldup!

That leads me nicely onto my PhD family. I particularly want to thank KJ, Rob, Ben, Ed (especially for the template!), Joby, Marzia, Phil, Mariya, Vikki, Rawan, Joey, Geoff, Harry, Mark, Cath, Jamie, Vaishali, Mathieu and Elise. You guys have been my support system and lifeline and light in the dark days! From day one til day crazy, I am so grateful for you amazing bunch of people. I want to double thank my Southampton Family; to Cath for a home when I needed one, and to all of you for putting up with Stressed Jess – you are all angels! I also want to show my utmost love and appreciation to Linda; my chemistry wifey, partner in crime through absolutely everything for eight years! I really and truly could not have done it without you by my side.

Thanks to my PhD panel members; Prof. Igor Larossa, Dr Chris Bray, Prof. Marina Resmini and Dr Caroline Brennan; and to all of the people at SBCS for all your help along the way, especially John Hayes for all the free chemicals and hydrogen taps! You were all integral to my research. To Professor Guy Rutter and Dr David Hodson at Imperial College for your collaborative efforts and for making our chemistry come to life in cells. It was a great experience and without your hard work and efforts the paper would not have been possible. I would also like to thank the chemistry department at the University of Southampton for accepting me into the fold in times of emergency characterisation!

To my wonderful parents! I know this has been difficult for us both to handle a lot of the time, and I know you often wished for things to be different, but thank you for understanding what this has meant to me and for all your support. I am so grateful for your love. I also really want to thank Vimal and Hiral Bhabhi and my little munchkins Viraj and Krish for giving me a home away from home and for all the love and amazing food for my soul - it means so much!

Special thanks to my long suffering friends who have not seen me properly for 4 years! Even my London girls Louise, Bodge, Nicola and Gabi – thank you all for being my cheerleaders to the finish line. Special love to my bestie Laura for all the phonecalls and tears and drinks and laughter and dancing and love and hugs and for generally rocking like a stone and being the greatest best friend in the whole entire universe. You are MY little tiramisu!

My final acknowledgements go to London, the greatest city in the whole world, my first and forever love, and to Jamie, again, for always holding my hand on every adventure.

I would like to dedicate this thesis to my brother Karan, for being my biggest supporter and the best Panch, through stress and strain and hardship. I hope I can do the same for you in life and I hope this labour of love shows you that anything is possible!

Chapter 1: Introduction

1.1. What is a Sensor?

A sensor, by definition, is an entity designed to detect and provide a signal for an aspect of its environment. They exist in both everyday items and complicated systems; from mercury in thermometers to measure temperature, to seismometers to measure ground motion during and after natural disasters. These sensors provide a readable output for the end user to make sense of the signals, generally in an optical or electrical format.

Even humans and living organisms contain sensors for the detection of important changes in external and internal environments. We have specialised cells that can act as sensors for various stimuli, such as temperature, sound, light, and especially for allergens and toxins.

The detection of toxins and poisons is as essential in industry as in biology. The detection of ultra-low concentrations of toxins, for example lead deposits in everyday substances such as make up, requires a rapid, facile and efficient measurement during quality control procedures, with a simple readable signal to provide the level and/or absence of the analyte being detected. Similarly, in biotechnology and medicine, the ability to quickly detect the presence of biomarkers and/or the expression of abnormal proteins in many disease states allows for faster diagnosis and treatment for the patient. In these instances, chemosensors are the specific sensors of choice.

Chemical sensors (also interchangeably called chemical probes[1]) provide a response to the detection of otherwise silent chemical analytes in the form of a measurable signal related to the amount of analyte it is detecting. This signal is often colorimetric, fluorescent, or luminescent, but can also be electrochemical (Figure 1.1). All chemosensors have a recognition element to their structure and composition, for selective interaction with the

intended analyte, be it a binding event or inducing a change in the receptors' shape and structure.

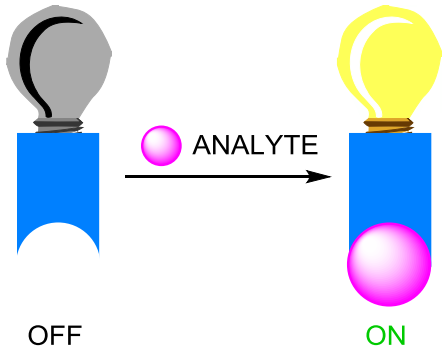

Figure 1-1 Schematic representation of an optical response from a probe, induced by analyte binding.

1.2. General Targets for a Sensor or Probe

In general, the common targets for a chemosensor include poisons, proteins, and other biomarkers for disease. A particularly successful field of chemosensing, and one in which this body of work is focused on, is metal cation sensing.

The burgeoning field of chemical biology and bioinorganic chemistry has been helping to ascertain the roles and functions of these metal cations in biology. Redox-active copper and iron are the two most studied metal cations, along with calcium, potassium and magnesium. All of these, and many others, play an active role in cellular and organ-level support and function. Their uses can be structural or enzymatic. Iron for example, is essential to life due to its role in the oxygen carrier protein haemoglobin. This often means that alterations in their abundance, location and function can lead to severe disorders in the organism. Other heavier metals such as mercury, lead and cadmium can promote serious toxicity and aging in biological systems, so their detection could be vital to help to identify a need for treatment.

The ability to successfully image these metal ions *in vivo*, and study their normal, abnormal and toxic behaviours in real time can help to determine whether they are a cause or effect of these disorders, and even utilise them as markers or indicators for the presence of abnormalities in the cells or organs.

1.3. Targeting Biological Zinc

Zinc is the second most abundant d-block metal in the body, and its role in a number of biological processes in the body has come to the forefront of contemporary research in the field of chemical biology. In 1996, a key paper by Berg and Shi was published, as a call for scientists to study zinc in the same way as iron and calcium had been investigated.[2] Berg's manifesto drew attention to the nature of bound zinc cations as key structural features of many proteins, and the core role it plays in the activity of enzymes, such as carbonic anhydrase. It is now known to be associated with over 3000 enzymes and proteins in the human body compared, for example, to 178 for iron and 63 for copper. As an example, alcohol dehydrogenase contains a zinc atom at its active site which is vital to enzymatic activity, but a second zinc ion is also present in a structural site that is key to the stability of the protein. Berg highlighted the importance of zinc ions as part of important biological components, specifically for the role they play in interactions with important macromolecules such as DNA; zinc finger proteins have been found to be involved in transcription of DNA, where a zinc transcription factor facilitates the interaction between the protein chain and the DNA helix.

As well as these bound forms, zinc is also present in many cells in a loosely bound and chelatable form, often referred to in literature as 'free' or 'mobile' zinc.[3] It is these pools of zinc that have attracted particular interest. Berg briefly mentioned the potential for zinc to work as an 'information carrier', and indeed, it has since been found to play a vital role in stimulating regulation of cellular function, or homeostasis.[4] These pools exist in many vital

organs in the body, such as the brain, pancreas, eyes, intestine, prostate and nervous system, and as such, zinc is implicated in regulating brain function and pathology, cell growth and proliferation, and in the maintenance of the normal function of these organs.

Many investigations have highlighted the potential link between the role that zinc plays at a cellular level, and a range of disease states, indicating the potential use of 'mobile' zinc as a marker for specific pathologies. As a specific example, Type 2 Diabetes mellitus (T2DM) is a global epidemic and as of 2013, cases in the UK hit an all-time high of 3.2 million.[5] Scientists have identified polymorphisms in the gene which encodes for the secretory granule zinc transporter ZnT8 in insulin-producing pancreatic β-cells, thus directly linking zinc deficiency with the presence of the disease. The biological trafficking of zinc has also been linked with other diseases including Alzheimer's disease,[6] epilepsy,[7] ischemic stroke,[8] infantile diarrhoea,[9,10] age related macular degeneration[11] and prostate cancer.[12]

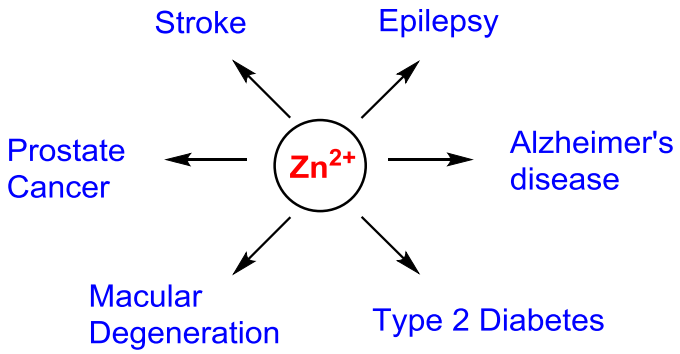

Figure 1-2 Some of the disease states linked to the abnormal homeostasis of Zn^{2+}

All of these disease processes are examples that arise from the breakdown of zinc homeostasis in the body, where the increase or reduction in the amount of zinc has been highlighted to be extremely significant. The exact role of zinc in the progression of these diseases, however, is still largely unknown. There is still a need to monitor the regulation of zinc in cells, its trafficking in and out of cells and around the body, and to study the pools of

chelatable zinc, to develop a better general understanding of the processes zinc is intrinsically involved in and how zinc-related diseases develop. This in turn, may help scientists use zinc to find and create efficient tools for diagnosis, or perhaps even treatment of these diseases.

Traditional methods of detecting zinc levels *in vivo* have involved invasive techniques to identify the cellular content or, as an example, using a zinc selective stain such as dithizone in tissues.[13] For obvious reasons, invasive procedures are undesirable, and dyes such as dithizone are very dependent on the external environment (factors such as light and heat), and as such there is a move to use alternative non-invasive imaging agents.

There are already many detection systems available for a range of other biologically relevant metal cations, like calcium, magnesium and potassium. Even though there is between 2 and 3 grams of zinc in the adult human, 'mobile' chelatable zinc is significantly less abundant than these cations, with concentrations varying in different compartments from micromolar to picomolar. Consequently any sensing systems would also need to be carefully tuned to have the required sensitivity over this range of concentrations.

1.4. Mechanisms for Zinc Sensing

It is important to appreciate the co-ordination chemistry of the zinc cation. Zinc in the body is in the divalent ion form, Zn^{2+}, and this gives it a number of important properties. Firstly, it has a d^{10} configuration, giving it a filled d-shell. The most important outcome of this is that it is rendered spectroscopically silent for the majority of techniques that have proved useful in probing the action of other cations in biological systems, such as UV-Vis and EPR spectroscopies. Ideas towards the design of chemical sensors for it can be obtained by looking at the factors that make it so successful in its biological roles in enzymes and proteins. Zn^{2+} is not redox active, the filled d-shell also means it has no preference for

coordination geometry and it can interact very strongly with a wide variety of ligands.[2,14] With this in mind, the majority of detection systems developed in the last fifteen to twenty years have concentrated on small molecule bio-imaging agents, in particular fluorescent probes.

Due to their high sensitivity and operational simplicity, fluorescent sensors have been used by a number of research groups in testing for many biologically relevant species, which has also become easier due to advancements in technology and fluorescence instrumentation. These types of probes are small, relatively easy to synthesise, are often able to cross cell membranes to successfully access the zinc sources *in vivo*, and are well suited to real-time *in cellulo* study.

These zinc reporters have many interesting mechanisms of action which determine the sensitivity and output signal, and whilst in this section some successful sensors of each example will be highlighted, the reader is directed to more comprehensive reviews of small molecule zinc sensors for a more exhaustive list of examples.[4,15–19]

The majority of chemosensors reported follow the same basic supramolecular structure (Figure 1-3). They typically consist of a fluorophore as the output site for the response to a binding event, attached to a receptor as the binding or chelation site for the species to be detected, in this case zinc. They can be directly ligated, but commonly are separated *via* a small spacer, typically $C_{2\text{-}3}$.

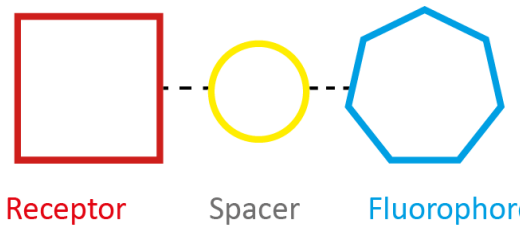

Figure 1-3 Representation of the typical structure of a small molecule fluorescent chemosensor

The photophysical mechanisms these constructs use to act as a sensor vary with structure, and the most common mechanisms of response are:

- Photoinduced Electron Transfer
- Internal/intramolecular Charge Transfer (and its related processes)
- Förster Resonance Energy Transfer
- Excimer/Exciplex formation

A summary of each approach of sensing is noted here. Again, these processes have been extensively reviewed, and these reviews also include accounts of other emerging and less common pathways of fluorescent signalling not discussed here.[15,20]

1.4.1. Photoinduced Electron Transfer (PET)

PET is one of the most common mechanisms of zinc sensing. PET sensors commonly adopt the fluorophore-spacer-receptor scaffold. The receptor contains high energy non-bonding electron pairs from heteroatoms like nitrogen and oxygen. Upon excitation of the system in the absence of the analyte, electron transfer that takes place from these high-energy electrons to the excited state of the fluorophore, inducing quenching of the fluorescent output and giving an 'off' state in this form. (Figure 1-4)

Chelation of zinc to the receptor lowers the HOMO of the ligand lone pair, thermodynamically disfavouring the quenching process *via* electron transfer, thus resulting in an emissive process upon excitation of the molecule. This is known as the 'switch-on' process that quenching of PET can provide upon chelation, resulting in Chelation Enhanced Fluorescence (CHEF). The role of the spacer is merely to keep the receptor and emissive components separate, but still close enough to allow the electron transfer process to efficiently occur.

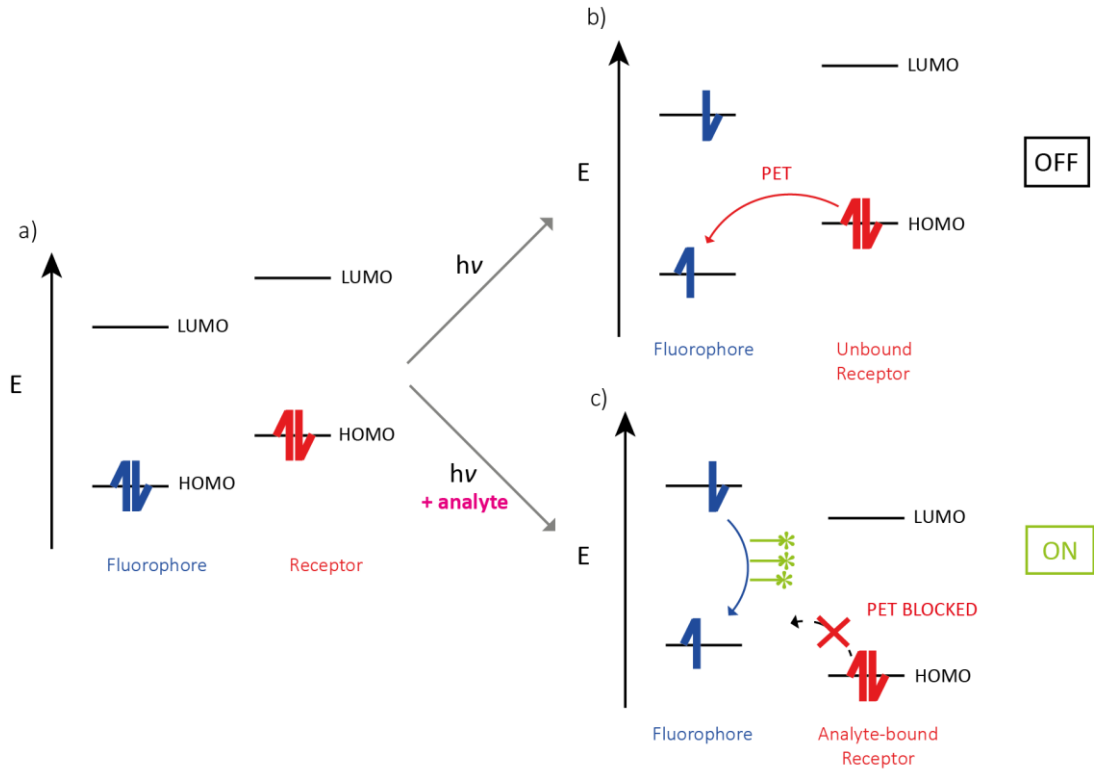

Figure 1-4 Orbital energy diagram to demonstrate the 'off' and 'on' states of a fluorescent chemosensor upon photoinduced electron transfer, or the blocking thereof.

Figure 1-5 demonstrates four successful examples of sensors selective for zinc using the PET 'off-on' mechanism for sensing.[21–24] All show selectivity for zinc, and in particular bodipy-based probe **5** was used to image zinc in living cells (Figure 1-5 (a) and (b)). These probes do also respond to Cd^{2+} ions in a similar manner to zinc, but as cadmium is not biologically relevant, this result is considered unimportant.

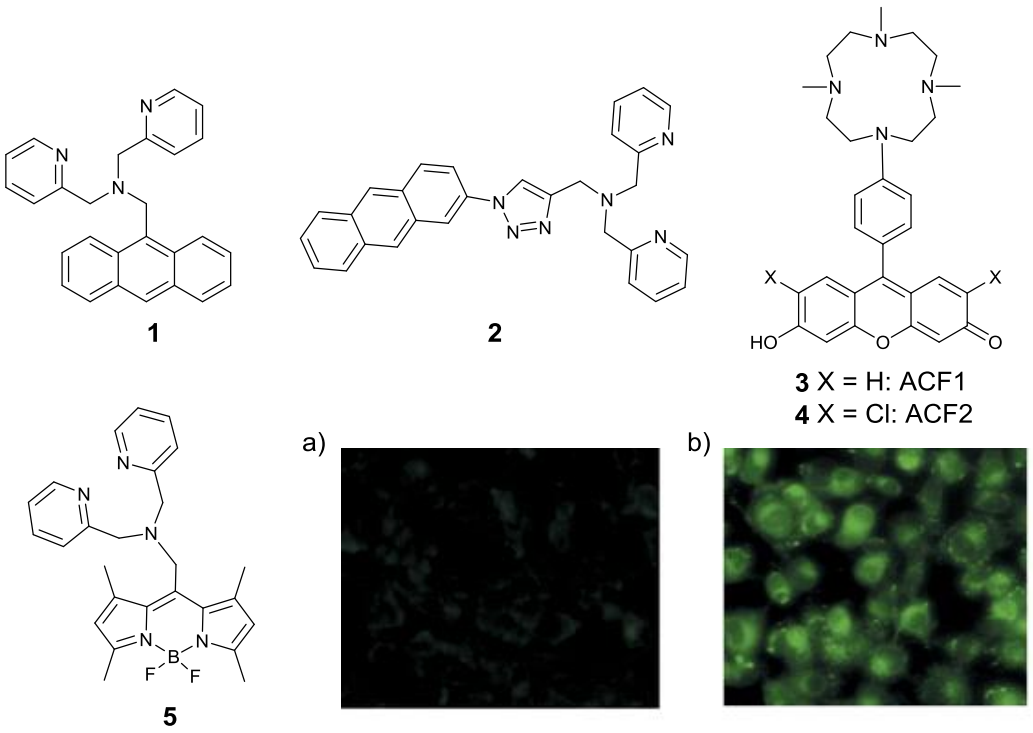

Figure 1-5 Selected examples of probes employing PET mechanisms for zinc sensing. a) Fluorescence image of TCA cells loaded with probe **5** (10 μM). b) Fluorescence image of stained cells loaded with Zn^{2+} (50 μM) for 30 min. Images reproduced with permission from the Royal Society of Chemistry. [24] Copyright © 2005, Royal Society of Chemistry.

1.4.2. Internal/Intramolecular Charge Transfer (ICT)

Sensors that utilise ICT mechanisms often consist of a fluorophore and receptor with no spacer, forming a π-electron rich conjugated system with an electron-rich and electron-deficient region. If the charge distribution in the molecule is altered, this is manifested as a change in fluorescent signal. Binding of zinc to an ICT-based chemosensor causes an observable change in fluorescence emission, often accompanied by a red or blue shift depending on whether the receptor is the electron donor or acceptor. This is distinctly different to the PET-mechanism of sensing, which generally has no observable band shift but merely a hyperchromic enhancement. ICT mechanisms are also often highly solvent dependent, as polarity plays a role in stabilising the electronic state of the molecule.

This behaviour often lends to ICT sensors being ratiometric, meaning the emission ratio at the two different wavelengths can be attributed to cation concentration, and these sensors

can potentially allow for the quantification of zinc present in the sample, be it solution, cells or tissues.

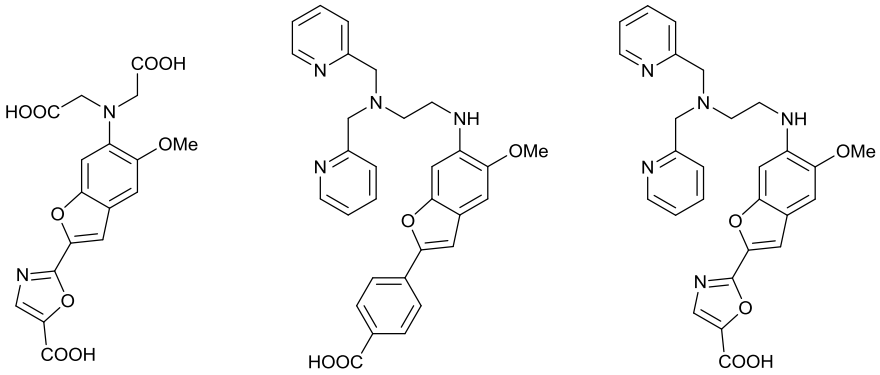

6 FuraZin **7** ZnAF-R1 **8** ZnAF-R2

Figure 1-6 Examples of ICT-based probes **6 – 8**

FuraZin **6**, and its related derivatives ZnAF-R1 **7** and R2 **8** are successful examples of ICT based probes, with the latter also being ratiometric.[17,25] In these examples, the binding of zinc alters the electron donating properties of the electron rich ligands used in these examples, thus affecting the photophysical properties of its response to a binding event. Probes **6**-**8** have been used to successfully image zinc in cellular environments.[25,26] Recently, an ICT-based zinc selective probe **9** was reported by Liu *et al.* that demonstrates effective imaging in zebrafish as a living animal model, with a ratiometric response and excellent selectivity for zinc.[27]

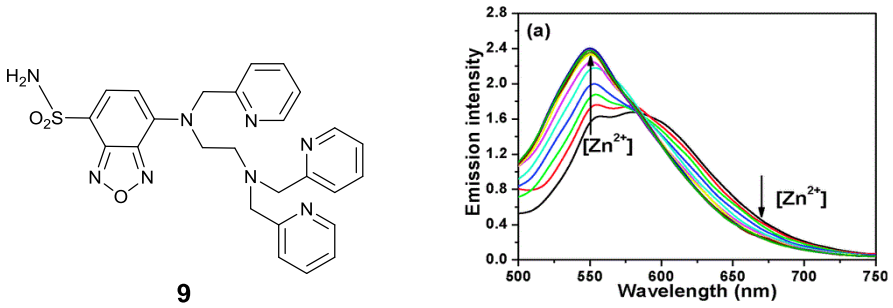

9

Figure 1-7 ICT-based Zn^{2+} selective probe **9** designed by Liu *et al.* and its ratiometric emission profile. Image reproduced with permission from the Royal Society of Chemistry.[27] Copyright © 2014, RSC.

1.4.3. Förster Resonance Energy Transfer (FRET)

Sensors that utilise the FRET mechanism to elicit a fluorescence response to binding always incorporate a 'switch-on' response. FRET is classified as a distance-dependent transfer of energy from an excited donor fluorophore to a ground-state acceptor fluorophore which is consequently excited and exhibits fluorescence.

The fluorophores of the FRET pair need to have the appropriate degree of spectral overlap between the emission of the donor fluorophore and the absorption spectra of the acceptor. By binding a cation to these types of probes, the distance between the FRET pair can be altered, thereby altering/arresting the FRET mechanism. This type of mechanism is generally employed when using two fluorescent proteins for a FRET-based probe. Alternatively, in the case of small molecule probes, it is possible to disrupt the degree of overlap between the FRET pair of fluorophores by altering the emission of the donor fluorophore upon a binding event.

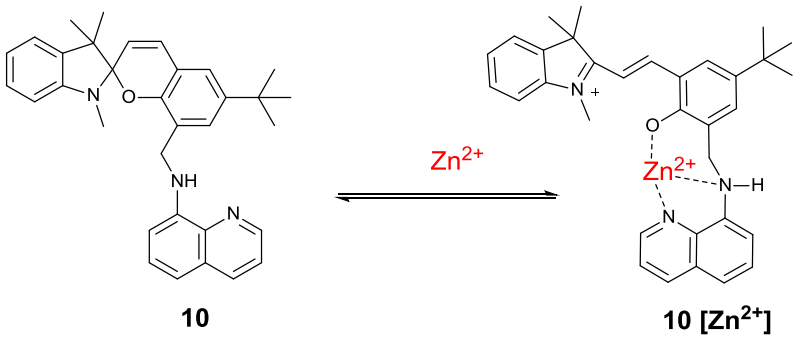

10 **10 [Zn^{2+}]**

Figure 1-8 FRET-based chemosensor selective for Zn^{2+} in EtOH, and its binding mode with Zn^{2+}

In 2010, a novel FRET-based chemosensor **10** was designed and demonstrated to show a CHEF response for zinc in ethanol solution. [28] The aminoquinoline moiety acts as the donor, and binding of zinc at the donor site causes ring opening and a change in FRET to occur between that and the acceptor moiety, resulting in a ratiometric response to binding.

Whilst this is advantageous, the inability to test this probe in an aqueous environment limits this probe's use in biological settings. This mechanism has been used successfully in genetically encoded zinc sensors with pairs of fluorescent proteins as donor and acceptor (see Section 1.6.1).

1.4.4. Excimer/Exciplex Formation

An excimer is defined as a complex formed when an excited fluorophore interacts with another fluorophore of the same structure in its ground state. Either a dual emission is observed, with excimer emission distinctly red shifted from that of the monomer, or only the excimer emission is observed.

When the molecule in the ground state is not identical, the excited complex formed is known as an exciplex. Often the emission bands for excimers/exciplexes are broad. With these sensors, the analyte can be used to template formation of, and promote emission of the complex, or peturb the interaction between the two fluorophores and switch off the emission.

A recent example of a zinc chemosensor exploiting this type of behaviour is shown in Figure 1-9.[29] Pyrene-based molecules are particularly known for their propensity to form excimers. The incorporation of them into this sensor meant the group observed characteristic pyrene excimer bands in the fluorescence spectra of sensor **11** in a H_2O/MeCN mixture. Upon binding of zinc however, no pyrene stacking occurs, and so monomer emission is observed. The subsequent addition of pyrophosphate means zinc is no longer bound inside the molecule, allowing the pyrene molecules to stack and so the excimer emission is once again observed.

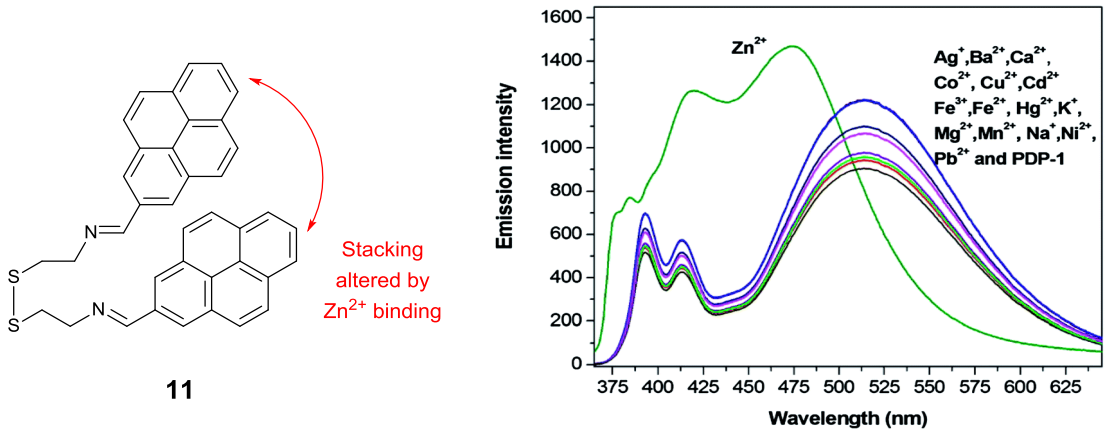

Figure 1-9 Zn^{2+} selective probe **11** and its emission profile in the presence of other analytes. Image reproduced with permission from the Royal Society of Chemistry. [29] Copyright © 2014, RSC.

1.5. Characteristics of an Ideal Zinc Sensor

Regardless of its mechanism of action, there are a number of rules that it is important to follow when designing a zinc-selective chemosensor. Many reviews and publications from zinc biologists and chemists alike often refer to the following essential criteria required for zinc sensing *in vivo* in real time.[4,16,18]

a) Selectivity for zinc over other competing cations, including protons

One of the strictest requirements for a successful probe is that it has high selectivity for zinc and retains this selectivity in the presence of other biologically abundant cations. Sensors must also be able to give a response over a wide range of concentrations of the cation and so display appropriate binding constant, as the concentration of zinc varies significantly according to biological setting.

b) Biological properties – toxicity/availability/solubility

The sensor molecule should ideally be completely biocompatible. Essential features include water solubility, very low or no toxicity, and insensitivity and high stability towards varying changes in environment such as pH and ionic strength of solution.

c) Optimal brightness and luminescence profile

There are also optical requirements for the fluorescent component of the molecule; the ideal sensor should have a large extinction coefficient and quantum yield to give high brightness or high fluorescence in response to a binding event, for ease of detection (visually or microscopically). Additionally, brighter probes can often be detected at lower concentrations, so reducing the disruption to metal homeostasis *in vivo*. Ideally the excitation and emission wavelengths of the sensors should be in the visible or low energy range. UV-radiation causes undesired photo-damage to tissues and cells, and also evokes cellular autofluorescence, which can contaminate the signal from the sensor. Near infra-red wavelengths are also of interest as these wavelengths can penetrate tissues more deeply.

d) Optimal sensitivity, with the ability to quantify the amount of analyte

A 'switch-on' response is preferred, as this can provide an ideal method of real-time observation of zinc chelation. A ratiometric response is also highly desirable to quantify the levels of zinc available in real time.

e) Simple and high yielding synthesis

One of the biggest drawbacks of the use of small molecule probes is that there is no guarantee that any probe will work *in-cellulo*. There is a need to be able to rapidly diversify and synthesise new probes quickly, so the synthetic route is very important. This can be likened to the pharmaceutical industry, where methodology is put in place for rapid synthesis, screening, and re-synthesis if needed of a large number of substrates to find a lead compound for drug molecules. To maximise the probability of efficacy in biological systems, access to multiple modified probes through a facile and expedient synthesis could prove to be highly beneficial for the field.

f) Control of probe distribution to monitor movement/presence of zinc.

A key current challenge is to develop these sensing systems further as targeted probes *in vivo*. This is to aid the study of chelatable pools of zinc in specific organs or cellular organelles, in order to develop a better understanding of the disease processes they are intrinsically involved with. All eukaryotic cells contain defined compartments, from the nucleus to vesicles, and zinc has a different role in each one. Control of probe localisation is vital as the user can then visualise zinc in specific areas. The ideal sensor or detection system for zinc should be able to detect zinc in cells and tissues with very little or no interference from any other factors.

1.6. Targeted Small Molecule Zinc Sensors – Evaluation of the Field

Whilst the development of probes for zinc with targeting capabilities is still in its infancy, there are successful examples of probes that have demonstrated subcellular localisation in an effort to meet all of the above criteria.

1.6.1. Protein Based Targeted Sensors

Protein-based fluorescent probes for zinc detection were amongst the first designed to localize to specific cellular compartments. These types of targeted sensors can essentially be divided into two categories.

The first are genetically encoded FRET sensors, where a zinc binding unit is placed between two different fluorescent proteins that alter in conformation upon binding of a zinc cation.[30] The genetically encoded sensor **12** developed by Dittmer *et al.* relies on zinc finger protein interactions to bind zinc, and their study found mitochondria to be a source and a sink for Zn^{2+} under different conditions, accumulating and releasing zinc in response to stimuli. The group also recently used these sensors to monitor the processes in the Golgi

apparatus and endoplasmic reticulum (ER), determining that elevated levels of Ca^{2+} in the cell gives rise to Zn^{2+} release from the ER.[31]

The second are sensors generated by labelling a genetically encoded tag with a small molecule sensor, as the Lippard group did with their SNAP-Tag based sensors.[32] The group, well-known for synthesising zinc-selective probes,[33] immobilized one of their family of Zinpyr fluorescent zinc probes onto targeted organelles, such as the Golgi apparatus and mitochondria, *via* labelling with alkylguaninetransferase (AGT) (Figure 1-10, **13**). The enzyme targets a protein known to be expressed in specific cellular compartments, to enable the localised imaging of Zn^{2+}. An advantage of sensors of this type is their ability to image zinc in localised compartments without worrying about the spontaneous distribution of the probe in the tissue or organ. Only the immobilised sensor is responsive to zinc, giving a desirable 'switch-on' response only when anchored and fused to the expressed protein.[34]

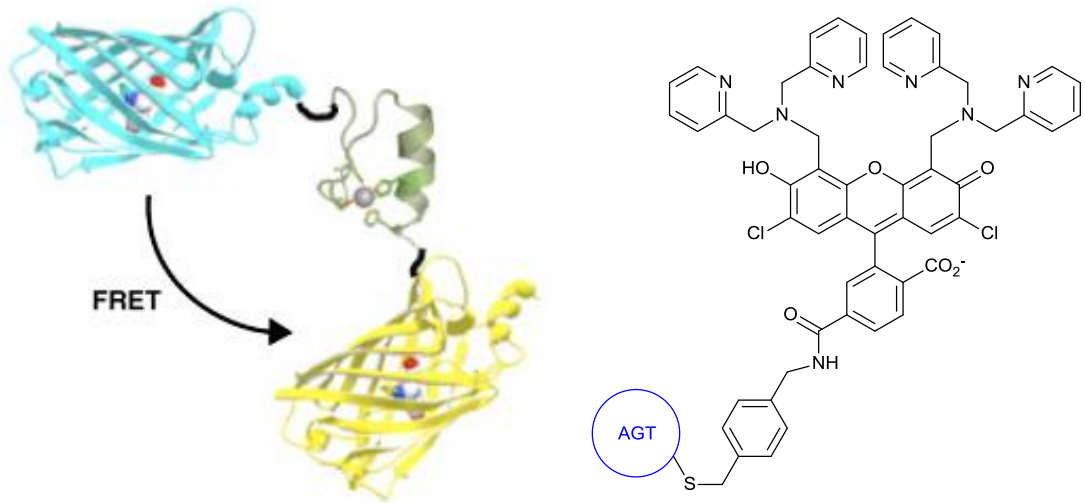

12 **13**

Figure 1-10 Protein based fluorescent sensors **12** and **13**.[1]

[1] Image for probe **12** reprinted from Current Opinion in Chemical Biology, volume 14, Elisa Tomat and Stephen J. Lippard, *'Imaging Mobile Zinc in Biology'*, p 225 – 230, Copyright © 2010, with permission from Elsevier.

Although these strategies have advantages in terms of the precise localisation of the probe they can give, both methods require extensive genetic modification procedures and long protein syntheses, which results in an undesirably complicated route to a simple imaging tool. These probes also suffer from low fluorescence outputs, but are available with a good range of binding constants needed to assess zinc levels in different biological settings.[35,36]

1.6.2. Biological Targeting with a Functional Group or Molecule

An alternative strategy is to use a sensor with a specific functional group or molecule, one that is not gene or protein based, and is known to interact at specific cellular sites, or localise at particular organelles. There are a growing number of recent examples in this field, some of which are described below. It is interesting to note that in many cases these probes are merely simple modifications of existing sensors with the additional functionality being applied *via* a synthetic handle on the probe. Whilst many of these sensors have a successful function, their synthesis is often challenging and low yielding.

1.6.2.1. Targeting Mitochondria

Mitochondrial zinc uptake occurs to clear the cytosol of the cell of zinc accumulation, but it is known that excessive accumulation of zinc inside the mitochondria promotes their dysfunction, and an increase in production of reactive oxygen species leading to toxicity and apoptosis. [37] To understand the implications of this, it is vital to monitor mitochondrial zinc uptake/movement in tissues or cells in real time.

In 2003, Rhod-Zin3 **14** (Figure 1-11) was found to detect changes in mitochondrial zinc at a nanomolar level, and the group made some important observations regarding the role of mitochondrial zinc and intracellular homeostasis in neuronal cells.[38] However, the localisation was serendipitous as it was not designed to image mitochondrial zinc specifically. Charged compounds are now commonly known to interact strongly with the

mitochondrial membrane, and in particular, lipophilic cations can accumulate inside the mitochondrial space. Therefore using cationic species as a way to target mitochondria is now a widely used and successful methodology.[39]

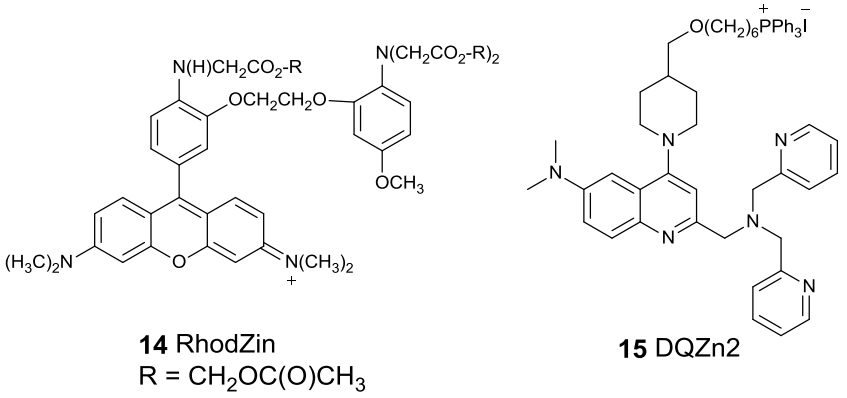

Figure 1-11 Lipophilic cation-bearing probes RhodZin **14**and DQZn2 **15,** for imaging of mitochondrial zinc.

In 2012, the development of a targeted fluorescent probe for zinc was published, DQZn2 **15**.[40] The sensor consists of a commonly-used di-2-picolylamine (DPA) metal chelating unit, with a quinoline based fluorophore and a triphenyl phosphonium targeting unit, separated from the sensor by a long linker to minimise its influence on the photophysical properties of the molecule. [41] Triphenylphosphonium cations are often used for anchoring a probe or other cargo to mitochondria in cells.[42,43] The sensor provided a basic quantitative measurement, as fluorescence intensity increases upon addition of zinc, but this is heavily influenced by pH, concentration of sensor, and photobleaching.

SZn-Mito **16** is another probe with an identical targeting group and metal chelating unit, but a different fluorescent reporter.[41] This PET-based probe was used to image zinc in the mitochondria in HeLa cells using both regular fluorescence and two-photon microscopy, to overcome unfavourable excitation and emission values of the probe and for imaging over extended periods of time with high resolution.[44] With 1:1 binding of probe and analyte, a 7-fold 'switch on' response to binding, excellent selectivity for zinc over other biologically

relevant metal cations, pH insensitivity and a K_d value of 3.1 nm, this probe has excellent characteristics to apply to real time *in cellulo* imaging.

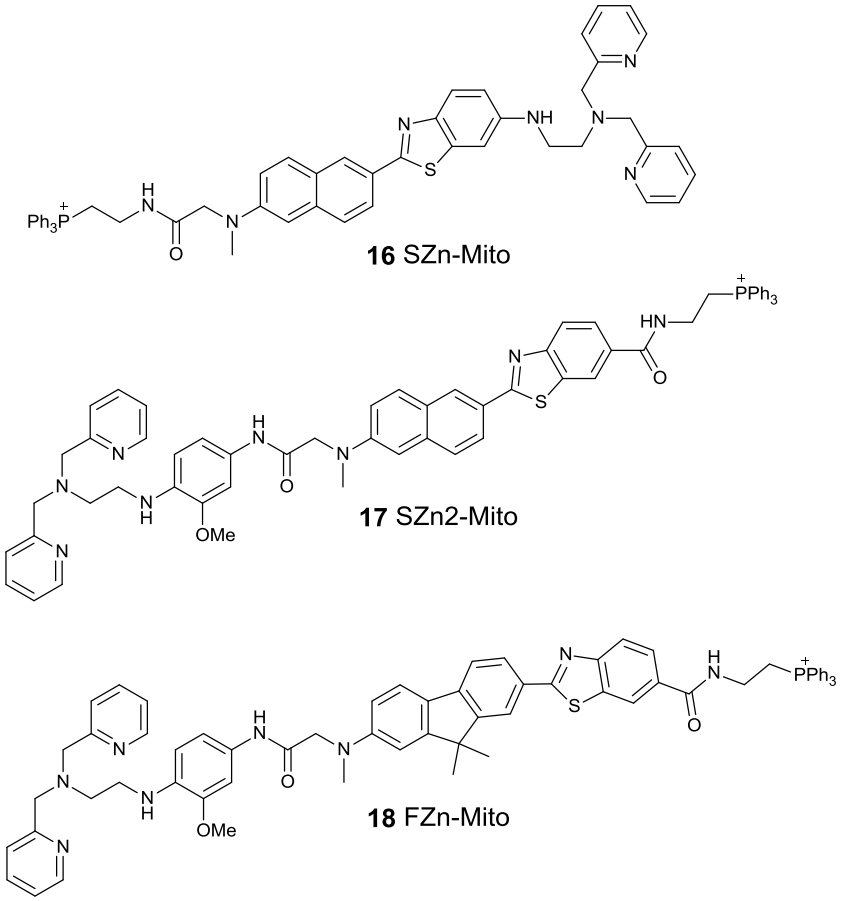

Figure 1-12 Other mitochondria-targeted Zn^{2+} probes **16 – 18** synthesised by the Cho Group.

The group followed this up with SZn2-Mito **17**, observing an improvement in fluorescent enhancement and a smaller K_d value of 1.4 nM, but with retention of the excellent characteristics of the parent probe.[45] They also synthesised a third probe, FZn-Mito **18**, with a different fluorophore core, but similar two photon characteristics and behaviour.[46] It displayed a 16-fold switch on CHEF in the presence of zinc and a favourable emission at 550 nm for both one- and two-photon imaging in HeLa cells. Mitochondrial presence was confirmed by co-localisation with the Mitotracker dye, with a Pearson's co-localisation coefficient of 0.86.

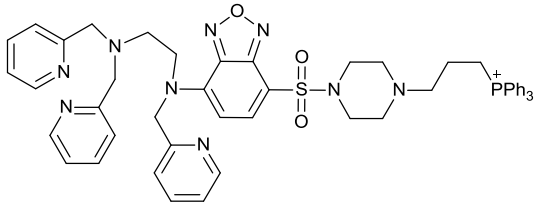

19 Mito-ST

Figure 1-13 ICT-based Zn^{2+} probe Mito-ST **19** for monitoring mitochondrial zinc.

In a similar manner, Guo and co-workers developed Mito-ST **19**, an ICT-based ratiometric probe used to monitor zinc release from mitochondria in response to stimuli like H_2O_2 and NO.[47] This provided a reliable method of monitoring the efflux of zinc from the mitochondria in response to toxic cell stimuli such as excess H_2O_2.

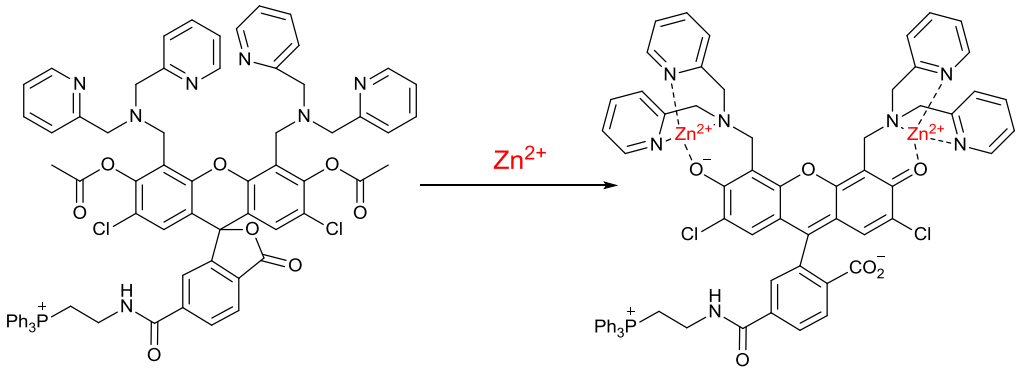

Scheme 1-1 Mitochondrial probe DA-ZP1-TPP **20** synthesised by Lippard *et al.*, and its binding mode with Zn^{2+} (1:2) to give complex Zn^{2+}[ZP1-TPP]

The Lippard group extended the utility of their commercially available Zinpyr-1 probe by appending a triphenylphosphonium cation to target the probe to mitochondrial space (Scheme 1-1, DA-ZP1-TPP **20**).[48] Acetylating the probe completely quenched fluorescence in the 'off'-state, resulting in a large 'on-off' difference and increasing the dynamic range of the probe, as zinc both mediates the hydrolysis of the acetyl groups and binds the ligand to produce a selective switch-on response. Without acetylation, the probe was sequestered in lysosomes and endosomes, and so the structure as well as the targeting group became vital

for successful *in-cellulo* imaging. DA-ZP1-TPP-stained cells responded to changes in intracellular zinc levels in both healthy and cancerous prostate cells, and showed the diseased cells lose the ability to accumulate zinc into the mitochondria.

1.6.2.2. Targeting the Cell Membrane

The extracellular membrane is another region of interest when studying zinc trafficking. Visualisation of zinc influx/efflux at a cell membrane can contribute to studies on zinc release related to neuronal activity, disease states of a cell, or of apoptosis.

The Taki group have recently synthesised a cholesterol conjugated fluorescent sensor, which binds to the plasma membrane of cells.[49] The probe **21** follows a modular design consisting of three clear units; a zinc-binding moiety, a fluorescent reporter component based on fluorescein, and a cholesterol molecule, linked to the fluorophore with a triethylene glycol linker (Figure 1-14). The cholesterol molecule has a high affinity for lipid membranes, and using this, the group demonstrated this sensor localised to the cell membrane. This was proved by fluorescence microscopy studies, confirming its presence in the extra cellular region due to the hydrophilic properties of the rest of the compound. The group commented on the ability to change the fluorophore in future, as well as the bioconjugation component, to allow multi-colour imaging at different compartments to facilitate our understanding of the way zinc is trafficked in a cell, though no further studies have been reported to date.

In a further demonstration of extracellular imaging, Li, Rutter and co-workers have synthesised ZIMIR **22**, a variant of the ZnAF sensor developed by Lippard, functionalised with two long alkyl chains that anchor the sensor to the extracellular region of the cell membrane, aiming to monitor the influx and efflux of zinc.[50] In particular, **22** was used to image intact murine pancreatic islet β-cells to exploit the fact that insulin granules contain

high levels of 'free' zinc co-ordinated to insulin, and both are co-released upon insulin secretion. This has been carried out before with commercial probes such as Newport Green DCF, RhodZin-3 (**14**) and Zinquin, but these all suffer from a lack of localisation, selectivity and also from operational problems associated with background fluorescence from the bulk solution in the extracellular space upon loading of the cells. ZIMIR-labelled cells were stable in the presence of the probe, and reliably reported changes in zinc concentration at the cell surface into the extracellular space upon stimulation to promote insulin release. It also aided the discovery of new information about the methods and precise locations of exocytosis from these types of cells, which could prove important in helping the study of type-2 diabetes melitus.

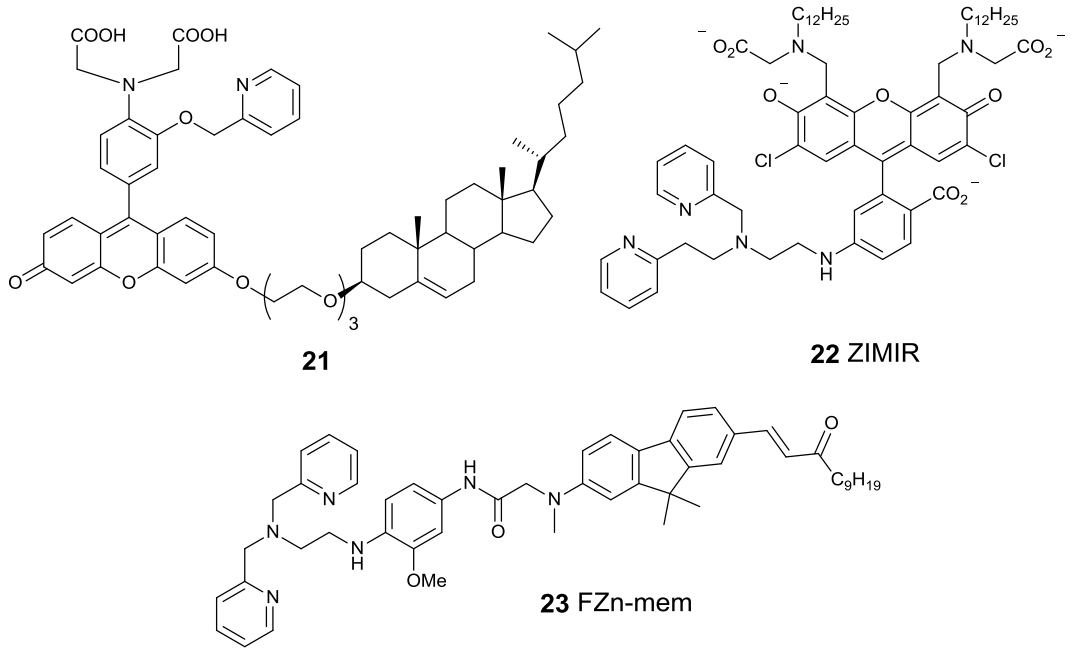

Figure 1-14 Zn^{2+} specific probes **21 – 23** designed to target extracellular membranes.

In a similar vein, the Cho group also synthesised a zinc-specific probe **23** with a dodecyl arm like ZIMIR, to anchor the probe extracellularly.[51] Much like FZn-Mito **18**, FZn-mem **23** had the extra advantage of being a two-photon chemosensor, with a 7-fold increase in emission

upon binding of zinc. The probe proved to be highly stable, imaging extracellular zinc ions in intact HeLa cells for extended periods of time, with little interference from other metal ions.

1.6.2.3. Targeting Lysosomes

The lysosome is an acidic compartment in the cell designed to aid degradation of other cellular elements. Like the mitochondria, the influx and accumulation of zinc into lysosomes have been known to contribute to their dysfunction, and particularly contributes to cell death in neurons under oxidative stress by causing lysosomal membrane permeabilization.[52] A better understanding of these mechanisms could contribute to the study of the causes and effects of various neurodegenerative disorders.

After their development of DQZn2 **15** as a successful mitochondrial stain (*vide supra*), the Jiang group also synthesised DQZn4 **24** with an identical core of fluorophore and DPA receptor, but a different targeting group.[53] The dimethyl ethylamino moiety is known to accumulate in acidic lysosomal space after being protonated and so can be used to help deliver cargo and probes to these compartments.[54–56] This was the first known example of a small molecule lysosomal-targeted zinc probe. Probe **24** retains the selectivity and sensitivity of **15**, despite the change in targeting group, performs well at the acidic pH of its intended compartment and was successfully utilized for imaging lysosomal zinc changes in living cells.

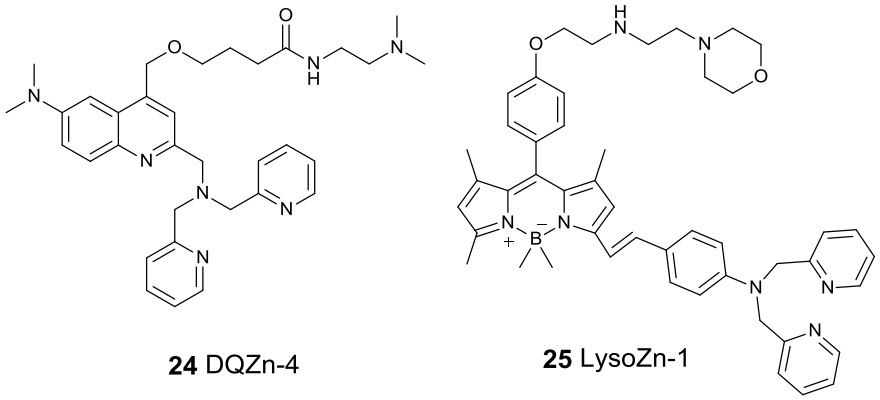

Figure 1-15 Small molecule probes DQZn4 **24** and LysoZn-1 **25** designed to target lysosomal space in cells.

Following this, Zhu *et al.* also designed a ratiometric zinc selective sensor **25** designed to localise in lysosomal space, based on a BODIPY scaffold with DPA again as the receptor unit.[57] They used a similar targeting group, also based on ethylenediamine, designed to protonate in acidic conditions and channel the probe into lysosomal compartments, but terminated with a morpholine unit rather than the dimethylamine moiety used in **24**. This ratiometric probe **25** was effective across an acidic pH range (pH 3–8), and was successfully used to monitor zinc concentrations in lysosomes in neural stem cells upon stimulation with H_2O_2. Considering H_2O_2 is a strong oxidant, the group found it has no effect on the behaviour of the probe, meaning any changes observed in fluorescence could be attributed solely to a change in zinc concentration.

1.6.2.4. Other Cellular Compartments

Cho and co-workers reported the synthesis and testing of BZn-Cyto **26** [46] alongside the report of FZn-Mito **18** and used both probes in live HeLa cells to demonstrate multicolour imaging of different compartments. BZn-Cyto was designed to localise in cytosolic space, and successful *in-cellulo* imaging via two photon microscopy was demonstrated, with a fluorescent enhancement of 27 fold in the presence of zinc and a nanomolar K_d, although

the localisation of **26** to cytosolic space was only qualitiatively observed and noted, not confirmed.

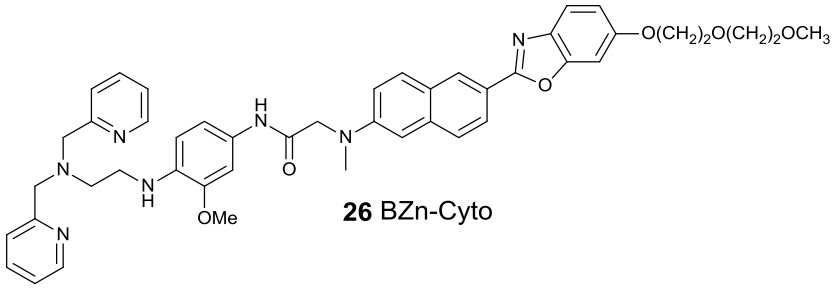

Figure 1-16 Cytosolic Zn^{2+} specific probe BZn-Cyto **26**

Mikata and co-workers designed a quinoline based, glucose appended sensor **27** that was selective for Zn^{2+}.[58] They hypothesised that the glucose units would aid cellular uptake via glucose transport channels in cells for visualisation in the membrane. Whilst the sensor proved selective for zinc with some favourable characteristics *in vitro*, the group found only a small enhancement of fluorescence in the presence of zinc during *in vitro* screening (two-fold) and during fluorescence microscopy (1.8 fold) in PC-12 cells (typical cell line for neurobiology study). The fluorescent response was only observed upon destruction of the cell membrane and addition of extra zinc, confirming its internalisation. However, sugars also have applications in targeting the surface of cells by binding subcellular lectins. This has been used by the Scanlan group in developing targeted zinc-porphyrins as photodynamic therapy agents, with various mono and di-saccharides.[59] Dong and co-workers recently reported the glycosylation of a naphthalimide-based Zn^{2+} probe enhances aqueous solubility and its targeting capabilities, whilst reducing its cytotoxicity.[60]

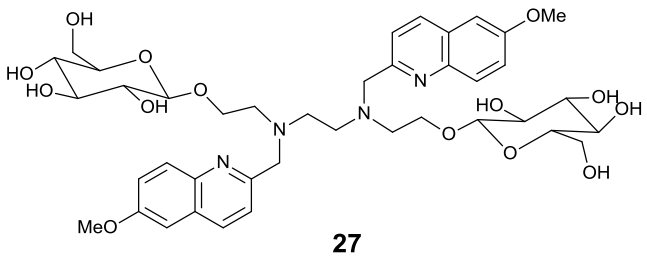

27

Figure 1-17 Glycosylated zinc probe **27** for intracellular imaging of Zn^{2+}

Most probes for other compartments are genetically encoded, hybrid or peptide sequence-based sensors. Spontaneous localisation has in fact been observed with some small molecule probes to other cell compartments. Whilst these probes, just as with RhodZin **14**, are successful at imaging zinc in certain cellular compartments, this is unplanned and unpredictable and can even vary between cell types/lines for the same probe. Nevertheless there are some examples of successful imaging of different compartments.

The ZBR probes **28a – c** (Figure 1-18), though not designed to show specific localisation, were found to localise in the endoplasmic reticulum (ER) in various cell lines.[61] This was confirmed by co-localisation studies with many known cell stains, and the consistency throughout the cell lines tested supports its reliability. These probes were used to image zinc exocytosis from the ER in response to stress in neural cells.

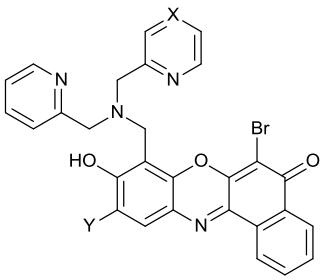

28a ZBR1 X = N Y = H
28b ZBR2 X = N Y = Cl
28c ZBR3 X = CH Y = H

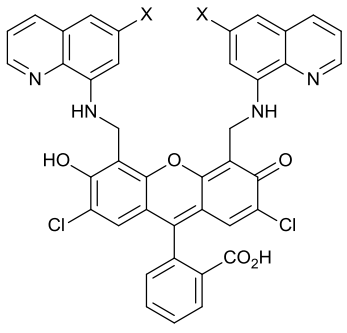

29 QZ2E X = OCH_2CO_2Et

Figure 1-18 Small molecule probes for Zn^{2+}, ZBR **28** and QZ2E **29,** that showed spontaneous localisation in cell lines.

A probe designed in the Lippard laboratory was shown to localise spontaneously in the Golgi apparatus, known as QZ2E (**29**).[62] The di-ester is cell permeable, and upon hydrolysis by intracellular esterases becomes trapped inside the cell. This probe in particular has a large dynamic range for zinc with an exceptional 'switch-on' response to zinc (ϕ(**29**) = 0.4 +/- 0.1%, ϕ(**29** + Zn^{2+}) = 73 +/- 3%), and excellent co-localisation demonstrated with a Golgi-specific stain in HeLa cells.

1.6.2.5. General Remarks

Despite the utility and success of these reported probes, their drawbacks are also notable. Often the overall yields of the targeted probes discussed here were less than 10%, with ZIMIR **22** for example being as low as 3%, due to complicated synthetic routes. The work of the Cho group in synthesising a variety of probes (**16 – 18**, **23**, **26**) for targeting different cellular compartments also demonstrates that despite having the same or similar core structure, the modifications required to alter the targeting capabilities of each probe were not easy to carry out.

The nature of probes such as the ZBR probes (**28**) showing spontaneous localisation, and the unpredictability of a probe's behaviour *in cellulo* is also another concern in the field. The rapid generation and study of these types of successful probes could help to study the factors governing their behaviour and localisation, and incorporate these advantageous characteristics into a general marker for the study of zinc *in vivo*.

1.7. Overall Aims of this Project

We set out to work towards overcoming these limitations and this thesis presents efforts to develop novel Zn^{2+} selective chemosensors that can meet contemporary criteria for successful and simple imaging of specific cellular regions with a modular and facile synthesis.

We aimed to utilise 'click' chemistry to a) synthesise novel sensors that incorporate a targeting unit to develop successful zinc-specific imaging tools, and b) to develop a zinc selective version of a novel structure with the potential to bind metals, with a new mechanism of sensing. Overall we wanted to demonstrate that 'click' chemistry can help to rapidly diversify the probe structures available to meet specific criteria for functional supramolecular structures.

1.8. Copper(I)-catalysed Azide-Alkyne Cycloaddition (CuAAC) and its Merits

'Click' chemistry is a term coined by Barry Sharpless,[63] as an easy, effective way to join two small, separate units together. There are many different reactions under the 'click' chemistry umbrella, but the reaction utilized most commonly is copper catalysed, and works *via* a cycloaddition of an azide group to an alkyne group, hence the term copper(I)-catalysed azide-alkyne cycloaddition (CuAAC).[64,65] It provides regiocontrol, only giving the 1,4- triazole (unlike the thermally driven cycloaddition which produces both the 1,4 and 1,5 triazoles), and proceeds as shown in Figure 1-19 to generate a 1,2,3-triazole bridge between the two 'click' units.

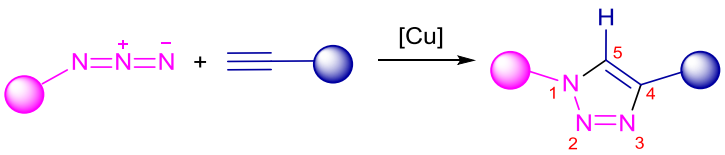

Figure 1-19 Schematic diagram to show the copper-catalysed reaction between an azide and an alkyne to regioselectively form a 1,4-triazole

While the reaction appears simple, it is in fact mechanistically very complex, and this complexity accounts for the regioselectivity of CuAAC reactions in exclusively forming 1,4-substituted triazole products.[66] The formation of a copper acetylide species is thought to account for the directing nature of the catalysis. However, as there are thought to be many other fast forming organocopper species in equilibrium in the reaction, the full mechanism

has yet to be conclusively elucidated. The cycle shown in Scheme 1-2 has recently been proposed by Fokin *et al.* following extensive study, calculations and calorimetry experiments.[67] Whilst it is widely accepted that the formation of a terminal copper acetylide species plays an important role in the catalytic cycle, Fokin and others [68] have proposed that this is not the only catalytically active species and argue a case for a weak π-bond interaction with another copper atom which leads to the regiocontrol observed.

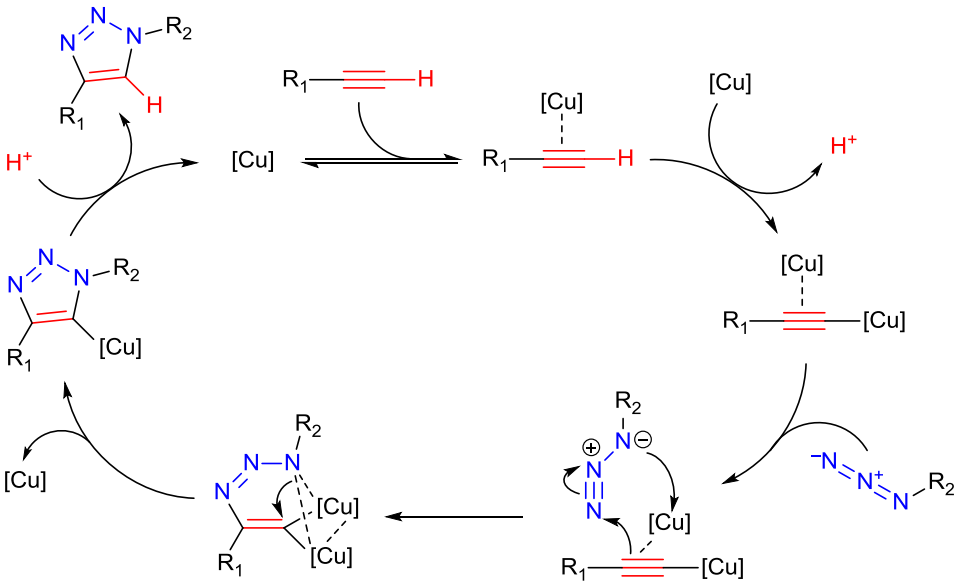

Scheme 1-2 Proposed catalytic cycle from Fokin *et al.*, for a typical CuAAC reaction to account for the observed 1,4- regioselectivity

Despite such points of contention, since Sharpless described it as the "premier example of a 'click' reaction",[69] the effectiveness of the CuAAC has led to its use as a robust method to introduce covalent linkages in an enormous number of molecular structures. It has applications in organic synthesis, medicinal chemistry, the generation of large supramolecular structures, and biomimetic polymers, dendrimers and chains.[70]

1.9. Existing Triazole-containing Zinc Sensors

In terms of chemosensing, many groups have chosen to use this reaction to join together their fluorescent reporter and metal binding unit. This allows not only for chemoselective

ligation but also maintains a small enough distance between the fluorophore and ligand to allow for optimal electron transfer processes upon a binding event. As well as acting as a spacer, in some instances the triazole can act as an additional co-ordinating motif to the metal centre in question. This is true in the case of chemosensor **2** (*vide supra*) synthesised by Zhu *et al*., whereby the triazole plays both a structural (ligating) role, alongside one contributing to the sensor's function.[22] For a full comprehensive review up to 2010, the review by Todd and Watkinson *et al*., covers many examples of triazole-containing sensors. [71] Some recent notable and successful examples since the 2010 review include those chemosensors shown in Figure 1-20Figure 1-21Figure 1-22.

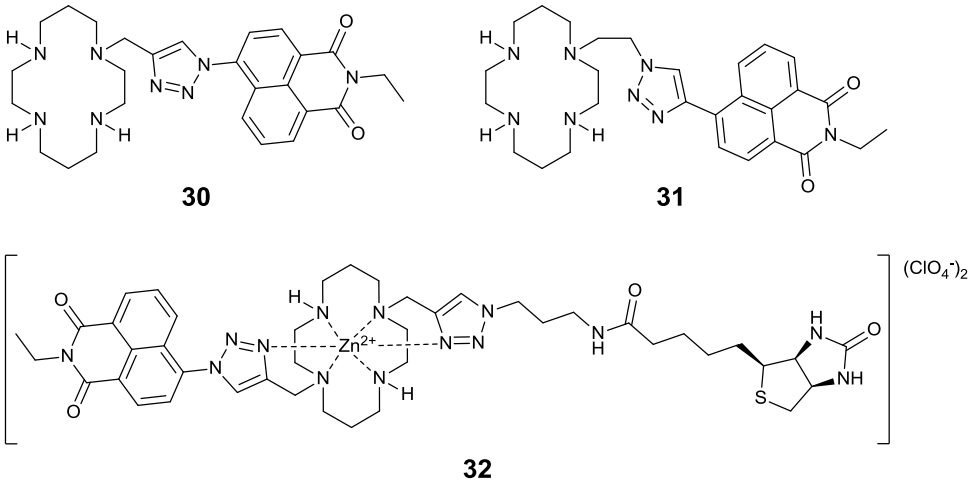

Figure 1-20 Triazole containing probes **30** and **31** studied by Todd *et al.* for their differing photophysical response to Zn^{2+}, and their biotinylated complex **32** for binding studies with avidin.

The Todd group have synthesised many triazole-ligand scaffolds with a fluorescent reporter for zinc sensing in aqueous media. The probes **30** (originally synthesised in 2009[72]) and **31** are identical apart from a reversed orientation of the triazole.[73,74] The study of both PET based sensors concluded that they are selective for zinc with a 7-fold and 5 fold CHEF effect observed respectively. Probe **31** was found to be a brighter probe, and differential pulse voltammetry was used to elucidate a reason for the reduced efficiency of PET quenching upon binding of zinc to this sensor. Noting the photophysical properties of these probes

were not optimal due to their UV-emission, the group attempted to incorporate a piperidinyl group to alter the excitation/emission wavelengths and extend the fluorescence lifetime of the probe, and whilst this was successful, the probes lost their selectivity for zinc, demonstrating the often unpredictable nature of designing zinc sensors.[75]

Complex **32** was also synthesised and was noted as the first fluorescent biotinylated metal complex. The zinc complex was used to monitor binding of biotin to avidin, as a more sensitive alternative to EPR methods previously used to study this interaction.[76]

There are many examples of calixarenes furnished with other groups via CuAAC reactions to function as zinc sensors, such as **33** (Figure 1-21).[77] Similar triazole-appended calixarenes have been used as PET sensors and excimer/monomer emission sensors for selective recognition of zinc,[78] and these fluorescent zinc complexes have been used for sensing pyrophosphate and display reversible logic-gate properties.[79]

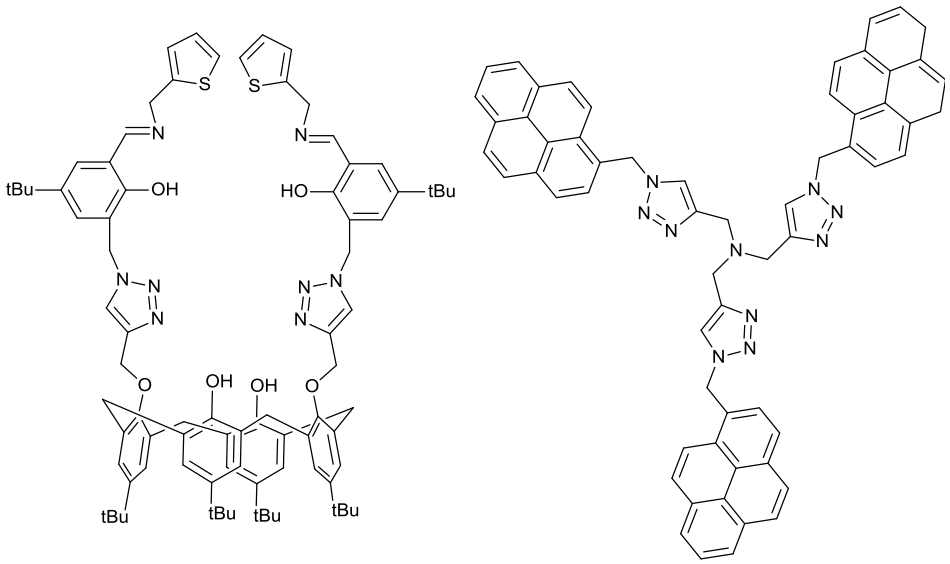

33 **34**

Figure 1-21 Calixarene probe **33** and tris-triazole pyrene probe **34**

Sensor **34** is also of note as a triazole-furnished sensor, as the pyrene units 'clicked' to the tripropargylamine core strongly encourage excimer formation and stacking of the units. [80] Upon binding of zinc, the group observe breakdown of the excimer and an increase in the emission band of the monomer, making it ratiometric.

Peptide based sensor **35** synthesised by Datta *et al.* shows 2:1 sensor:Zn^{2+} binding, excellent selectivity and some reversibility, with an ON-OFF phenomenon observed with alternative additions of $Zn(ClO_4)_2$ and $HClO_4$.[81] These properties indicate its potential use as an optical tool/switch.

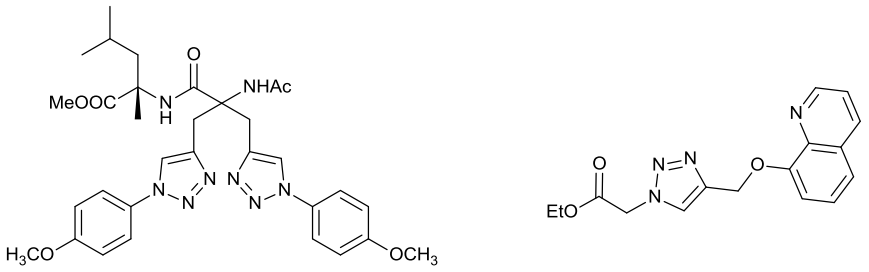

35 **36**

Figure 1-22 Peptide based Zn^{2+} probe **35** and quinoline appended 'click' probe **36**

Triazole containing sensor **36,** with a hydroquinoline chromophore, was synthesised in 2 steps using CuAAC.[82] In an aqueous environment the probe acts as a 'turn-on' CHEF sensor with a 10 fold increase in fluorescence upon binding together with a marked blue shift in the emission of 62 nm. In MeCN, the sensor demonstrates a ratiometric response to zinc, which the authors attributed to a lack of photoinduced proton transfer in the aprotic solvent.

Combined with the selectivity of the molecules for zinc over other transition metals, these are all excellent examples of simple CuAAC reactions successfully building bright functional molecules. As outlined previously the simple, rapid and high yielding nature of the CuAAC, combined with the wealth of reaction conditions available, can provide groups with a

simple method to construct novel potential sensors using this versatile reaction in a facile manner.

1.10. One-pot Multicomponent CuAAC Reactions

1.10.1. Introduction to Iterative 'Click' Chemistry

In our efforts towards the synthesis of an 'ideal sensor', we turned to the wealth of literature available regarding multicomponent coupling reactions, and in particular those utilising the copper-catalysed azide-alkyne cycloaddition (CuAAC).

Molecules with multiple triazoles can be synthesised in a stepwise manner, but this can decrease the efficiency of the reaction through the extra manipulations required for working up reactions and purification techniques. However, there are many excellent examples of the synthesis of complex molecules containing triazole moieties in a one-pot fashion. They benefit from using simple pre-functionalised units, high atom economy, huge savings in waste and purification costs, control of the final product outcome (i.e., the ability to avoid unwanted oligomerisation) and excellent yields.

Examples from the literature can be grouped by their synthetic strategy used into four distinct areas;

a) Using a CuAAC reaction in combination with another alternative coupling to build a molecule,

b) The use of 'masked' azides, introduced at a later stage via a chemical transformation,

c) The use of alkynes with and without protecting groups (commonly silyl-based), and

d) Control via reactivity, with no protecting groups involved.

These types of reactions are commonly used in peptidomimetic strategies, other large biomolecule mimics such as DNA analogues, and to synthesise bi-aryl ligand scaffolds for large supramolecular structures like cages and rotaxanes.

1.10.2. Using a CuAAC/Alternative Coupling Combination [83]

The high chemoselectivity of an azide and alkyne in the CuAAC reaction often means it can be used in tandem with other reactions in a synthetic route, as many other functional groups, with or without protecting groups, are tolerated under the reaction conditions. This is particularly common in peptide synthesis, where a triazole unit is commonly used as a bioisostere of an amide bond. The dimensions of a triazole are somewhat similar to that of an amide bond (Figure 1-23), and it is of note that the triazole moiety is known to be biocompatible and has been incorporated into small molecule drug candidates.[84]

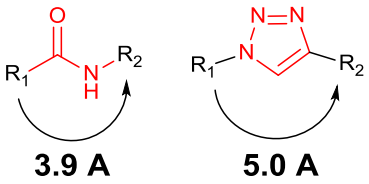

Figure 1-23 Demonstrating the use of a triazole as a bioisostere of an amide bond.

A particularly elegant example of a one-pot Ugi/CuAAC reaction was demonstrated by Cai and co-workers, to synthesise triazole-containing amino acid derivatives and peptidomimetic fragments.[85] The group employed a classical 4-component Ugi reaction in MeOH to readily furnish two bis-amides **37** and **38** with an azide and alkyne respectively, and then carried out the CuAAC reaction using copper(II) acetate, sodium ascorbate and NEt_3 in the same pot to construct the peptidomimetic **39**. (Scheme 1-3)

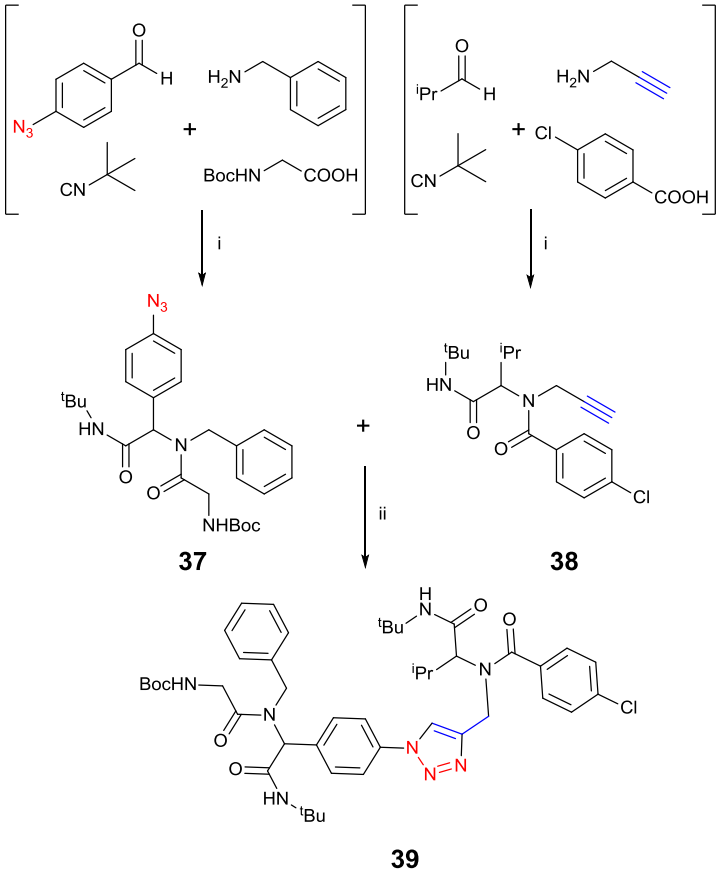

Scheme 1-3 One pot tandem Ugi/CuAAC reaction to construct peptidomimetics as reported by Niu and co-workers. Conditions: i) MeOH, rt. , ii) $Cu(OAc)_2$, Na. ascorbate, NEt_3, r.t.

CuAAC reactions are also commonly employed alongside palladium-based cross-coupling reactions, as the conditions can be complementary and, if the substrates are added in the correct sequence, can synthesise the desired product efficiently in high yields. Often used in the synthesis of bi-aryl and other cyclic and aromatic small molecule drug candidates or biologically active molecules, a common synthetic route incorporates the CuAAC first, followed by a cross coupling reaction on the combined molecule. Many examples of this have been noted in the review by Sokolova and Nenajdenko, but there are some notable examples in which the CuAAC has been utilised as the final step of the synthetic route.[83]

An efficient one-pot Sonogashira-CuAAC reaction was reported by both Novak *et al.* in 2009,[86] carried out under ambient temperature and pressure, and by Friscout and Boons in 2010 in a microwave-assisted reaction.[87]

The reaction typically follows the sequence in Scheme 1-4, with some variation. In the conditions by Novak *et al.*, the CuI employed for the Sonogashira reaction was also utilised for the CuAAC, which occurs concurrently with the slow addition of a solution of TBAF to deprotect the TMS-alkyne. The authors state that no particular care was taken to ensure air was excluded from the reaction, and that the slow addition of TBAF was to avoid the homocoupling of the deprotected alkyne moieties under their conditions. The yields are still only good to moderate (53-77%), and particularly low in the case of 4-nitro phenyliodide as the starting material, and also with bulky adamantyl azide as the CuAAC partner.

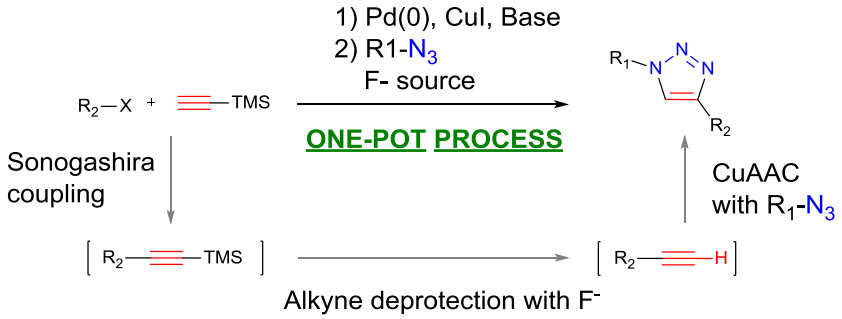

Scheme 1-4 A general one pot Sonogashira-CuAAC reaction to install and alkyne and perform a CuAAC to synthesise triazoles, as exemplified by Novak *et al.*

Nevertheless, this was advanced to a microwave assisted version by Friscourt and Boons, with high yielding results within the scope of substrates they examined. The group also observed low yields using a 4-nitro phenyl-halide starting material, but higher catalyst loadings and longer reaction time for the Sonogashira coupling vastly improved the final yield of the 'click' product from 11% to 53%, suggesting that electron-withdrawing moieties require longer reaction times.

This methodology has been put into practice for the synthesis of complex molecules, such as *N*-heterocyclic kinase inhibitors,[88] and also in the synthesis of some fused heterocycles of biological interest, also including the use of acetylene gas as the alkyne component.[89] In

2012 Kim *et al.* suggested the TMS protected alkyne intermediates produced in the previous one-pot reactions mentioned were unstable intermediates, and proposed that the use of TIPS-protected alkynes was bulky enough to provide extra stability, leading to higher yields of triazole-containing products.[90]

1.10.3. The Use of 'Masked' Azides, Introduced at a Later Stage *via* a Chemical Transformation

One of the drawbacks of the one-pot Sonogashira-CuAAC reaction, especially with some smaller substrates, involves the synthesis, isolation and handling of organic azides.[91] This is because some azide-containing substrates, particularly those that are polyvalent or of a low molecular weight, can be very unstable, difficult to handle and unsafe to work with due to their potentially explosive nature. In the last ten years a large number of papers report the synthesis of these organic azides *in-situ* before the addition of an alkyne-containing substrate to perform the CuAAC in a two-step one-pot fashion.

The first important example of this was demonstrated by Fokin *et al.* in 2006, in which triazole-containing structures were prepared from alkyl, aryl and vinyl halides, sodium azide and a chosen acetylene partner under classical CuAAC conditions with $CuSO_4$ and a reductant.[92] The reaction conditions were relatively mild and simple, and in most cases the final product was simply isolated by filtration in very high yields, including some structures with multiple triazole moieties (**40–42**, Scheme 1-5). The utility of this procedure was further extended by the group's report of a microwave assisted three component 'click' reaction, using slightly modified conditions to those previously employed (*vide supra*) but still with excellent yields.[93] The procedure was used to synthesise a conjugated variant of TBTA, a common ligand used in the CuAAC reaction to stabilise Cu(I) species.[94]

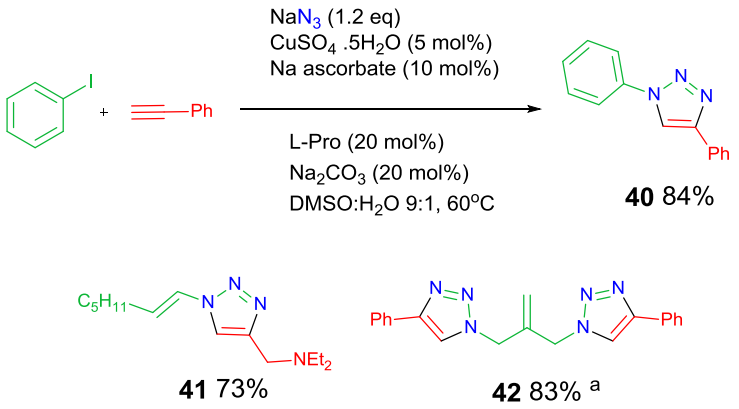

Scheme 1-5 Standard conditions for *in-situ* generation of azides for direct CuAAC reactions in one pot, as exemplified by triazole **40**, and other examples **41** and **42**. (a) uses alkyl chloride as the halide component.

Many other reports have appeared using this type of halide substitution method for forming azides,[95–97] and this was used to great effect by the Crowley group in a simple, modular and high yielding method to generate functionalised ligand scaffolds. Circumventing the isolation of potentially dangerous low molecular weight organic azides, the group obtained alkyl, benzyl and aryl substituted pyridyl-1,2,3-triazole ligands from the one-pot, three-component reaction in high yields, and in some cases in higher yields than from the corresponding isolated azide. A typical example (Scheme 1-6) demonstrates the mild reaction conditions employed and typical yields obtained, i.e., for compound **45**, 92%. The ligands were used for complexation with silver and copper salts.[98] They also synthesised some novel polydentate triazole ligands in the same manner with a view to their use in large metallosupramolecular structures.[99]

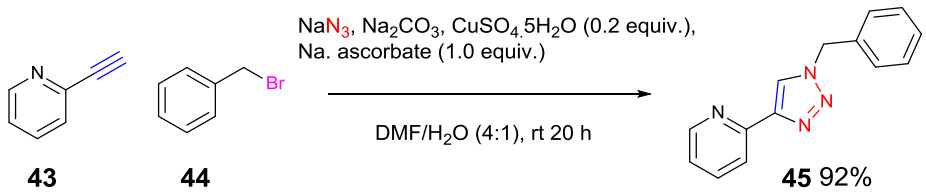

Scheme 1-6 A typical one pot procedure followed by Crowley *et al.* for a multicomponent CuAAC reaction.

Many other reports have appeared with a view to making this process 'green' as well as safe, and discuss the use of recyclable catalysts, ionic liquids, ball-milling procedures, and using water as the reaction solvent.[100–106]

Boronic acids are also synthetically useful in the context of forming these types of low molecular weight azides. After noting that other nitrogen containing nucleophiles have been able to substitute boronic acids, Guo and co-workers used inorganic NaN_3 to substitute aryl and vinyl boronic acids with an azide moiety, and demonstrated the reaction's efficacy in a one-pot reaction to synthesise the corresponding 'click'-products in moderate to high yields (Scheme 1-7).[107] They state this method to be better than using aryl and vinyl halides as the conditions are mild and a higher substrate tolerance was observed, but since this publication appeared, methodology for these halide substitutions has been optimised and vastly improved, as shown in the many examples previously discussed.

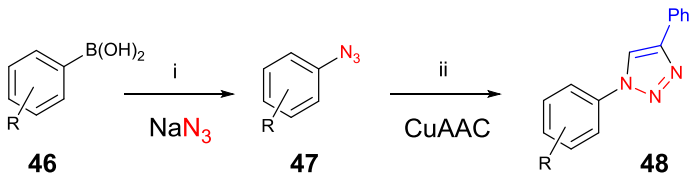

Scheme 1-7 One pot substitution-CuAAC reaction to generate aromatic triazole products **48** from boronic acid precursors **46**. Conditions: i) $CuSO_4$ (10 mol%), MeOH, rt., ii) PhCCH, rt..

This methodology was used in a one-pot, iterative CuAAC reaction on ferrocene boronic acid with a protected acetylene group installed, as the corresponding azide compound was found to be unstable when isolated. The group synthesised a double-triazole functionalised ferrocene compound in moderate yields, and demonstrated the efficiency of the one-pot route over the stepwise synthesis.[108]

The direct transformation of alcohols to azides, without the prior need to convert the alcohol into a leaving group first, is another strategy implemented into a one-pot scheme for synthesising triazoles. Most of the work in this area has been carried out by the Sreedhar group from India. They first reported a multicomponent coupling of secondary alcohols, trimethylsilyl-azide (TMS-N_3) and alkynes in the presence of copper to furnish 1,4-substituted triazoles in excellent isolated yields, including alkyne coupling partners with heterocycles such as pyridine.[109] TMS-N_3 is necessary as the azide nucleophile, as sodium azide (NaN_3) gave no reaction, and while common solvents such as DMSO and MeCN gave moderate yields, nitromethane gave the highest yields. This is a drawback as it is not generally regarded as a conventional solvent. The group also developed a method to convert homoallylic secondary alcohols in a similar manner, but with the addition of $PdCl_2$ to help avoid any sigmatropic rearrangement of the allylic azide formed.[110] This not only gave access to challenging allylic azides, but also their CuAAC products in one pot in good yields, this time in a simple solvent mixture of $CHCl_3/H_2O$.

One of the most common routes to azides, after halide substitution, is a simple diazotransfer method to transform an amine into an azide. In 1991, Eaton *et al*. first reported the use of trifluoromethylsufonyl azide, or TfN_3, in the preparation of azahomocubanes.[111] They reacted a cubyl amine with this reagent in the presence of triethylamine to produce cubyl azide precursors in high yields (74-85%). Azides also originally found their use as amine protecting groups,[112] and in 1996 Wong and co-workers reported a useful metal-catalysed method of preparing azides from amines using TfN_3, and demonstrated a diazotransfer on many representative amine-functionalised sugars such as **49** in a process they deemed to be mild and scaleable (Scheme 1-8).[113]

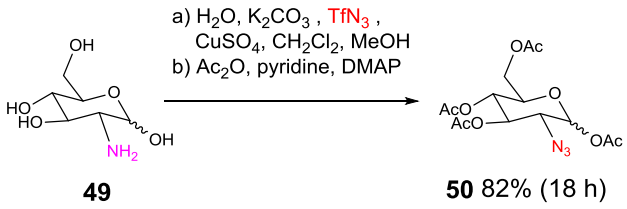

49 **50** 82% (18 h)

Scheme 1-8 Typical diazotransfer reaction to protect amines using TfN_3, as reported by Wong *et al.*

This procedure has found many applications for one-pot synthetic routes,[114–116] notably with Arora and co-workers who combined this diazotransfer with a CuAAC to develop a one-pot multicomponent procedure to synthesise triazole-containing biomimetic oligomers (replacing the amide bond).[117,118] The iterative sequence recycles the copper source used as a Lewis acid to perform the cycloadditions, and results in high yields both in solution and solid state syntheses of oligomers containing up to four triazoles.

A particularly important point to highlight at this stage is the great dangers and drawbacks that these procedures could potentially create in the laboratory. Aside from Tf_2O being an expensive starting material, limiting its use in scale-up, TfN_3 is a huge detonation hazard. It is often made in solutions of $CHCl_3$ or CH_2Cl_2, but the volatility of these solvents could prove to be dangerous upon storage as dry TfN_3 is highly explosive.[119] Moreover, these azide sources in chlorinated solvents could generate the very explosive azido-chloromethane or diazido-methane. Using these reagents in safer conditions, making fresh reagents each time without storing them and not isolating any intermediate until the final stage of the reaction makes TfN_3 easier to manipulate and handle, hence the utility of the one-pot pseudo-peptide scheme from Arora *et al*..

This was further demonstrated by a one-pot multicomponent reaction reported by Wittman and Beckmann in 2007, using these reaction conditions to perform a diazotransfer-CuAAC iterative sequence which was not limited to amino acid residues (Scheme 1-9).[120] They demonstrated short reaction times using a microwave reactor. No

reaction intermediates were isolated, and a freshly prepared solution of TfN_3 in dichloromethane was made before each reaction. They also investigated the reaction in toluene instead of CH_2Cl_2 due to the potential hazard it presents, and whilst the yield of the final triazole product **52** drops from 94% to 77%, it is still a moderate result that could be utilised in scale-up procedures. Even so, each solution of TfN_3, however freshly and carefully made, does not have the same concentration due to variable reaction yields, and as a consequence the reactions always require a significant excess of the reagent to be used. Combined with its poor shelf life and huge safety concerns, this does not make TfN_3 an ideal candidate for a simple iterative CuAAC in the laboratory on any scale.

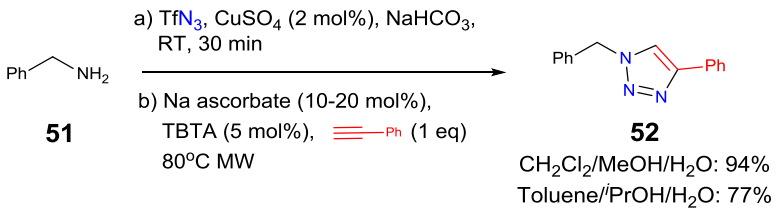

Scheme 1-9 One pot diazotransfer-CuAAC reaction using TfN_3 reported by Wittman and Beckmann.

Alternative conditions have been investigated for diazotransfer reactions of this nature.[121,122] TMS-N_3 is regarded as a 'safer' reagent as there are no inherent explosive properties associated with it. However it is very sensitive to moisture and oxidising agents, where it will decompose to hydrogen azide, and so must be stored in a dry moisture-free atmosphere.[123] TMS-N_3 (and ^{t}BuONO) was the diazotransfer reagent of choice for Moses *et al*. in their development of a one-pot procedure, in a simple and atom-efficient multicomponent reaction to give triazole containing aromatic compounds in high yields.[124] However, they only investigated the transformation of simple substituted anilines, and did not demonstrate any scope in the acetylene coupling partner used in the one-pot procedure either, limiting the utility of their study.

An important advancement in the development of safe and easy to handle diazotransfer reagents came with the characterisation and use of imidazole-1-sulfonyl azide **54**. Imidazole-1-sulfonates demonstrate a similar reactivity to trifluoromethanesulfonates, but this has the added benefits of being more stable and less expensive. Goddard-Borger and Stick reported imidazole-1-sulfonyl azide to have analogous behaviour to TfN_3 in synthesising azide containing compounds.[125] The HCl salt was crystalline, did not require purification and could be stored safely, with no detonation occurring upon severe impact testing and high temperatures. It furnished a wide range of azide-containing alkyl, aromatic, amino acid and carbohydrate compounds from their corresponding amines in high yields under mild conditions. This reagent was utilised in an interesting example of a one-pot three step synthesis of triazole containing compounds from aldehydes and amines, in which the final 'click'-products were isolated in moderate to high yields (Scheme 1-10).[126,127]

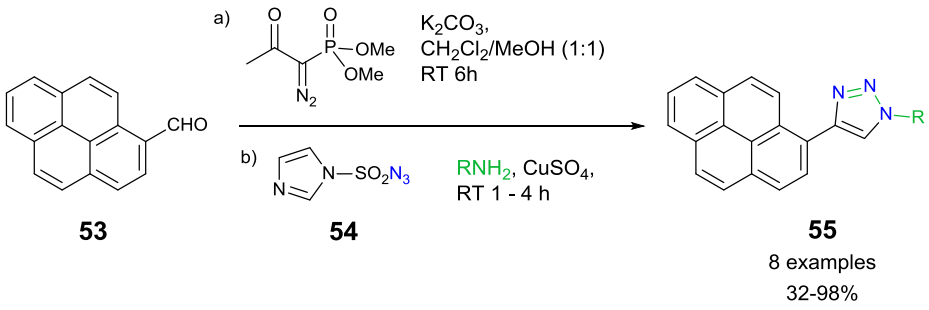

Scheme 1-10 *In situ* generation of both azide and alkyne coupling partners from an aldehyde **53** and and amine, and subsequent CuAAC to synthesise pyrene furnished triazoles.

This is the first noted instance of both CuAAC coupling partners being generated *in situ* in the same reaction, and whilst the yields are not always exceptional, the group demonstrate scope of the chemistry with a good range of amine substrates (although a smaller set of aldehyde substrates was investigated) and extend the methodology to the synthesis of triazole linked sugars, demonstrating its potential utility in oligosaccharide synthesis.

1.10.4. The Use of Alkynes With and Without Protecting Groups

Other reported one-pot CuAAC reactions have focused on developing a reaction using protected alkyne precursors straight into the reaction mixture. This avoids the extra steps of deprotection and isolation of any alkyne 'click' partners before the CuAAC reaction. This is particularly useful when, for example, one is using low molecular weight acetylenes to make small triazole containing products, or to conveniently allow control over reactivity when the compound contains more than one alkyne unit.

An important study towards this methodology was reported in 2006, where Leigh and Aucagne demonstrated a methodology for a 'click-click' reaction of three components in one pot.[128] The group took advantage of orthogonal reaction conditions and utilised molecules containing both TMS-protected and free acetylenes, 'clicking' one and then deprotecting *in situ* to release the second acetylene for CuAAC ligation, under mild conditions (Scheme 1-11).

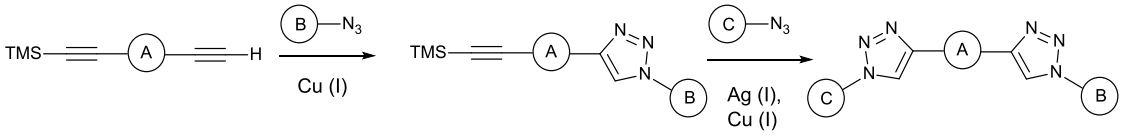

Scheme 1-11 Schematic of the one pot 'click-click' reaction methodology developed by Leigh and Aucagne.

The group found that during initial optimisations, $Cu(MeCN)_4PF_6$ was compatible alongside $AgBF_4$ for the orthogonal reactions. Upon applying these conditions to peptides, the solvent system of $^tBuOH/H_2O$ required the use of more classical CuAAC conditions using $CuSO_4$ and sodium ascorbate to generate Cu(I) *in-situ*. The reaction was very sluggish, and trying to solve this with higher catalytic loadings, and the use of heat/microwave conditions encouraged Cu(I) promoted desilylation. Gentle warming of the reaction proved to be a successful compromise.

However, many groups, noting the instability of TMS, moved to the alternative triisopropylsilyl (TIPS) protecting group. This gave greater control and stability, and yet was still compatible with their CuAAC conditions.[129,130] This, combined with the report from Gramlich and co-workers, on their combined use of TIPS and TMS to synthesise oligonucleotides,[131] prompted Aucagne and co-workers to investigate alternatives to TMS as alkyne protecting groups, and to develop a more robust methodology for successive iterative cycloadditions.[132] The group settled on a combination of TES and TIPS, with their orthogonal deprotection conditions, and demonstrated three iterative 'clicks' on a single molecule.

Despite being the most common alkyne protecting group, alternatives strategies to silyl protecting groups have also appeared. In 2011 two groups reported the one pot synthesis of triazoles using both aryl halides and protected alkynes, generating the azide *in situ* and the tandem CuAAC/deprotection of the respective protecting groups. Zysman-Colman *et al.* utilised the classic TMS protected alkynes and obtained moderate yields, and, in some cases, also observed the formation of an undesired 1,5-triazole product,[133] [2] while interestingly Kolarovic *et al.* reported the first use of alkynoic acids to deliver acetylene groups for CuAAC, with the aim to circumvent the use of low molecular weight alkynes, which are sometimes desirable for producing terminal triazole moieties.[134] The CuAAC proceeds alongside the transformation of the aryl iodide to the azide, under classical CuAAC conditions of Cu(II) with a reductant, and *in-situ* decarboxylation of the protecting group on the alkyne leaves the triazole product **56** (Scheme 1-12). This decarboxylation is presumed to be copper-catalysed,[135] and this one-pot process furnished very high yields of products with a range of azides and alkynoic acids. Li and Flood also reported the use of

[2] Other groups have also reported similar reactions of note. [212–214]

butyn-2-ol as an alternative protecting group cleaved readily under strong basic conditions, to allow sequential 'click' reactions in the synthesis of triazolophanes.[136]

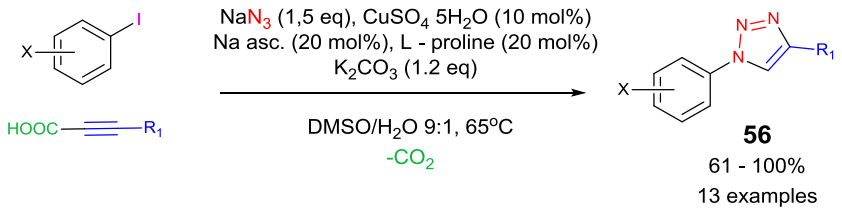

Scheme 1-12 One pot substitution-CuAAC-decarboxylation multicomponent sequence, as reported by Kolarovic *et al.*

Nevertheless the silver-catalysed in-situ deprotection of TMS groups in tandem with a CuAAC reaction in one pot as shown in Scheme 1-11 still proved popular due to its evident simplicity and utility, and this methodology found uses in supramolecular chemistry,[137] synthetic peptide synthesis,[138] convenient fluorescent labelling of biomolecules [139] and also in the construction of analogues of DNA.[140]

1.10.5. Control *via* Reactivity Without Protecting Groups

Perhaps the least studied method of iterative CuAAC reactions, controlling the reactivity to ensure sequential 'click' ligation of different moieties is not so popular due to its potential unpredictability and often very slow reaction times. These types of reactions however, are advantageous in that they remove the need for a protection/deprotection sequence altogether, and there are some notable examples in the literature to draw inspiration from.

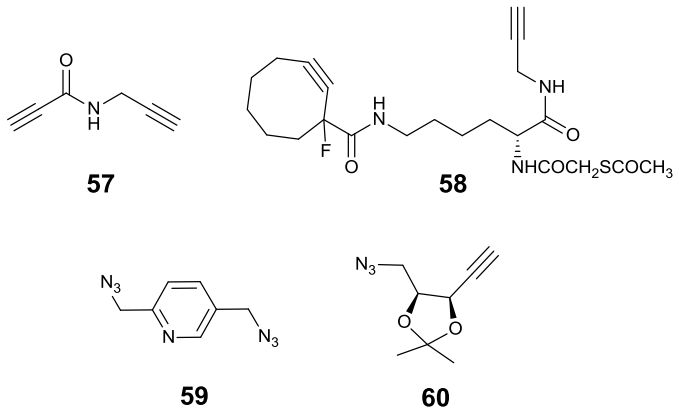

Figure 1-24 Central molecules with two 'clickable' moieties for the formation of bistriazole products without the need for protecting or 'masking' groups.

Bis-alkyne linker **57** (Figure 1-24) was synthesised by Girard *et al.* for the exact reason of circumventing protecting groups.[141] The methodology relies on the conjugated alkyne being activated by the amide group, thus making this the more reactive alkyne of the two in the molecule. After first carrying out a neat AAC on the activated alkyne with no catalyst involved (or in acetone if solvent was required), the 1,4-triazole isomer was isolated from a crude mixture of regioisomers by a simple trituration. This was carried forward to a CuAAC reaction for the second inactivated alkyne to form iterative triazoles on the same molecule with moderate and excellent yields for each cycloaddition respectively.

The drawbacks to this methodology are evident. The formation of a mixture of both isomers (in some cases intractable) during the first cycloaddition reaction does not identify this as a fully efficient iterative 'click' methodology. Furthermore, whilst exclusively affording the 1,4-regioisomer, the second copper-catalysed 'click' reaction is very slow, and in the case of many substrates it can take up to 48 h to complete. On a positive note, the catalyst used for the CuAAC was a solid-supported Cu(I) catalyst, and this provided a facile work-up at the end to afford the bis-triazole product in a simple fashion without any copper residues remaining from the reaction.

Strain-promoted azide-alkyne cycloaddition, or SPAAC, is a popular method to install triazoles in large biomolecules and other drug-like target molecules without the use of copper, avoiding metal residues. Despite copper being an essential element in the body, these catalytic residues can promote oxidative damage by the formation of reactive oxygen species, and SPAAC is now commonplace as a bioconjugation strategy in biological systems and some drug targets.[142] The ring strain, as demonstrated by the cyclooctyne moiety in **58**, allows the AAC to proceed without the need for a thermal or catalytic push.[143,144] Beal *et al.* took advantage of this when designing **58**, and demonstrated a sequential SPAAC/CuAAC on this large molecule to selectively generate one triazole after another, and synthesised a bis-triazole compound capable of binding to bovine serum albumin.[145] The group demonstrate that a range of biomolecules can be ligated to the framework, including biotin, peptides, disaccharides, and fluorescent tags. However, again the SPAAC is sluggish unless carried out at high concentrations, and synthesis of the cyclooctyne itself can be challenging and low yielding.

As well as bis-alkynes, a procedure for iterative CuAAC reactions on a bis-azide compound has recently been reported.[146] Utilising Cu(II)-chelation assisted CuAAC,[147,148] Zhu and co-workers designed various pyridine-containing bis-azides like **59**, where Cu(II) chelates to the pyridine nitrogen and its adjacent azide, selectively forming that triazole first. Only upon addition of a reductant to increase the concentration of a Cu(I) species *in-situ* does the pendant azide participate in a CuAAC, thereby giving control and selectivity when performing iterative CuAAC ligations. The group found they obtained a greater yield of the bis-triazole product in one-pot than with stepwise iterations, making this an efficient iterative CuAAC procedure. There was also very little material loss, as the intermediate mono-'click' product is not isolated. The group also demonstrated that there was no loss of

reactivity when the reaction was performed in aqueous HEPES buffer at pH 7, thus demonstrating its potential application in bioconjugation strategies.

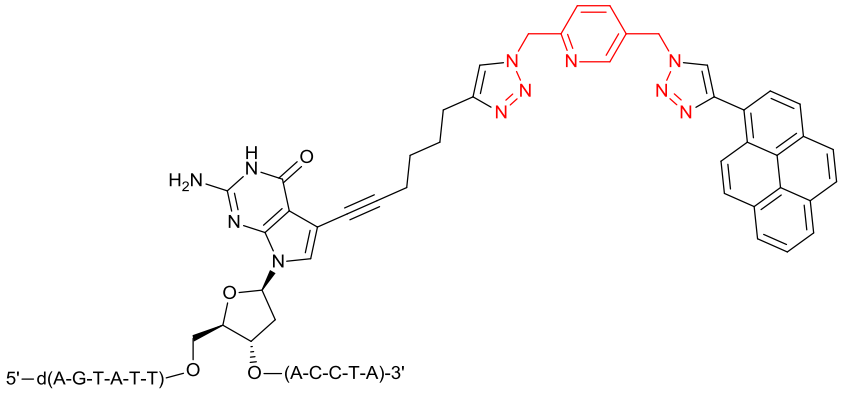

61

Figure 1-25 Pyrene tagged DNA product reported by Ingale and Seela, using bis-azide **59**

Indeed, Ingale and Seela used **59** to synthesise cross-linked and fluorescent pyrene-tagged DNA (such as **61**).[149,150] The methodology allowed them to sequentially ligate two molecules to the bis-azide core in one pot in a desired controlled manner, after many previous attempts to do so with varying success.[151–153] One serious drawback of this methodology is that the bis-azide core **59** used by both groups for their study is classed as a low-molecular weight azide, and the dangers of synthesis and handling of this compound (as previously discussed) require great care and attention. Zhu and co-workers also synthesised larger molecules whereby the pendant, non-chelating azide is attached to the pyridine by a longer alkyl linker, thereby increasing molecular weight and removing any inherent dangers associated with bis-azide manipulation.

Finally, Kaliappan *et al.* reported a unique approach to iterative CuAAC reactions with a view to linking carbohydrates through triazoles.[154] The group designed sugars with both an azide and alkyne moiety attached, as compound **60**, and successively 'clicked' first the azide, and then the alkyne moiety without oligomerisation to furnish a bis-triazole sugar

using simple building blocks such as methyl propiolate, and small phenyl and benzyl azides. However, the yields of bis-triazole obtained were very low (23-46%) due to the instability of the central building block **60** both on standing and in solution, and the group isolated the CuAAC product of the two external azide and alkyne building blocks in higher yield than the desired bis-triazole, as well as other unknown by-products from the decomposition of the sugar. This particular report highlights the need for stable building blocks, high chemoselectivity and control over reaction partners in one-pot multi-component procedures like this one to ensure high yielding successful reactions.

1.11. Concluding Remarks

This chapter highlights only a selection of the wide variety of zinc-specific probes already reported. After highlighting precise cellular localisation as one of the key objectives for the design of novel fluorescent probes for zinc, we can see a number of groups have made efforts towards this aim. The probes presented are of a wide variety of structures with a variety of cellular compartments targeted, but their challenging and low yielding synthetic route detracts from the success of the sensors themselves. Modifications to the core structure are not available in a rapid, facile manner, and this prevents further studies to develop more structurally diverse biologically targeted sensors for zinc in different biological settings.

'Click' chemistry, namely the CuAAC reaction, could readily provide a path to access these types of probes. Their utility in the synthesis of zinc-specific probes has already been realised in many examples presented here, with high yielding reactions and high molecular diversity of the 'click' components for each reaction. To maintain the ideal supramolecular structure set out for a probe we can envisage a method to incorporate sequential 'click' reactions into an existing core scaffold to append additional functionality. There are many

methods of iterative CuAAC ligation to draw experience from, and this methodology, and 'click' chemistry in general, could be utilised to aid the rapid generation of a successful library of probes.

Chapter 2: Design and Development of a Novel Iterative Double-'Click' Reaction

2.1. Introduction and Aims

Previous work by Watkinson and co-workers had utilised CuAAC chemistry towards Zn^{2+}-specific chemosensors. In 2009 the group synthesised probe **30** consisting of the metal chelating azamacrocycle, cyclam, linked to a naphthalimide fluorophore *via* a triazole linker (Scheme 2-1).[72]

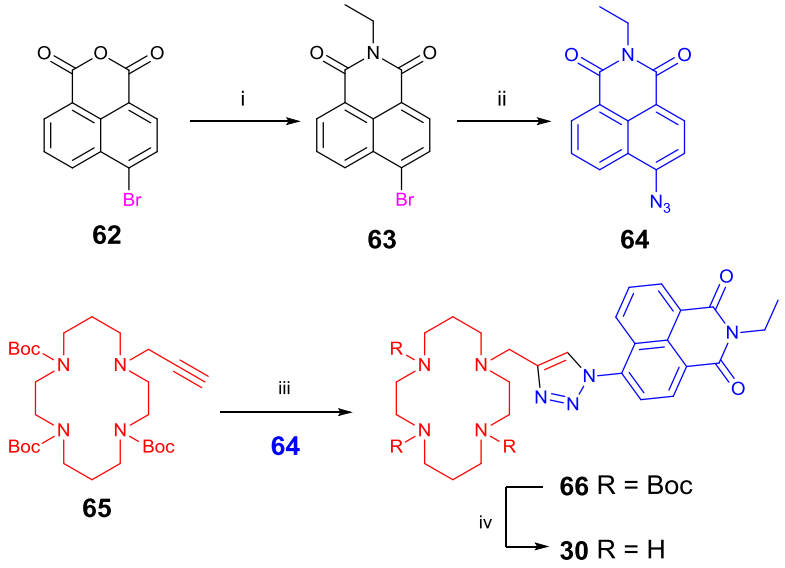

Scheme 2-1 Synthetic route to 'Clickate' probe **30**. Conditions i) Ethylamine, 1,4-dioxane, 70 °C, 82%. ii) NaN_3, NMP, rt 24 h, 50%. iii) $CuSO_4.5H_2O$, Na. ascorbate, THF/H_2O, 82%. iv) TFA/ CH_2Cl_2 (1:5), 88%.

The synthesis, as expected for 'click' chemistry, was simple and high-yielding, and the sensor showed 1:1 binding of the zinc ion to the sensor with a desirable 'switch-on' fluorescent response (6 fold increase), and also demonstrated an effective response over a broad pH range (pH 4-10). The probe also showed excellent selectivity for Zn^{2+} over all other first row transition metals. Probe **30** was also tested *in vivo* in murine thymocyte cells, and appeared to detect cellular levels of zinc in apoptotic cells without the addition of extracellular zinc. This work was a particularly novel modular approach to the design of a

sensor molecule and is one of the first instances reported where a triazole acts as an extra metal ligand on a probe of this type.

The simple modular nature of the 'click' synthesis of probe **30** allowed the group to investigate an alternative yet similar ligand and investigate its effects on the efficacy of the sensor. Based on work by Kimura *et al.*,[155] the group incorporated an alternative azamacrocyclic ligand, cyclen, to synthesise probe **68** in similarly high yields to **30**.[156] It also demonstrated a significant (approx. 5-fold) increase in fluorescence in response to zinc, across the same pH range, and displayed a broadly similar selectivity profile to probe **30**, with a difference in fluorescence response to Cd^{2+}.

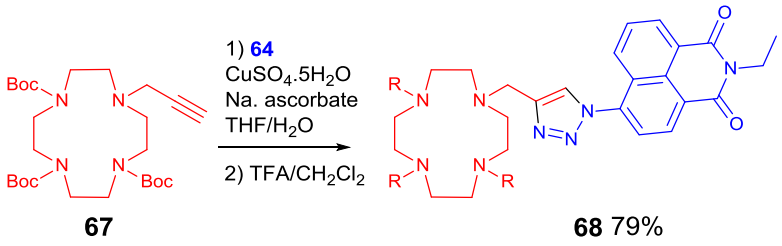

Scheme 2-2 Synthesis of cyclen 'clickate' analogue **68** [156]

Both probes demonstrated efficacy in imaging in live organisms *in vivo*, as shown in Figure 2-1. *In vivo* results in zebrafish showed localisation of the probes in the intestine, biliary system and the eye, suggesting potential application of these small molecule sensors as organ-level imaging agents for zinc in zebrafish models.

This study clearly demonstrated how the simple modular construction of the sensor allowed the ready investigation of different novel zinc-selective probes. It showed how a small structural change to the ligand induced slight changes in metal binding behaviour and metal detection, whilst maintaining the overall efficacy as a zinc-selective probe.

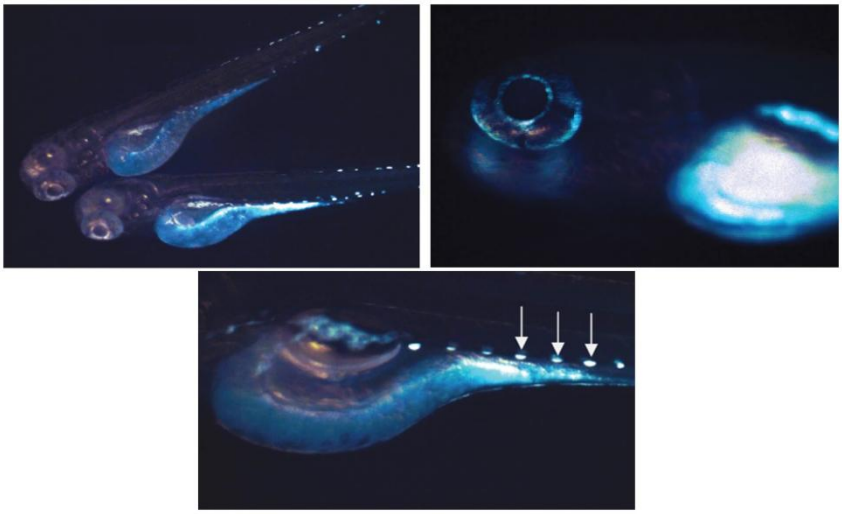

Figure 2-1 Fluorescence microscopy images of *Danio rerio* (zebrafish) embryos incubated with sensors 21 and 22. [156] These images indicate the probes localise in the eye and gut region of the embryo. Arrows indicate iridophores in the embryo, these are not illuminated due to the probe.

We felt all the properties of probe **30** and **68** were promising, despite the UV-excitation and emission wavelength (λ_{em} **30** = 407nm, **68** = 420nm), and so we envisaged the next step was to develop this system further, as a targeted probe *in vivo* to aid the study of chelatable pools of zinc in a specific organ or at cellular organelles. We anticipated the sensor itself could be conjugated to a biomolecule marker that is known to bind to specific sites *in cellulo,* as demonstrated by many of the small molecule probes discussed in Chapter 1, thereby targeting the sensor to specific cellular locations. We planned to extend the synthetically simple, modular design of the previously synthesised fluorescent probes to create a library of easily tailored, targeted probes to overcome the complexities of existing targeted sensors that require challenging synthetic protocols for their preparation.

This chapter will discuss in detail the design and optimisation of the synthetic route developed towards a number of novel sensors, drawing inspiration from literature precedent of sequential iterative CuAAC ligations in one-pot. It will describe the eventual success of utilising a simple *in-situ* azide formation to synthesise a range of three unit, bis-triazole constructs with model substrates.

2.2. Synthetic Strategy and Target Molecules

There was potential for different ligation strategies to be applied to the 'clickate' sensor **30**. The naphthalimide based fluorophore has a viable point of conjugation, at the nitrogen atom at the imide position of the molecule, as well as a facile means of adding alternative metal binding units *via* 'click' chemistry (as shown with probe **68**) to alter the binding capabilities of the probe (Figure 2-2). This would make the fluorophore component the core of these new probes.

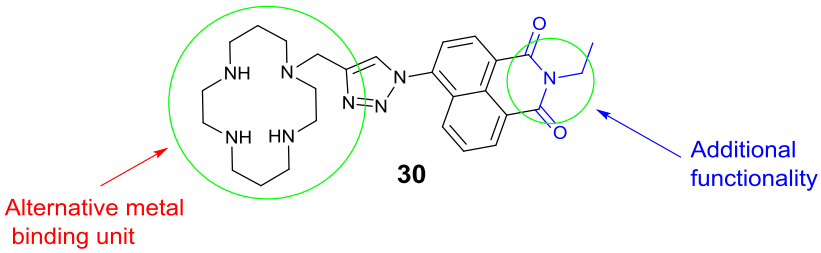

Figure 2-2 Potential points of modification highlighted on 'Clickate' probe 21

We aimed to design a modular synthesis based on a central building block of a naphthalimide fluorophore, with various 'clickable' units of ligand and biological targeting group. Many of the targeted small molecule probes reported in the literature are limited by their challenging and low yielding syntheses, and this is even more evident for recombinant probes and those probes that utilise peptides. Whilst they are efficient and demonstrate excellent behaviour for imaging purposes, their use is limited by the expensive and difficult requirements for synthesis and purification, the need to tag the probes with large peptide chains, or the transgenic approaches required for gene delivery. As well as the numerous benefits previously described of one-pot multicomponent reactions, our main focus was to use it to provide a facile synthesis of a multicomponent molecule. We aimed to overcome all of these complexities with pre-functionalised building blocks, to allow tailored design and production of a successful targeted small molecule fluorescent probe capable of

detecting biological zinc. Triazoles themselves are specifically noted for their biocompatibility and inertness to metabolic conditions,[157] making them an ideal conjugation approach for our desired purpose. A basic representation of our initial design of the possible 'click' pairs is shown in Figure 2-3.

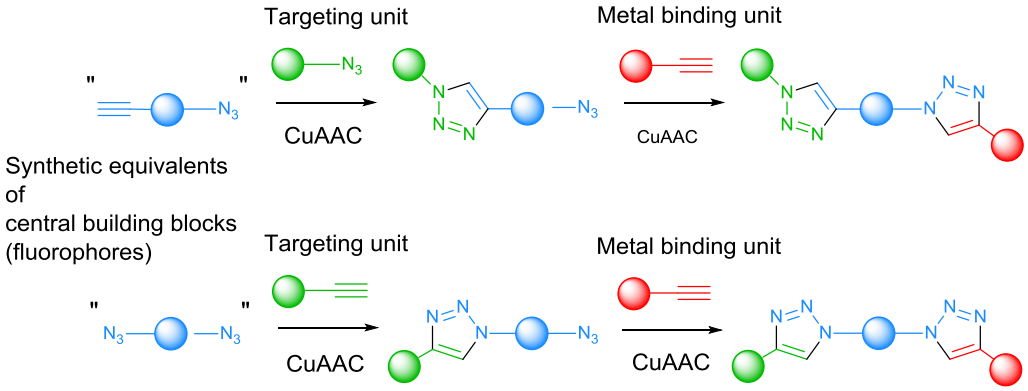

Figure 2-3 Schematic to demonstrate proposed synthetic routes to novel bis-triazole constructs using a clickable fluorescent central building block (in blue)

Targeting groups and ligands can be readily functionalised with either an azide or alkyne group, which 'clicks' to a central building block chosen to match with the appropriate click partners, using synthetic equivalents of molecules with two 'clickable' moieties to synthesise novel three-unit constructs. It is important to note that only one loading of catalyst was envisioned, as both CuAAC steps could utilise the same catalyst, reducing reaction costs even further, removing purification steps and also reducing metal waste.

2.3. Results and Discussion

2.3.1. Design and Synthesis of Central Building Blocks

The key to a successful synthetic route using these synthons was to retain control over the CuAAC taking place at any one time. The bromide in the 4-position of the naphthalimide was presented as a potential functional group to act as a masked 'clickable' functional group.[158,159] By starting from the commercially available anhydride **62**, this would allow

facile installation of one 'click' component upon formation of the imide, with the bromide subsequently transformed at a later stage to allow the sequential iterative clicks to take place.

We took inspiration from the reports previously described on the *in-situ* substitution of halides to azides with a subsequent and one-pot CuAAC, particularly the work of *Crowley et al*. (Scheme 1-6)[98,99] Unlike this method, the nucleophilic displacement of the bromide to the azide in the case of our naphthalimide core is catalyst free. The synthesis of the new central building blocks **69** and **70** (Figure 2-4) would hopefully allow us to perform a CuAAC at one end of the naphthalimide, to install a potential targeting group first, and then transform the bromide and 'click' a ligand at the other end without isolating any (potentially unstable) reaction intermediates, and maintaining the ability to control the iterative CuAAC reactions in constructing our three component molecule as desired in a high yield.

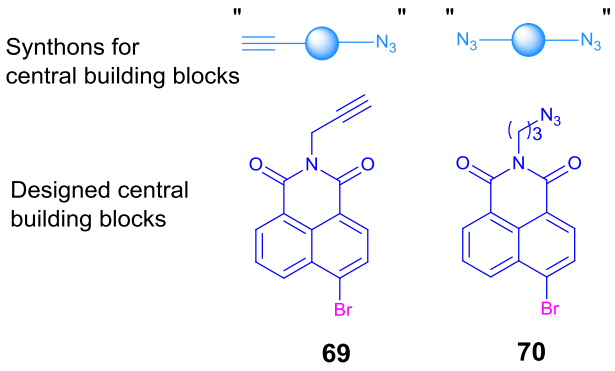

Figure 2-4 Synthetic targets for new central building blocks **69** and **70** (derived from commercially available naphthalic anhydride **62**)

The synthesis of central building block **69** was a simple and readily scaleable one-step condensation between the anhydride **62** and propargylamine in 1,4-dioxane that is very high yielding at 96% (Scheme 2-3).

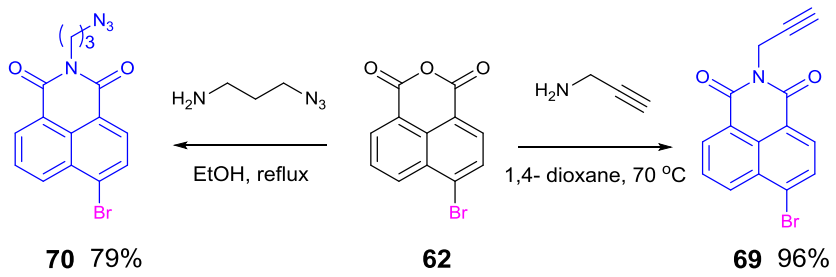

70 79% **62** **69** 96%

Scheme 2-3 One step syntheses of central building blocks **69** and **70**

Li and co-workers reported the installation of an azide at the anhydride position of the fluorophore in a similar manner to the installation of the alkyne in **69**. The group incorporated 3-azido-propan-1-amine into naphthalenediimide structures to create a 'clickable' unit (in this instance for the formation of [2] and [3]catenanes).[160,161] This led us to the design of central building block **70**, which we hoped would allow the sequential ligation of two different alkyne functionalised groups. We were able to synthesise the desired building block in high yield on a gram scale (Scheme 2-3).

The cyclam and cyclen ligands from 'clickate' probes **30** and **68**, and many other known zinc-binding ligands in the literature,[22,72,156,162,163] are most commonly functionalised with an alkyne. The design of both fluorophores meant that the second CuAAC ligation for the metal binding unit would readily be able to incorporate these easily accessible alkyne-functionalised compounds upon application to probe synthesis.

2.3.2. Optimisation of Synthetic Route for One-pot Synthesis

2.3.2.1. Initial Stepwise Iterations

Initial investigations were applied to the central building block **69**, using benzyl azide and phenylacetylene as model 'template' CuAAC partners for our actual desired building blocks. This allowed us to optimise the reaction using inexpensive and analytically simple substrates. First, we set out to identify each of the desired intermediates and to confirm a

stepwise synthesis of a model three unit construct (Scheme 2-4). For the first CuAAC with benzyl azide we used classical 'click' conditions of $CuSO_4$ and a reductant in a THF/H_2O mixture, as with the 'clickate' sensor **30** and its cyclen analogue. Triazole **71** was isolated after column chromatographic purification in good yield. The S_NAr reaction was performed with 1.2 equivalents of sodium azide in *N*-methyl pyrrolidinone (NMP), with moderate yield of **72** after isolation, and the final CuAAC under the same conditions with phenylacetylene gave a yield after purification of 68% for the bistriazole three unit construct **73**.

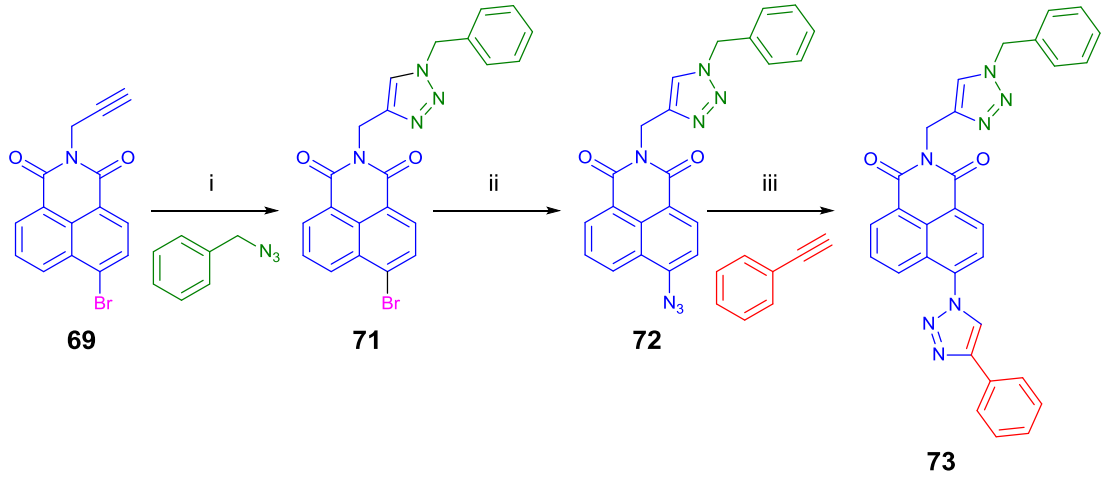

Scheme 2-4 Initial stepwise iterations to obtain each intermediate and intended final product in the one-pot synthetic route, using classical CuAAC conditions. Conditions i) $CuSO_4.5H_2O$ (10 mol%), Na. ascorbate, THF:H_2O (7:3) 16 h, 76%. ii) NaN_3, NMP, rt, 24 h, 41%. iii) as stage (i), 68%.

It was evident from the outset that the major limitation on the implementation of this synthetic route into a one-pot procedure was the choice of solvent. Polar aprotic solvents such as DMF, DMSO and NMP are the most effective for the nucleophilic aromatic substitution (S_NAr) of the aromatic bromide on the naphthalimide to the azide. This meant that for a one-pot route we were limited to the use of these solvents, thus ruling out THF/H_2O and the classical 'click' conditions used in Scheme 2-4. Due to successful precedence within the group, we elected to use NMP as our solvent of choice.

We identified a literature procedure for the use of CuI as a CuAAC catalyst in NMP, and employment of this copper source in the first CuAAC formed **71** in good yield (Scheme 2-5). With an established procedure in hand for the synthesis of the azide intermediate, we moved on to optimise the final CuAAC.

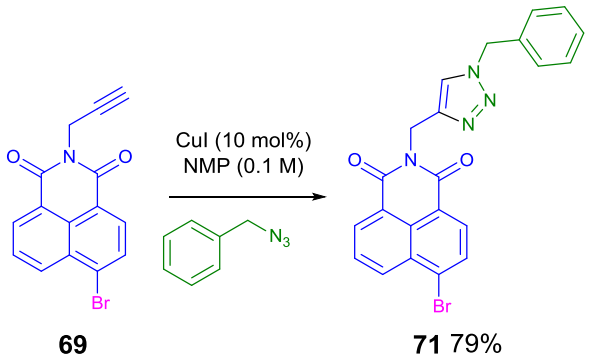

69 **71** 79%

Scheme 2-5 CuAAC reaction between **69** and benzyl azide in NMP to synthesise **71**

2.3.2.2. CuAAC Catalyst Screening

An initial test using ethyl-naphthalimide azide **64** as a model substrate for the reaction proved that the addition of CuI and phenylacetylene did not result in the desired triazole product **75** (Scheme 2-6), and it became clear a screen of copper salts was necessary to obtain conditions specific to the requirements of this reaction.

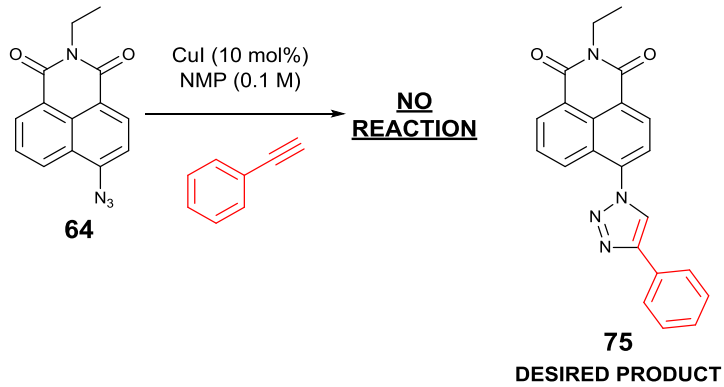

64

75
DESIRED PRODUCT

Scheme 2-6 Failed CuAAC from model substrate **64** to form triazole **75**

Entries 1 – 3 in Table 2-1 show the range of Cu(I) and (II) catalysts screened for a test CuAAC with azide **64** and phenylacetylene in NMP, including a reductant (sodium ascorbate) with the Cu(II) salts. The reactions were monitored at regular time intervals, and finally stopped at 72 h, after seeing no conversion to **75** in all cases.

Whilst **entry 1** demonstrates clearly that CuI on its own does not work in the designed system, it is commonplace to use a basic additive alongside CuI to accelerate the reaction and facilitate the CuAAC by aiding the formation of the active catalytic species in the cycle,[64,65,164–168] with each reaction displaying a particular sensitivity and specificity to base and solvent used. This literature precedent for addition of a basic additive in the presence of NMP [169,170] led us to test some commonly used bases. **Entries 4 – 6** show that all bases tested dramatically accelerated both the reaction time and increase the yield. The use of sodium acetate (NaOAc) as an inorganic base gave the highest yield at 98%, although the organic bases also displayed high yields, and so this was chosen as the basic additive. [3]

[3] It is important to note that the NaOAc base should be dried thoroughly before employment in the reaction. We found that any water present in the reaction had a marked effect on the yield of final product and we observed some formation of decomposition products by ^{1}H NMR analysis when water was present.

Table 2-1 Catalyst and additive optimisations for CuAAC from model substrate 64 to form 75

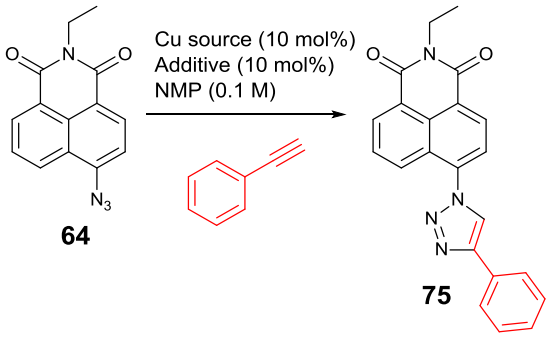

Entry	Cu source (10 mol%)	Additive	Yield %[a]
1	CuI	-	0 (72 h)
2	Cu(I)L [b]	-	0 (72 h)
3	Cu(II)L' [c]	Na. ascorbate	0 (72 h)
4	CuI	DIPEA	93 (3 h)
5	**CuI**	**NaOAc**	**98 (3 h)**
6	CuI	NEt_3	95 (3 h)

(a) NMR yield; (b) L = $PF_6(MeCN)_4$, I, Br, $(PPh_3)_3Br$, $(PPh_3)_3OAc$; (c) L' = $(ClO_4)_2.6H_2O$, $(acac)_2$, $(OTf)_2$.

We extended this model approach to optimising the one-pot S_NAr-CuAAC reaction to test the ability of these reaction conditions, and from bromide **63** we obtained triazole **75** in moderate yield of 58%, and so these conditions using CuI and NaOAc were chosen for our one-pot, double-CuAAC investigation from our intended central building blocks.

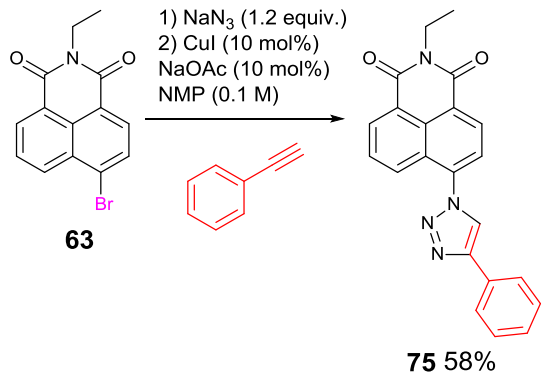

Scheme 2-7 Successful one-pot S_NAr-CuAAC sequence from bromide **63** to form **75**.

2.3.3. Stepwise Confirmation of New Conditions

Having established suitable conditions for each individual step, the synthetic route was investigated in both a stepwise manner and in one-pot using central building block **69** and the 'template' CuAAC partners benzyl azide and phenylacetylene, as previously shown in Scheme 2-4.

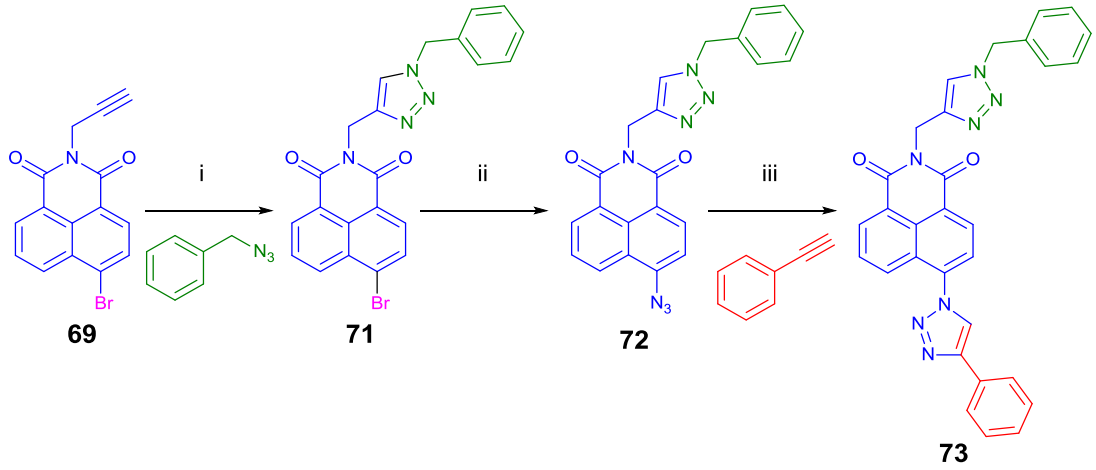

Scheme 2-8 Stepwise formation of bistriazole **73** from central building block **69** using the optimised conditions. Conditions i) CuI (10 mol%), NaOAc, NMP, rt, 1 h, 95%. ii) NaN_3, NMP, rt, 24 h, 55%. iii) as stage (i), 4 h, 80%.

It was clear that the reaction was efficient when carried out stepwise, as expected, with an overall yield of 41 % over three steps and purifications. The lowest yielding step is the S_NAr to form the azide **72**, and this was the main cause of such a low overall yield**.**

2.3.3.1. Investigations into Formation of Azide 72

After synthesising and isolating a large clean stock of bromide **71** we attempted to modify the reaction time in NMP, under the conditions developed. Heating the reactions promotes the complete conversion of bromide **71** to **72** in 4 h, but the yield of **72** formed is only 78% by ^{1}H NMR analysis of the reaction mixture. The remainder is a clear decomposition product formed *in-situ*, which was identified to be aniline **76** (Spectrum 2-1). This was consistently the major decomposition product formed throughout this study and reaction optimisation, and whilst it is only a minor contaminant, due to the very high quantum yield

of 4-amino naphthalimide derivatives in organic solvents the impurity needed to be removed, even when present in very small quanitites, which proved difficult.

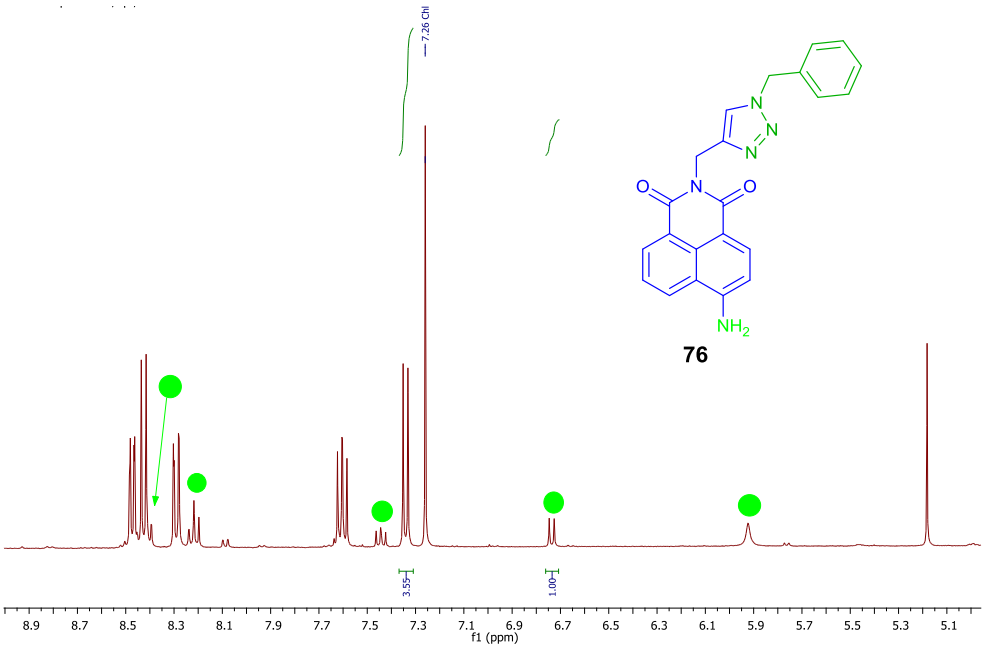

Spectrum 2-1 ^{1}H NMR spectroscopic analysis of formation of azide 72 in NMP at 60^{o}C.

Decomposition product corresponds to aniline **76** (highlighted in green).

At room temperature, analysis of the reaction mixture by ^{1}H NMR spectroscopy showed it proceeded cleanly and completely. It appears the azide intermediate **72** is ultimately not stable however, as decomposition product **76** begins to appear after work-up, and more is isolated after column chromatography. Heating the reaction was therefore detrimental to the overall yield, and it was decided to keep our original solvent conditions at room temperature in NMP. Additionally, the instability of azide **72** on isolation gave credence to the idea that this would be a successful one-pot multicomponent reaction however; as the intermediate would not require isolation this would likely give high yields of our desired double-triazole product **73**.

2.3.4. Preliminary One-pot Synthesis Attempt

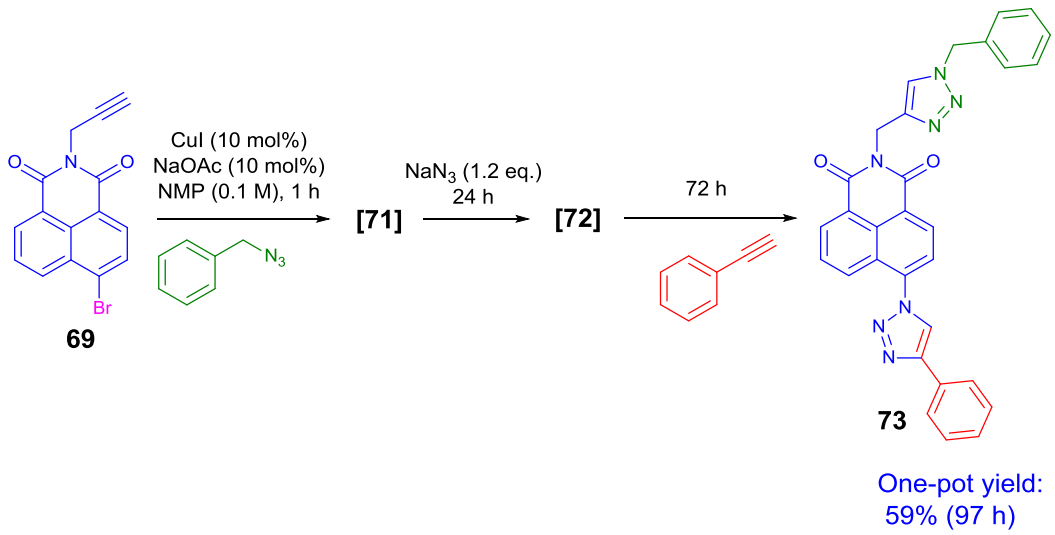

Scheme 2-9 Synthesis of bistriazole **73** using a one-pot procedure from central building block **69**

Upon applying our optimised conditions to a one-pot procedure, we found that whilst the first two stages of the reaction proceeded well, the final CuAAC was very slow (72 h) with a final yield of only 59% of **73** isolated after purification. This corresponded with the ^{1}H NMR yield from an aliquot taken before work-up, and many decomposition products of **72** were isolated upon purification, along with a small amount of unreacted azide **72**.

Therefore in an attempt to optimise this final CuAAC step we synthesised and isolated a stock of azide **72** and set up a number of CuAAC reactions with phenylacetylene under the standard conditions we had optimised, screening a variety of additives to determine which were having a detrimental effect on the reaction (Table 2-2).

2.3.4.1. Investigation into Slow Reaction Time of 72 to Form 73

Table 2-2 Effect of various additives on formation of double triazole **73** from azide **72**

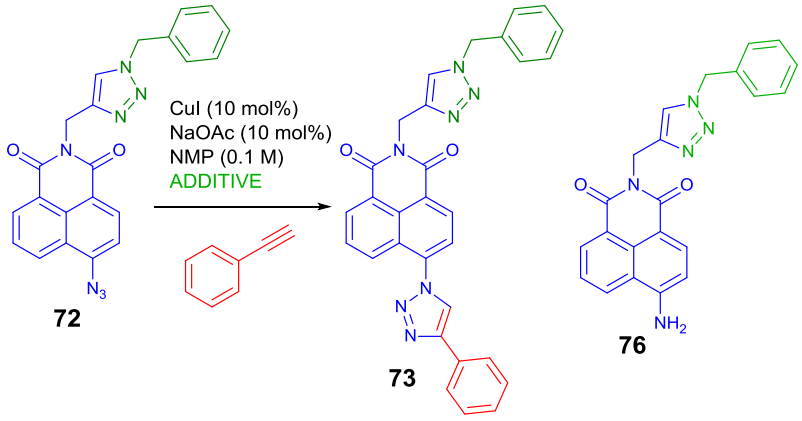

Entry	Additive	Time (h)	Product	Yield % [a]
1	0.05 eq. **76**	48	**73**	98
2	1 eq. NaBr	48	**73**	19
3	0.2 eq. NaN_3	48	**73**	83

(a) ^{1}H NMR yields

As the S_NAr reaction to form azide **72** is not 100% efficient, we decided to include aniline **76** as one of the additives. We found that 5 mol% of this had no effect on the reaction at all (**entry 1**), and neither did 0.2 equivalents of NaN_3, the potential excess present from the addition of 1.2 equivalents to perform the S_NAr (**entry 3**). However NaBr, an unavoidable by-product formed in stoichiometric amounts as a result of the S_NAr reaction, has a significant effect on the yield of triazole formed, and even after 48 h there was only 19% formation of **73** and significant levels of decomposition of azide **72** were observed by ^{1}H NMR analysis. To overcome this, rather than employ silver salts to scavenge the bromide ions, we decided to add a protic solvent to form a mixed solvent system for the final CuAAC, with a view to solvate the bromide ion instead. The solvent was to be added after the S_NAr was complete, so it could have not have a detrimental effect on the azide formation.

2.3.4.2. Protic Solvent Screen

Table 2-3 Effects of protic solvent on the formation of bistriazole 73

Entry	Starting Material	Solvent	Ratio (NMP:X)[a]	Time (h)	Product	Yield %
1	**71**	H_2O	4:1	48	**73**	82[b]
2	**71**	MeOH	4:1	48	**73**	86[b]
3	**71**	EtOH	4:1	48	**73**	88[b]
4	**71**	^{i}PrOH	4:1	48	**73**	63[b]
5[c]	**69**	EtOH	9:1	48	**73**	48
6[c]	**69**	EtOH	4:1	41	**73**	66
7[c]	**69**	EtOH	1:1	41	**73**	85

(a) Protic solvent added after completion of S_NAr. (b) ^{1}H NMR yields. (c) **69** to **71** 1h, 1.2 equiv. BnN_3, **71** to **72** 24 h, 1.4 equiv. PhCCH, **72** to **73** 16 h.

Initially, despite the previous decomposition observed in its presence, water was used as the protic solvent and was added as 1 part water to 4 parts NMP, so as not to drastically increase the volume of the reaction (Table 2-3, **entry 1**). After monitoring the reaction by ^{1}H NMR spectroscopy we were pleased to see a dramatic increase in yield of desired product **73** with no major decomposition observed. A switch to protic organic solvents for the same screen gave comparable results using MeOH and EtOH after 24 h (**entries 2 and 3**), with ^{i}PrOH showing a lower yield of 63% in the same timeframe (**entry 4**). As EtOH gave a marginally higher yield, this was our final choice of protic solvent.

A screen of the whole model one-pot multicomponent procedure as in Scheme 2-9 with different ratios of EtOH added for the final CuAAC (**entries 5 – 7**) showed that despite halving the concentration of the reaction mixture, the final CuAAC reaction completed in a faster time of 16 h, with an 85% isolated yield of bistriazole **73** when using a 1:1 ratio of

EtOH to NMP. As the ratio of EtOH:NMP got larger, the yield of **73** clearly diminished. **Entry 7** demonstrates our finalised conditions for a one-pot, double 'click' ligation procedure, as shown in Scheme 2-10.

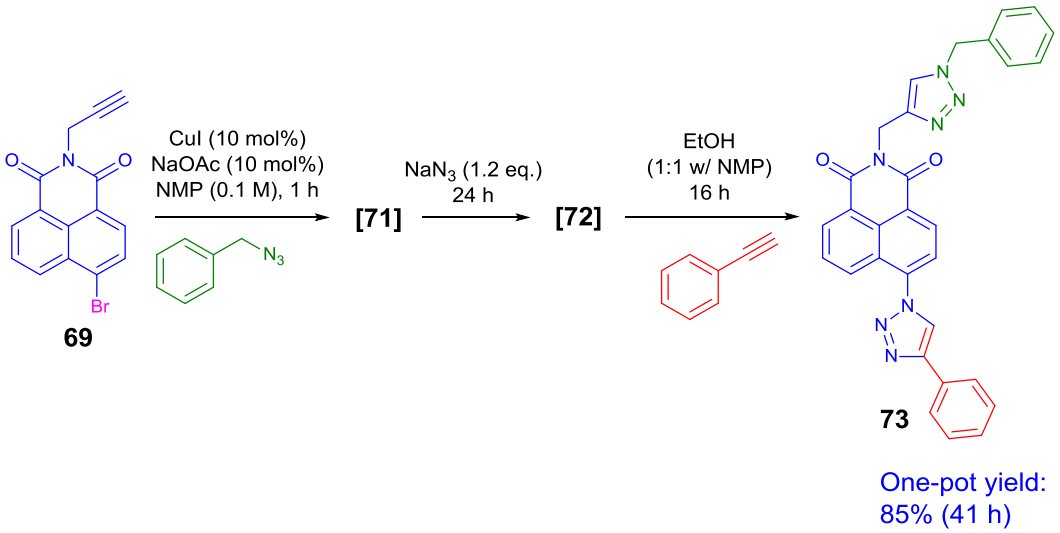

Scheme 2-10 Finalised one-pot, multicomponent procedure for the synthesis of bistriazole **73** from central building block **69**, benzyl azide and phenyl acetylene

Finally, whilst these reactions were carried out at 0.1 M, we also demonstrated this system gave similarly high yields at 0.2 M (86% NMR yield) and 0.3 M (85% NMR yield) as well, showing that the reaction is not limited by reaction concentration.

2.3.5. Application of Optimised Synthesis to Building Block 70

These optimised conditions (exemplified in Scheme 2-10) were then readily applied to central building block **70**. After the three stepwise iterations of CuAAC, azide formation and a second CuAAC and three purifications, the overall yield of final product **79** obtained from **70** was only 41%, but gratifyingly by following the designed one-pot protocol we obtained a final isolated yield of **79** of 72% (Scheme 2-11). During the stepwise iteration, it became apparent that the azide intermediate **78** formed after the S_NAr had a poor level of stability. Immediately after column chromatography, azide **78** appeared to be unstable as both a solid and in solution, even if kept in an air-free atmosphere and in the dark. For this reason

we were unable to characterise it fully. This is also a potential reason behind the slightly diminished yield of bis-triazole **79** compared to **73**, and more by-products are evident by analysis of the ^{1}H NMR spectrum of the crude reaction mixture after work-up procedures.

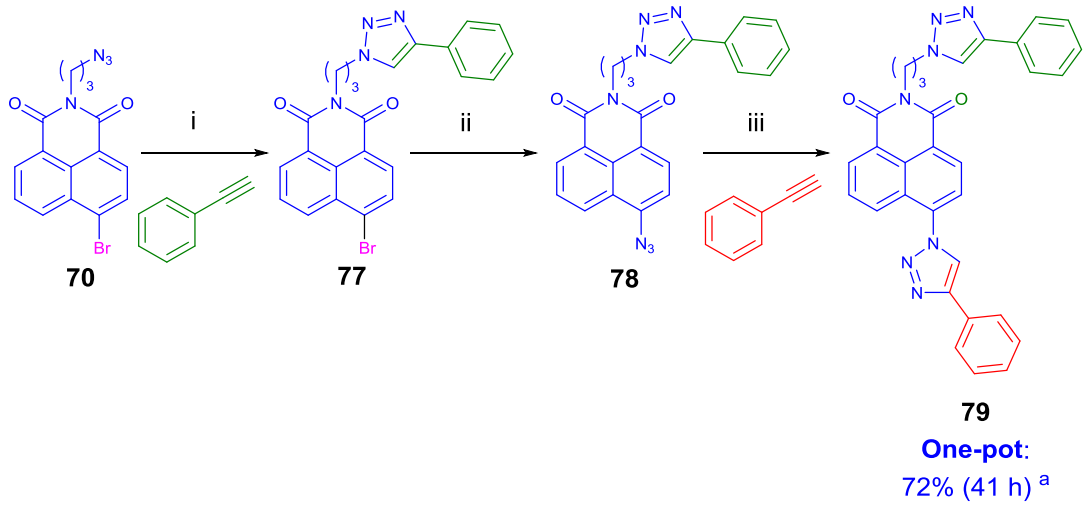

Scheme 2-11 Application of optimised multicomponent procedure to central building block **70** to form bistriazole **79**, both stepwise and in one-pot. Conditions: i) CuI (10 mol%), NaOAc, NMP, rt, 1 h, 67%. Ii) NaN_3, NMP, rt, 24 h, 76%. iii) as stage (i), 16 h, 81%. (a) EtOH (1:1 w/ NMP) added for final step when carried out in one pot. There was no second addition of copper source.

2.4. Conclusion

In conclusion, a novel one-pot three component iterative 'click' reaction to form double-triazole containing compounds with a naphthalimide core was designed and optimised. We utilised a simple S_NAr-CuAAC strategy to successfully design a novel 'click'-chemistry based reaction sequence with high yields and high purity of final bis-triazole products **73** and **79** **(**Scheme 2-12**)**. Excitingly, we were also able to isolate both products straight from the reaction mixtures by simple precipitation and filtration, with greater than 99% purity by ^{1}H NMR spectroscopy. The reaction was designed for future application in the synthesis of novel fluorescent bis-triazole constructs capable of acting as sensors for Zn^{2+} in an analogous manner to existing probes in our group, but with readily incorporated cell

targeting moieties to induce localisation in a cellular environment. Our efforts towards this are described in Chapter 3.

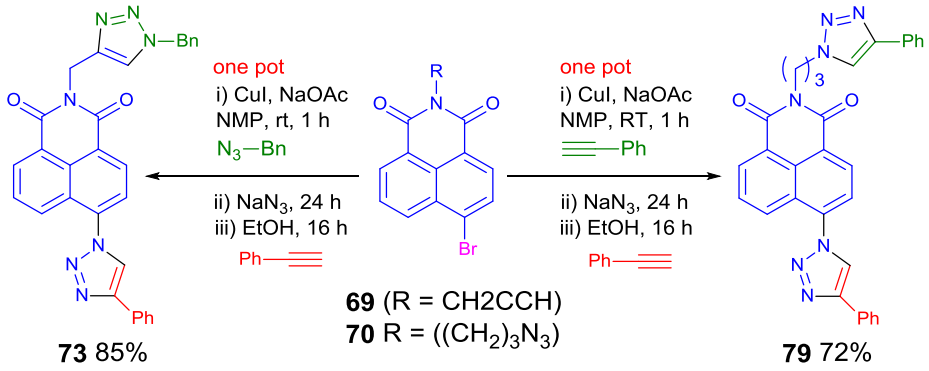

Scheme 2-12 A schematic representation of the final optimised multicomponent one-pot routes to synthesising bistriazole containing compounds from central building blocks **69** and **70**, and isolated yields (0.1 M reaction concentration)

Chapter 3: Design and Development of Biologically-Targeted Zinc Sensors

3.1. Introduction

Having designed a successful iterative one-pot ligation procedure that is high yielding and synthetically simple, we decided to demonstrate its utility by synthesising sensors with biological targeting groups, rendering them capable of localisation in cellular compartments with an end goal of using them for visualisation of zinc in these locations. The building blocks required for constructing these types of sensors would be pre-functionalised units, synthesised to incorporate either an azide or alkyne moiety to ligate them to the central building block core (Scheme 3-1).

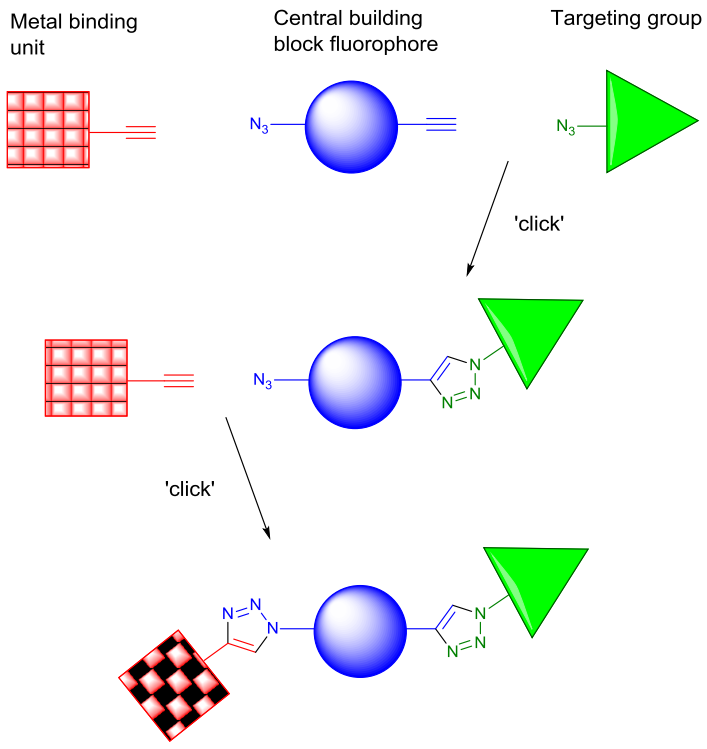

Scheme 3-1 Schematic representation of the synthesis of three-unit constructs for fluorescent sensing in cellular compartments

We chose to integrate metal binding units already demonstrated to be selective for Zn^{2+}. Many recent examples of biologically targeted fluorescent probes are described in Chapter 1, and it is interesting to note that in many cases these probes are merely simple modifications of existing sensors, with the additional functionality being easily applied *via* a synthetic handle on the probe. We aimed to take a similar approach when synthesising our biological targeted building blocks and took well-established targeting units from the literature to incorporate into our sensors.

Unlike the established targeted probes already reported (see section 1.6), we aimed to overcome their difficult and low yielding synthetic procedures by utilising our iterative multicomponent procedure to give compounds with the desired functionality in high yields. This chapter will discuss the routes taken to synthesise both the 'clickable' building blocks and a small family of fluorescent sensors, *in-vitro* testing of each sensor's fluorescent response to zinc, and also the successful *in-cellulo* testing of selected sensors in murine pancreatic islet cells.

3.2. Results and Discussion

3.2.1. Synthesis of Biological Targeting Groups

Our first task was to synthesise the 'clickable' building blocks that would allow us to incorporate a biological targeting group into our novel three unit sensor construct.

3.2.1.1. Azide-bearing Targeting Groups

We began by synthesising potential targeting units functionalised with an azide moiety. This would allow us to use the central building block **69** with an alkyne unit as the site for the first CuAAC to install the targeting group.

The ability to monitor the efflux of zinc out of cells using an extra-cellularly anchored zinc-specific probe was recently demonstrated by Li and co-workers in their development of the probe ZIMIR **22**, through the attachment of a pair of dodecyl alkyl chains for interdigitating the cell membrane extracellularly.[50] We envisaged that the incorporation of a didodecyl unit into our sensor motif would induce similar behaviour to ZIMIR.

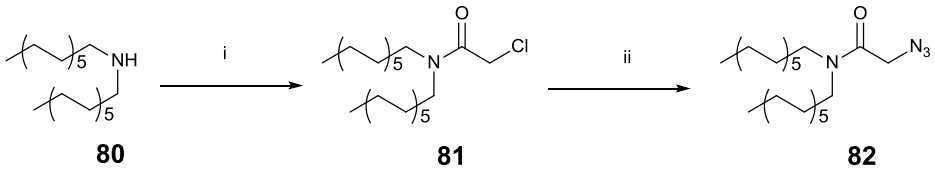

Scheme 3-2 Synthesis of didodecylamine unit **82**. Conditions: i) Chloroacetyl chloride, NEt_3, CH_2Cl_2, 24 h, 76%, ii) NaN_3, DMF, 65 °C, 24 h, 98%.

A 'clickable' didodecyl unit **82** was synthesised from commercially available didodecylamine **80** in 2 steps using established protocols (Scheme 3-2). The amide **81** was formed using chloroacetyl chloride and triethylamine in anhydrous CH_2Cl_2 in good yield after purification. The azide formation reaction in DMF was very high yielding at 98%, and no further product purification was required.

In light of the report of cholesterol conjugated probe **21** having efficacy in targeting the cellular membrane, we also decided to use cholesterol as a bioconjugate in our library, due to its ability to act as an alternative extracellular anchor. [49] Chloride **84** was synthesised in excellent yield from commercially available cholesterol, and azide **85** was synthesised in DMF in moderate yield after purification (Scheme 3-3).

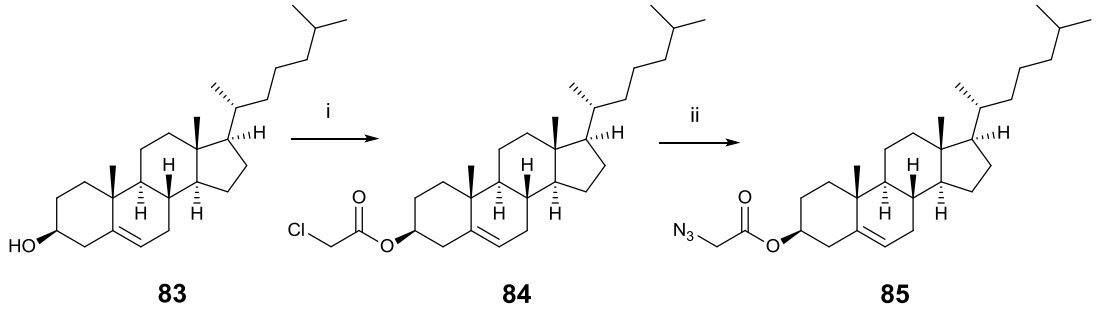

Scheme 3-3 Synthesis of cholesterol azide 13. Conditions: i) Chloroacetyl chloride, NEt_3, CH_2Cl_2, 24 h, 92%, ii) NaN_3, DMF, 65 °C, 24 h, 65%.

Another common and successful targeting group often incorporated into the framework of zinc specific sensors is the triphenylphosphonium cation, known to induce localisation of the organic molecule into the charged mitochondrial matrix. DQZn2 **15** and SZn-Mito **16** are two such examples.[40,41] We synthesised (4-azidobutyl)triphenylphosphonium bromide **89** in 2 steps from commercially available dibromobutane **86** following literature procedures (Scheme 3-4).[171] Following this, we carried out an ion exchange of the bromide for a tetrafluoroborate anion, to reduce the previously observed propensity of bromide anions to arrest the CuAAC one-pot process (see Chapter 2).

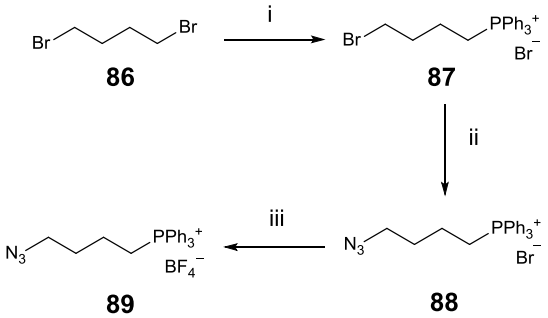

Scheme 3-4 Synthesis of (4-azidobutyl)triphenylphosphonium tetrafluoroborate **89**. Conditions i) PPh_3, toluene, reflux 16 h, 68% ii) NaN_3, $EtOH/H_2O$ (1:1), reflux 16 h, 73% iii) aq. NH_4BF_4, 96%. [171]

DQZn4 **24** has a structurally identical core to DQZn2 **15**, but instead of a triphenylphosphonium cation it uses an *N*,*N*-dimethyl ethylamino moiety to instead target

intracellular lysosomal space.[53] This molecule was the first reported lysosomal Zn^{2+} specific sensor, and so we also decided to append this unit to our fluorescent sensor to provide another targeting group option.

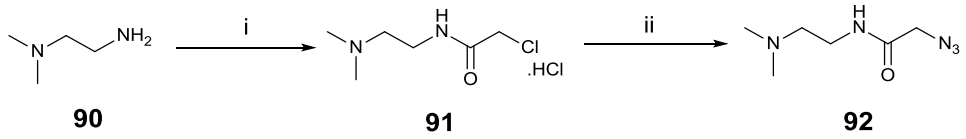

90 **91** **92**

Scheme 3-5 Synthesis of 2-azido-N-(2-(dimethylamino)ethyl)acetamide **92**. Conditions i) Chloroacetyl chloride, EtOAc, 0 °C, 1 h, 89% ii) NaN_3, H_2O, 60 °C, 48 h, 72%.

Following a modified literature procedure [172] we obtained the hydrochloride salt **91** in excellent yield, and this it was taken forward to react with sodium azide in water to give the azide **92** in a good yield of 72% (Scheme 3-5).

3.2.1.2. Alkyne-bearing Targeting Group

For the central building block **70**, which is designed to incorporate two alkyne units as the building blocks for the three unit constructs, we settled on the use of propargylated glycosides as a potential biological targeting unit.

Sugars have been incorporated into zinc-specific ligands previously, as demonstrated by the quinoline-based probes synthesised by Mikata and co-workers,[58] and there is a great precedent for 'clickable' glycosides as cell-targeting tools, particularly by the Scanlan research group.[59,173] Not only would these act as targeting moieties, they could also potentially aid the solubility and cellular uptake of our sensors.[60] Acetyl-protected propargylated glucose **94** was synthesised according to literature procedures from commercially available glucose penta-acetate **93** in moderate yield (Scheme 3-6).

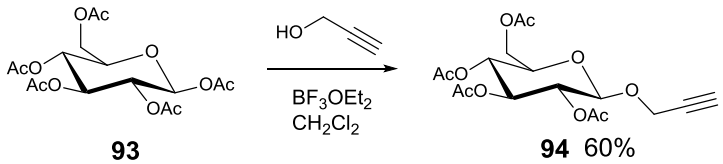

93

Scheme 3-6 Synthesis of propargylated glucose 15 [59]

3.2.2. Synthesis of Metal Binding Ligands

The design of the central building blocks dictated that the second CuAAC iteration for the zinc specific ligand must be carried out with an alkyne-appended 'click' partner. This led us to the synthesis of propargylated ligands **95–97** (Figure 3-1), all of which were readily synthesised.

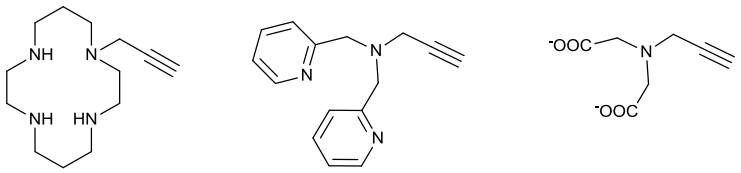

95 **96** **97**

Figure 3-1 Propargylated ligands chosen for this study

All of the ligands shown in Figure 3-1 are known metal chelators. Cyclam acetylene **95** has been used by the Watkinson group in our studies towards zinc sensing.[71–73] Di-2-picolylamine (DPA, **96**) and iminodiacetate (IDA, **97**) are commonly used in many small molecule fluorescent sensors and whilst they also known to chelate to other metals such as copper and manganese, both of these ligands have been employed in sensors specific to the detection of Zn^{2+}, and were chosen for this study for their varying binding affinities for zinc.[22,50,163] This variety is to ensure that the probes synthesised are able to detect mobile zinc at a wide range of biologically relevant concentrations.[174] These ligands were synthesised with appropriate protecting groups (when needed) for both ease of synthesis in the one-pot procedure, and to avoid unwanted binding of copper from the CuAAC.

Following literature procedures,[72] Boc-protected cyclam acetylene **65** was synthesised from commercially available starting material **98** in moderate yield after purification by column chromatography (Scheme 3-7).

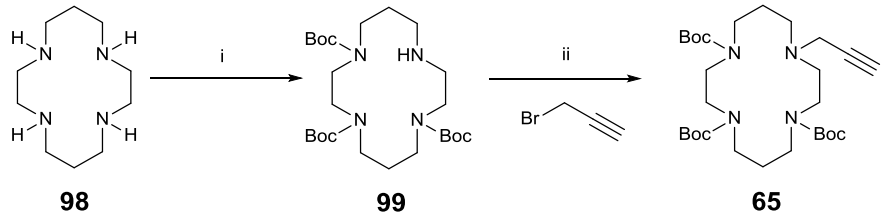

Scheme 3-7 Synthesis of Boc-protected propargylated cyclam ligand **65**. Conditions: i) Boc_2O, NEt_3, CH_2Cl_2, 16 h, 49%, ii) Na_2CO_3, MeCN, reflux, 16 h, 69%.[72]

Scheme 3-8 demonstrates the high-yielding one step synthesis of acetylene-functionalised DPA **96**. The product was synthesised, after column chromatography using ethyl acetate with 5% triethylamine as the eluent, in excellent yield. This particular ligand is useful in the synthesis of sensors as it requires no extra protection-deprotection steps.

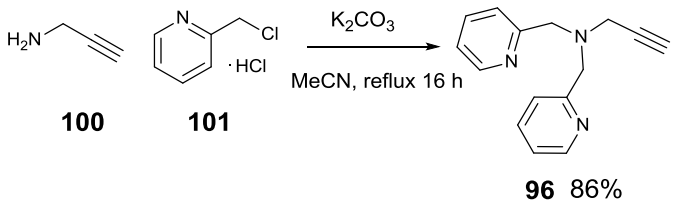

Scheme 3-8 Synthesis of propargylated DPA ligand **96**

IDA **97** has also previously been synthesised by Varazo *et al.*.[162] Following their procedures we obtained the protected variant of the desired ligand **104** in a moderate yield after column chromatography.

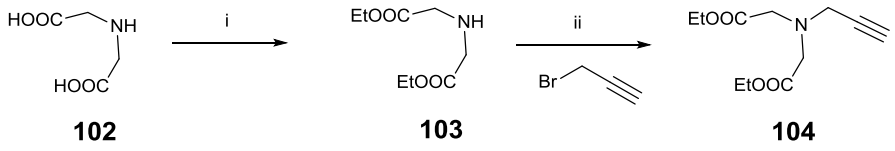

Scheme 3-9 Synthesis of protected IDA ligand **104.** Conditions: i) $SOCl_2$, EtOH, rt, 16 h, 33%. ii) K_2CO_3, MeCN, reflux, 16 h, 76%.[162]

3.2.3. Synthesis of Sensors Using One-pot Methodology

With our selection of desired building blocks in hand, we began synthesising a small library of sensors, using our optimised one-pot procedure to ensure high yields, high purity and minimal loss of material.

3.2.3.1. Didodecyl-Bearing Sensors

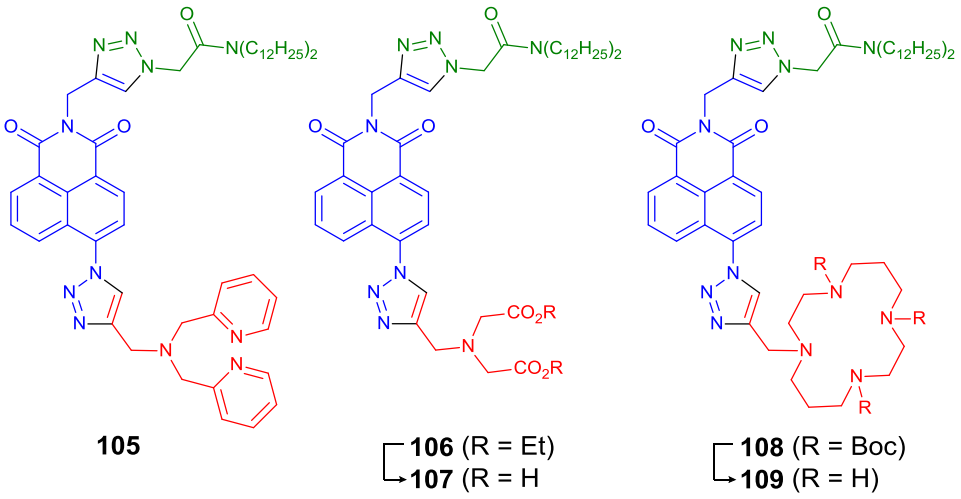

Figure 3-2 Didodecyl-appended sensors with different metal binding units, designed to target the extracellular membrane of a cell.

Sensors **105**, **107** and **109** were synthesised from central building block **69**, in order to demonstrate the modularity and flexibility of our synthesis with respect to the metal binding unit. Each was synthesised with the same extracellular targeting didodecylamine unit **82**, but contained a different metal binding ligand (Figure 3-2). This was to demonstrate that our synthetic approach can allow for the tailored synthesis of a probe with the appropriate binding constant, to reflect the concentration of mobile zinc in the intended area of study.

Following our optimised conditions, we were pleased to find the reaction proceeded extremely well for the synthesis of **105** from **69** on a 1 mmol scale, with an overall isolated yield of 82%, corresponding to an average of 95% yield for each step in the synthesis. This

and all of the one-pot iterative reactions noted in this study were monitored by ^{1}H NMR spectroscopy to ensure and confirm completion of each step before proceeding to the next addition for the iterative procedure. The pure product was isolated from the reaction mixture by column chromatography using neutral alumina, following work-up with a saturated basic solution of EDTA to ensure all copper residues were removed. Sensor **105** required no deprotection steps and the sensor was ready to use in the laboratory and *in cellulo* (Scheme 3-10).

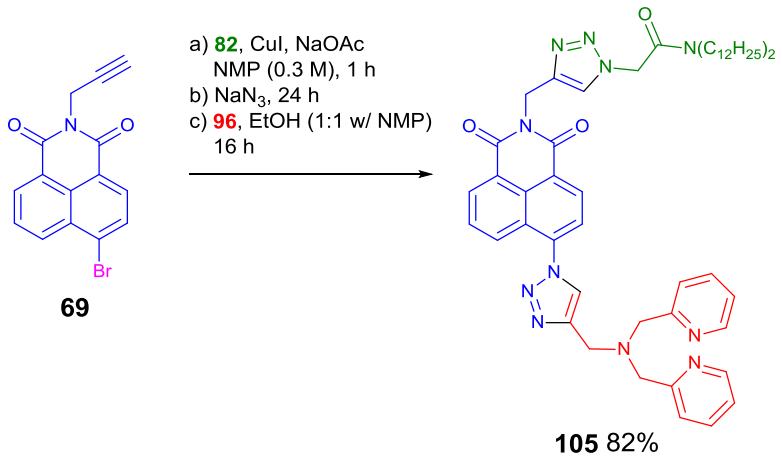

Scheme 3-10 One-pot synthesis of sensor **105** from central building block **69**

As with **105**, **106** was readily synthesised on a 1 mmol scale using didodecylamine azide **82** and protected IDA ligand **104** (Scheme 3-11). The protected sensor was isolated after column chromatography in good yield of 76%. Upon standing however, this compound appeared to show signs of degradation, both by ^{1}H NMR spectroscopy and by TLC analysis. After stirring this degradation mixture in diethyl ether, we were pleased to find that sensor **106** remained in solution, and the impurity was precipitated. Whilst this impurity was not identified, ^{1}H NMR spectroscopic analysis showed there was no second triazole present as seen by the absence of ligand **104**, and furthermore the chemical shifts did not match that

of what would be the corresponding azide intermediate. This was further confirmed by IR spectroscopy, where no characteristic azide band was observed.

Deprotection of **106** to give the ready-to-use sensor **107** proved to be problematic. Basic hydrolysis of the ester using potassium hydroxide caused complete degradation of the sensor, whilst sodium hydroxide gave a slight degradation but mostly recovered **106**, with very little of the desired product detectable. A third alternative, the use of lithium hydroxide in a THF/H_2O mixture, gave conversion to clean product **107** after work up with citric acid, but in only a moderate yield of 53%.[175]

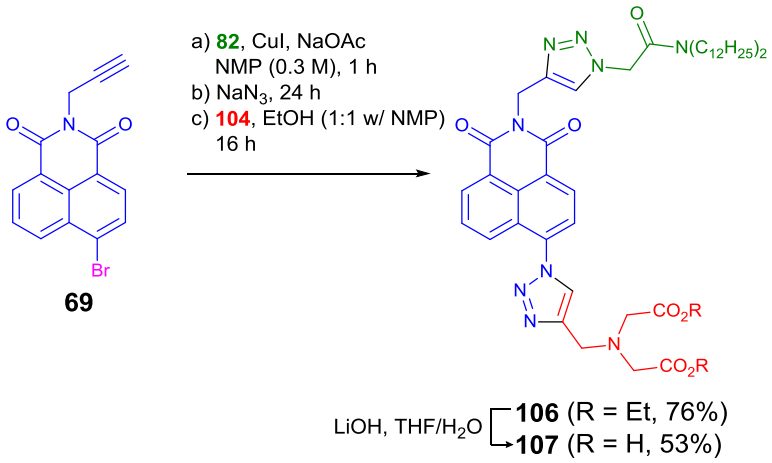

Scheme 3-11 One-pot synthesis of protected sensor **106** from central building block **69**, and subsequent deprotection to yield **107**.

Sensor **109**, similar in structure to the original 'clickate' sensor **30,** was also synthesised on a 1 mmol scale, in a good yield of 75% for the Boc-protected **108**, using the targeting group **82** and the protected cyclam alkyne ligand **65**. Deprotection by stirring **108** in TFA/ CH_2Cl_2 (1:5) followed by a basic work-up gave sensor **109** in excellent yield of 89% (Scheme 3-12).[72]

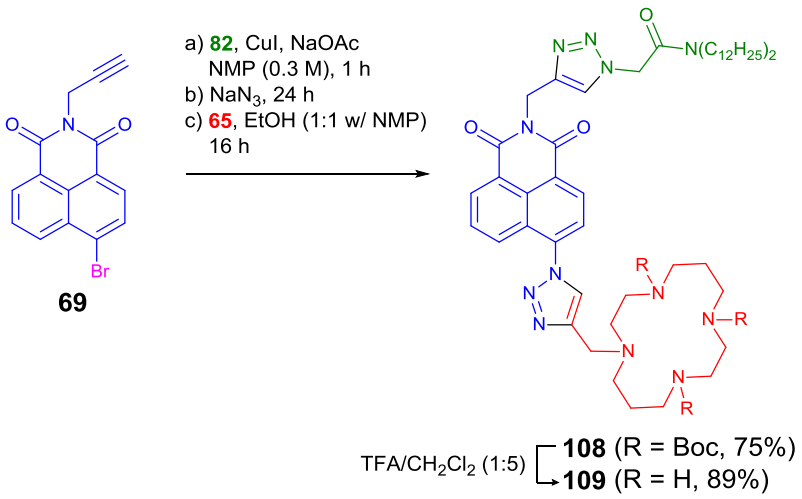

Scheme 3-12 One-pot synthesis of protected sensor **108** from central building block **69**, and subsequent deprotection to yield **109**.

3.2.3.2. Cyclam-appended Sensors

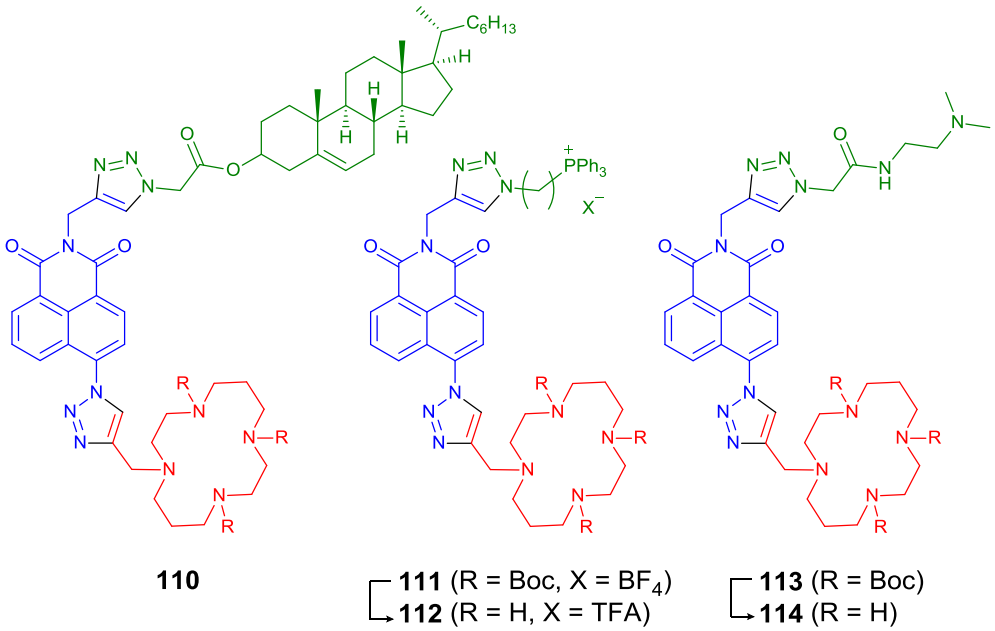

Figure 3-3 Cyclam-appended sensors with different biological targeting units, designed to target different compartments of a cell.

In a similar mix-and-match approach, sensors **110, 112** and **114** were synthesised from central building block **69**, in order to demonstrate the modularity and flexibility of our synthesis, this time with respect to the biological targeting unit (Figure 3-3). We

hypothesised that as the majority of the molecules were identical in structure to the 'clickate' sensor **30** that these probes would retain their zinc selectivity and sensitivity, but with the added bonus of specificity for a cellular location.

The synthesis of sensor **110** presented many difficulties in its handling during the synthetic stages of the one-pot route. The well-known tendency of cholesterol to aid the formation of gels via van der Waals and hydrogen bonding [176] caused our reactions to stall. The gelation prevented efficient mixing, and further dilutions with NMP did not aid the process of stirring. Despite this, after rigorous purification, one attempt yielded 28% of sensor **110** (Scheme 3-13). However, this result could not be consistently reproduced, and so synthesis of this sensor was abandoned due to lack of facile access to the desired product.

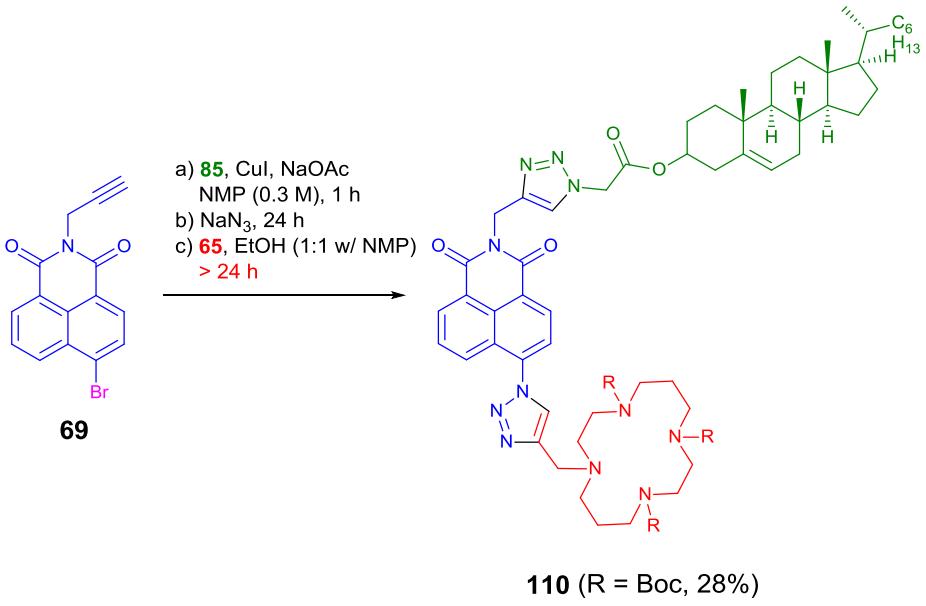

Scheme 3-13 Synthesis of sensor **110** from central building block **69**

Sensor **111** was also synthesised on a 1 mmol scale, in a moderate yield of 66% for the Boc-protected **111**, using the targeting group **89** and the protected cyclam alkyne ligand **65** (Scheme 3-14). The reaction and work up proceeded as expected but we found most of the crude material to be insoluble in chlorinated solvents CH_2Cl_2 and $CHCl_3$, and also observed

streaking upon TLC analysis. A simple trituration of the crude material with EtOAc resulted in the extraction of the final sensor and some minor impurities, whilst the remaining solid from the trituration was found to be further impurities and degradation products. Column chromatography of the separated product mixture in CH_2Cl_2-MeOH gave the desired protected sensor **111**. As with sensor **109**, deprotection of the Boc groups with TFA gave the final sensor **112** in good yield.

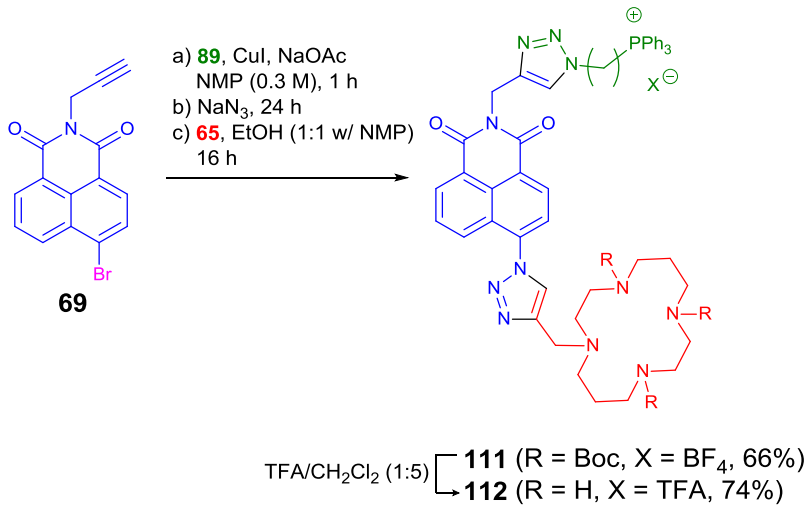

Scheme 3-14 One-pot synthesis of protected sensor **111** from central building block **69**, and subsequent deprotection to yield **112**.

The ethylene-diamine appended protected sensor **113** was also isolated in a moderate yield of 68% following the one-pot procedure with central building block **69**, azide **92** and cyclam alkyne **65** (Scheme 3-15)**.** Loss of material was identified during column chromatography due to the polar nature of the compound, with significant streaking on TLC plates occurring in the various solvent systems investigated, so the yield of **113** was diminished. The deprotection in acidic conditions proceeded smoothly to desired sensor **114** in moderate yield.

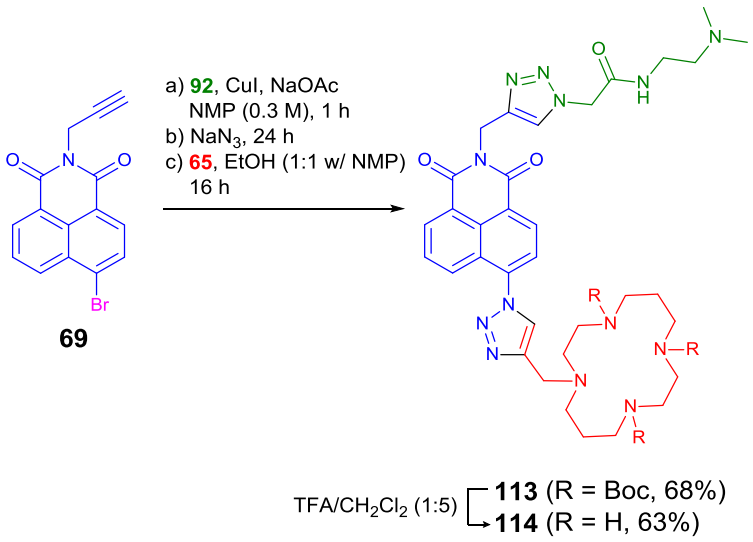

Scheme 3-15 One-pot synthesis of protected sensor **113** from central building block **69**, and subsequent deprotection to yield **114**.

3.2.3.3. D-Glucose-bearing Sensor

Sensor **116** was synthesised to demonstrate the ability of the methodology to incorporate alkyne-bearing targeting groups, with propargylated glycoside **94** designed for ligation to central building block **70** to showcase this. It was decided to utilise the propargylated DPA ligand **96** in the synthesis of this sensor to avoid any harsh deprotection conditions that could destroy the sugar moiety.

During the azide formation step of the procedure, as expected, ^{1}H NMR spectroscopic analysis of the reaction mixture showed the formation of an aniline intermediate in small quantities (~10%) as observed previously using this central building block **70** in optimisation studies (see Chapter 2.3.5). After completion of the reaction, upon work up a small amount of **116** was also identified in the reaction mixture. This, combined with the nature of the pyridine-based ligand made purification quite challenging, and we obtained **115** in a moderate yield of 61% following column chromatography on alumina in CH_2Cl_2-MeOH.

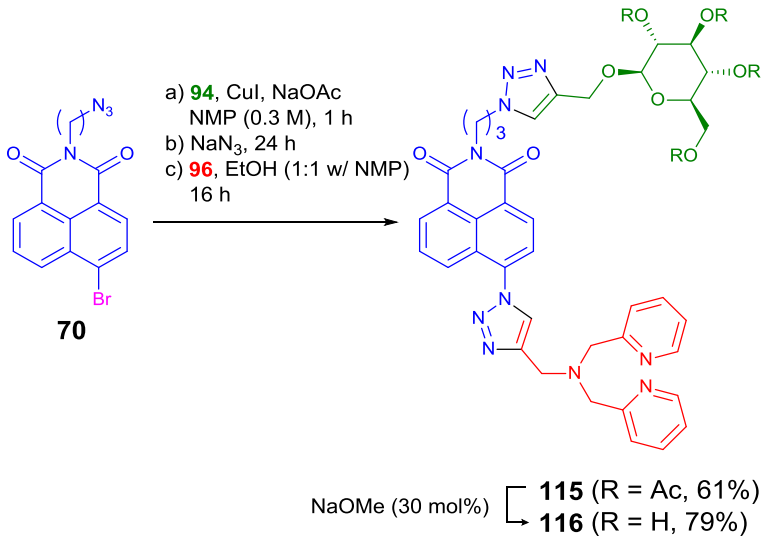

Scheme 3-16 One-pot synthesis of protected sensor **115** from central building block **70**, and subsequent deprotection to yield **116**.

Deprotection of the acetyl groups on the glycoside was carried out according to a modified literature procedure using 30 mol% sodium methoxide (NaOMe).[59] A longer reaction time of 18 h gave product **116** in 79% yield. The now-deprotected glycoside greatly increased the propensity of the compound to dissolve in water, and the obtained compound was not soluble in many organic solvents. Therefore sensor **116** was assumed to be a 30% Na-salt as it was obtained by simply evaporating the reaction solvent.

3.2.4. *In vitro* Testing of Sensors

With the synthesis of a small family of sensors complete, it was necessary to carry out testing in the laboratory to confirm that our novel three-unit constructs **105**, **107**, **109**, **112**, **114** and **116** had the desired fluorescent properties for a zinc probe. All of the ligands incorporated into our constructs were all based on previously reported sensors that displayed a desirable selective switch-on response upon zinc binding and with a 1:1 binding stoichiometry;[22,50,163] nonetheless we felt it was imperative to ensure each of our designed sensors still retained this behaviour even with the inclusion of an additional biological targeting unit in both aqueous and organic media.

3.2.4.1. Response to Zn^{2+} in Aqueous and Organic Media

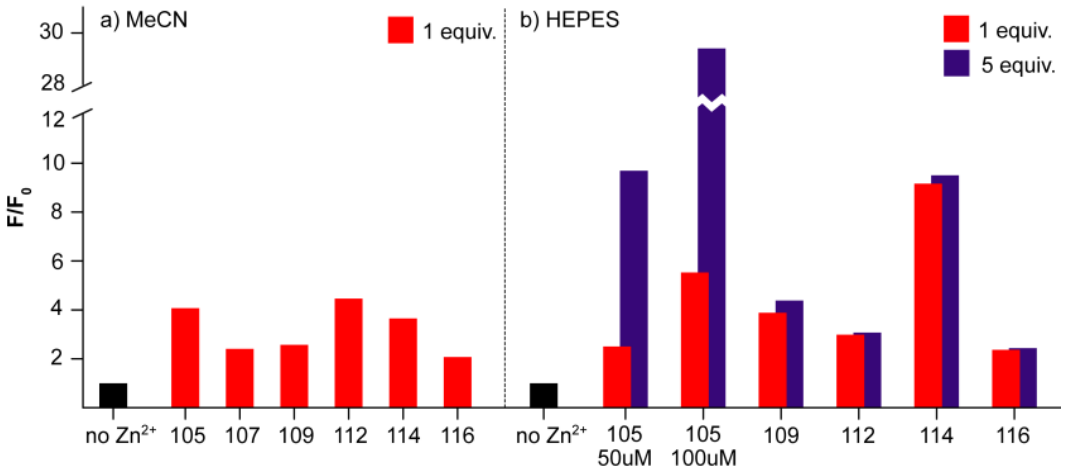

Figure 3-4 The switch on fluorescent response (F/F_0) of each sensor to 1 (red) and 5 (purple) equivalents Zn^{2+} in MeCN and aqueous HEPES buffer

As a first pass, to ensure full solubility of both free sensor, metal salt and metal bound sensor, we chose MeCN as the organic solvent to carry out our initial testing. The concentration of each sample was 100 µM of sensor, and the sensors were titrated with 1, and then 5 equivalents of zinc perchlorate hexahydrate, to demonstrate their response upon zinc-binding.

All of the sensors had a broad absorption band at 347 nm (obtained from UV-Vis spectroscopy), so this was determined as the wavelength of excitation for each to monitor the fluorescent response. The emission wavelength of each probe was also very close to that of the original 'clickate' probe **30** and its cyclen analogue **68**, with λ_{em} values between 400 and 420 nm.

As Figure 3-4 demonstrates, each of the sensors responded to 1 equivalent of zinc with the expected switch-on fluorescent enhancement of between 2- and 4.5- fold with no significant blue or red shift seen in any of the emission profiles, and very little or no enhancement with 5 equivalents of zinc added.

The exception appears to be sensor **112**, which showed a small decrease in fluorescence upon addition of excess zinc (Figure 3-5). However, despite the slight quenching, this effect was not investigated further as overall there was still a 3-fold fluorescence enhancement, and so this probe still generates a desirable response.

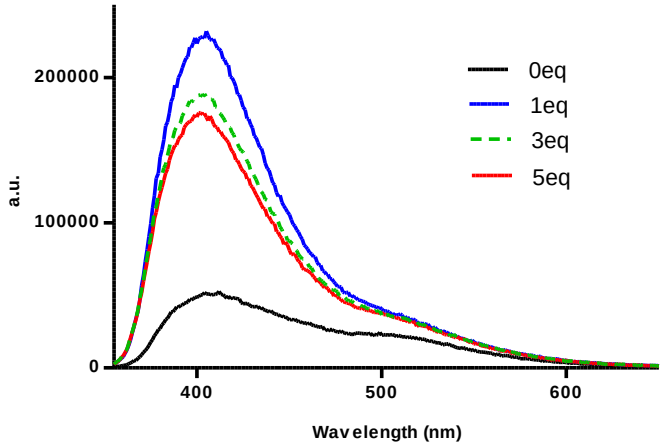

Figure 3-5 Fluorescence emission profile of sensor **112** (100 µM) in response to Zn^{2+} in MeCN

A key part of this study was to ascertain the sensors' response in an aqueous environment, both for a direct comparison to our previously synthesised sensors **30** and **68**, and also to obtain information about these targeted probes under biologically relevant conditions.

With the exception of **105** and **107** (*vide infra*), the probes **109, 112, 114** and **116** responded as expected in 0.1 mM aqueous HEPES buffer (pH 7.4) upon excitation at the same wavelength (λ_{ex} = 347 nm), demonstrating a similar, or in some cases enhanced, fluorescent enhancement in response to Zn^{2+} to that seen in organic media. For solubility purposes, the samples in HEPES buffer required a total 1% volume of DMSO, as this is also the most common solvent used to load other organic dyes onto cellular media with little to no toxicity.

No results in aqueous solution were obtained with sensor **107**, the IDA and didodecyl appended sensor designed for targeting the extracellular membrane. Despite the addition

of DMSO to aid solubility, the sensor precipitates in aqueous media upon the addition of zinc, therefore we were not able to collect data on its behaviour in HEPES buffer.

Overall these results demonstrate that the switch-on response of these sensors to zinc has not been affected by the inclusion of a biological targeting group.

*3.2.4.2. Investigations into Anomalous Behaviour of Sensor **105** in Aqueous Media*

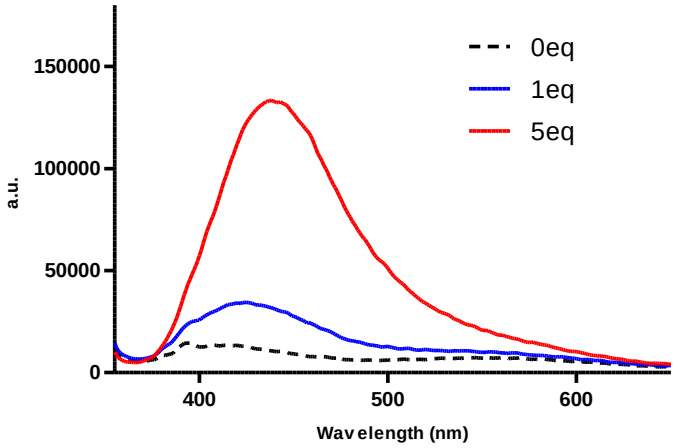

Figure 3-6 Fluorescence response of sensor **105** (100 μM) with increasing amounts of Zn^{2+} in aqueous buffer (0.1 mM HEPES, pH 7.4, ambient temperature, λ_{ex} = 347 nm).

Figure 3-4 and Figure 3-6 demonstrates the anomalous behaviour of sensor **105** in HEPES buffered water, where the addition of 5 equivalents of zinc produced a greater fluorescent response than 1 equivalent. We decided to further investigate these observations to ascertain a reason for it.

Addition of further equivalents of zinc(II) perchlorate resulted in further significant increases in the fluorescence emission of the probe, up to a maximum value of a 35 fold enhancement with 15 equivalents of zinc added (100 μM). This was also combined with a large red shift in the emission value; at 1 equivalent with a 5 fold increase we observed a 23 nm red shift, and at 15 equivalents with a 35 fold increase we observed a red shift of 31 nm (Figure 3-7).

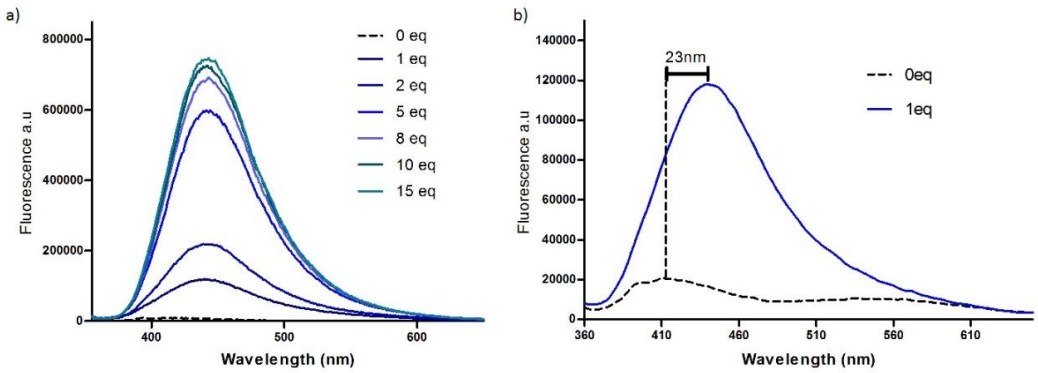

Figure 3-7 a) Fluorescence emission of sensor **105** with increasing amounts of Zn^{2+}. b) The red shift in emission value upon addition of 1 equiv. of Zn^{2+} to sensor **105**

Alongside these results from fluorescence studies, there was a strong visual difference in the appearance of the samples to the naked eye. It was clearly evident that the addition of zinc to the samples of sensor decreased the turbidity of the samples (see Figure 3-8(a)), and that this decrease in turbidity corresponded to the increased fluorescence output (Figure 3-8(b)). This effect was still visible even at lower concentrations of 50 µm and even 10 µm, with titrations also demonstrating a continual increase in fluorescence emission up to 15 equivalents of Zn^{2+} and a red shift in emission wavelength, as demonstrated by Figure 3-7(a). However, the effect was very slightly diminished upon reduction of sample concentration.

Figure 3-8 a) Samples of sensor **105** in HEPES buffered water (pH 7.4) with (L-R) 0, 1, 5 and 15 equivalents of Zn2+. b) the same samples illuminated with a UV-wavelength lamp to demonstrate their fluorescent output.

These observations suggested that sensor **105** was acting in a surfactant-like manner, with its structure bearing a lipophilic aliphatic tail and a polar metal binding head group, and we therefore hypothesised that the emission behaviour could be attributed to aggregation effects in aqueous solution. A similar photophysical response was observed for ZIMIR **22** but not realised or noted by the authors, suggesting similar behaviour, which could account for its large reported dynamic range.

Dynamic light scattering (DLS) experiments were performed to confirm the presence of aggregates, at a sensor concentration of 30 μm in HEPES buffer (1% DMSO). Sensor **105** demonstrated aggregation phenomena in aqueous solution, as shown by the large particle size observed in these samples. The aggregates were at their largest with no Zn^{2+} present (Z-average diameter 773 nm). In the presence of Zn^{2+} the particle size decreased greatly (15 equiv. Zn^{2+} Z-average diameter 247 nm), coinciding with an increase in fluorescence emission. These aggregates remained even when the concentration of the samples was dropped to 10 μm, although this phenomenon was not observed in MeCN solution.

Structurally similar samples to **105,** containing **116** with a different biological targeting unit, showed no significant aggregation. This was demonstrated by the low degree of scattering and poor signal quality by DLS, demonstrating the difference small structural changes can have on the behaviour of these probes.

To further examine the behaviour of probe **105** and its apparent solvent dependency we investigated the effect of solvent composition on its fluorescence emission in both the presence and absence of zinc (Figure 3-9).[177] We found that in the absence of zinc, as the volume of HEPES buffered water in MeCN was varied, there was little difference in the fluorescence output, albeit a small drop as the percentage of HEPES buffered water increased above 50% v/v. In the presence of 5 equivalents of zinc however, we observed a steady increase in fluorescence emission up to 60% v/v HEPES buffered water in MeCN, and

then a significant drop in the emission value after this point. This drop coincides with the observed red shift in fluorescence emission wavelength. This shows that the behaviour of this sensor can be attributed to a combination of PET quenching and aggregation-induced quenching.

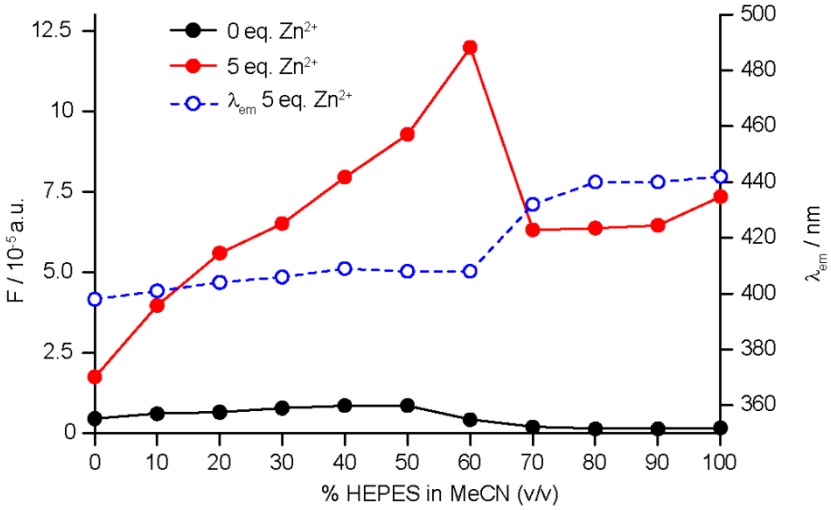

Figure 3-9 HEPES/MeCN titration of aggregating sensor **105** demonstrating both the change in fluorescence emission and red the shift of the emission wavelength upon increasing the percentage of HEPES in MeCN.

It was possible that the binding of other metal ions could possibly influence aggregation significantly leading to a loss of selective Zn^{2+} sensing behaviour. Given the important role that aggregation plays in the performance of sensor **105** *in vitro*, we validated the selectivity of **105** for zinc ions. Pleasingly, only Cd^{2+} and Hg^{2+} produced a fluorescent response, which is to be expected based on previous studies using this particular ligand, and is not biologically relevant as the presence and interference of cadmium and mercury in living cells is negligible.[178] All other metal ions tested led either to no change in fluorescent output or quenching of the background fluorescence.

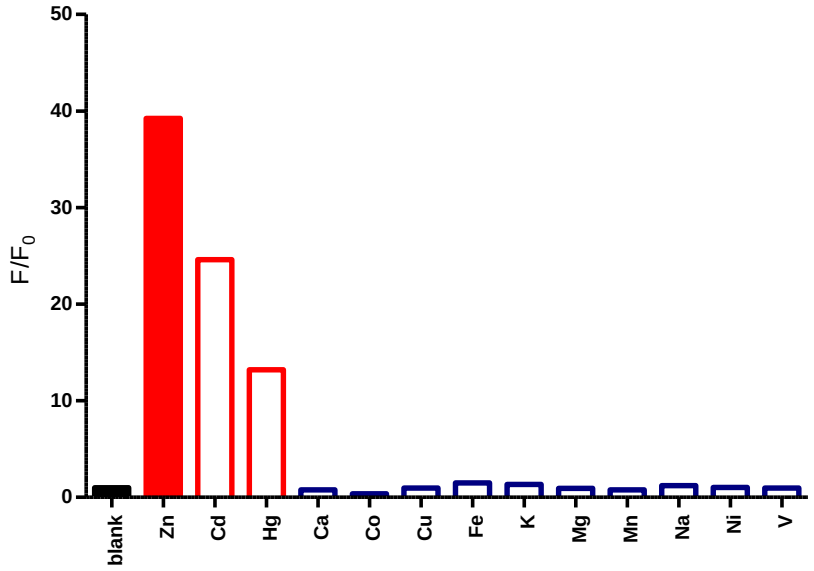

Figure 3-10 Fluorescence response of sensor **105** (100 μm) in HEPES buffered water (1% DMSO) to 5 equivalents of metal cations (as the perchlorate salt)

3.2.5. Determination of K_d values for sensors 109, 112, 114 and 116 [179]

Dissociation constants (K_d) were determined by non-linear regression analysis of titrated samples of sensors **109**, **112**, **114** and **116**. Sensor **105** could not be evaluated due to the aggregation observed in aqueous media, and nor could sensor **107** due to the aforementioned precipitation upon addition of zinc. In the case of probes **112** and **114** that target the lysosome and mitochondria respectively, titrations were also performed at the relevant pH of the organelle.

$$L + M \rightleftharpoons [LM]$$

Equation 3-1 Equation for a 1:1 binding model of ligand (L) and metal (M)

$$\frac{F}{F(0)} = 1 + \left(\frac{F(max)}{2F(0)} - 0.5\right) \times \left(1 + \frac{CM}{CL} + \frac{Kd}{CL} - \left[\left(1 + \frac{CM}{CL} + \frac{Kd}{CL}\right)^2 - \frac{4CM}{CL}\right]^{0.5}\right)$$

Equation 3-2 Equation used to determine K_d values for sensors **109**, **112**, **114** and **116** where CM and CL concentrations of Zn^{2+} and probe respectively, F is the observed fluorescence, F(0) is the observed fluorescence of the probe alone (i.e. CM = 0). Non-linear regression analysis was used to determine F(max)/F(0) and Kd.[72]

$$L + M \rightleftharpoons [LM] \rightleftharpoons [L_2M] \rightleftharpoons [L_3M] \ldots$$

Equation 3-3 Equation to demonstrate more complex equilibria for species potentially formed between ligand (L) and metal (M) in solution

Titrations were carried out in HEPES buffered aqueous solution, by measuring the fluorescent output upon the addition of Zn^{2+}. Assuming our sensors follow a simple 1:1 binding model (Equation 3-1), by using Equation 3-2, the K_d of the four sensors was evaluated from the data obtained. Although reasonable values of K_d were obtained when compared to those reported for structurally similar ligands,[22,163] the goodness of fit to a 1:1 binding model varied considerably, as demonstrated in Figure 3-11.

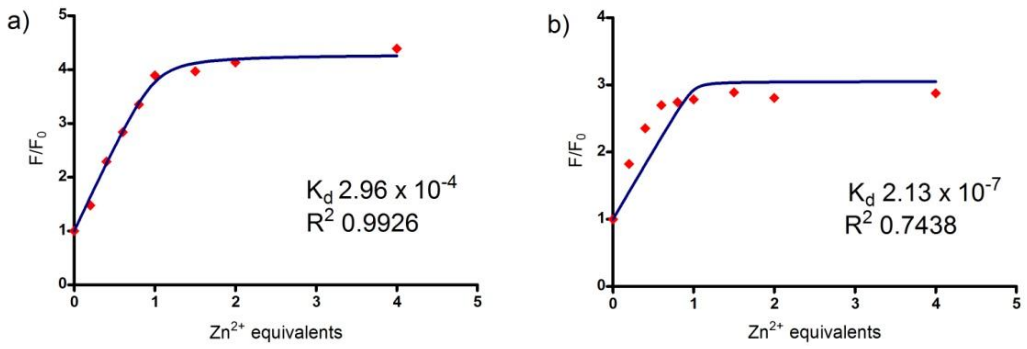

Figure 3-11 Representative examples of non-linear fitting of fluorescence titration data using Equation 3-2 for a) sensor **109** and b) sensor **112**, demonstrating the varied goodness of fit to the model.

The values obtained for probes **109**, **112**, **114**, and **116** are shown in Table 3-1. It is of note that the value obtained for sensor **109** is a lower K_d value than that of the analogous 'Clickate' probe **30**, but we obtained a better goodness of fit in our calculations than those for sensor **30**.[72]

We observed poor fitting of sensors **112** and **114**, and similar issues have recently been identified by Vögtle and co-workers in their investigations of dendrimeric cyclam sensors for Zn^{2+}.[180] This assumes that instead of the simple, one species model as approximated for these systems, there exists instead a series of complex equilibria of species where multiple

ligands can bind to the metal ion (Equation 3-3). Lippard and McQuade also observed similar characteristics with their Zn^{2+}-specific probes QZ2E **29** and QZ2A, and were unable to obtain accurate binding constants, due to the unexplored nature of a complex equilibria of species in solution.[62]

Attempts to try and obtain further data on these probes by ^{1}H NMR spectroscopic studies were unsuccessful. Whilst we can speculate that our probes behave similarly, this was not further investigated as it would require extensive study and calculation to ascertain the reasons behind the observed data. This was considered to be a separate study outside the scope of this thesis, as the main focus remained the successful demonstration of function and utility of the synthesised sensors in biological milieu.

Table 3-1 Values for K_d and F(max)/F(0) obtained by non-linear regression analysis of sensors **109**, **112**, **114** and **116**.

Sensor	K_d (calculated)	F(max)/F(0)	R^2	K_d Lit. value[72,163]
109	2.96×10^{-6} (pH7.4)	4.3	0.9926	4.3×10^{-8} M^{-1}
112	2.13×10^{-7} (pH 7.4)	3.1	0.7438	4.3×10^{-8} M^{-1}
	1.85×10^{-7} (pH 7.8)	3.3	0.7150	
114	9.80×10^{-8} (pH 7.4)	11.5	0.9223	4.3×10^{-8} M^{-1}
	1.38×10^{-7} (pH 5.8)	10.0	0.9019	
116	2.12×10^{-7} (pH 7.4)	2.6	0.6482	1.2×10^{-8} M^{-1}

3.2.6. *In-cellulo* Testing

3.2.6.1. Introduction and Background to Cell Testing Work

The biological trafficking of zinc has been strongly linked to type 2 diabetes associated with the pancreas.[181–183] The release of insulin from pancreatic β-cells is associated with the

concomitant release of zinc from Zn^{2+}-containing granules, which allows the changes in the concentration of Zn^{2+} on the exterior of the plasma membrane to be used as a proxy for the release of insulin. This approach has been refined in recent work by Li and co-workers through the development of ZIMIR **22**, a selective sensor for Zn^{2+} that utilises two dodecyl chains as a targeting group (Figure 3-12).[50] The group demonstrated ZIMIR anchors on the extracellular face of the plasma membrane, and can be used to monitor the response of the pancreatic cells in releasing zinc to various stimuli with high spatial resolution.

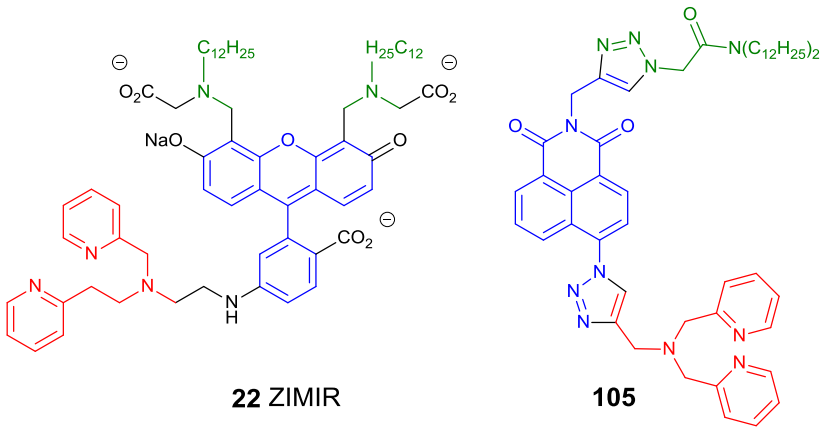

Figure 3-12 ZIMIR, an extracellular-membrane probe for Zn^{2+} and **105** .

As Figure 3-12 demonstrates, the structure and *in vitro* behaviour of sensor **105** bears remarkable similarities to ZIMIR in that both: i) possess a surfactant-like structure, which in the case of ZIMIR has been shown to localize the sensor to the extracellular face of the plasma membrane; ii) display a large increase in fluorescence output in the presence of excess Zn^{2+} (70-fold in the case of ZIMIR, 35 fold in the case of sensor **27**); and iii) demonstrate selectivity for Zn^{2+} over other biologically available divalent metal ions.

Given the utility of ZIMIR **22** in monitoring the stimulated efflux of zinc, we decided to evaluate probe **105** *in cellulo* in collaboration with Prof. Guy Rutter and Dr David Hodson, based at Imperial College and who worked on ZIMIR, to see if it displayed similar membrane targeting behaviour in pancreatic islet cells. We also decided to screen a

selection of the other sensors we synthesised for this study to validate our hypothesis and visualise the targeting capabilities of both our intra- and extra-cellular targeted fluorescent probes.

As predicted in our *in-vitro* testing, sensor **107** was not viable for cell studies due to its immediate precipitation in physiological buffer (HEPES-bicarbonate buffer (120 mM NaCl, 4.8 mM KCl, 24 mM $NaHCO_3$, 0.5 mM Na_2HPO_4, 5 mM HEPES, 2.5 mM $CaCl_2$ and 1.2 mM $MgCl_2$) saturated with 95% O_2/5% CO_2 and adjusted to pH 7.4). Probe **116** was also not tested in this context as the glucose unit appended as the targeting group on the probe could stimulate random and unwanted zinc secretions from these types of pancreatic islet cells. Importantly, all of the other probes tested retained their 'switch-on' response towards Zn^{2+} in the physiological buffer, and so were deemed viable for loading onto cells.

*3.2.6.2. Testing of Sensor **105** [4]*

Sensor **105** (30 μm) was incubated with pancreatic islet cells for 1 h, which were then washed under a steady flow of biological buffer for the remainder of the experiment to remove unbound sensor. In order to overcome the less favourable absorption/emission profile of sensor **105** compared with ZIMIR **22** (λ_{ex} = 493 nm, λ_{em} = 518 nm *vs* λ_{ex} = 347 nm, λ_{em} = 443 nm), the cells were imaged using 2-photon excitation (λ_{ex} = 850 nm), to visualise the distribution of the probe within the first few islet layers. Two-photon microscopy is fast becoming the imaging tool of choice, particularly at a sub-cellular level, as it allows for deeper imaging in tissues and cells and sharper imaging compared with conventional fluorescence microscopy.[184] The low energy excitation wavelengths are also advantageous in minimising photobleaching and cellular damage, something which was particularly key

[4] Isolation of murine pancreatic islet cells, and MIN6 cells for toxicity studies, and all microscopy work was carried out by Dr David Hodson. JP assisted with the loading of probes onto pancreatic islet cells and making of solutions used, as well as observation of the epifluorescence studies on all probes tested.

for us using UV-excitatable naphthalimide fluorophores in our sensors. Two-photon microscopy allowed us to overcome any limitations of UV-bleaching when imaging the islet cells and allowed for longer imaging times with little cell damage.

After incubation and irrigation with buffer, the imaging showed sensor **105** remained clearly localised on the cell surface, appearing to stain the plasma membrane in a manner similar to ZIMIR with little or no internalisation of the probe over the time scale of the experiment. (Figure 3-13**a**) This clearly demonstrates that **105** targets the extracellular membrane with our chosen targeting group.

We also investigated the response of **105** to changes in the extracellular concentration of Zn^{2+} using fluorescence microscopy. Trivially, addition of extracellular Zn^{2+} led to an increase in fluorescence, to confirm the presence and localisation of **105** as anchored on the extracellular face of the plasma membrane (Figure 3-13**b**). More interestingly, when KCl was administered, to cause membrane depolarisation and concomitant release of insulin and Zn^{2+} into the extracellular space, sensor **105** exhibited a strong fluorescence response (Figure 3-13**c** and **d**) in a manner similar to that previously observed with ZIMIR, and the epifluorescence images in Figure 3-13**d** clearly demonstrate the success and intensity of the 'switch-on' response *in-cellulo.* Using glucose as a stimulus for the cell also gave a moderate response, but still a definite 'switch-on' visible by microscopy. Therefore these results suggest that not only does readily available sensor **105** successfully localise on the extracellular membrane, but it could also be used to map the release of insulin at the cellular level.

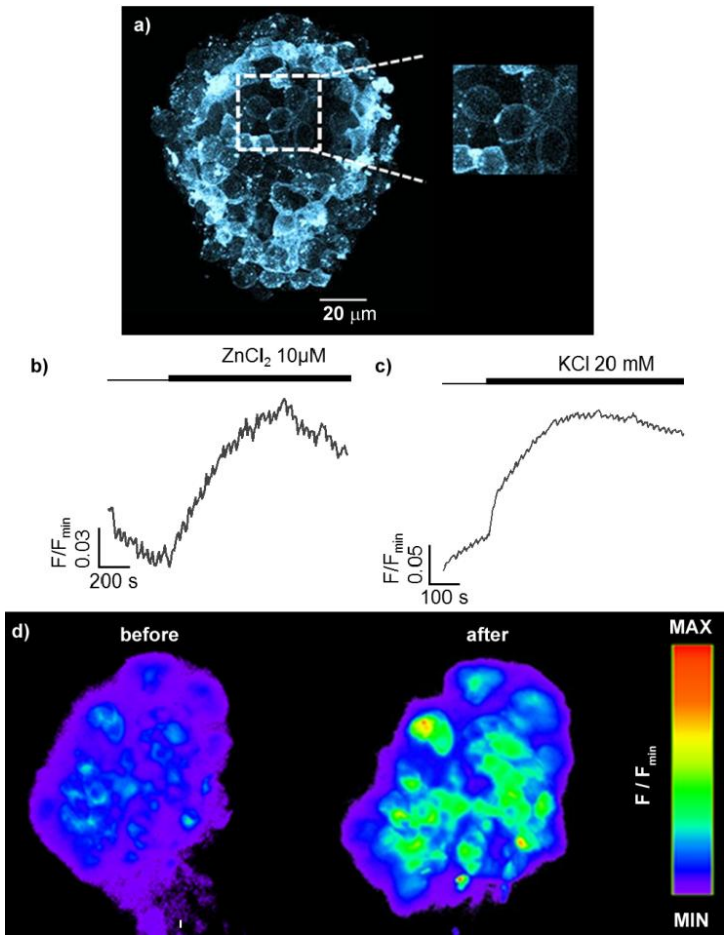

Figure 3-13 Fluorescence study of primary mouse islets of Langerhans incubated for 1 h with **105** (30 μM). a) Two photon image (λ_{ex} = 850 nm, λ_{em} = 400-550 nm, max z-projection 80-100 μm); Response of sensor **105** over time to exogenous b) 10 μM $ZnCl_2$ and c) 20 mM KCl measured by epifluorescence microscopy. d) Epifluorescence images demonstrating the response to Zn^{2+} co-released with insulin from dense core secretory granules after stimulation with KCl (20 mM)

Intriguingly, when the same experiment was attempted with sensor **109**, despite the structurally similarity to sensor **105** (polar metal binding unit, lipophilic tail), no increased fluorescence response in the cell membrane was observed, which once again demonstrates the unpredictable behaviour of designed probes in biological settings, and highlights the need to be able to rapidly modify probe structures at any stage of a study.

*3.2.6.3. Testing of Probes **112** and **114***

We also investigated the *in cellulo* behaviour of probe **112**, appended with a triphenylphosphonium ion for targeting mitochondrial space, in the same manner as probe

105. As Figure 3-14a clearly shows, the qualitative appearance of the two photon microscopy image is not only distinctly different to that of sensor **105** (Figure 3-13a), but demonstrates a stippled, internalised appearance commonly seen with mitochondrial stains. Epifluorescence imaging using cell stimuli (both exogenous $ZnCl_2$ and KCl to fully depolarise the membrane) clearly demonstrate a lack of response of the probe to extracellular events (Figure 3-14**c**). To further confirm its internalisation into cell compartments, using pyrithione to compromise the cell membrane and additional $ZnCl_2$ we were able to visualise a significant increase in fluorescence (Figure 3-14**d**).

The two photon microscopy imaging of probe **114**, appended with the ethylenediamine unit to localise the probe into lysosomal compartments, was also carried out. Figure 3-14**b** shows that whilst **114** also displayed an extranuclear localisation with a punctate appearance, consistent with its presence in or on intracellular organelles, the appearance of islets incubated with sensor **114** is qualitatively different to those incubated with mitochondria targeted probe **112**, with **114** localised in larger bodies. In a similar manner, it also demonstrated no response to extracellular stimuli during epifluoresence imaging, and a significant 'switch-on' response upon administration of pyrithione and $ZnCl_2$ to the islets.

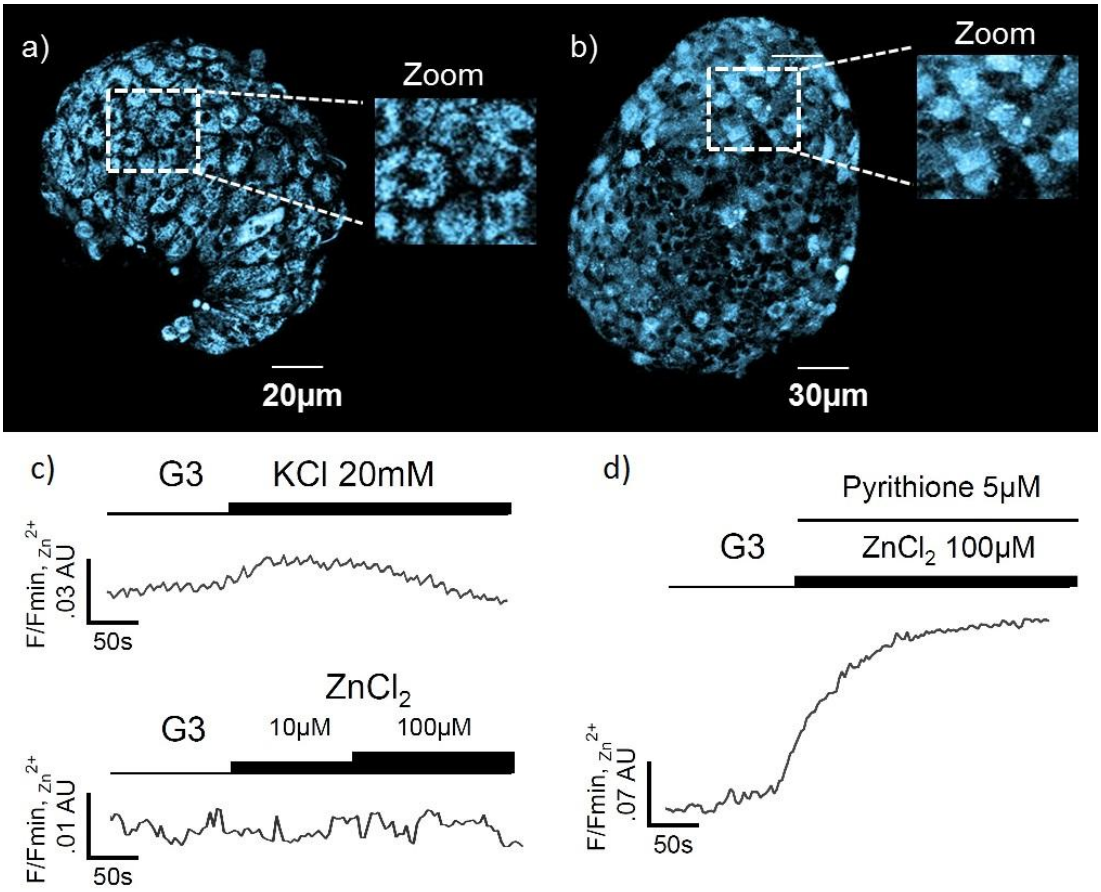

Figure 3-14 Fluorescence study of primary mouse islets of Langerhans incubated for 1 h with **112** (30 µM) and **114** (300 µM). Two photon image (λ_{ex} = 850 nm, λ_{em} = 400-550 nm, max z-projection 80-100 µm) of a) **112** and b) **114**. Response of sensor **112** over time to exogenous c) 10 µM $ZnCl_2$ and 20 mM KCl, and d) 5 µm pyrithione co-administered with 100µm $ZnCl_2$, measured by epifluorescence microscopy.

*3.2.6.4. Co-localisation and Cytotoxicity Studies of Probes **105**, **112** and **114***

The selective and differential localisation of **112** and **114** in the cell was confirmed by co-localisation with Mitotracker and Lysotracker respectively (Figure 3-15**c**). Both are commercially available dyes commonly used in cell staining for their respective organelles, and we observed efficient co-localisation, as demonstrated by the correlation co-efficients obtained. The very strong correlation of **112** and **114** with their respective stains is a clear indicator of successful localisation of our probes in the intended compartments of the cell. Finally, we were also able to show that none of the probes were cytotoxic as incubation of

mouse islets with probes **105**, **112** and **114** does not significantly induce cell death (necrosis) compared to DMSO alone (Figure 3-15**a** and **b**).

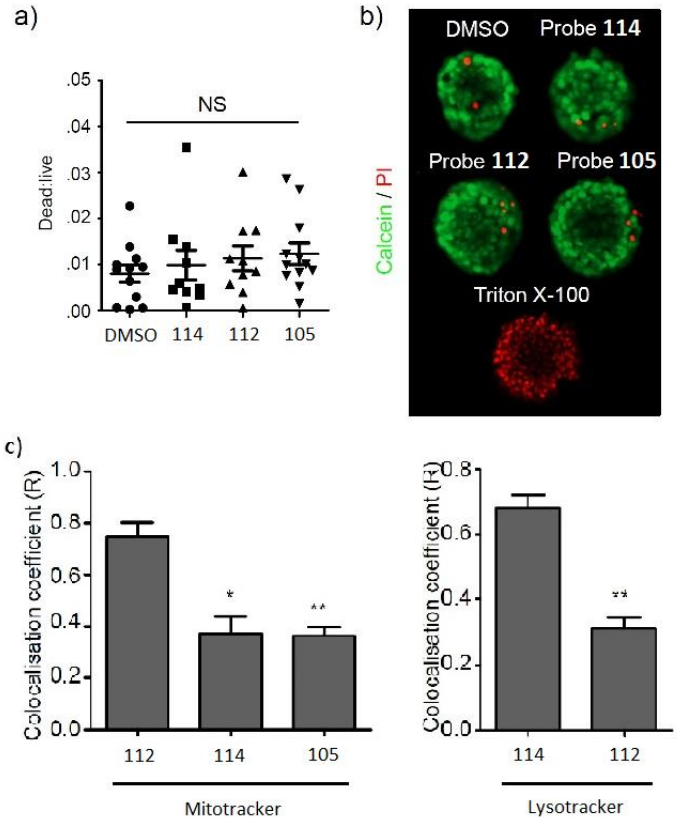

Figure 3-15 Cytotoxicity and co-localisation assays for probes **105**, **112** and **114**. a) Incubation of mouse islets with probes **105**, **112** and **114** does not significantly induce cell death (necrosis) versus DMSO-alone (1:333) (NS, non-significant; P<0.54). b) Representative images showing calcein and PI staining in islets treated with DMSO and probes **105**, **112** and **114**. Below is a positive control (Triton X-100; to permeabilise the membrane). c) Statistical analysis of probe localisation with Mitotracker and Lysotracker.

3.3. Conclusions and Future Work

These results clearly show that the one-pot iterative method can be used to synthesise fluorescent sensors efficiently and rapidly, by utilising biological targeting groups bearing either an azide or an alkyne with central building blocks **69** or **70** respectively, and metal binding ligands incorporating an alkyne moiety. All six successful sensors were isolated in good to excellent yields over three steps that correspond to an average of 85-92% for each chemical step. We anticipate that this approach will significantly accelerate the

development of probes for application in biological systems, as the units and the probes as a whole are accessible in a synthetically flexible and expedient manner.

The importance of ease of synthesis in order to overcome the difficulties associated with their unpredictable behaviour *in cellulo* was inadvertently exemplified through the different responses of **105**, **107** and **109**, all of which were originally designed for staining the plasma membrane in biological systems.

Testing of sensors **105**, **112** and **114** bearing different targeting units in pancreatic islet cells demonstrated not only their differential localisation but also their divergent responses to extracellular stimuli, suggestive of applications in the study of Zn^{2+} trafficking in the subcellular space. In particular, sensor **105** successfully allowed us to monitor insulin release *in vitro* in living pancreatic islet cells, using Zn^{2+} as a proxy, in a manner analogous to ZIMIR **22** but with the advantage of being significantly less challenging to prepare and showing improved dynamic range *in cellulo*. This is suggestive of great potential for probes like ours in the high resolution imaging of insulin secretion, an important goal in the study of diabetes. We believe our modular synthetic approach will facilitate the future optimisation and application of targeted Zn^{2+} sensors for biology, allowing the manufacture of tailor-made probes, such as **105**, with applicability for the study of Zn^{2+}-signalling and insulin exocytosis.

Often chemosensors that have been developed for sensing are very specific for the cation they intend to probe, and cannot be readily modified to sense other analytes. As a future application, our approach potentially allows us to expand the scope of cation sensing and incorporate other ligands with known specific affinity for other metals and incorporate those into our scaffolds to readily create other new sensors for toxic metals and other biologically relevant species. The same could also be said for expanding the scope of targeting group, to include small molecules to target synapses and neurotransmitters, or

even short peptide sequences known to interact with specific proteins or with specific cell types.

It would also be of interest to investigate the behaviour of the glucose appended sensor **116** *in cellulo*. It is known that cancerous cells overexpress lectins on their surface that partake in known interactions with carbohydrates, and the ability to target these lectins could allow for facile and specific imaging of cancerous cells,[59] particularly those associated with prostate cancer, a disease that zinc is known to be implicated in. In a similar manner to the work carried out by Scanlan and co-workers,[59] our methodology would allow for the rapid synthesis of a library of probes with mono and di-saccharides intended to target these cells for imaging purposes.

The blue-emission characteristics of these probes can additionally allow for multicolour imaging of a cell when used alongside other alternative cell stains for different compartments, and collaborations are currently ongoing towards this aim. Ultimately, the ease of this synthetic route could help to overcome many barriers currently being faced by cell biologists in the field of imaging of cells and organelles in many disease states associated with zinc.

Chapter 4: Chapter 4 Header

4.1. Introduction to Rotaxanes

A rotaxane, specifically a [2]rotaxane, is an interlocked structure consisting of a ring shaped molecule, known as a macrocycle, threaded onto a dumbbell shaped molecule known as a thread. This type of structure allows the macrocycle to move freely across the thread without slipping off at the ends, as the ends of the thread act as stoppers to prevent this. The two components are not covalently linked, but their separation would require the breaking of a covalent bond in the structure. Rotaxanes with more than two components, for example with two macrocycles on one thread, are known as [3]rotaxanes; and so with *n* components, these types of supramolecular structures are [*n*]rotaxanes (Figure 4-1).

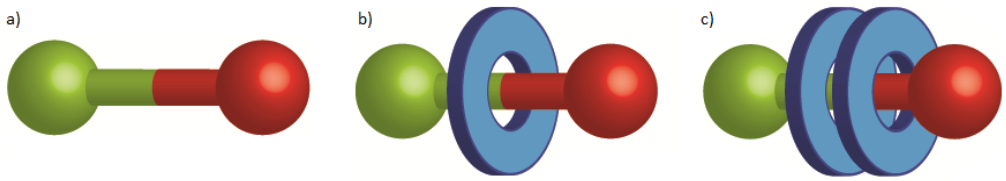

Figure 4-1 Representation of a) a thread and its corresponding b) [2]rotaxane and c) [3]rotaxane

4.2. Synthesis of Rotaxanes

One of the first accounts of rotaxane formation in 1967 relied on the statistical probability that in the presence of a macrocycle, the joining of two half thread components would occur through the ring (Scheme 4-1). [185] Whilst this gave a 6% yield of the interlocked structure **119**, the methodology was cumbersome and inefficient; clearly unreliable for a desired high-yielding synthesis.

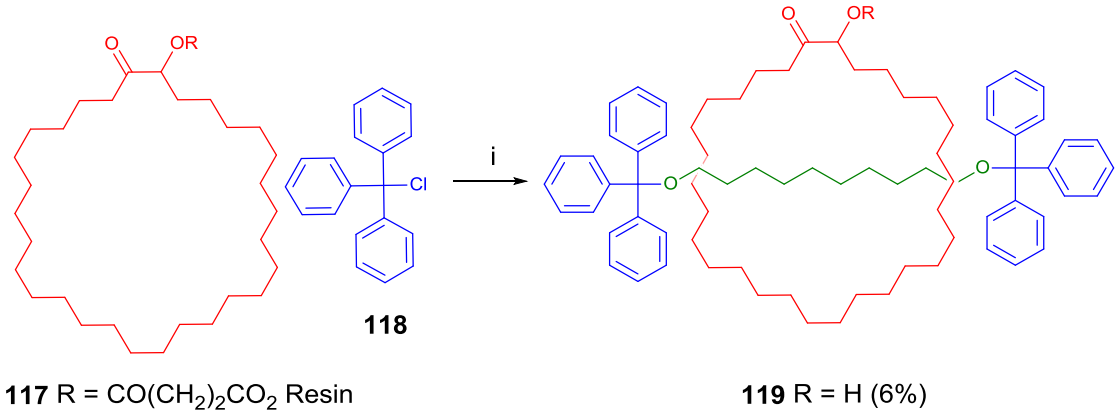

Scheme 4-1 [2]Rotaxane **119** as synthesised by Harrison and Harrison in 1967. Conditions: i) Decane-1,10-diol, pyridine/DMF/toluene, 70 repetitions, followed by resin removal from macrocycle.

The development of the 'Passive Template' methodology pioneered by Sauvage and co-workers made the synthesis of interlocked molecules much easier.[186] In this approach the components are pre-arranged by a template before formation of the final covalent bond to form the interlocked structure. In the case of [2]rotaxane formation, this commonly involves one of two methods: [187]

a) Stoppering or capping, the threading of a molecule through the macrocycle cavity and then stoppering either end of the thread;

b) Clipping, the formation (closing) of a macrocycle from its precursor around the pre-formed stoppered thread.

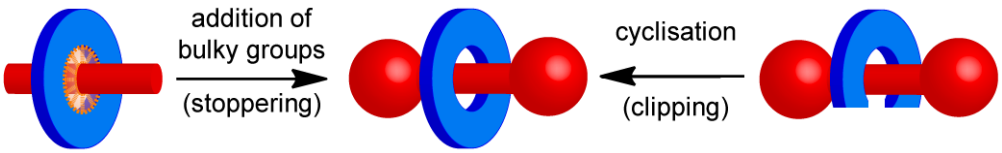

Figure 4-2 Representation of the stoppering and clipping methods of forming [2]rotaxanes

This pre-arrangement can be mediated by templates such as hydrogen bonding, electrostatic interactions, halogen bonding, and can also be metal mediated. In these instances, the metal used merely acts as an aid to pre-arrangement of the components. Its inherent reactivity is ignored and unused for the subsequent covalent bond formation to yield the final interlocked product.

4.3. Active Template Methodology of [2]Rotaxane Synthesis

The active template methodology was first reported by the Leigh group, and this has greatly facilitated access to structures like rotaxanes, catenanes and other interlocked structures.[187–189] This approach uses transition metal-catalysed reactions such as Pd-catalysed Heck reactions, and the CuAAC reaction to both template the formation and catalyse the joining of the half-thread components together to successfully form rotaxanes (Figure 4-3). This offered many advantages to the passive template methods. These methods can provide shorter reaction times and an operationally-simple synthesis, only use sub-stoichiometric amounts of the metal which effectively acts as a traceless mediator of formation, and allow for higher molecular diversity not previously possible with passive template components due to a need for recognition sites for the template.

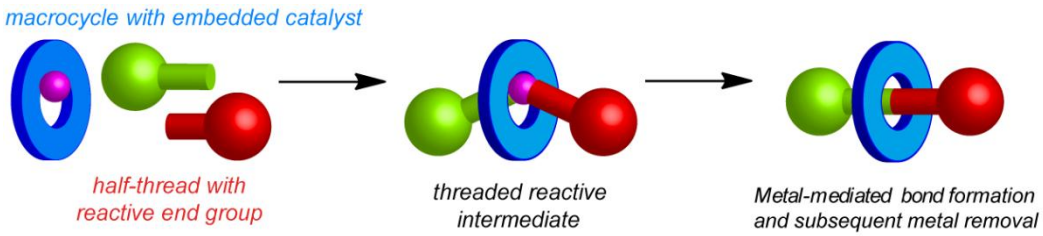

Figure 4-3 Representation of the metal-mediated active template synthesis to form [2]rotaxanes.

The first active template-CuAAC (AT-CuAAC) for the formation of [2]rotaxanes was reported in 2006 (Scheme 4-2)[190] and since then has provided access to many novel rotaxanes, catenanes and molecular machines with varying properties and function. However, these

reactions employed large macrocycles, and therefore bulky half threads to form rotaxanes such as **120**, limiting the architectures that could be accessed and their diversity.

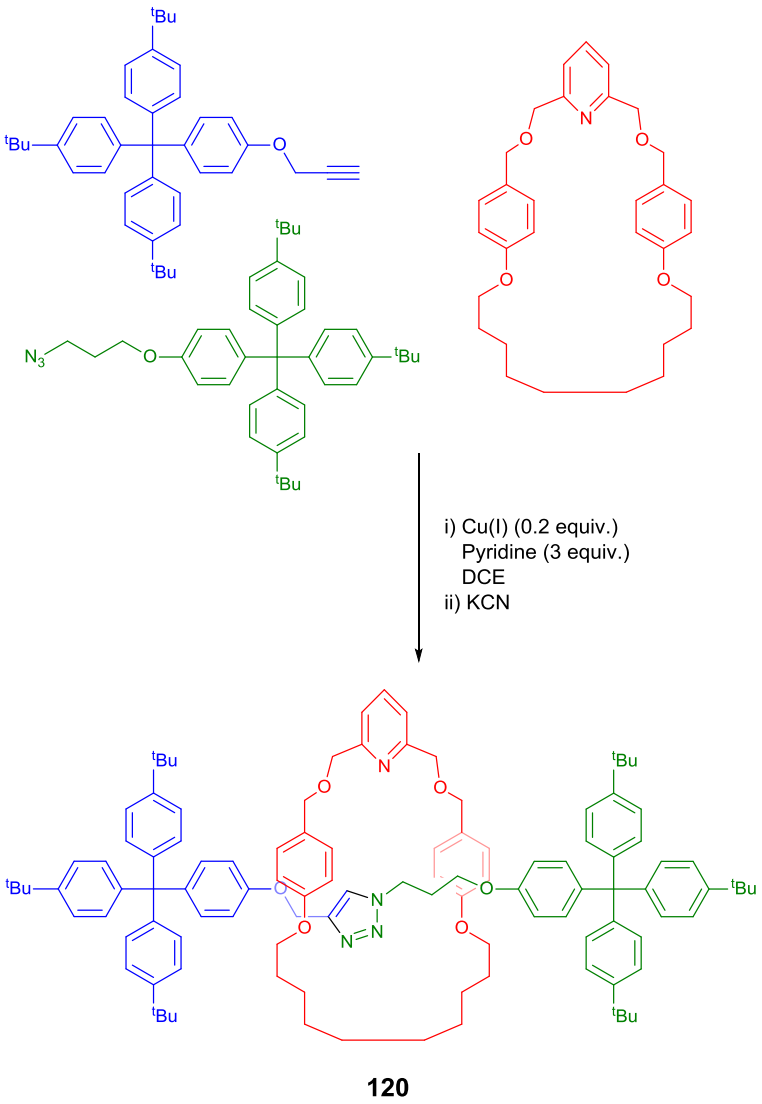

120

Scheme 4-2 AT-CuAAC synthesis from Leigh and co-workers to synthesise [2]rotaxane **120**

More recently, the Goldup group reported the use of small macrocycles with small half threads as stoppers, such as **122** and **123** to synthesise [2]rotaxanes with the highest yielding AT synthesis to date.[191] As with all CuAAC reactions, this readily allows for the synthesis of supramolecular constructs with high molecular diversity, and the structures obtained can be easily modified to investigate and facilitate novel functions and applications.[192] A particular highlight was the serendipitous isolation and characterisation of

an interlocked Cu(I) triazolide **124**, sterically protected by the crowded nature of these small rotaxanes which was found to be very stable.[193] This was the second time the triazolide intermediate had been observed, and the first time it was isolated from a direct CuAAC reaction, and is an example of how active template synthesis can help in the elucidation of key steps and intermediates in transition metal-catalysed reactions.

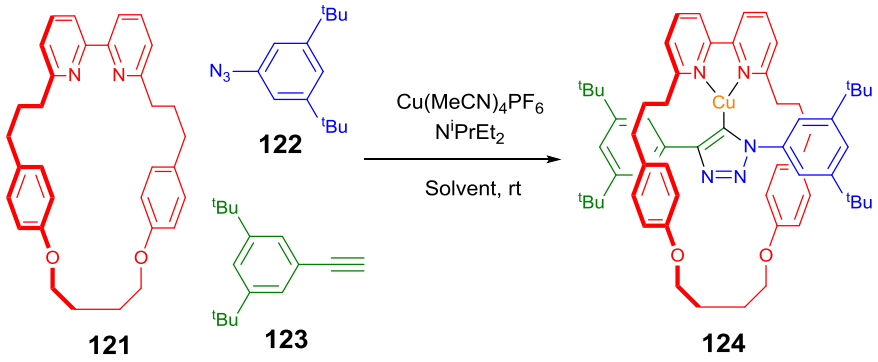

Scheme 4-3 Synthesis of Cu-triazolide **124** by Goldup and co-workers

4.4. Rotaxanes as Fluorescent Sensors

There are many examples of luminescent rotaxanes in the literature. Their interesting features and properties come from the restricted motion of the components of the rotaxanes; the mechanical motions of a shuttling and pirouetting macrocycle can alter the photophysical properties of these molecules in relation to their non-interlocked components, and means these types of molecules can be used as chemosensors for recognition of binding events.

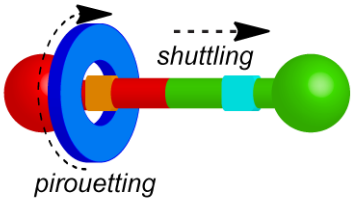

Figure 4-4 Representation of pirouetting and shuttling of a macrocycle on a [2]rotaxane.

Perhaps the most popular use for rotaxanes as chemosensors are those used as anion detection systems. Generally these systems are synthesised by passive anion-templated methods, and working examples have been reported and summarised in excellent reviews by Beer and co-workers,[194,195] and Ma *et al.*.[196]

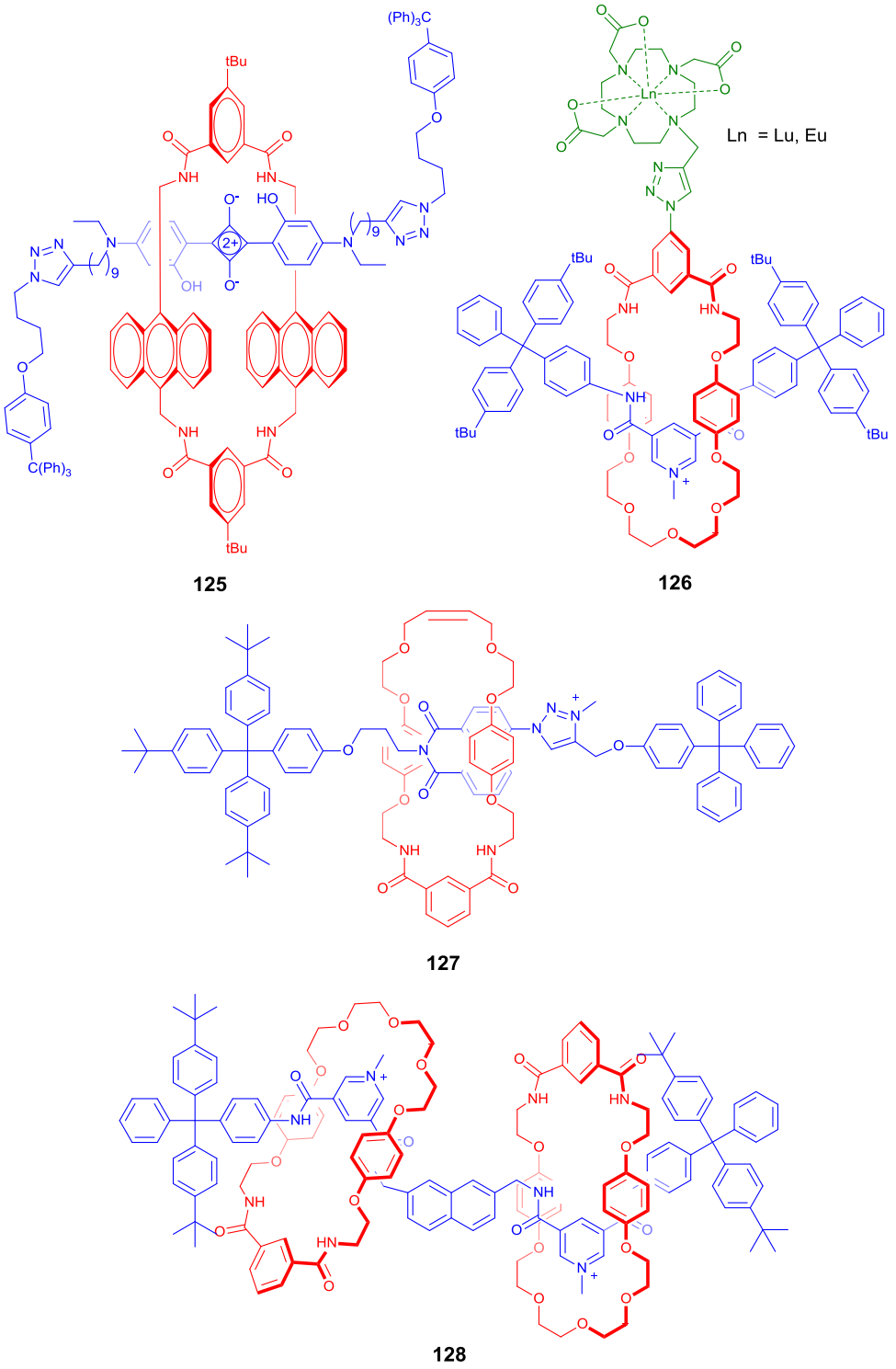

Figure 4-5 Anion-sensing [2]rotaxanes **125–127**, and [3]rotaxane **128**.

Some interesting examples are shown in Figure 4-5, incorporating commonly available organic luminescent units that work effectively to aid selective sensing of the desired anion, such as naphthalenes,[197] squaraines,[198] naphthalimides [199] and additional lanthanide motifs.[200]

In contrast, there are limited examples of rotaxanes which elicit a photophysical response based on cationic guest/host interactions. One of the earliest examples is from 1996, when Swager and co-workers presented a polyrotaxane polymer **129**, in which the binding of Cu^+ resulted in greater conductivity of the polymer and a red-shift of the UV-Vis absorption, rendering the polymer a successful Cu^+ sensor in CH_2Cl_2. [201]

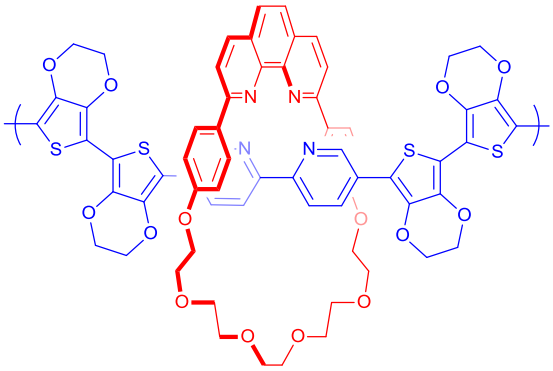

129

Figure 4-6 Cu^+ binding polyrotaxane synthesised by Swager and co-workers.

Hiratani and co-workers synthesised a [1]rotaxane **130** stoppered by an anthracene group, in which the binding of Li^+ in CH_2Cl_2/MeCN (9:1) selectively induced a conformational change in the position of the anthracene group to the macrocycle, resulting in a greater energy transfer from macrocycle to fluorophore and chelation enhanced fluorescence (CHEF). [202] The binding was monitored by fluorescence spectroscopy with a broad emission band centred around 420 nm (Figure 4-7).

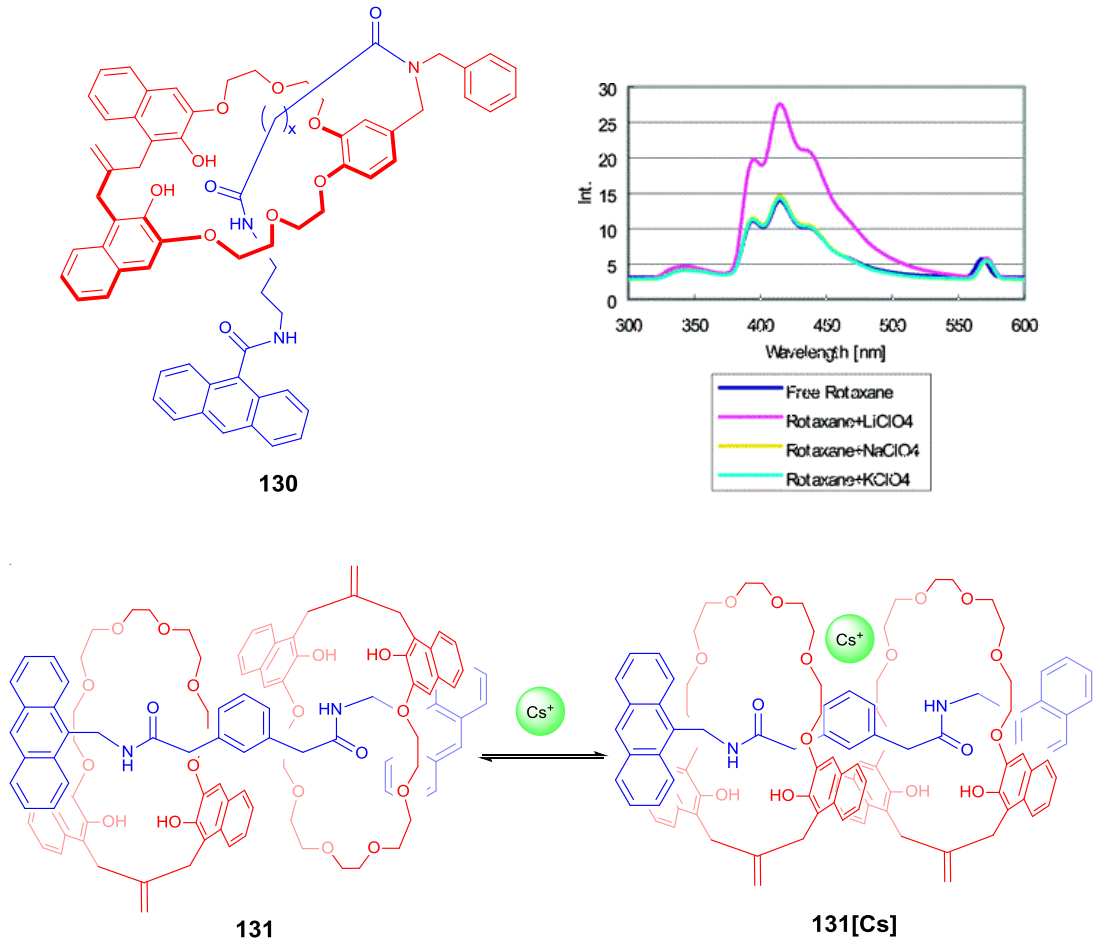

Figure 4-7 Anthracene-appended [1]rotaxane **130** and its emission spectra in the presence of analytes tested. Image reproduced with permission from Journal of the American Chemical Society, 2004, 126, p 13568 - 13569. Copyright © 2004 American Chemical Society b) [3]rotaxane **131** and its binding mode with Cs^+

The same group also synthesised a [3]rotaxane **131** as shown in Figure 4-7, with anthracene groups again, this time as appended stoppers on the two-macrocycle system. [203] They observed when binding to Li^+, two cations ions were incorporated into the [3]rotaxane, but in the case of Cs^+ 1:1 binding with the [3]rotaxane was observed (figure 4-7). They proposed that the Cs^+ ion encouraged a change in orientation of both macrocycles to form a sandwich complex with the cation, and confirm this by NOESY NMR spectroscopy and mass spectrometry. The addition of Cs^+ and the conformational change also induced CHEF which was observed by fluorescence spectroscopy, with excitation at 285 nm.

Li *et al.* synthesised a fluorescent switchable [2]rotaxane **132** with two different recognition sites on the thread, an amide and an amine.[204] The addition of acid and base causes the macrocycle to shuttle between the two stations, as did the addition of either Li^+ or Zn^{2+}. The fluorescence output of the anthracene moiety on the thread is dependent on the motion and station choice of the macrocycle. In the case of Li^+, the fluorescence of the [2]rotaxane is weak as the macrocycle binds and sits at the amide station, so the amine is available to participate in PET quenching of the anthracene stopper (**132[Li]**, Scheme 4-4). Binding of Zn^{2+} both displaces the Li^+ ion and results in the shuttling of the macrocycle to the amine station (**132[Zn]**), resulting in enhanced fluorescence of anthracene by eliminating PET quenching (λ_{ex} **132[Zn]** 370nm, λ_{em} **132[Zn]** max 422nm).

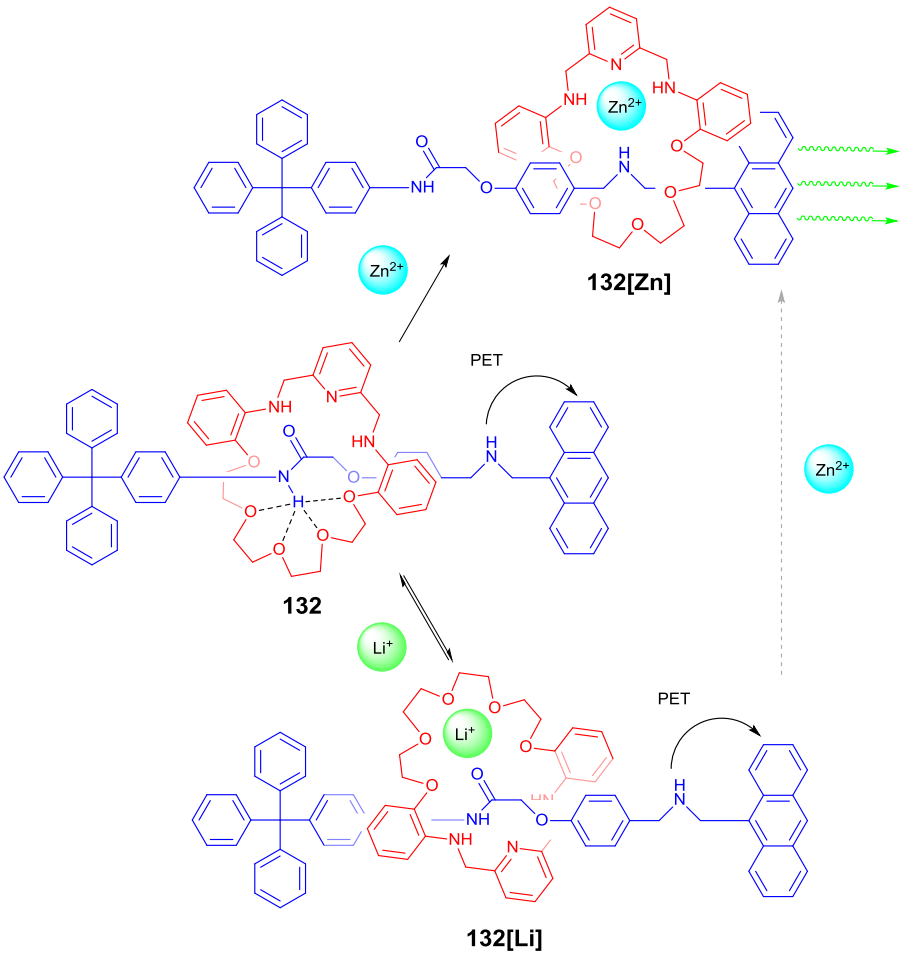

Scheme 4-4 [2]Rotaxane **132** by Li *et al.* and its shuttling modes with Li and Zn.

More recently, Smith and co-workers reported the synthesis and testing of squaraine rotaxane endoperoxides such as **133,** with sites for metal chelation and their response to metal cations.[205] Whilst the rotaxanes are not selective for a particular metal, the binding of Co^{2+}, Zn^{2+} and Ni^{2+} at the appended dipicolylamine binding sites on the thread induced quenching of the observed fluorescence of the rotaxane in MeCN (Figure 4-8, (a) and (b)).

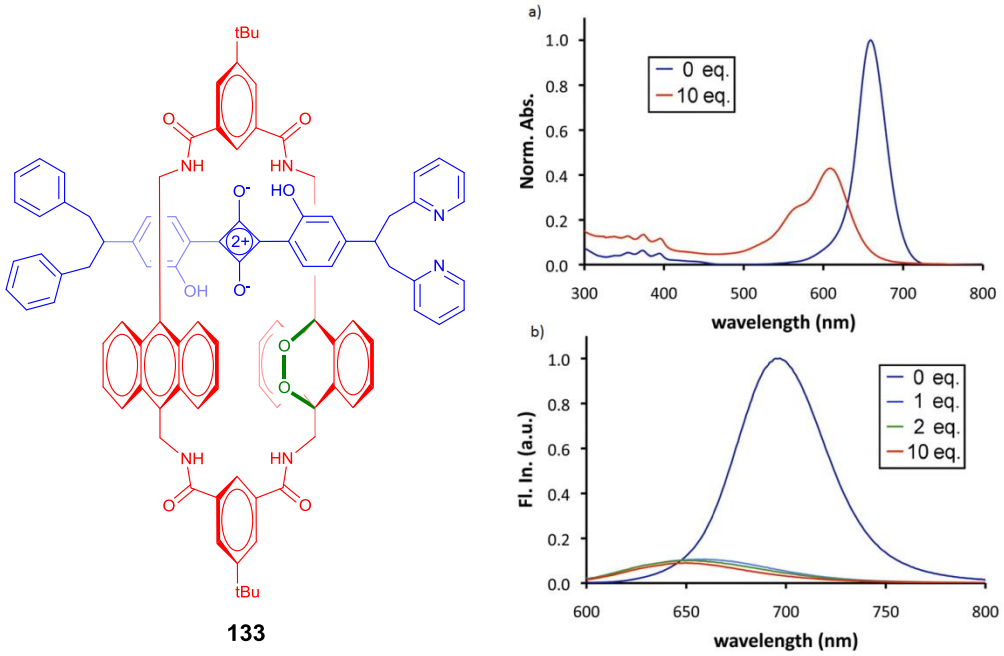

Figure 4-8 Squaraine endoperoxide rotaxane **133**, and its a) absorption and b) emission spectra in the presence of Zn^{2+}. Images reproduced with permission from Taylor & Francis.[205] Copyright © 2012, Taylor & Francis.

4.5. Aims for This Project

Whilst each of these systems has interesting properties, it is of note that all of them suffer with difficult and low yielding syntheses. They also often require mixtures of solvent due to solubility issues of such large structures. Additionally, as AT-CuAAC methodology could allow for the incorporation of a fluorescent unit into related structures this could provide a facile route into novel mechanically chelating rotaxane ligands, perhaps with the ideal optical properties to act as sensors.

Previously, when reporting the investigation into smaller [2]rotaxanes, the Goldup group synthesised a novel fluorescent rotaxane **134** incorporating a naphthalimide unit as one of the half-threads to demonstrate the utility of the synthesis and the smaller macrocycles.[191] The naphthalimide was shown to act as an efficient bulky stopper which prevented de-threading.

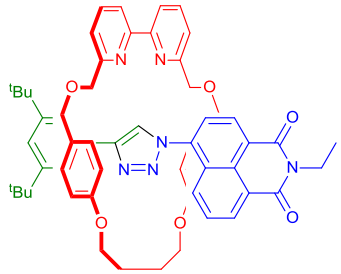

134

Figure 4-9 Naphthalimide [2]rotaxane **134** synthesised by Goldup and co-workers.

The incorporated bipyridine macrocycle is non fluorescent but is known to be able to act as a ligand for metal cations inside the rotaxane cavity, demonstrated in particular by the active template methodology used to synthesise the rotaxanes. We therefore anticipated that the rotaxane may be able to function as a sensor for metals *via* the unique movements of the macrocycle and perhaps a charge transfer mechanism from the macrocycle to the fluorophore during a signalling event. We aimed to investigate the capability of these systems for sensing metals, and ideally with Zn^{2+} in particular considering our previously demonstrated success in this field.[72,156] We also wanted to utilise the modularity of the AT-CuAAC to synthesise novel fluorescent rotaxanes with modified naphthalimide fluorophores to hopefully induce selectivity and a desirable 'off-on' response as a Zn^{2+} chemosensor, without perturbing the binding abilities of the macrocycle.

4.6. Preliminary Work [206]

Preliminary studies within our group focused on the photophysical properties of rotaxanes **134** and **137** in MeCN (Scheme 4-5). The synthesis was found to be very straightforward, with both the macrocycle **136** and half thread components **64**, **122** and **123** known in the literature. The alkyne-bearing fluorescent half thread **135** was synthesised in two steps in good yield, following a Sonogashira coupling of trimethylsilyl acetylene and bromo-naphthalimide **63,** and the subsequent removal of the TMS group with K_2CO_3. Using one equivalent of each respective half thread and macrocycle, 0.96 equivalents of Cu(I) and heating for 72 h in CH_2Cl_2 gave the desired rotaxane **134** and **137** in 99% and 91% yield respectively.

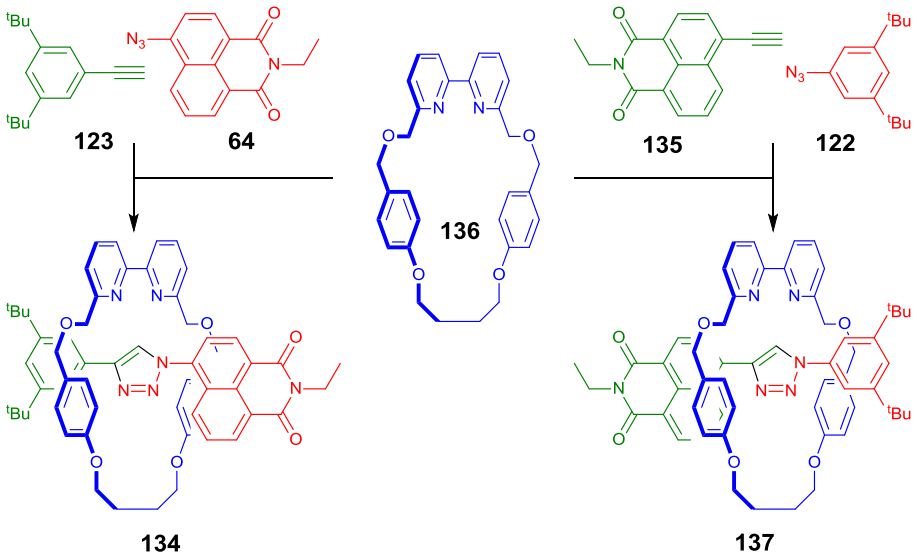

Scheme 4-5 Synthesis of rotaxanes **134** and **137**. Conditions: $[Cu(MeCN)_4]PF_6$, CH_2Cl_2, reflux 72 h, 99% (**134**), 91% (**137**).

Rotaxane **134** displayed an absorption at 344 nm in MeCN. Interestingly we observed two fluorescence emissions at 430 and 553 nm. Monitoring the binding of Zn^{2+} to the rotaxane clearly demonstrated a quenching effect of the metal binding event on the observed fluorescence of the more intense second band (Figure 4-10, (a)). In contrast the thread on

its own demonstrates no binding of zinc by both fluorescence and UV, and only has a single observed emission (Figure 4-10, (b)).

We thus tentatively attributed the second emission band to energy transfer between the aromatic groups on the macrocycle and the fluorophore upon excitation; i.e. exciplex formation. The metal binding in the macrocycle cavity presumably perturbs this interaction, causing a breakdown of the exciplex.[207,208]

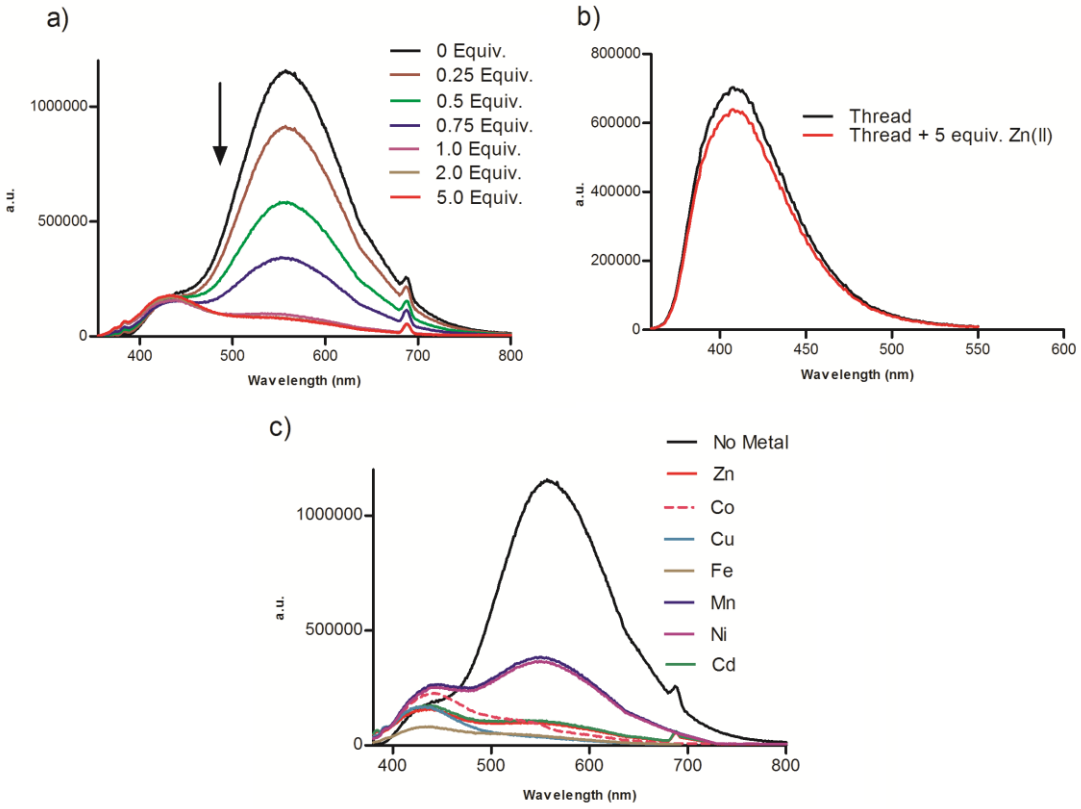

Figure 4-10 a) Fluorescence emission spectra of rotaxane **134** in MeCN titrated with increasing amounts of Zn^{2+}. b) Emission spectra of the thread component only in the absence and presence of Zn^{2+}. c) Emission spectra of rotaxane **134** in the presence of other metals, in MeCN.

Unfortunately this observed quenching of emission was not unique to Zn^{2+}, and we found that a range of biologically relevant metal ions induced the same quenching effect (Figure 4-10 (c)), rendering this rotaxane ineffective as a chemosensor.

In the case of rotaxane **137**, despite the only difference in structure being the orientation of the triazole, the system displays a single emission. Upon excitation at 381 nm in MeCN, the

emission is centred at λ_{max} 465nm. Interestingly, the emission increases at first, and is then quenched after the addition of 0.3 equivalents of Zn^{2+}, with a hypsochromic shift to 455 nm in emission. Overall this corresponds to a 'switch-off' response to Zn^{2+} with a blue shift in emission. The thread demonstrates no significant response to Zn^{2+}, again confirming the need for the interlocked structure form cation binding. As with rotaxane **134**, this response is not limited to Zn^{2+} (Figure 4-11).

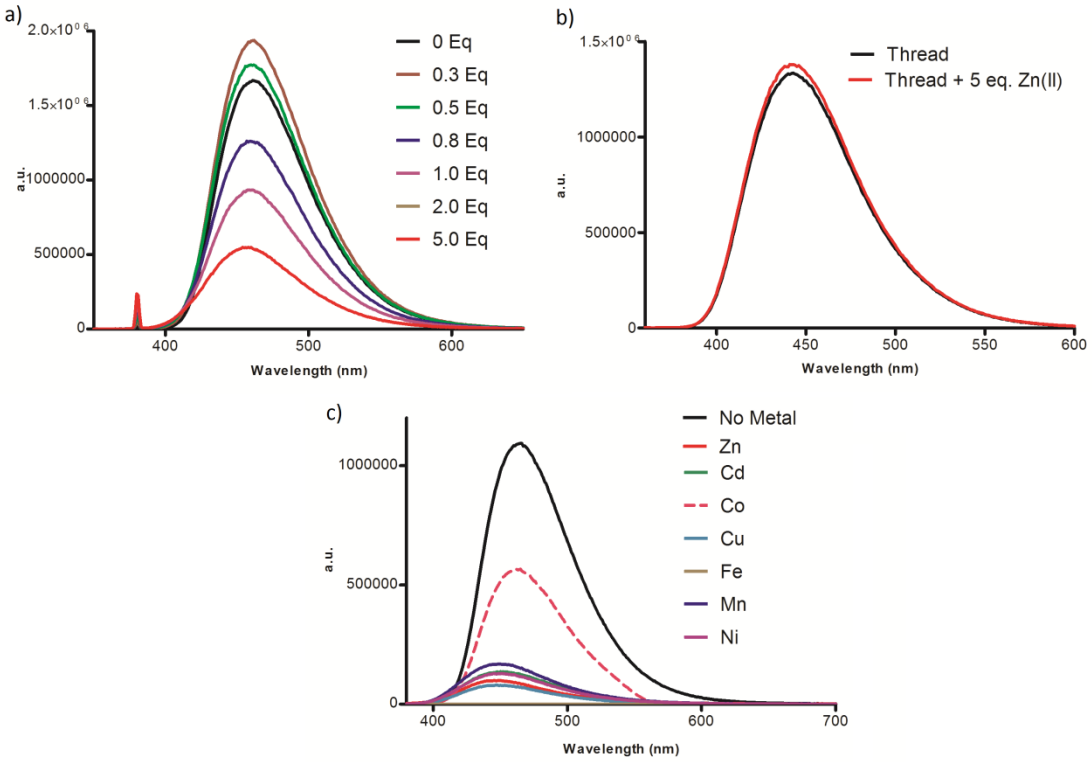

Figure 4-11 a) Fluorescence emission spectra of rotaxane **137** in MeCN titrated with increasing amounts of Zn^{2+}. b) Emission spectra of the thread component only in the absence and presence of Zn^{2+}. c) Emission spectra of rotaxane **137** in the presence of other metals, in MeCN.

4.7. Results and Discussion

4.7.1. Designing Modified Fluorescent Rotaxanes

The studies on rotaxanes **134** and **137** and their observed lack of selectivity led to a redesign in strategy. It is well known that the substitution at the 4-position of a naphthalimide fluorophore dictates the absorption and emission profile of these dyes, and

we felt we could utilise this to tune the optical output and aid the development of a cation-selective rotaxane.

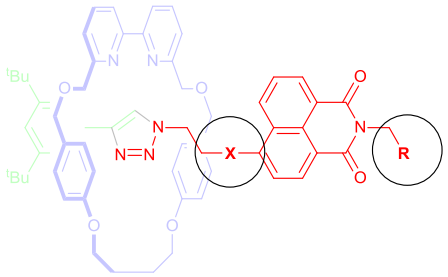

Figure 4-12 Proposed points of modification on a [2]rotaxane that will both lengthen the thread and incorporate an additional stoppering moiety

Figure 4-12 demonstrates our proposed points of modification. To incorporate an alternative substitution at the 4-position of the fluorescent half thread, an extra linker needed to be incorporated, thereby increasing the overall thread length. Recent work in the Goldup group has shown that in the case of more flexible threads, the ethyl-naphthalimide fluorophore is unable to prevent the macrocycle escaping the interlocked system. For this reason we decided to replace the ethylamine group with a 2,2-diphenyl ethylamine group.

4.7.2. Additional Stoppering of Rotaxanes

To confirm the incorporation of a 2,2-diphenyl ethylamine group at the imide position did not greatly affect the behaviour of the rotaxane, we first synthesised rotaxane **140**, an analogue of **137** with the additional stoppering group incorporated.

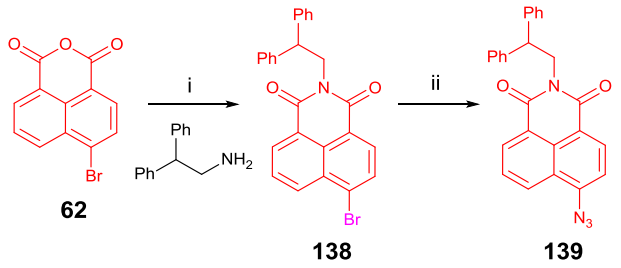

Scheme 4-6 Synthesis of half thread **139** incorporating the new 2,2-diphenyl ethylamine stopper. Conditions: i) EtOH, reflux 18 h, 97% ii) NaN_3, NMP, rt 24 h, 59%.

The fluorescent half thread was synthesised in an analogous manner to half thread **64**. After refluxing the naphthalic anhydride with diphenyl ethylamine in EtOH, the bromide **138** was obtained in quantitative yield. Stirring with NaN_3 in NMP at room temperature for 24 hours gave the azide half thread **139** in 59% yield after purification. Following a modified rotaxanation procedure,[193] the corresponding rotaxane was obtained in 88% yield following purification by column chromatography.

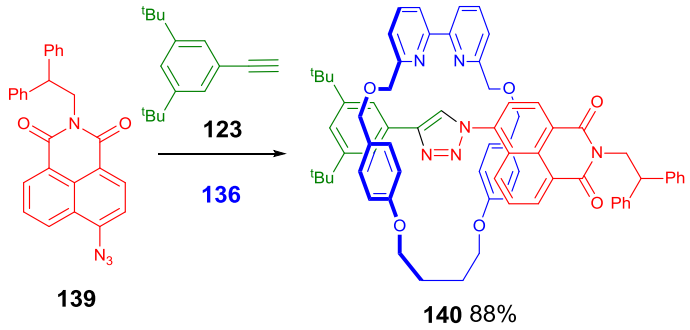

Scheme 4-7 Synthesis of rotaxane **140**. Conditions: $[Cu(MeCN)_4]PF_6$,(0.96 eq.), DIPEA (1 eq.), EtOH, rt, 16 h

Fluorescence spectroscopy studies on rotaxane **140** indicated the behaviour in MeCN in response to Zn^{2+} was analogous to that of **134**. The same dual band emission was observed, with the second more intense band being quenched upon addition up to 1 equivalent of Zn^{2+}, and remaining at a plateau as increasing equivalents were added. Similarly Rotaxane **140** failed to display any selectivity for first row biologically relevant transition metals or Cd^{2+}.

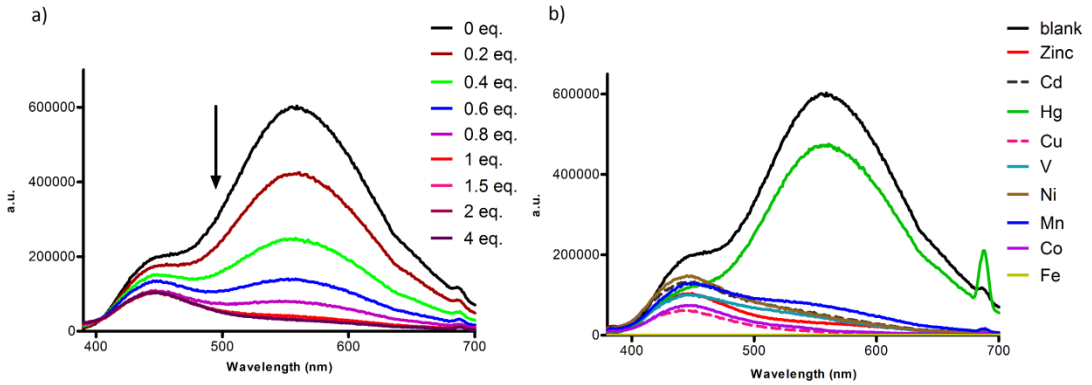

Figure 4-13 a) Fluorescence emission spectra of rotaxane **140** (100 µM) in MeCN titrated with increasing amounts of Zn^{2+}. b) Emission spectra of rotaxane **140** in the presence of other metals (5 equiv.) in MeCN.

Satisfied that the addition of the diphenyl stopper did not affect the binding behaviour and fluorescent profile of the rotaxanes, we could now study the effects of additional modifications of the fluorescent half-thread on the behaviour and selectivity of these rotaxane scaffolds.

4.7.3. Incorporation of Heteroatoms into the Fluorescent Half Thread

It is well known that the incorporation of heteroatoms, in particular at the 4-position of naphthalimide fluorophores, introduces an electron donation site, and so gives rise to highly emissive compounds. It was also hypothesised this extra potential co-cordination site for metals could help to induce selectivity, in the case of a 4-amino or 4-thio-naphthalimide. The desired half threads are demonstrated in Figure 4-14, incorporating an amine, amide and thio-ethanol derived group as shown.

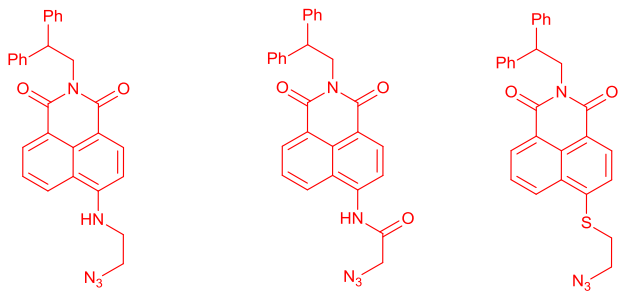

141 **142** **143**

Figure 4-14 New half threads **141-143** designed to incorporate heteroatoms into the rotaxane thread.

4.7.4. Synthesis of Azide Half Threads **141-143**

The synthetic route to the amino- and thio-ethanol derived **141** and **143** was identical. Heating bromide **138** in DMSO for 16 h with 2-aminoethanol or 2-mercaptoethanol under basic conditions gave the alcohol intermediates in good yields. Following this, the alcohol was transformed to the azide-furnished half thread using diphenylphosphoryl azide in a Mitsunobu-type reaction.

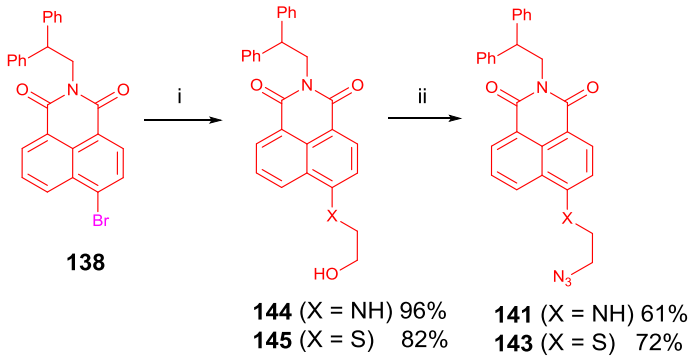

Scheme 4-8 Synthesis of half threads **141** and **143**. Conditions: i) 2-aminoethanol or 2-thioethanol, Cu_2O, K_2CO_3, DMSO, 80 °C, 16 h. ii) PPh_3, DEAD, diphenylphosphoryl azide, 0 °C, 2 h.

The amide-containing half thread **142** proved to be more challenging to synthesise. Starting from the 4-nitro naphthalic anhydride **146**, formation of the imide with diphenyl ethylamine was trivial, but the subsequent reduction to the 4-amino naphthalimide **148** was limited by the solubility of the nitro-compound **147**. A reduction using palladium-on-carbon in a 1:1 mixture of EtOAc/MeOH proved successful, with good yields of **148** obtained without the need for purification. Amide formation using chloroacetyl chloride was quantitative, and subsequent displacement of the chloride with an azide using NaN_3 gave half thread **142** in 84% yield.

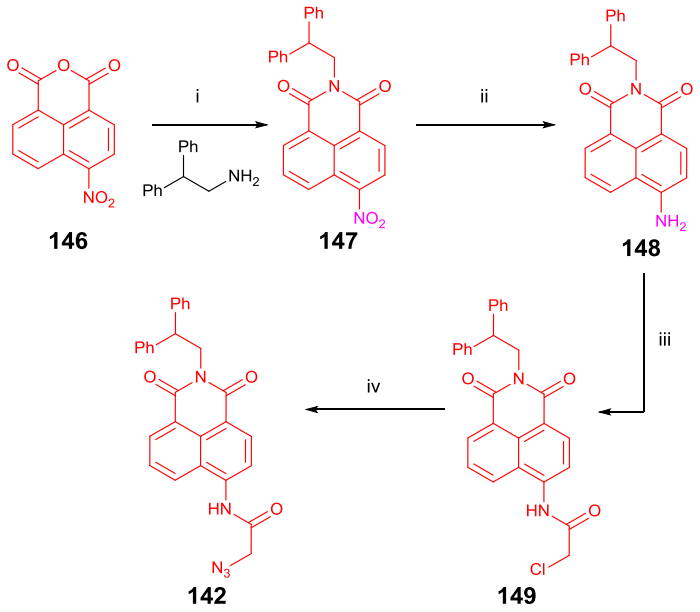

Scheme 4-9 Synthesis of half thread **142**. Conditions: i) EtOH, reflux, 16 h, 86%. ii) Pd/C (10 mol%), EtOAc/MeOH (1:1), rt, 4 h, 97%. iii) 2-chloroacetyl chloride, DMAP, THF, 0 °C to rt, 6 h, 98%. iv) NaN_3, DMF, rt, 24 h, 84%.

4.7.5. Rotaxane Synthesis and Testing

4.7.5.1. Amine-functionalised Rotaxane

Using the same conditions as in Scheme 4-7 for the synthesis of rotaxane **140**, amine-containing rotaxane **150** was synthesised from half thread **141,** 3,5-di-*tert*-butyl phenylacetylene and macrocycle **136** in 72% yield after purification (Scheme 4-9).

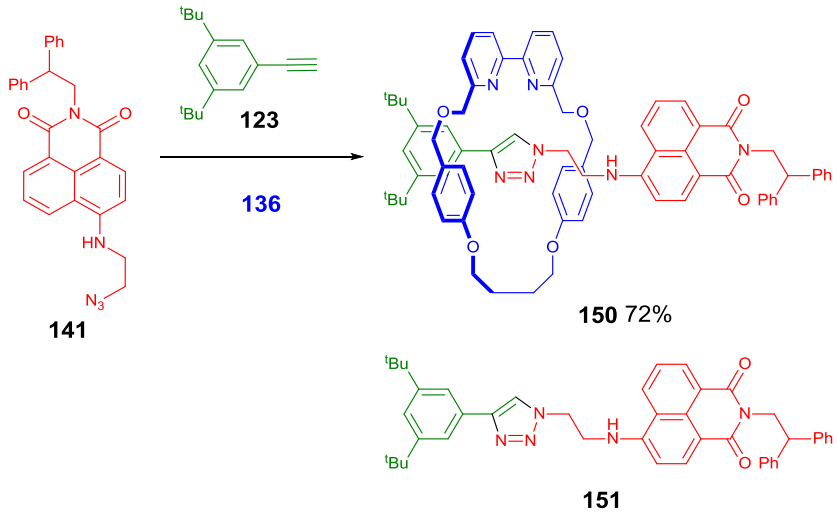

Scheme 4-10 Synthesis of rotaxane **150**. Conditions: $[Cu(MeCN)_4]PF_6$ (0.96 eq.), DIPEA (1 eq.), EtOH, rt, 16 h

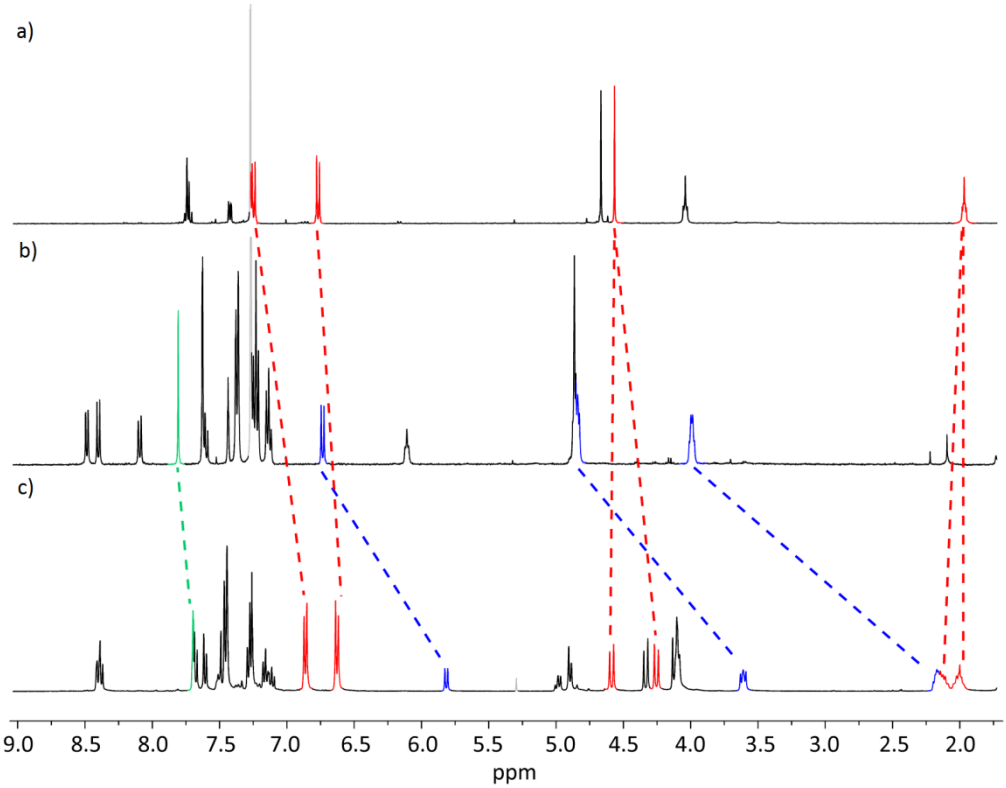

Figure 4-15 Partial 400 MHz 1H NMR spectra of a) macrocycle **136**, b) thread **151** and c) rotaxane **150** in CDCl3. Assignments as indicated in Section 5.3

Rotaxane **150** was identified as the most emissive of the rotaxanes synthesised with an intense yellow colour in solution, due to the electron donating nature of the 4-amino substitution pattern on the naphthalimide. A simple titration with zinc perchlorate showed the fluorescence was quenched upon addition of Zn^{2+}. The emission spectrum demonstrates a small hypsochromic shift in emission wavelength, from 510 nm for the free rotaxane, to 500 nm when bound with Zn^{2+}, indicating a binding interaction of the amine moiety. The UV absorption profile demonstrates a similar blue-shift from 440 nm to 420 nm.

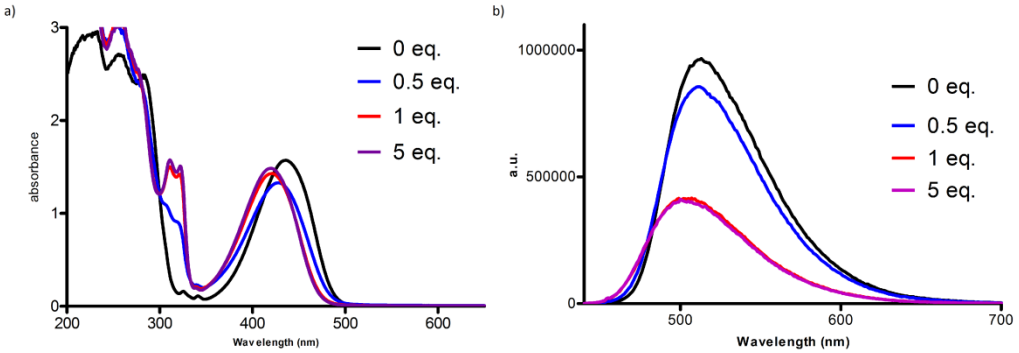

Figure 4-16 a) UV-Vis absorption spectra of samples of rotaxane **150** (100 µM) in MeCN titrated with increasing amounts of Zn^{2+}. b) Fluorescence mission spectra of samples of rotaxane **150** in MeCN titrated with increasing amounts of Zn^{2+}.

The emergence of 2 sharp bands at 314 nm and 322 nm, increasing with binding of Zn^{2+} to rotaxane **150** is clearly observed in the absorption profile (Figure 4-16), however, a UV-Vis spectroscopic titration of the macrocycle **136** on its own with Zn^{2+} shows the same emission bands, indicating the absorptions are due to the binding of metal to the bipyridine moiety.

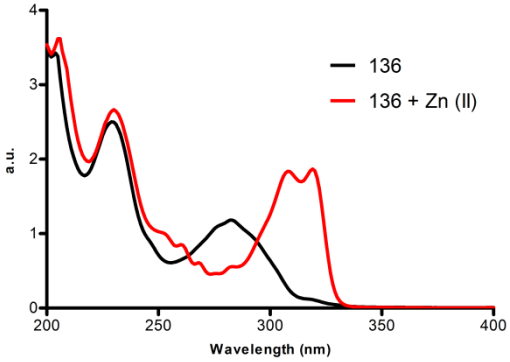

Figure 4-17 UV-Vis absorption spectra of samples of macrocycle **136** (100 µM) in MeCN in the absence (black) and presence (red) of 5 equiv. Zn^{2+}.

This binding can also be observed by ^{1}H NMR spectroscopy. It is interesting to note that whilst the triazole peak in these interlocked systems is generally shifted significantly downfield due to hydrogen bonding effects with the bipyridine macrocycle, in this system the triazole peak is restored to its expected shift position in the aromatic region of the spectrum analogous to the thread (see Figure 4-15). We hypothesise this to be due to the macrocycle hydrogen bonding at the amine position on the thread. Upon addition of Zn^{2+} to

the rotaxane, the shift and broadening of the bipyridine macrocycle signals is clearly evident, as is the shift of the triazole peak to 5.7 ppm (Figure 4-18). This indicates shuttling of the macrocycle away from the amine position on the thread, thus potentially disrupting any previous interaction between the macrocycle and naphthalimide component.

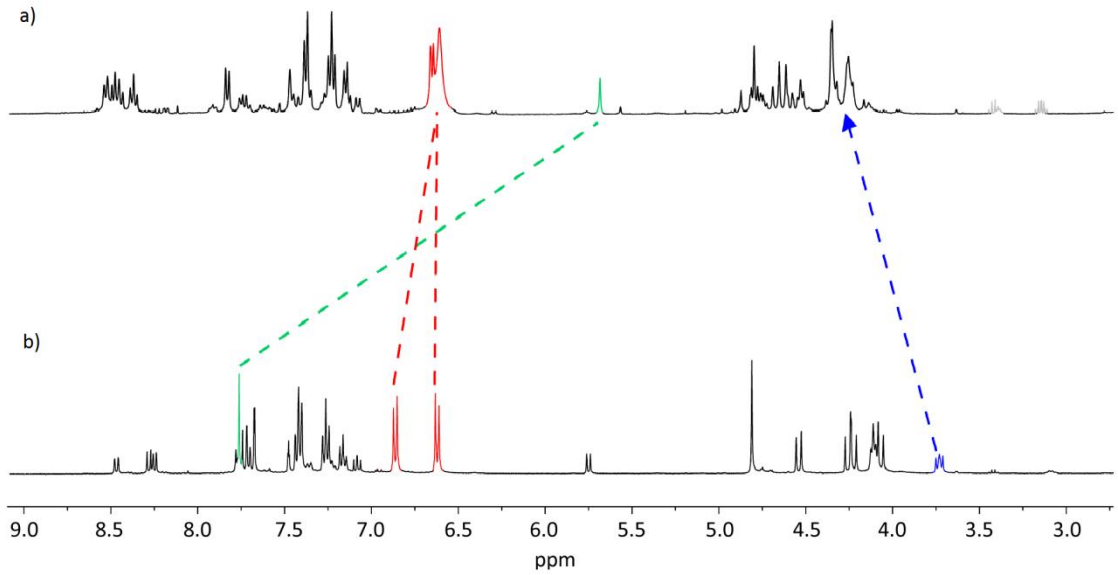

Figure 4-18 Partial 400 MHz 1H NMR spectra of a) rotaxane **150** in the presence of Zn^{2+} and b) rotaxane **150** in d-MeCN. Assignments as indicated in Section 5.3.

These observed characteristics could account for the 'on-off' behaviour observed by fluorescence spectroscopy upon binding. We can hypothesise that in the free rotaxane, the proposed hydrogen bonding with the amine moiety on the thread could help to stabilise the excited state of the molecule, accounting for the brightness. Upon binding, the movement of the macrocycle destabilises the excited state, thus altering the optical output.

The thread **151** on its own, as expected, displays no significant spectral changes to indicate any binding, thus affirming the need for the interlocked structure to display these changes in absorption and emission spectra.

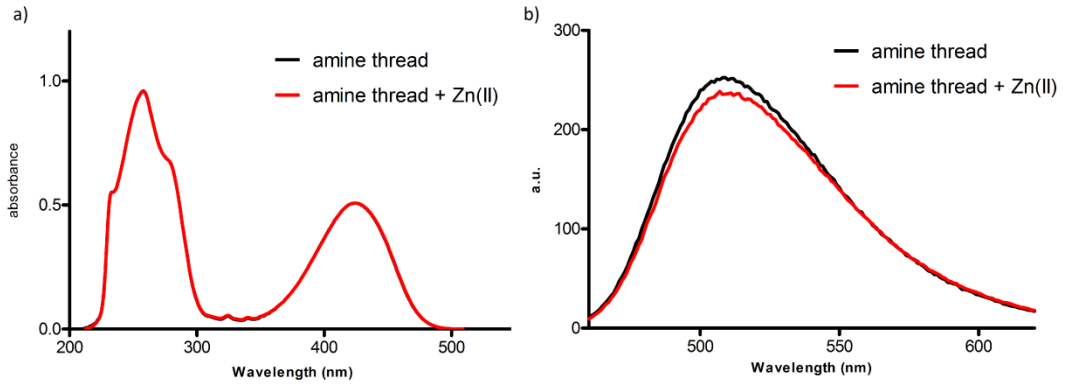

Figure 4-19 a) UV-Vis absorption spectra of samples of thread **151** (100 µM) in MeCN in the presence and absence of Zn^{2+}. b) Fluorescence mission spectra of samples of thread in MeCN in the presence and absence of Zn^{2+}.

Despite these properties, a screen of metals indicates rotaxane **150** also displays a lack of selectivity upon addition of 5 equivalents of each metal. Group 1 and 2 alkali and alkali earth metals appear not to bind to the rotaxane scaffold as no response is obtained. Interestingly, both Mn^{2+} and Hg^{2+} displays a similar profile to **140**, also perhaps indicating no binding. All other first-row transition metals, and Cd^{2+} display the same quenching behaviour as Zn^{2+}, but to differing extents (Figure 4-20).

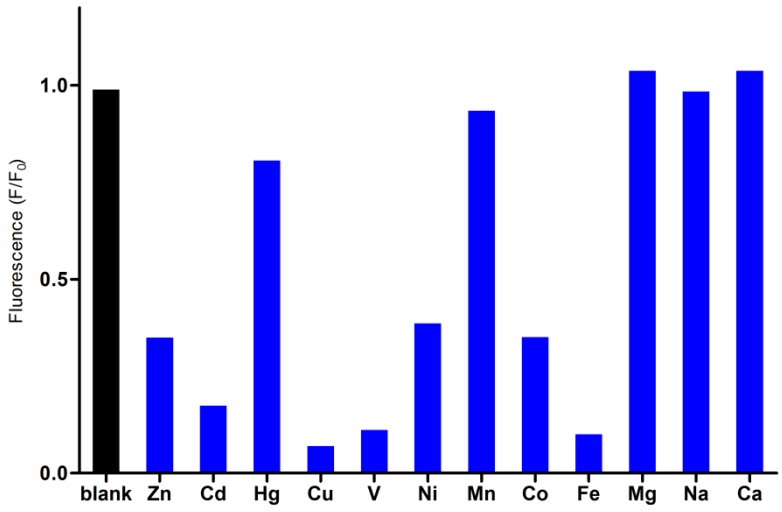

Figure 4-20 Fluorescence emission (F/F_0) of samples of rotaxane **150** (100 µM) in the presence of 5 equiv. of different metals.

4.7.5.2. Amide-functionalised Rotaxane

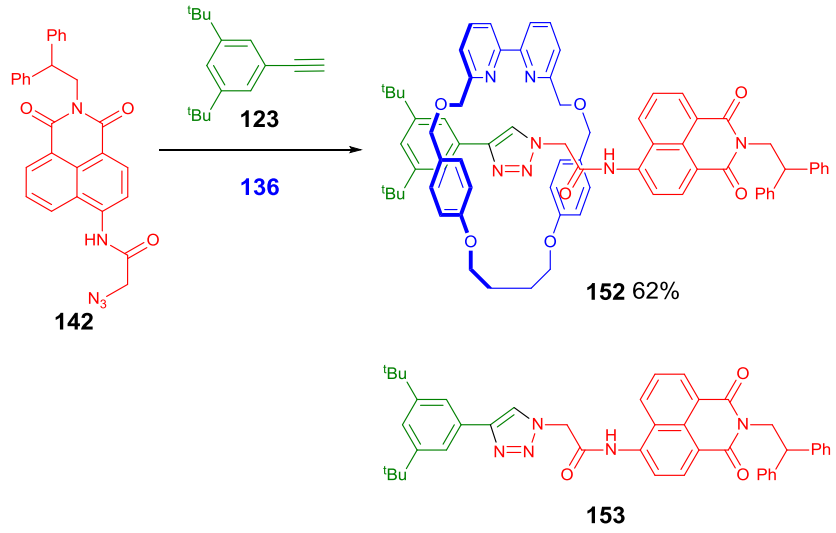

Scheme 4-11 Synthesis of rotaxane **152**. Conditions: $[Cu(MeCN)_4]PF_6$ (0.96 eq.), DIPEA (1 eq.), EtOH, rt, 16 h

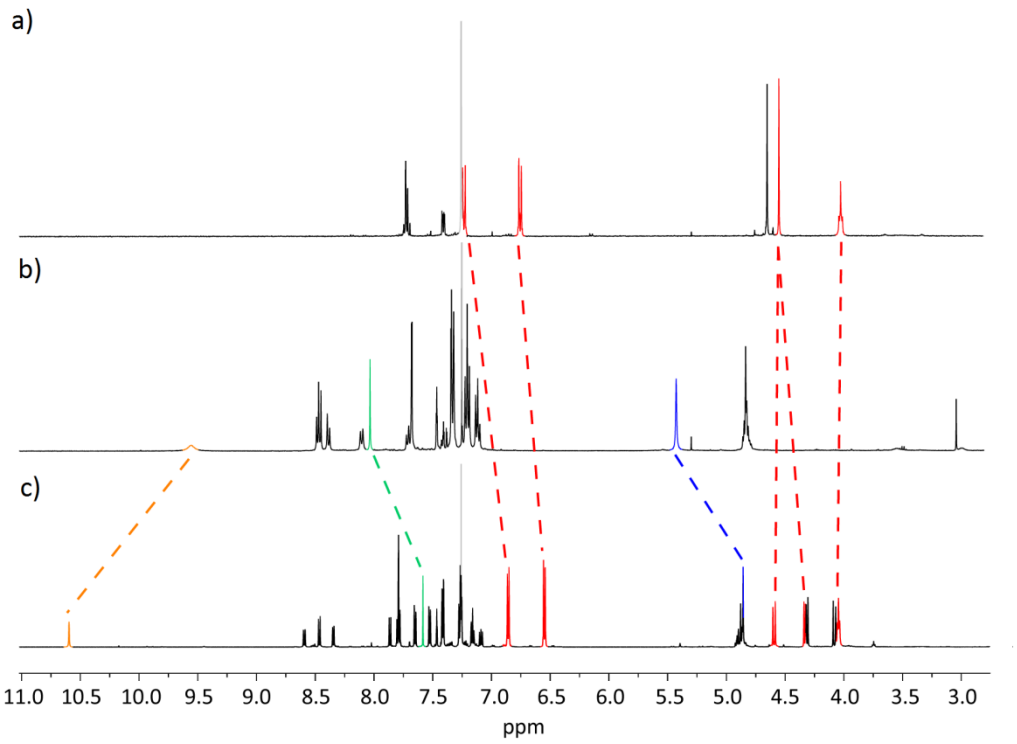

Figure 4-21 Partial 400 MHz 1H NMR spectra of a) macrocycle **136**, b) thread **153** and c) rotaxane **152** in CDCl3. Assignments as indicated in Section 5.3.

Amide functionalised rotaxane **152** was synthesised and tested in an analogous manner. **152** was synthesised in 61% yield under the same conditions, using half thread **142**. The

absorption spectra of a basic titration with increasing equivalents of Zn^{2+} displayed a decrease in a broad absorption band centred around 378 nm, and a concomitant increase in absorption at 350 nm, with an isosbestic point at 361 nm. The same absorption bands for the bipyridine binding are observed at 310 nm and 318 nm, indicating binding inside the rotaxane scaffold.

When its fluorescence spectrum was measured, exciting the samples at the wavelength of the isosbestic point (361 nm), an interesting response was observed which was comparable to that of rotaxane **137**, with an initial increase in emission, along with a blue shift, followed by an incremental decrease in emission and a further blue shift. Overall, this contributes to a slight 'switch-on' response, with a significant blue shift of 20 nm from 450 nm (no Zn^{2+}) to 430 nm (5 equiv. Zn^{2+}). Emission spectra obtained by exciting at the other notable wavelengths from the excitation spectra (351 nm and 378 nm) show similar characteristics (Figure 4-22).

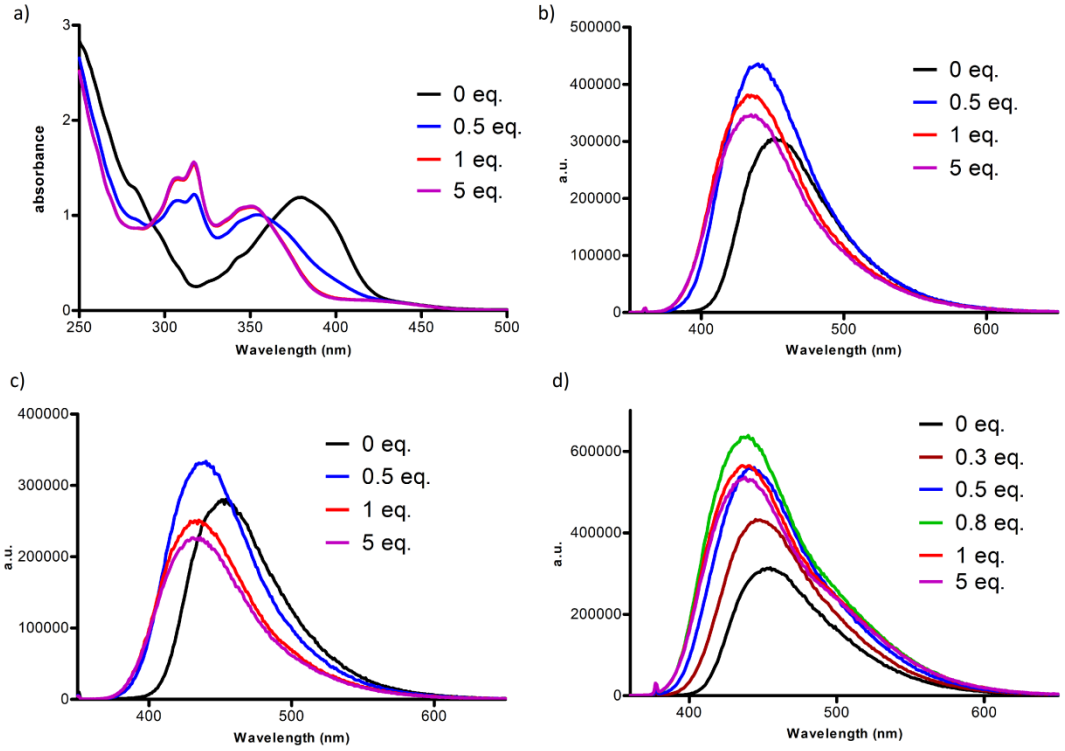

Figure 4-22 a) UV-Vis absorption spectra of samples of rotaxane **152** (100 µM) in MeCN titrated with increasing amounts of Zn^{2+}. b) Fluorescence mission spectra of samples of rotaxane **152** in MeCN titrated with increasing amounts of Zn^{2+} (λ_{ex} 361 nm (isosbestic point)). c) as (b), λ_{ex} 351 nm. d) as (b), λ_{ex} 378 nm.

Analysis of rotaxane **152** by ^{1}H NMR spectroscopy in the absence and presence of Zn^{2+} in MeCN clearly demonstrates the binding of Zn^{2+} to the rotaxane, as observed by the broadening of the bipyridine macrocycle signals at 6.5 and 6.8 ppm. In a similar manner to rotaxane **150**, the triazole signal in the free rotaxane is observed in the aromatic region, whilst the NH proton of the amide group is observed at 10.6 ppm. This indicates a potential hydrogen bonding interaction between the macrocycle and the amide station on the thread in the free rotaxane. Upon binding of zinc, the macrocycle appears to shuttle to the triazole station, restoring the amide signal to 9.9 ppm. The equivalent ^{1}H NMR spectrum of the non-interlocked thread component shows the triazole proton present at 7.95 ppm, and also the amide NH signal at ~9.5 ppm (Figure 4-21).

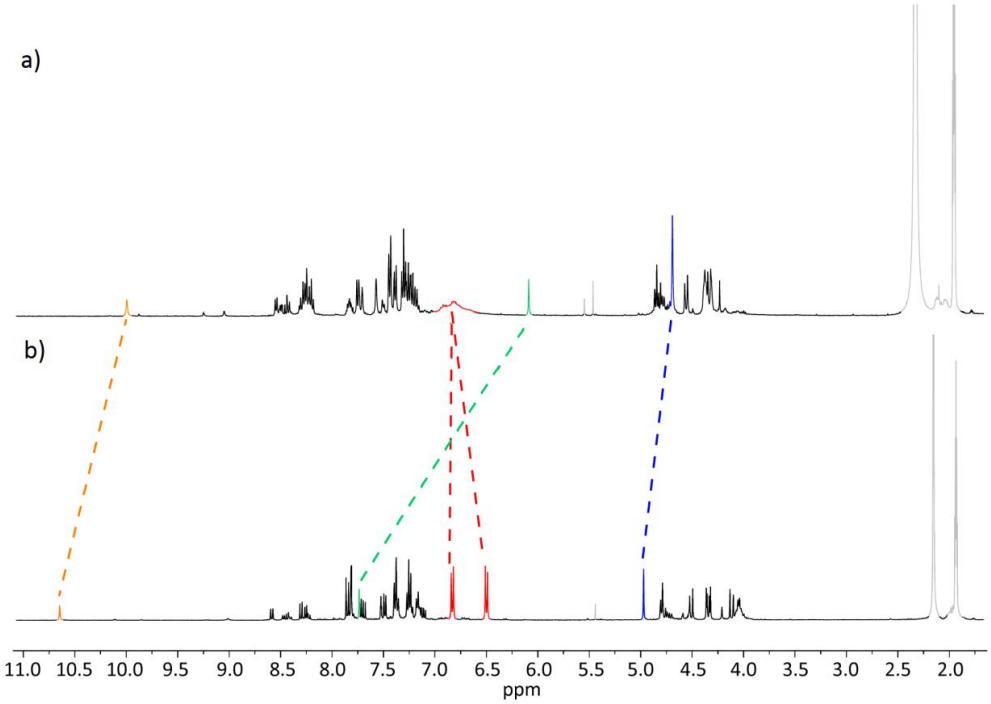

Figure 4-23 Partial 400 MHz 1H NMR spectra of a) rotaxane **152** in the presence of Zn^{2+} and b) rotaxane **152** in d-MeCN. Assignments as indicated in Section 5.3.

The triazole proton also moves upfield to 6.1 ppm, as observed with the previous rotaxanes. We also see a shift of the α-CH_2 on the thread between the amide and triazole from 4.9 to 4.6 ppm, indicating a change in interaction inside the interlocked molecule (Figure 4-23). Both absorption and emission spectra of the thread alone, which is more emissive than the interlocked component at the same concentration, demonstrate no changes in their spectra upon addition of Zn^{2+}, indicating no metal binding.

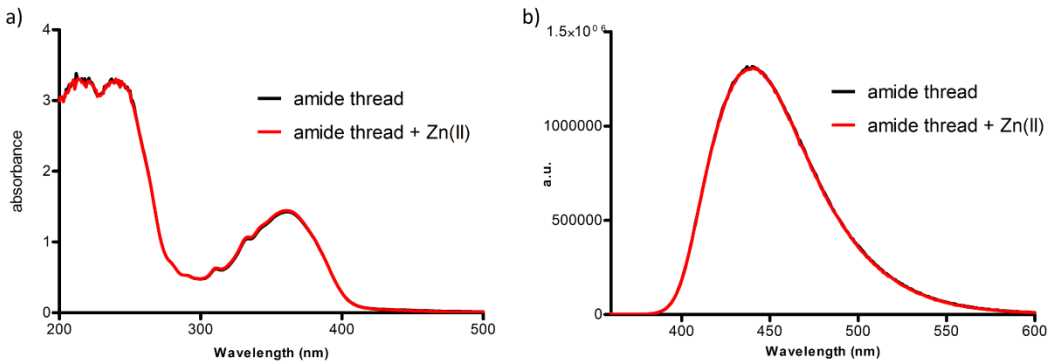

Figure 4-24 a) UV-Vis absorption spectra of samples of thread **153** (100 µM) in MeCN in the presence and absence of Zn^{2+}. b) Fluorescence mission spectra of samples of thread in MeCN in the presence and absence of Zn^{2+}.

The metal screen provided an interesting result as an approximately 3-fold switch-on response was observed for rotaxane **152** in the presence of both Cd^{2+} and V^{2+}. Given that both atoms have very different ionic radii [209] it is quite clear that factors other than the size of cavity are influencing the selectivity of these structures.

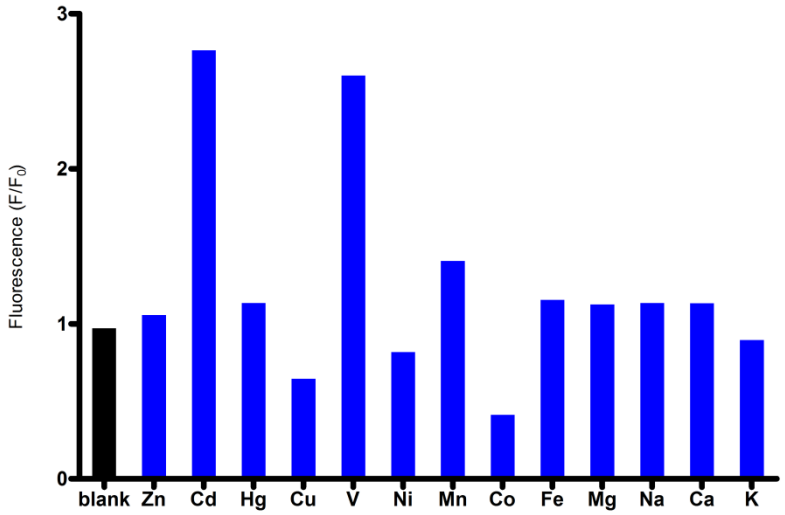

Figure 4-25 Fluorescence emission (F/F_0) of samples of rotaxane **152** (100 µM) in the presence of 5 equiv. of different metals.

4.7.5.3. Sulfur-functionalised Rotaxane

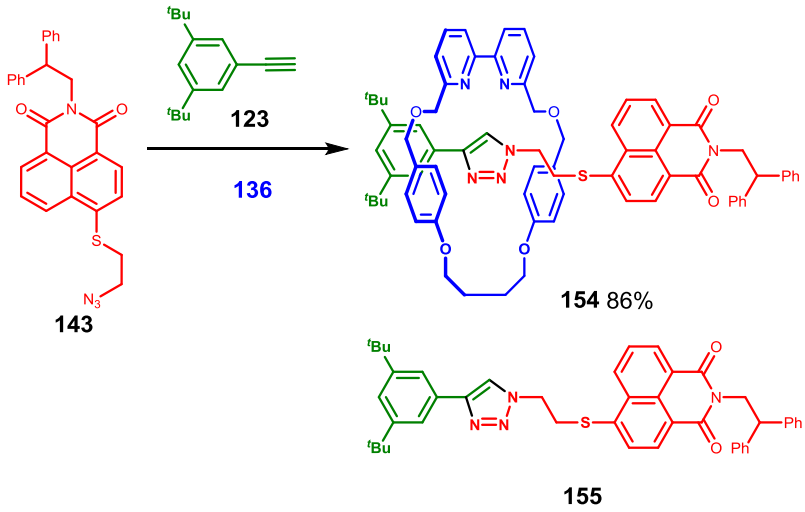

Scheme 4-12 Synthesis of rotaxane **154**. Conditions: $[Cu(MeCN)_4]PF_6$ (0.96 eq.), DIPEA (1 eq.), EtOH, rt, 16 h

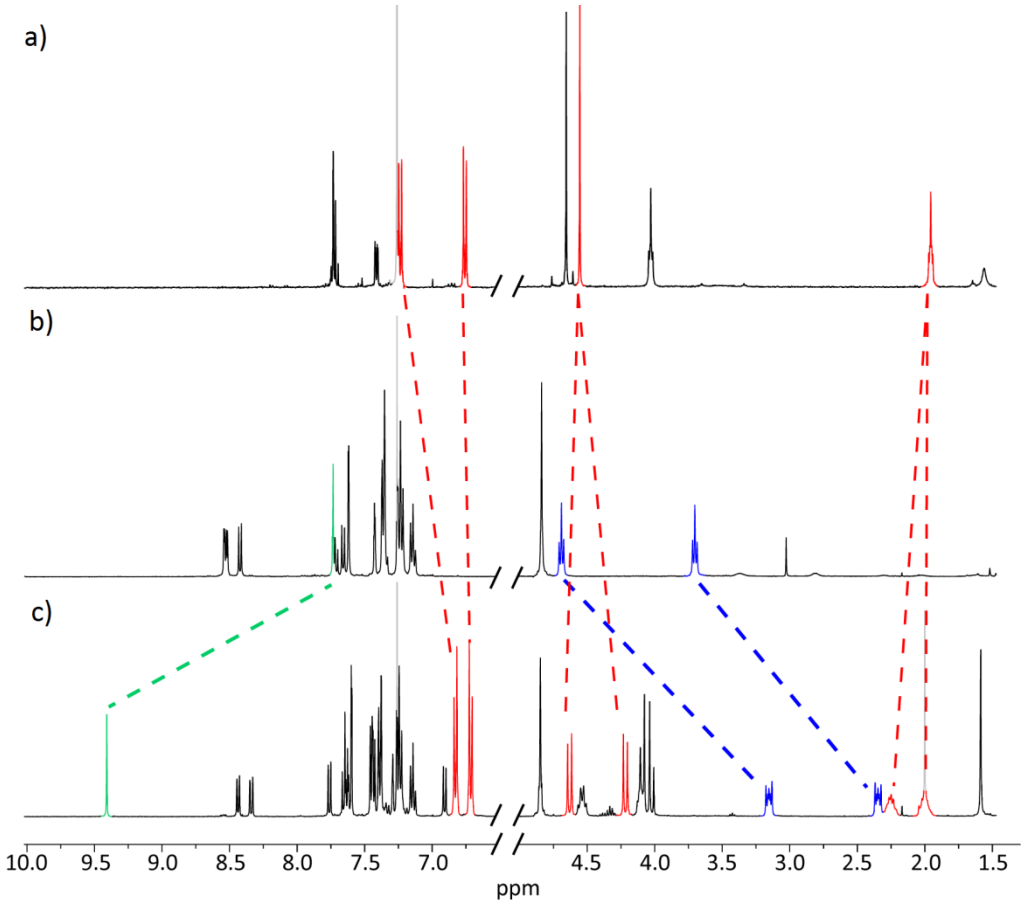

Figure 4-26 Partial 400 MHz 1H NMR spectra of a) macrocycle **136**, b) thread **155** and c) rotaxane **154** in CDCl3. Assignments as indicated in Section 5.3.

The sulfur-functionalised rotaxane **154** was synthesised in 86% yield following the same conditions as the previous rotaxanations. As observed with rotaxane **150**, this rotaxane was also highly emissive, due to the sulfur lone pairs donating into the fluorophore.

The absorption profile observed by UV-Visible spectroscopy revealed a slight increase and blue shift of the main absorption band centred at 380 nm upon addition of Zn^{2+}, and also the previously observed bipyridine binding from the emergence of two strong bands at 312 and 322 nm. A simple titration with Zn^{2+} in MeCN indicated this rotaxane has a highly desirable switch-on response to the metal. Upon excitation at 380 nm we observed a broad emission at 468 nm, which incrementally increased in output to a maximum emission at 1 equivalent, blue-shifted by 18 nm to 450 nm.

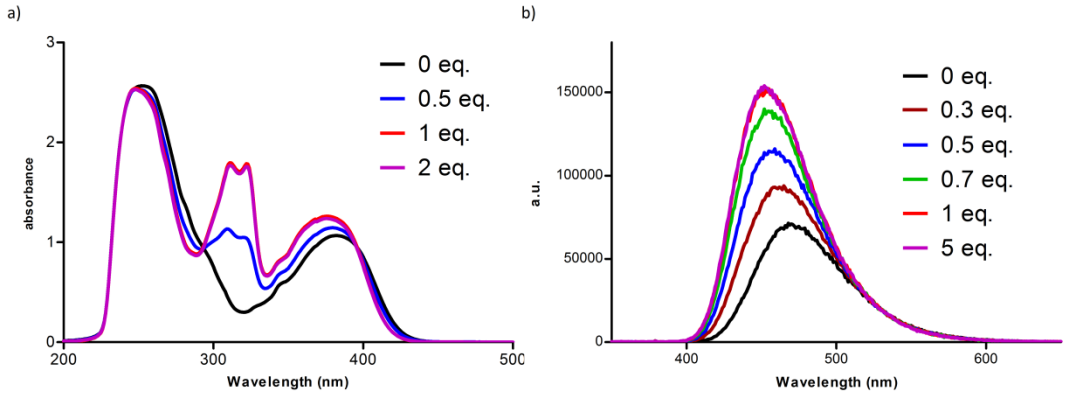

Figure 4-27 a) UV-Vis absorption spectra of samples of rotaxane **154** (100 µM) in MeCN titrated with increasing amounts of Zn^{2+}. b) Fluorescence emission spectra of samples of rotaxane **154** in MeCN titrated with increasing amounts of Zn^{2+}

A ^{1}H NMR titration of rotaxane **154** with Zn^{2+} in MeCN indicates that upon addition of Zn^{2+} the spectrum resolves into a single species at or above one equivalent of zinc, with both the free rotaxane and the Zn-bound product observed when titrated with 0.5 equivalents of the metal (Figure 4-28). This is another indicator of 1:1 binding stoichiometry. We clearly observe the binding through the same characteristic signals as previously observed. The broadening of bipyridine macrocycle signals is shown from two distinct doublets to a broad multiplet at approx. 6.5 ppm. A large downfield shift of the triazole proton signal from 9.3 to 5.5 ppm is also observed, as is the shift of the ethylene CH_2- proton signals upfield. This combined with the observed hypsochromic shift in fluorescence emission indicates a potential interaction of the bound metal with the sulfur heteroatom.

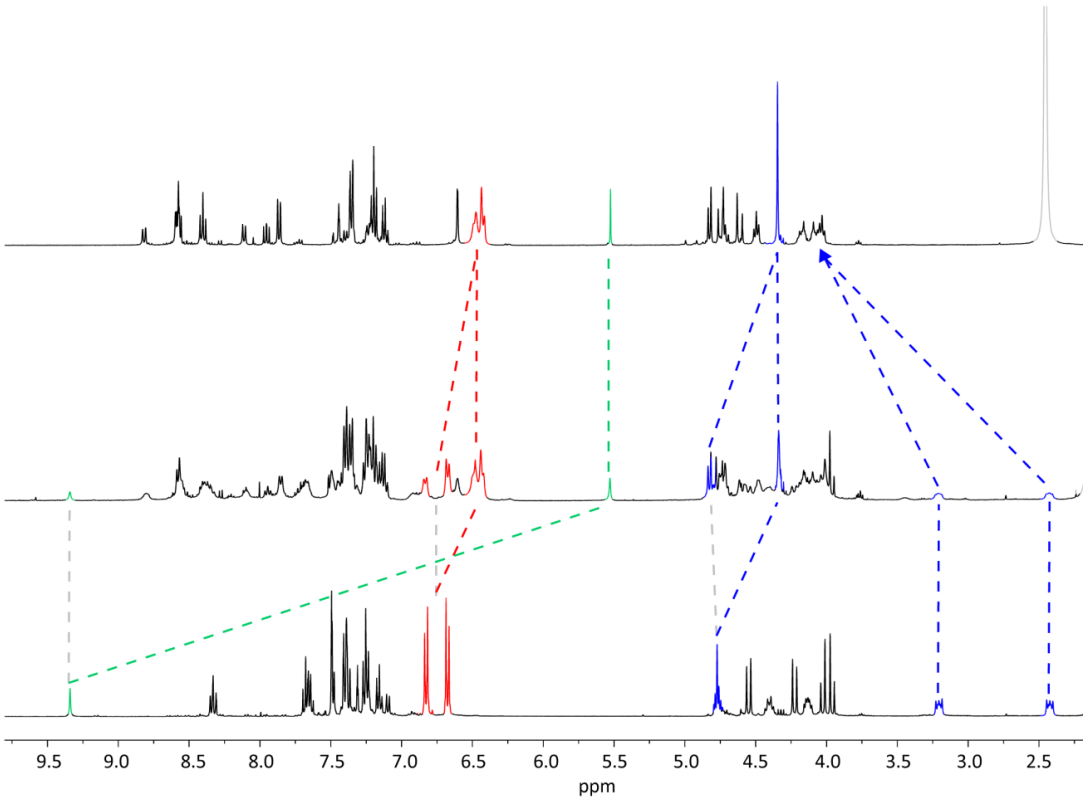

Figure 4-28 Partial 400 MHz 1H NMR spectra of a) rotaxane **154** in the presence of 1 equiv. Zn^{2+} , b) rotaxane **152** in the presence of 0.5 equiv. Zn^{2+} and b) rotaxane **154** in d-MeCN. Assignments as indicated in Section 5.3

To ensure the selectivity and behaviour was dependent on the interlocked structure the thread **155** was tested for its response to Zn^{2+}. Both excitation and emission profiles for the thread show no change upon addition of 5 equivalents of zinc, indicating no binding.

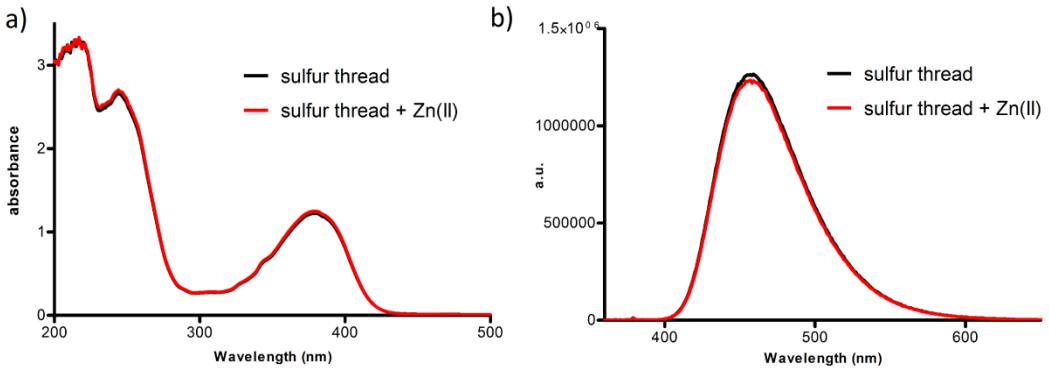

Figure 4-29 a) UV-Vis absorption spectra of samples of thread **155** (100 µM) in MeCN in the presence and absence of Zn^{2+}. b) Fluorescence mission spectra of samples of thread in MeCN in the presence and absence of Zn^{2+}.

As this rotaxane displayed such favourable characteristics for zinc binding we wanted to test its selectivity, and we were pleased to find rotaxane **154** was selective for Zn^{2+} over all metals tested, including $Cd^{2+}$and Hg^{2+}, with an approximate ~2 fold switch-on at maximum saturation (Figure 4-30, blue bars). It is notable that the sensor is selective for Zn^{2+} over Cd^{2+}, as Zn^{2+} sensors often show a similar response to both metals due to their analogous co-ordination chemistry.

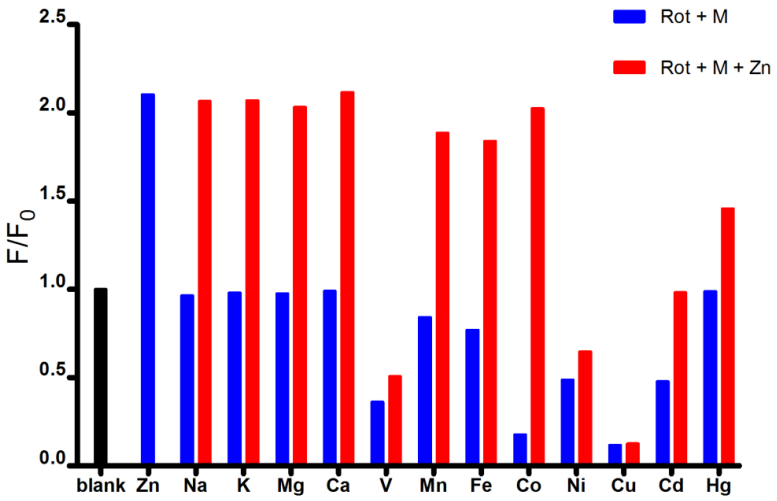

Figure 4-30 Fluorescence emission (F/F_0) of samples of rotaxane **154** (100 µM) in the presence of 5 equiv. of different metals (blue), and then 5 equiv. Zn^{2+} (red).

An important feature of any potential Zn^{2+} probe is the ability to selectively function in the presence of other biologically relevant metal ions. A typical test for this carried out *in vitro* is a fluorescence recovery experiment, which we carried out in organic media, with a view to modifying these rotaxanes in future to function in aqueous media. In this experiment, five equivalents of a metal ion were added to a sample of the rotaxane, the fluorescence response measured, and then five equivalents of Zn^{2+} were added to the same sample and fluorescent output compared (Figure 4-30, red bars).

We observed that almost all of the metals gave a recovery in fluorescence output upon addition of Zn^{2+} to the samples, apart from V, Ni and Cu. With the exception of V this is

consistent with the Irving-Williams series,[209] whereby the stability constants are higher for those metals than Zn.

4.7.6. Calculation of Binding Constants of Rotaxanes 150, 152 and 154

We can quantify the interaction of zinc and rotaxane by calculating a binding constant (K_d) by monitoring the interaction by NMR, UV-Vis, or even fluorescence spectroscopy. After observing bands indicating binding of bipyridine in the UV-Visible absorption spectra for each rotaxane, we decided to use the absorbance spectra to calculate an approximate binding constant.

By plotting the maxima of each absorbance measurement emission against the equivalents of Zn^{2+} added, we could obtain a visual representation of binding and use this data to extrapolate a K_d value for the ligand. The dissociation constant was determined by non-linear regression analysis previously used for calculations in Chapter 3 (Equation 4-1).[72] As the ^1H NMR, UV-Vis and fluorescence spectroscopy titration data for each rotaxane indicated a 1:1 binding of Zn^{2+}:rotaxane, we could confidently assume that the ligand follows a 1:1 binding model.

$$\frac{F}{F(0)} = 1 + \left(\frac{F(max)}{2F(0)} - 0.5\right) \times \left(1 + \frac{CM}{CL} + \frac{Kd}{CL} - \left[\left(1 + \frac{CM}{CL} + \frac{Kd}{CL}\right)^2 - \frac{4CM}{CL}\right]^{0.5}\right)$$

Equation 4-1 Equation used to determine K_d value for rotaxanes, where CM and CL concentrations of Zn^{2+} and rotaxane respectively, F is the observed absorbance, F(0) is the observed absorbance of the rotaxane alone (ie CM = 0). Non-linear regression analysis was used to determine F(max)/F(0) and K_d.[72,179]

To begin with, a full titration was carried out of macrocycle **136** alone with Zn^{2+} to obtain a binding constant. Samples were made from 0 to 1 equivalents of Zn^{2+} in 0.1 equivalent increments, and further data points were obtained at excess amounts of Zn^{2+} to confirm the maximum response was achieved. The absorbance value at 319 nm (one of the $\pi - \pi^*$

bands) was measured (F) and the relevant values inserted into Equation 4-1 to give a K_d value of 4.17 x 10^{-11} M with excellent 'goodness of fit',

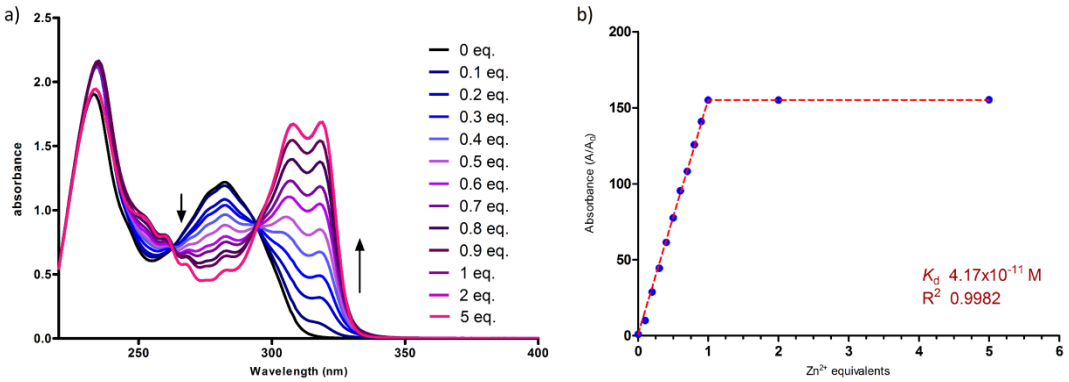

Figure 4-31 a) UV-Vis absorption spectra of samples of macrocycle **136** (100 µM) in MeCN titrated with increasing amounts of Zn^{2+}. b) Non-linear fitting of data of data from (a) using Equation 4-1.

A full titration of rotaxane **154** was also carried out. By applying the same formula to the UV-Vis titration data obtained for this zinc-selective rotaxane, we obtain an ambiguous K_d value of ~1.14 x 10^{-17} M, also with an excellent goodness-of-fit. The ambiguous value merely indicates that the values obtained are outside the limits of calculation using this methodology. [179]

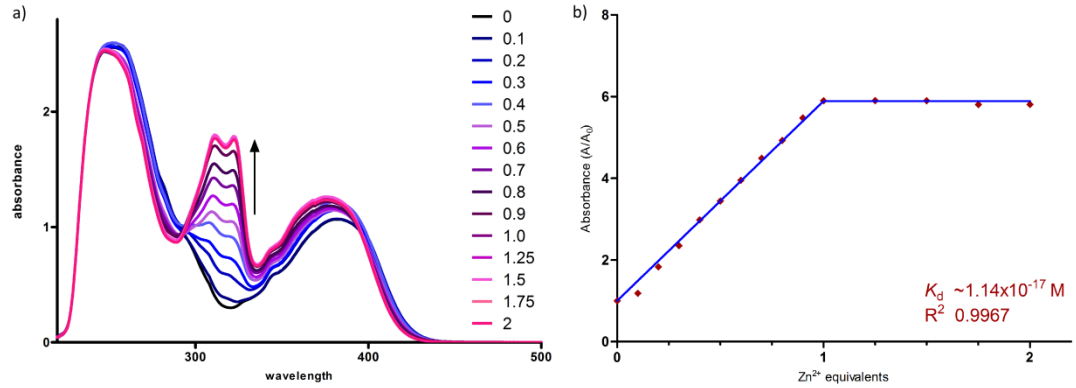

Figure 4-32 a) UV-Vis absorption spectra of samples of rotaxane **154** (100 µM) in MeCN titrated with increasing amounts of Zn^{2+}. b) Non-linear fitting of data of data from (a) using Equation 4-1.

In a similar manner, K_d values were obtained for both rotaxanes **150** and **152** using the same absorption band, and we obtained a similar ambiguous value for rotaxane **150**, with

an estimated K_d of ~5.33 x 10^{-17} M. Titration of rotaxane **152** gave a poorer fit with a value of 3.09 x 10^{-7} M. This variation can be accounted for by experimental error; titration by UV-Vis spectroscopy is very sensitive to concentration of sensor and analyte, dilution and many other effects. A small loss of accuracy can lead to a large deviation in results.

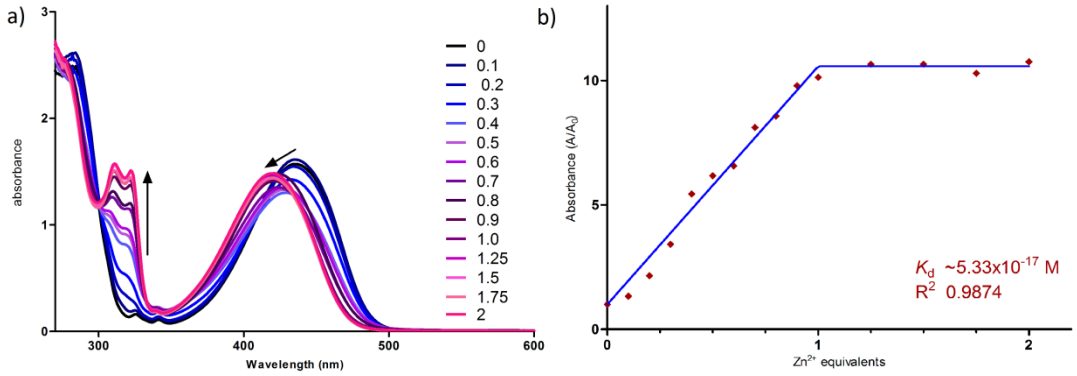

Figure 4-33 a) UV-Vis absorption spectra of samples of rotaxane **150** (100 µM) in MeCN titrated with increasing amounts of Zn^{2+}. b) Non-linear fitting of data of data from (a) using Equation 4-1.

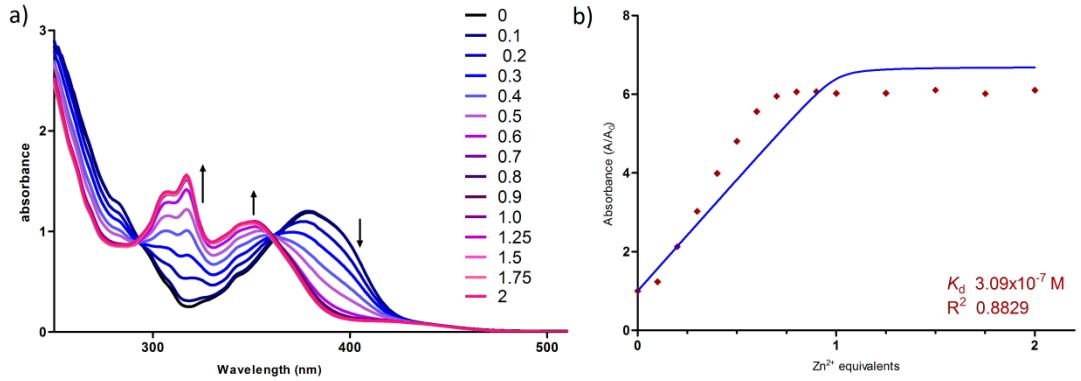

Figure 4-34 a) UV-Vis absorption spectra of samples of rotaxane **152** (100 µM) in MeCN titrated with increasing amounts of Zn^{2+}. b) Non-linear fitting of data of data from (a) using Equation 4-1.

Whilst all of the molecules are utilising the same binding motif (bipyridine), there are some factors that govern the binding to each ligand that could account for the difference in behaviour. For example, the macrocycle is less sterically restricted than the rotaxane. Both of the oxygen atoms from its ether linkages can participate in binding the metal inside the cavity. The rotaxanes have more severe steric restrictions due to the presence of the thread

in the macrocycle, and also will likely have a different co-ordination motif consisting of a different number of solvent molecules, and number of ether linkages participating in binding the metal. Attempts to obtain X-Ray crystallographic data of these rotaxanes with Zn^{2+} bound have been unsuccessful to date, but a solid state structure would help to clarify how these rotaxanes bind metal guests in solution.

4.8. Conclusions and Future Work

In conclusion, we were able to exploit the metal-binding abilities of a bipyridine macrocycle to develop novel, fluorescent mechanically interlocked structures with different responses to metals. We have demonstrated that the AT-CuAAC is an effective route to simple and facile modifications of ligand design, and shown that even small changes in molecular structure can account for very different results.

The study allowed for the discovery of a'switch-on' sulfur- containing fluorescent rotaxane **154** in the presence of Zn^{2+}, in MeCN. As a chemosensor in organic media, it has an estimated K_d value appropriate for potential biological study, and although it retains its selectivity in the presence of several other first row transition metals, the binding of Cu^{2+}, Ni^{2+} and V^{2+} quenches the fluorescence in a non-recoverable manner. This suggests that whilst this system has the optimal energy levels and conformations to produce a desirable optical response, this scaffold would perhaps need further adjustments to overcome its selectivity problems, which could possibly come from modification to the macrocycle component.

A synthetic 'trial-and-error' study like this one provides no insight into the exact mechanisms working to give each rotaxane its unique optical response. To complete the study we would need to carry out extensive computational studies on these structures and obtain more information about the relative orbital energies and the processes governing

the fluorescence output. This in turn could allow for a more precise design process for selective [2]rotaxanes with desirable optical properties, including more bathochromically-shifted emissions (with biological applications in mind), which are more desirable than those in the UV-range.

We have seen through previous work and our own studies with designing biological sensors that their behaviour *in cellulo* can be highly unpredictable. With the 'clickate' sensor previously designed by the Watkinson group [72] they also observed a lack of recovery of fluorescence upon sequential addition of Cu^{2+} and then Zn^{2+}, and the probe was still utilised successfully in both cells and organisms.

To this end, despite the lack of recovery in the presence of some cations, there is still some merit in ascertaining the behaviour of a rotaxane scaffold as a novel *in cellulo* sensor. This too would require modification of the ligand scaffold primarily to make it water-soluble. Efforts towards this are currently being realised in the laboratory through the synthesis of water soluble macrocycles, and also particularly by appending water soluble di-carboxylic acid groups that act as both a stopper to avoid de-threading and to increase the solubility of these rotaxanes in aqueous media (**156**, Figure 4-35). We have already shown that modification to the stoppering element of the rotaxane has no significant effect on their photophysical behaviour, as exemplified by rotaxanes **134** and **140**, and we anticipate this approach to work in a similar manner in this instance.

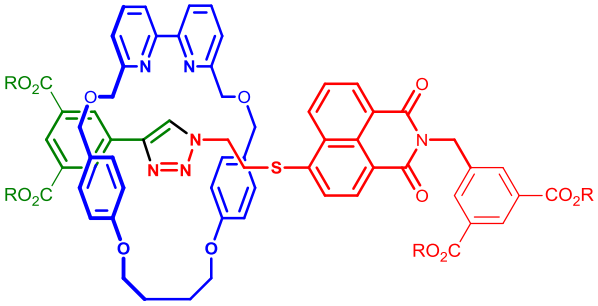

156 (R = H or PEG group)

Figure 4-35 Potential structure of a hypothetical water-soluble rotaxane based on successful Zn^{2+} sensor rotaxane **152**

The AT-CuAAC approach will not only make this a facile modular way to access and fine-tune these types of structures, but also allow for the generation of a novel class of optical probes suitable for selective cation-imaging purposes for specific cells and even disease models.

Chapter 5: Experimental Section

5.1. General Experimental Information

All commercially available reagents, unless otherwise stated, and solvents for column chromatography were used as supplied without further purification. EDTA refers to ethylenediaminetetraacetic acid. EtOH was stored over 4 Å-molecular sieves. Et_3N was stored over KOH under a N_2 atmosphere. Reaction solvents were supplied dry from an MBRAUN MB SPS-800 solvent purification system. Petrol refers to the fraction of petroleum ether boiling in the range 40-60 °C. All glassware and needles were oven dried and cooled under an inert atmosphere prior to experimental use.

Infrared spectra were recorded in the range 4000-600 cm^{-1}, obtained directly from the compound as a solid or neat liquid on a Bruker Tensor 37 FTIR spectrometer. ^{1}H and ^{13}C NMR spectra were recorded on a Bruker AV400 or AVIII 400 NMR spectrometer. Chemical shifts were reported in δ (ppm) and referenced to residual solvent. Multiplicities of signals are reported using standard abbreviations: s = singlet, d = doublet, t = triplet, q = quartet, quint = quintet, m = multiplet, br = broad, and coupling constants measured in Hertz (Hz) and reported to 1 d.p.. Low resolution mass spectrometry was carried out by the mass spectrometry service at the University of Southampton using either a MaXis (Bruker Daltonics, Bremen, Germany) mass spectrometer equipped with a Time of Flight (TOF) analyser or solariX (Bruker Daltonics, Bremen, Germany). High resolution electrospray ionisation mass spectrometry was carried out by the EPSRC National Mass Spectrometry Service, University of Wales, Swansea on a Thermofisher LTQ Orbitrap XL. Melting points were measured on a Stuart SMP3 melting point apparatus and are uncorrected.

Flash column chromatography, unless stated otherwise was performed using VWR silica gel 60 (220-240 mesh), and TLC was carried out using pre-coated aluminium backed plates with

Merck Kieselgel 60 F254. The plates were visualised under a UV lamp (254 nm), or by staining with basified aqueous $KMnO_4$ solution followed by gentle heating.

Fluorescence spectroscopic/spectrophotometric studies for characterisation were performed using a Jobin Yvon Horiba Fluorormax®-3 machine, in a 1 cm path length cell without an incident ray filter. Solutions of deprotected sensors **105**, **107**, **109**, **112**, **114** and **116** were prepared from a stock solution in DMSO such that each 3 mL testing sample contained 1% DMSO. All aqueous testing was carried out using HEPES buffered water (0.1 mM, pH 7.4) at ambient temperature. Testing of all sensors and rotaxanes in MeCN was carried out using HPLC grade MeCN (VWR) which was used without any further purification.

Dynamic light scattering (DLS) measurements to determine average aggregate size of solutions of sensors were obtained on a Malvern Zetasizer Nano ZS instrument equipped with a 633 nm laser. The measurement angle was 173 degrees. Samples were prepared as for the fluorescence measurements.

The following compounds were all prepared following previously reported literature procedures. All spectroscopic data obtained matched those previously reported; **63**, **64** and **65**,[72] **87** and **88**,[171] **91**,[172] **94**,[59] **96**,[210] **103**,[162] **123** and **136,**[191] and 3-azido-1-aminopropane.[211]

5.2. General Procedures

5.2.1. General Procedure A: One-pot Synthesis of a Sensor from Building Block 69

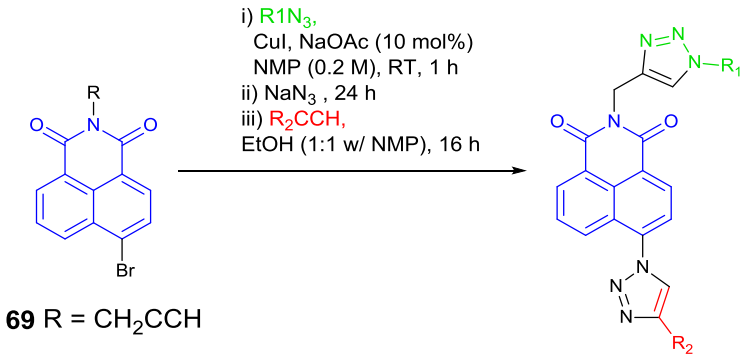

69 R = CH_2CCH

Acetylene **69** (314 mg, 1.0 mmol), an azide (1.0 mmol), CuI (19.0 mg, 10 mol%) and NaOAc (8.2 mg, 10 mol%) were combined in a sealed CEM microwave vial which was wrapped in foil and purged with N_2. Anhydrous NMP was added, and the reaction was stirred at r.t. for 1 h. Upon complete consumption of **69** (determined by ^{1}H NMR spectroscopy), NaN_3 (78 mg, 1.2 mmol) was added in a single portion to the reaction vial, which was resealed and the reaction stirred for a further 24 h. Upon completion of azide formation (determined by ^{1}H NMR spectroscopy), an acetylene (1 mmol) and EtOH (1:1 w/ NMP) were added to the reaction vial, and the final mixture was stirred for a further 16 h, at which point the reaction was complete (determined by ^{1}H NMR spectroscopy).

5.2.2. General Procedure B: One-pot Synthesis of a Sensor from Building Block 70

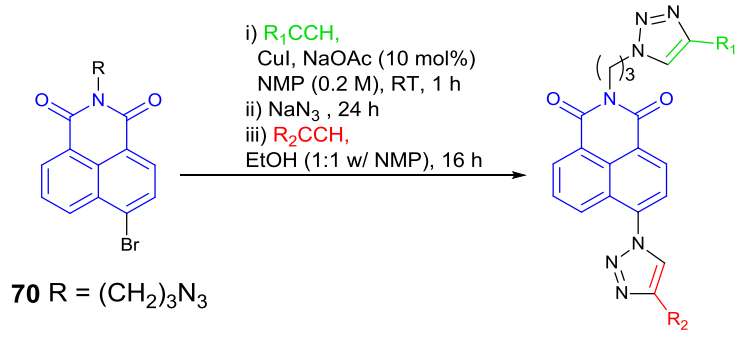

70 R = $(CH_2)_3N_3$

Azide **70** (359 mg, 1.0 mmol), an acetylene (1.0 mmol), CuI (19.0 mg, 10 mol%) and NaOAc (8.2 mg, 10 mol%) were combined in a sealed CEM microwave vial which was wrapped in

foil and purged with N_2. Anhydrous NMP was added, and the reaction was stirred at r.t. for 1 h. Upon complete consumption of **70** (determined by ^{1}H NMR spectroscopy), NaN_3 (78 mg, 1.2 mmol) was added in a single portion to the reaction vial, which was resealed and the reaction stirred for a further 24 h. Upon completion of azide formation (determined by ^{1}H NMR spectroscopy), an acetylene (1 mmol) and EtOH (1:1 w/ NMP) were added to the reaction vial, and the final mixture was stirred for a further 16 h, at which point the reaction was complete (determined by ^{1}H NMR spectroscopy).

5.2.3. General Procedure C: Rotaxane Synthesis

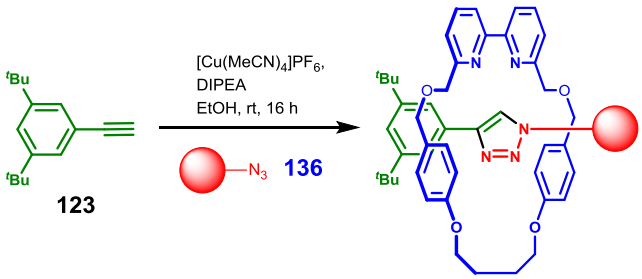

The macrocycle **136** (1 eq.), azide (1 eq.), alkyne **123** (1 eq.), $[Cu(MeCN)_4]PF_6$ (0.96 eq.) and DIPEA (1 eq.) were weighed dry into a sealed flask and purged with N_2. EtOH was added to make a 0.02 M solution (wrt. macrocycle), and the mixture stirred at r.t. for 16 h. The solvent was evaporated, and the resulting residue diluted with CH_2Cl_2 and washed with 16% aqueous EDTA tetrasodium-saturated ammonia solution. The organic layer was retained and the aqueous layer extracted twice further with CH_2Cl_2. The organic extracts were combined, dried over $MgSO_4$, filtered and dried in vacuo. The crude mixture was purified by flash column chromatography (1:1 Petrol/ CH_2Cl_2 to 10% MeCN/1:1 Petrol- CH_2Cl_2) to yield the desired [2]rotaxane.

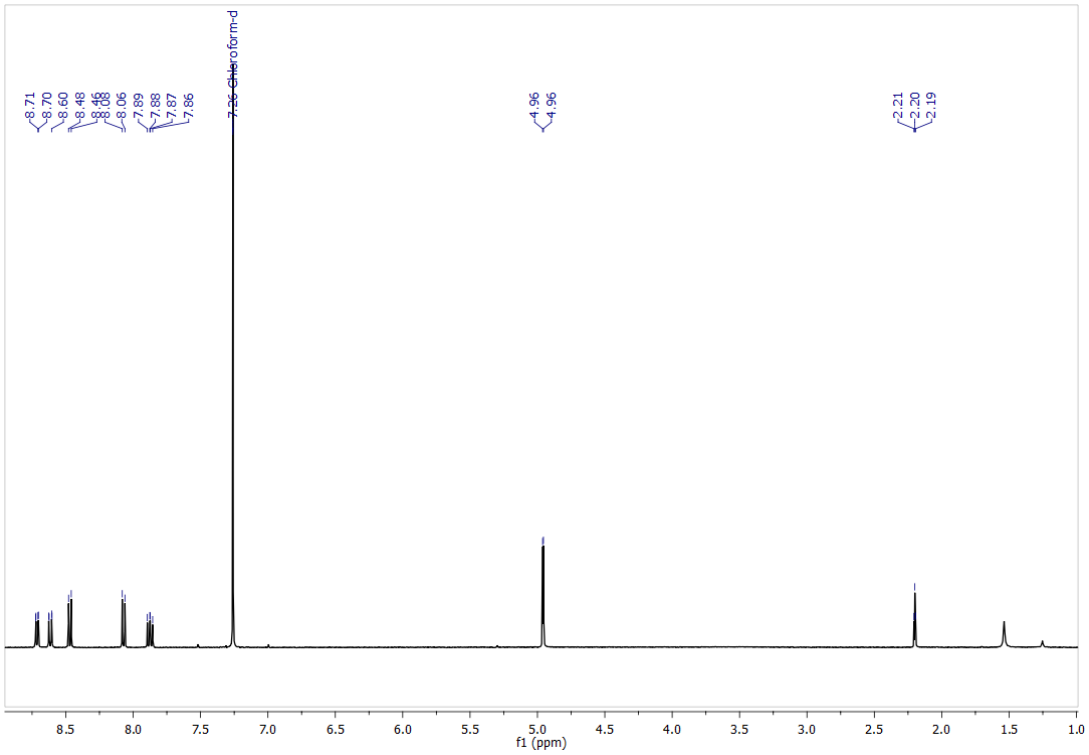
8.71
8.70
8.60
8.48
8.06
7.89
7.88
7.87
7.86
7.26 Chloroform-d
4.96
4.96
2.21
2.20
2.19
f1 (ppm)

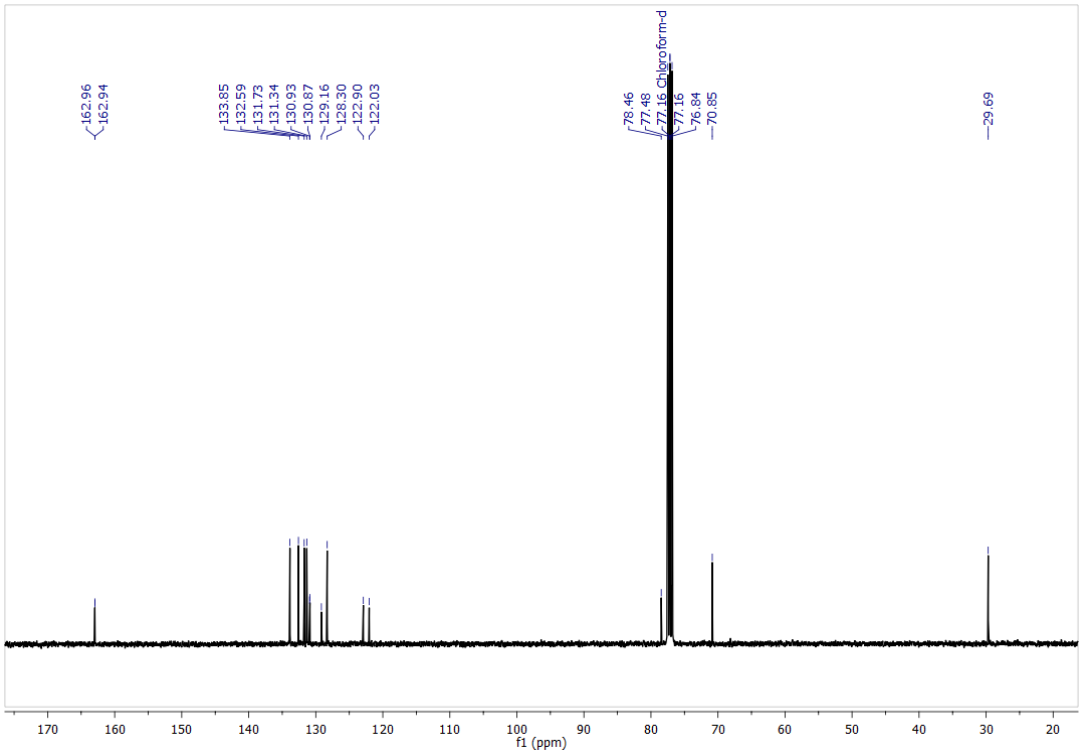
162.96
162.94
133.85
132.59
131.73
131.34
130.93
130.87
129.16
128.30
122.90
122.03
78.46
77.48
77.16 Chloroform-d
77.16
76.84
70.85
29.69
f1 (ppm)

5.3. Experimental Data

*6-Bromo-2-(prop-2-yn-1-yl)-1H-benzo[de]isoquinoline-1,3(2H)-dione (**69**):*

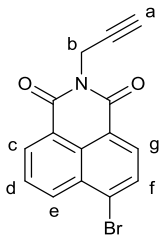

Following a modified literature procedure,[72] 4-bromo-1,8-naphthalic anhydride (1.0 g, 4.1 mmol) was dissolved in 1,4-dioxane (30 mL). One portion of propargyl amine (0.26 mL, 4.1 mmol) was added to the solution. This was stirred at r.t. for 1 h, and then heated at 70 °C for 2 h. After cooling the reaction mixture to r.t., a further portion of propargyl amine (0.05 mL, 0.8 mmol) was added, and the reaction left to stir at 70 °C overnight. After cooling to r.t, the reaction mixture was slowly poured into iced water (120 mL). The resulting precipitate was collected by suction filtration and dried *in vacuo* to give bromide **69** as a brown solid (1.1 g, 96%). ^{1}H NMR (400 MHz, $CDCl_3$) δ_H 8.70 (d, J = 7.3, 1H, H_c), 8.60 (d, J = 8.5, 1H, H_e), 8.46 (d, J = 7.9 , 1H, H_g), 8.06 (d, J = 7.9 , 1H, H_f), 7.87 (dd, J = 8.4, 7.4 , 1H, H_d), 4.95 (d, J = 2.4 , 2H, H_b), 2.20 (t, J = 2.4 , 1H, H_a); ^{13}C NMR (101 MHz, $CDCl_3$) δ_C 162.9, 162.9, 133.8, 132.5, 131.7, 131.2, 130.9, 130.8, 129.1, 128.2, 122.8, 121.9, 78.3, 70.7, 29.6; IR (ν_{max}/cm^{-1}) 3391, 3257, 2923, 2106, 1700, 1659, 778; M.p. (°C) 177-179; HRMS (EI) calcd for $C_{15}H_8{}^{79}BrNO_2$ $[M + H]^+$ 313.9811, found: 313.9809. UV: $\lambda_{max}(CH_2Cl_2)$/nm (ε / mol^{-1}cm^{-1}dm^3) 357 (8379), 343 (10173), 328 (6896).

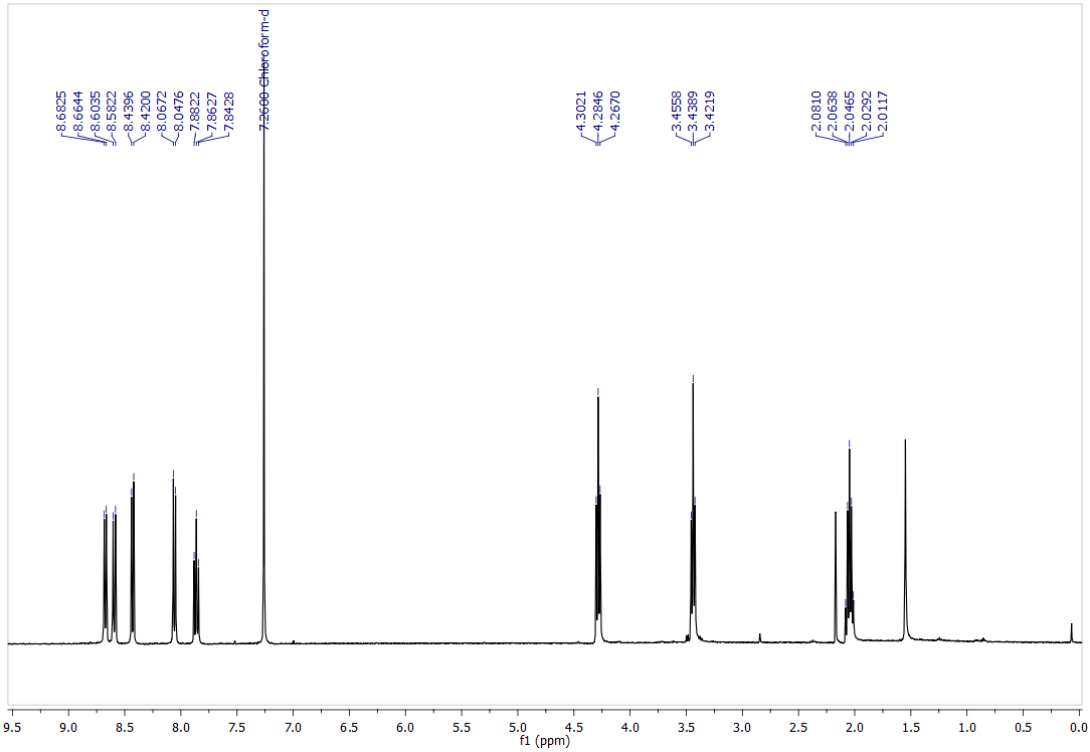
8.6825
8.6644
8.6035
8.5822
8.4396
8.4200
8.0672
8.0476
7.8822
7.8627
7.8428
7.2666 Chloroform-d
4.3021
4.2846
4.2670
3.4558
3.4389
3.4219
2.0810
2.0638
2.0465
2.0292
2.0117
f1 (ppm)

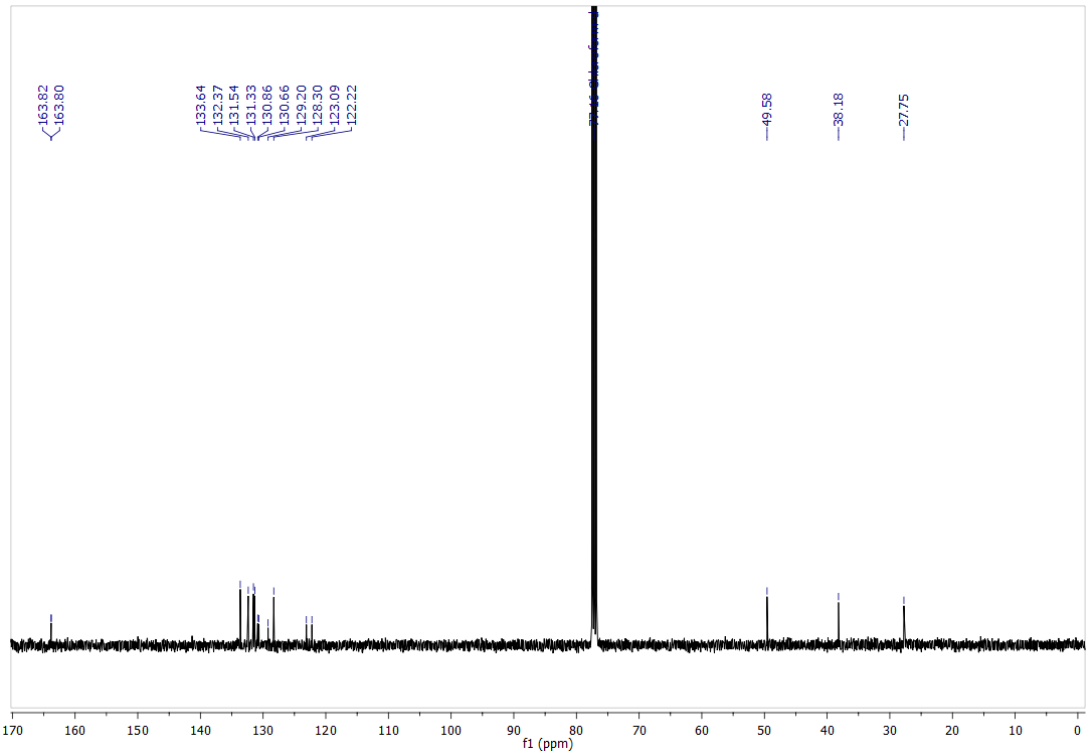
163.82
163.80
133.64
132.37
131.54
131.33
130.86
130.66
129.20
128.30
123.09
122.22
49.58
38.18
27.75
f1 (ppm)

*2-(3-Azidopropyl)-6-bromo-1H-benzo[de]isoquinoline-1,3(2H)-dione (**70**):*

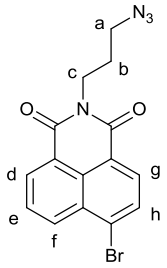

4-Bromo-1,8-naphthalic anhydride (0.25 g, 0.91 mmol) was dissolved in EtOH (30 mL). 3-azido-1-aminopropane (0.46 g, 4.6 mmol) was added to the solution and the reaction left to stir at reflux overnight. After slow cooling to r.t, the resulting precipitate was collected by suction filtration and purified by flash column chromatography (4:1 CH_2Cl_2/EtOAc) to give bromide **70** as a brown solid (0.26 g, 79%). ^{1}H NMR (400 MHz, $CDCl_3$) δ_H 8.67 (d, *J* = 7.2, 1H, H_d), 8.59 (d, *J* = 8.5, 1H, H_f), 8.42 (d, *J* = 7.8, 1H, H_g), 8.05 (d, *J* = 7.8, 1H, H_h), 7.86 (m, 1H, H_e), 4.28 (t, *J* = 7.0, 2H, H_c), 3.44 (t, *J* = 6.8, 2H, H_a), 2.04 (app. quint, *J* = 6.8, 2H, H_b). ^{13}C NMR (101 MHz, $CDCl_3$) δ_C 163.8, 163.8, 133.6, 132.4, 131.5, 131.3, 130.8, 130.6, 129.2, 128.3, 123.1, 122.2, 49.6, 38.2, 27.7. M.p. (°C) 92-93. HRMS (EI) calcd for $C_{15}H_{11}{}^{79}BrN_4O_2$ $[M + H]^+$ 359.0138, found 359.0141. UV: $\lambda_{max}(CH_2Cl_2)$/nm (ε / $mol^{-1}cm^{-1}dm^3$) 357 (11646), 343 (13675), 327 (9214).

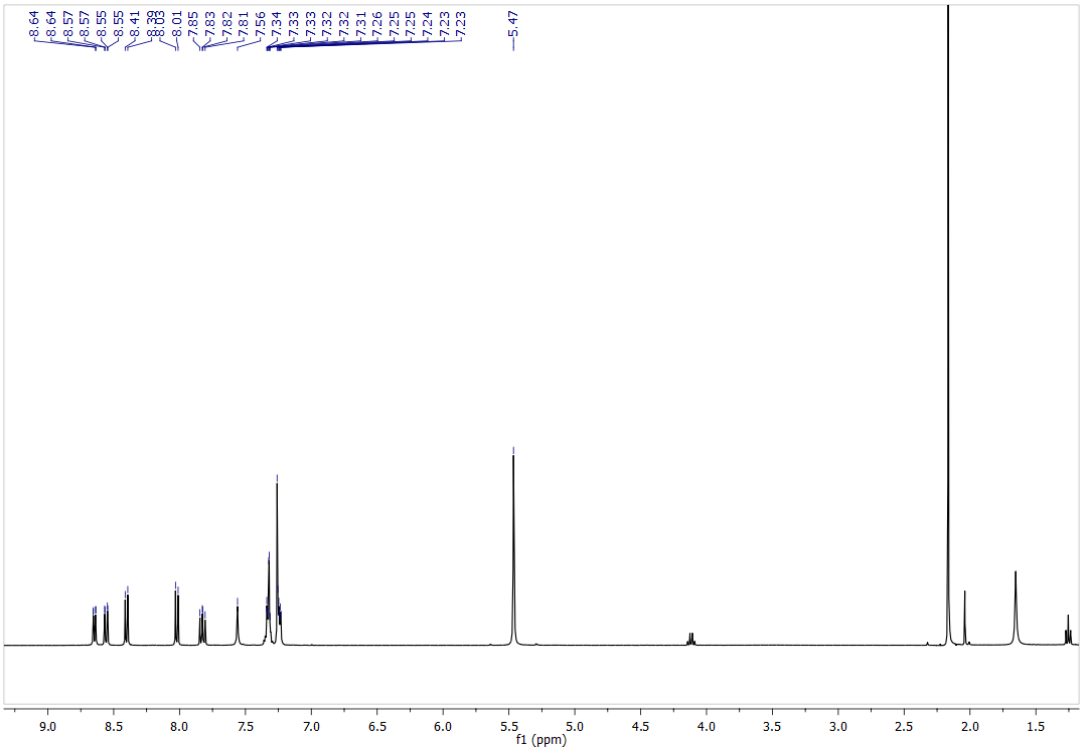
8.64
8.64
8.57
8.57
8.55
8.55
8.41
8.39
8.03
8.01
7.85
7.83
7.82
7.81
7.56
7.34
7.33
7.33
7.32
7.32
7.31
7.26
7.25
7.25
7.24
7.23
7.23
5.47
9.0
8.5
8.0
7.5
7.0
6.5
6.0
5.5
5.0
4.5
4.0
3.5
3.0
2.5
2.0
1.5
f1 (ppm)

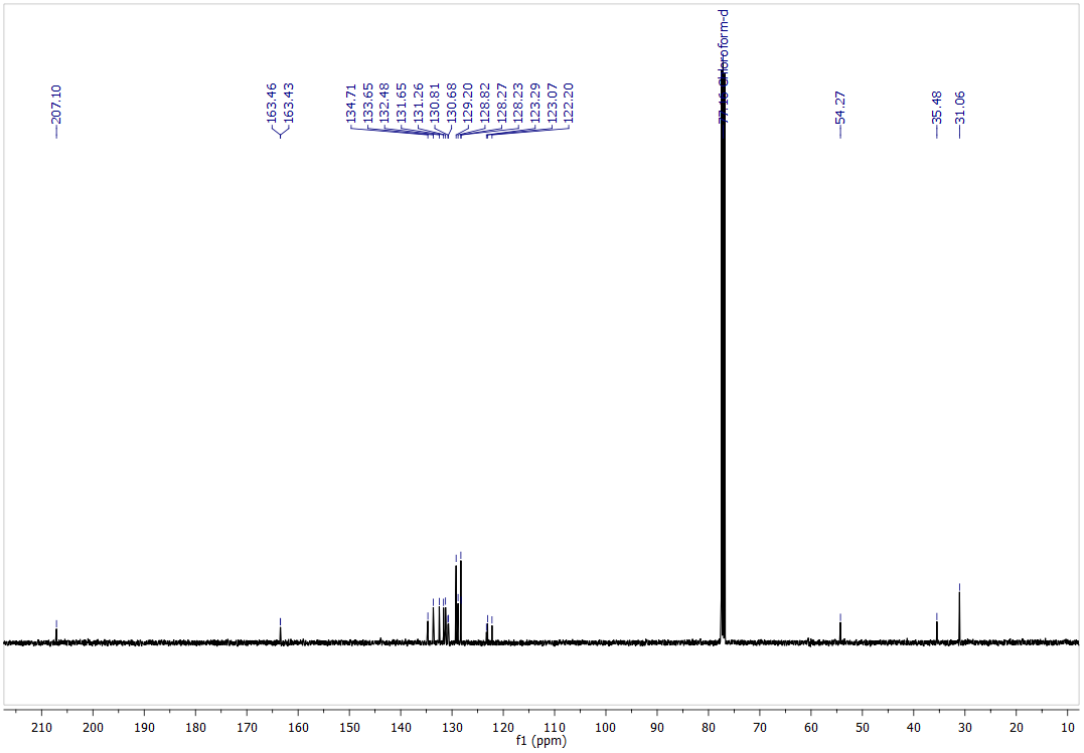
207.10
163.46
163.43
134.71
133.65
132.48
131.65
131.26
130.81
130.68
129.20
128.82
128.27
128.23
123.29
123.07
122.20
77.16 deuterochloroform-d
54.27
35.48
31.06
210
200
190
180
170
160
150
140
130
120
110
100
90
80
70
60
50
40
30
20
10
f1 (ppm)

*2-((1-Benzyl-1H-1,2,3-triazol-4-yl)methyl)-6-bromo-1H-benzo[de]isoquinoline-1,3(2H)-dione (**71**):*

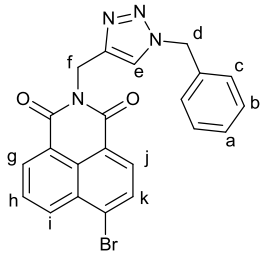

Acetylene **69** (1.0 g, 3.2 mmol), benzyl azide (0.43 g, 3.2 mmol), and CuI (60 mg, 10 mol%) were combined in a sealed CEM microwave vial which was purged with N_2. Anhydrous NMP (16 mL) was added, and the reaction stirred at r.t. for 1 h. The reaction mixture was diluted with a saturated solution of EDTA in 17.5% aqueous NH_3 (30 mL) and stirred for 5 min. The resulting precipitate was collected by suction filtration and purified by flash column chromatography (4:1 to 1:1 CH_2Cl_2/EtOAc) to yield triazole **71** as a pale yellow powder (1.35 g, 95%). ^{1}H NMR (400 MHz, $CDCl_3$) δ_H 8.64 (d, *J* = 7.3, 1H, H_g), 8.55 (d, *J* = 8.5, 1H, H_i), 8.40 (d, *J* = 7.8, 1H, H_j), 8.02 (d, *J* = 7.8, 1H, H_k), 7.82 (dd, *J* = 8.5, 7.3, 1H, H_h), 7.56 (s, 1H, H_e), 7.37-7.29 (m, 4H, H_b and H_c), 7.26-7.22 (m, 1H, H_a), 5.46 (s, 4H, H_d and H_f); ^{13}C NMR (101 MHz, $CDCl_3$) δ_C 207.1, 163.5, 163.4, 134.7, 133.6, 132.5, 131.6, 131.2, 130.8, 130.8, 129.2, 128.8, 128.3, 128.2, 123.3, 123.1, 122.2, 54.3, 35.5, 31.1; IR: (ν_{max}/cm^{-1}) 3133, 1700, 1653, 1586, 1337, 1049, 959, 779. M.p. (°C) 128-131. HRMS (EI) calcd for $C_{22}H_{16}{}^{79}BrN_4O_2$ $[M + H]^+$ 447.0451, found: 447.0450. UV: $\lambda_{max}(CH_2Cl_2)$/nm (ε / mol^{-1}cm^{-1}dm^3) 358 (3459), 343 (4066), 328 (2753).

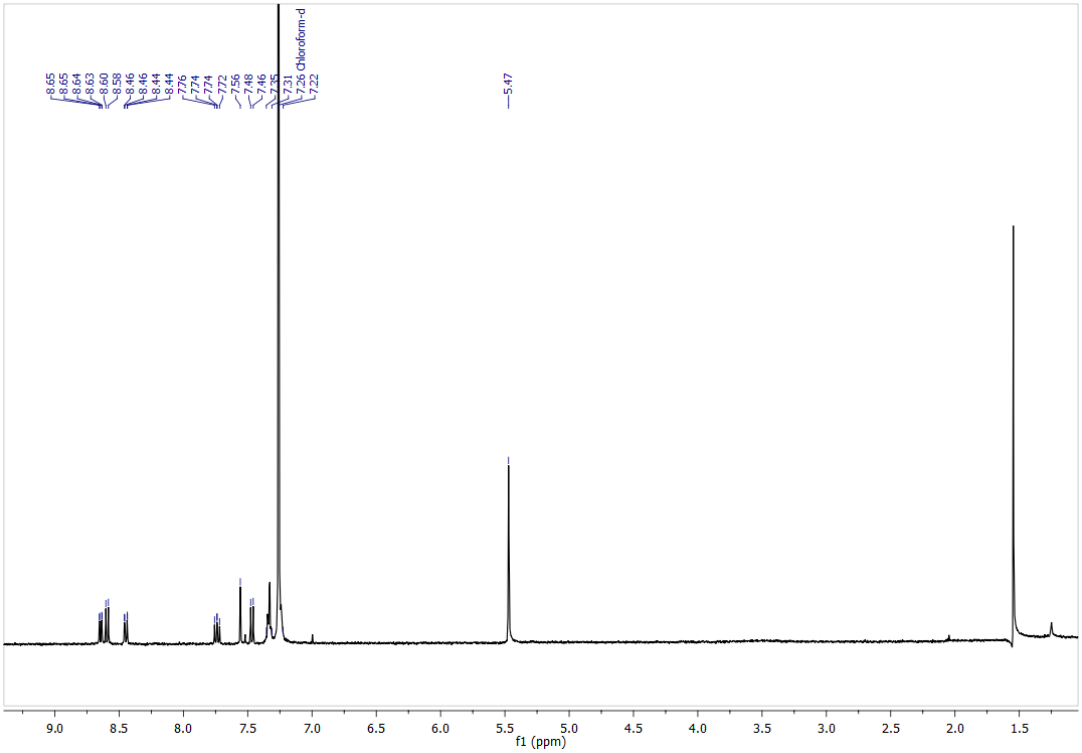
8.65
8.65
8.64
8.63
8.60
8.58
8.46
8.46
8.44
8.44
7.76
7.74
7.74
7.72
7.56
7.48
7.46
7.35
7.31
7.26 Chloroform-d
7.22
5.47
9.0
8.5
8.0
7.5
7.0
6.5
6.0
5.5
5.0
4.5
4.0
3.5
3.0
2.5
2.0
1.5
f1 (ppm)

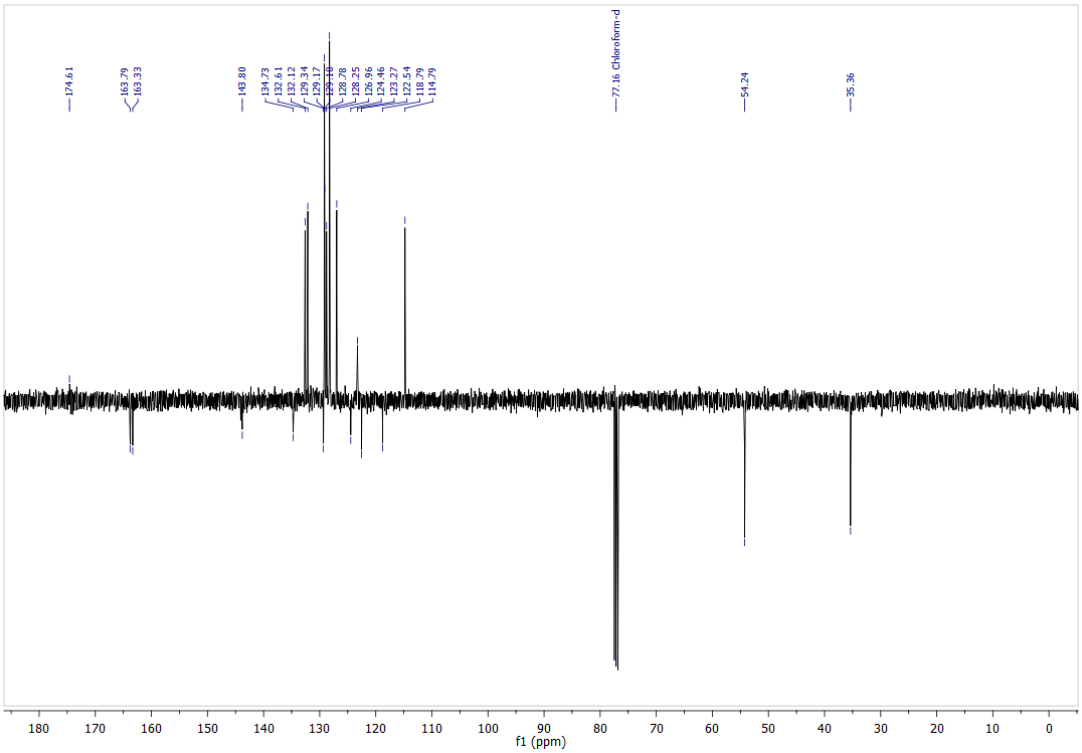
174.61
163.79
163.33
149.80
134.73
132.61
132.12
129.34
129.17
129.10
128.78
128.25
126.96
124.46
123.27
122.54
118.79
114.79
77.16 Chloroform-d
54.24
35.36
180
170
160
150
140
130
120
110
100
90
80
70
60
50
40
30
20
10
0
f1 (ppm)

*2-((1-Benzyl-1H-1,2,3-triazol-4-yl)methyl)-6-azido-1H-benzo[de]isoquinoline-1,3(2H)-dione (**72**):*

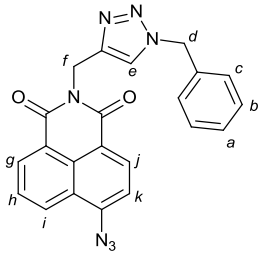

Bromo-triazole **71** (1.4 g, 3.2 mmol), and NaN_3 (0.25 g, 3.80 mmol) were combined in a sealed CEM microwave vial which was purged with N_2 and wrapped in foil. Anhydrous NMP (16 mL) was added, and the reaction stirred at r.t. for 24 h. The reaction mixture was diluted with water (30 mL) and stirred for 5 min. The resulting precipitate was collected by suction filtration and purified by flash column chromatography (1:1 Petrol/EtOAc) to yield azide **72** as a yellow powder (0.72 g, 55%). ^{1}H NMR (400 MHz, $CDCl_3$) δ_H 8.64 (d, *J* = 7.2, 1H, H_g), 8.59 (d, *J* = 8.1, 1H, H_j), 8.44 (d, *J* = 8.4, 1H, H_i), 7.73 (dd, *J* = 7.4, 8.4, 1H, H_h), 7.55 (s, 1H, H_e), 7.46 (d, *J* = 8.0, 1H, H_k), 7.35-7.31 (m, 3H, H_a and H_b), 7.26-7.22 (m, 2H, H_c). 5.47 (s, 4H, H_d and H_f). ^{13}C NMR (101 MHz, $CDCl_3$) δ_C 174.6, 163.8, 163.3, 143.8, 134.7, 132.6, 132.2, 129.3, 129.2, 129.1, 128.8, 128.3, 126.9, 124.5, 123.3, 122.5, 118.8, 114.8, 54.2, 35.4. IR: (ν_{max}/cm^{-1}) 3142, 2923, 2120, 1655, 1579, 1325, 1233, 1046, 780. M.p. (°C) 160-162. HRMS (EI) calcd for $C_{22}H_{16}N_7O_2$ $[M + H]^+$ 410.1360, found: 410.1358. UV: $\lambda_{max}(CH_2Cl_2)$/nm (ε / mol^{-1}cm^{-1}dm^3) 384 (9103), 367 (11295), 344 (7235).

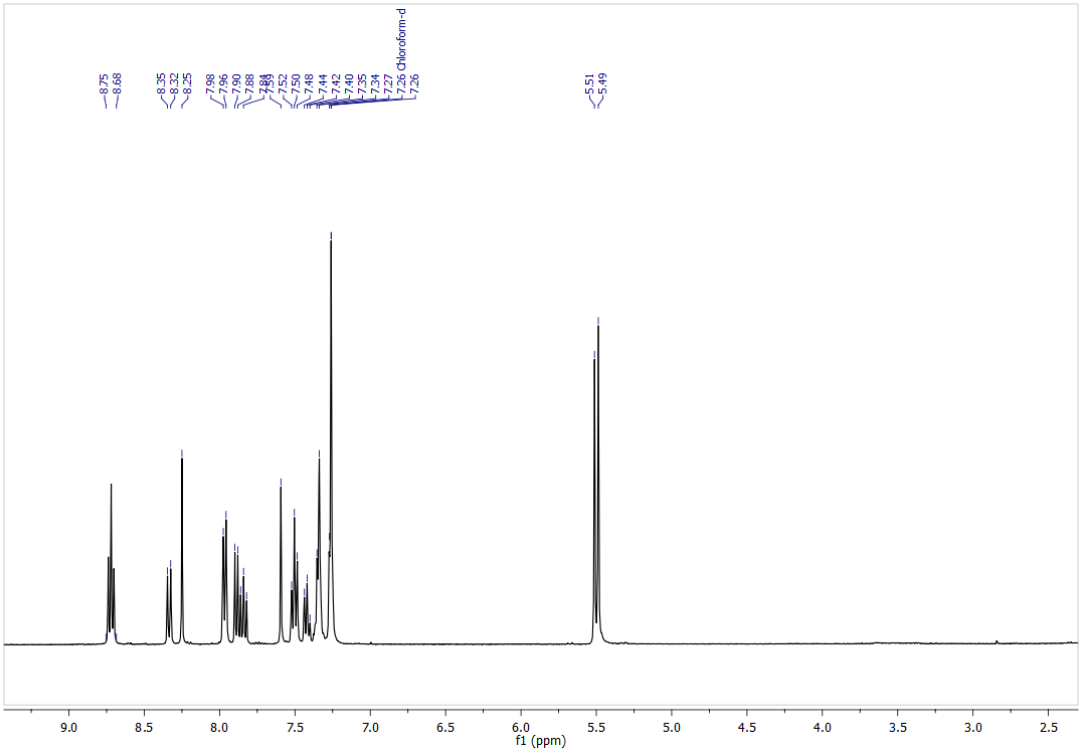
8.75
8.68
8.35
8.32
8.25
7.98
7.96
7.90
7.88
7.84
7.82
7.52
7.50
7.48
7.44
7.42
7.40
7.35
7.34
7.27
7.26 Chloroform-d
7.26
5.51
5.49
9.0
8.5
8.0
7.5
7.0
6.5
6.0
5.5
5.0
4.5
4.0
3.5
3.0
2.5
f1 (ppm)

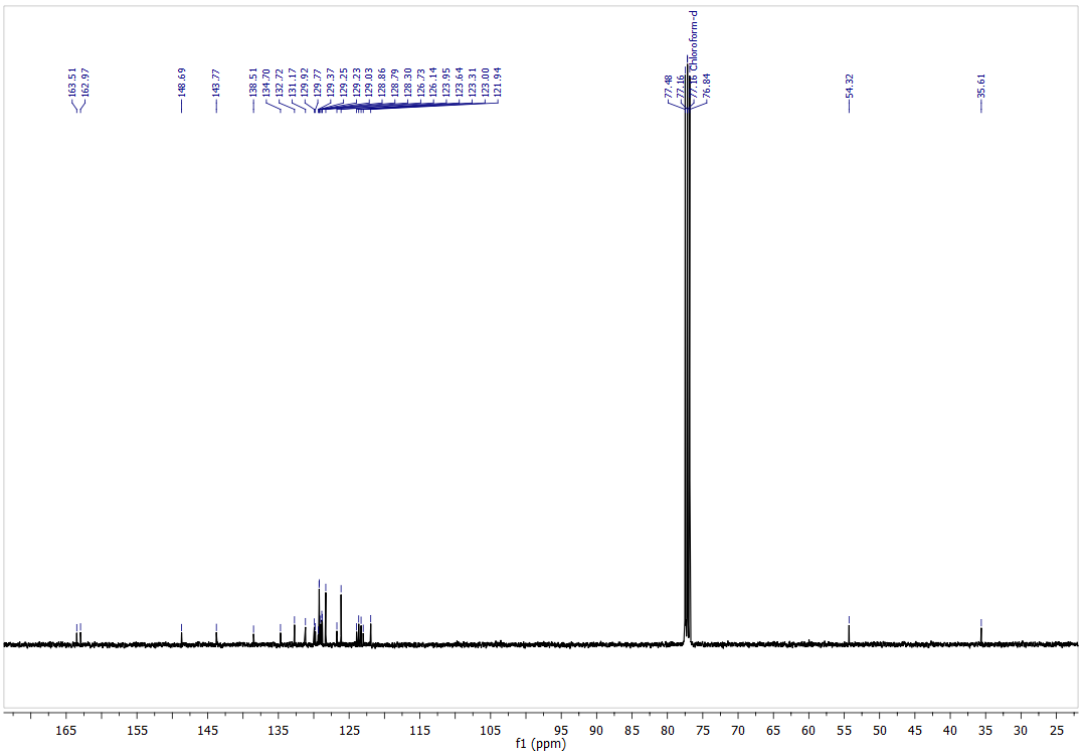
163.51
162.97
148.69
143.77
138.51
134.70
132.72
131.17
129.92
129.77
129.37
129.25
129.23
129.03
128.86
128.79
128.30
126.73
126.14
123.95
123.64
123.31
123.00
121.94
77.48
77.16
77.16 Chloroform-d
76.84
54.32
35.61
165
155
145
135
125
115
105
95
90
85
80
75
70
65
60
55
50
45
40
35
30
25
f1 (ppm)

*2-((1-Benzyl-1H-1,2,3-triazol-4-yl)methyl)-6-(4-phenyl-1H-1,2,3-triazol-1-yl)-1H-benzo[de]isoquinoline-1,3(2H)-dione (**73**):*

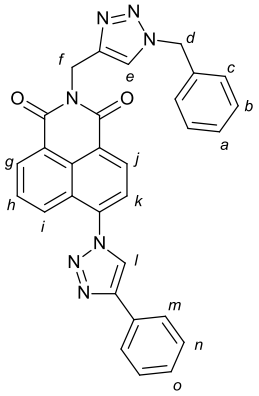

Triazole-azide **72** (0.050 g, 0.12 mmol), phenylacetylene (0.014 mL, 0.12 mmol), CuI (2.3 mg, 10 mol%) and NaOAc (1.1 mg, 10 mol%) were combined in a sealed CEM microwave vial which was purged with N_2. Anhydrous NMP (0.61 mL) was added, and the reaction stirred at r.t. for 16 h. The reaction mixture was diluted with a saturated solution of EDTA in 17.5% aqueous NH_3 (5 mL) and stirred for 5 min. The resulting precipitate was collected by suction filtration and purified by flash column chromatography (100% CH_2Cl_2 to 1:1 CH_2Cl_2/EtOAc) to yield bis-triazole **73** as a pale yellow powder (0.051 g, 81%). ^{1}H NMR (400 MHz, $CDCl_3$) δ_H 8.75-8.68 (m, 2H, H_g and H_j), 8.33 (d, J = 8.5, 1H, H_i), 8.25 (s, 1H, H_l), 7.96 (d, J = 7.4, 2H, H_m), 7.88 (d, J = 7.8, 1H, H_k), 7.86-7.82 (m, 1H, H_h), 7.59 (s, 1H, H_e), 7.52-7.48 (m, 2H, H_n), 7.43-7.40 (m, 1H, H_o), 7.36-7.31 (m, 3H, H_a and H_b), 7.27-7.23 (m, 2H, H_c), 5.51 (s, 2H, H_f), 5.49 (s, 2H, H_d). ^{13}C NMR (101 MHz, $CDCl_3$) δ_C 163.5, 162.9, 148.7, 143.7, 138.5, 134.7, 132.7, 131.1, 129.9, 129.7, 129.4, 129.3, 129.2, 129.0, 128.8, 128.7, 128.3, 126.7, 126.1, 123.9, 123.6, 123.3, 123.0, 121.9, 54.3, 35.6. IR: (ν_{max}/cm^{-1}) 3128, 3066, 1705, 1658, 1584, 1401, 1121, 1023, 953, 850, 781, 761, 718. M.p. (°C) >230. HRMS (EI) calcd for $C_{30}H_{22}N_7O_2$ $[M + H]^+$ 512.1829, found: 512.1829. UV: $\lambda_{max}(CH_2Cl_2)$/nm (ε / mol^{-1}cm^{-1}dm^3) 344 (9099).

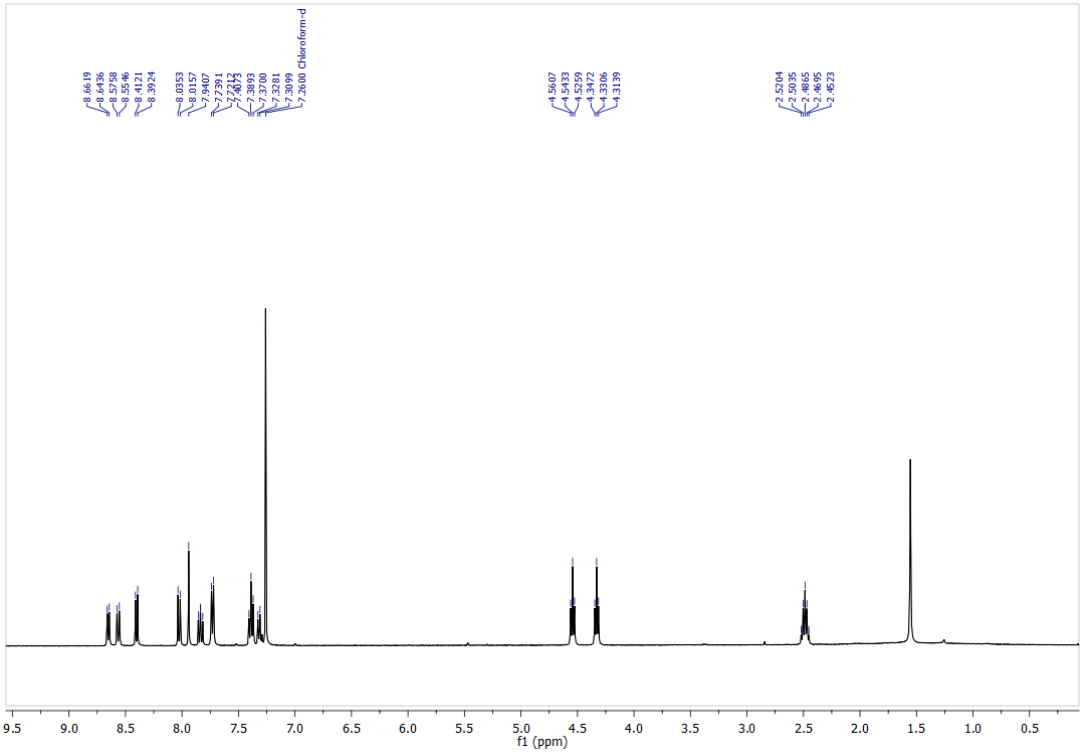
8.6619
8.6436
8.5758
8.5546
8.4121
8.3924
8.0353
8.0157
7.9407
7.7391
7.7212
7.4073
7.3893
7.3700
7.3281
7.3099
7.2660 Chloroform-d
4.5607
4.5433
4.5259
4.3472
4.3306
4.3139
2.5204
2.5035
2.4865
2.4695
2.4523
f1 (ppm)

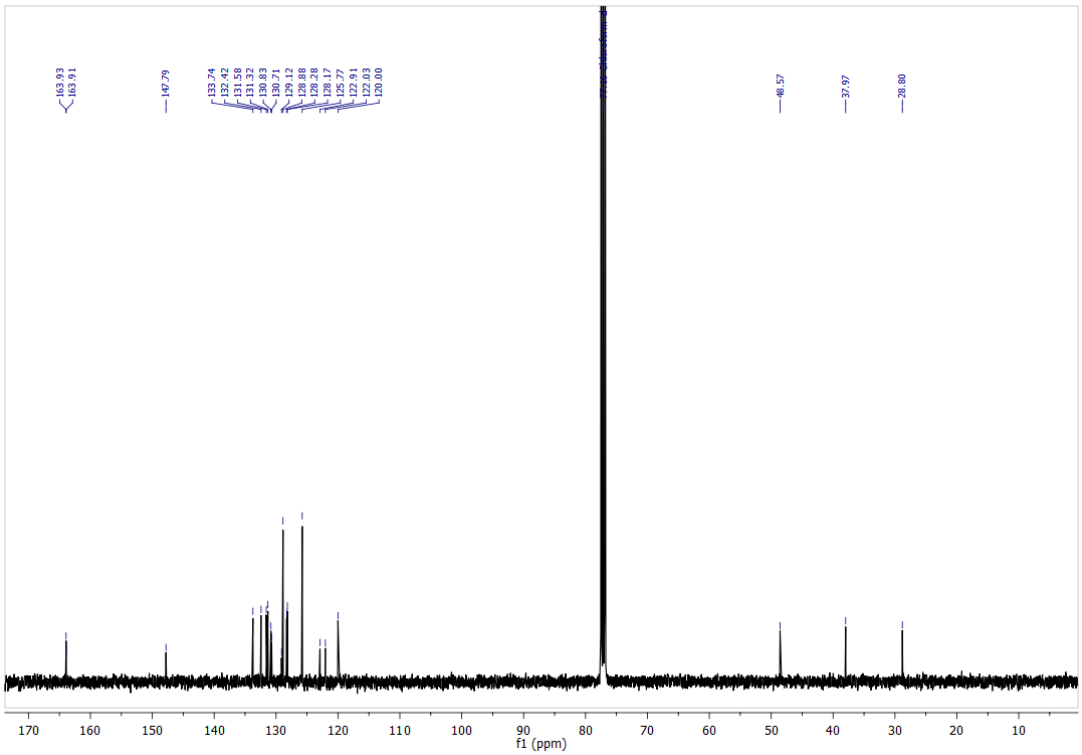
163.93
163.91
147.79
133.74
132.42
131.58
131.32
130.83
130.71
129.12
128.88
128.28
128.17
125.77
122.91
122.03
120.00
48.57
37.97
28.80
f1 (ppm)

*6-Bromo-2-(3-(4-phenyl-1H-1,2,3-triazol-1-yl)propyl)-1H-benzo[de]isoquinoline-1,3(2H)-dione (**77**):*

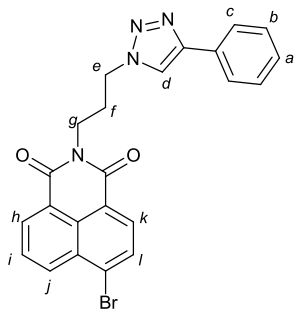

Azide **70** (0.20 g, 0.56 mmol), phenylacetylene (0.062 mL, 0.56 mmol), and CuI (10 mg, 10 mol%) were combined in a sealed CEM microwave vial which was purged with N_2. Anhydrous NMP (2.8 mL) was added, and the reaction stirred at r.t. for 1 h. The reaction mixture was diluted with a saturated solution of EDTA in 17.5% aqueous NH_3 and stirred for 5 min. The resulting precipitate was collected by suction filtration and purified by flash column chromatography (4:1 to 1:1 CH_2Cl_2/EtOAc) to yield triazole **77** as a pale yellow powder (0.17 g, 67%). ^{1}H NMR (400 MHz, $CDCl_3$) δ_H 8.65 (d, *J* = 7.3, 1H, H_h), 8.56 (d, *J* = 8.5, 1H, H_j), 8.40 (d, *J* = 7.9, 1H, H_k), 8.02 (d, *J* = 7.9, 1H, H_l), 7.94 (s, 1H, H_d), 7.83 (dd, *J* = 8.3, 7.4, 1H, H_i), 7.75 (m, 2H, H_c), 7.42-7.36 (m, 2H, H_b), 7.34-7.28 (m, 1H, H_a), 4.54 (t, *J* = 6.9, 2H, H_g), 4.33 (t, *J* = 6.6, 2H, H_e), 2.48 (app. quint, *J* = 6.8, 2H, H_f). ^{13}C NMR (101 MHz, $CDCl_3$) δ_C 163.9, 163.9, 147.8, 133.7, 132.4, 131.6, 131.3, 130.8, 130.7, 129.1, 128.9, 128.3, 128.2, 125.7, 122.9, 122.0, 120.0, 48.6, 37.9, 28.8; IR: (ν_{max}/cm^{-1}) 3142, 3061, 1698. 1659, 1586, 1568, 1460, 1345, 1225, 1055, 970, 918, 810, 767, 696. M.p. (°C) 200-202. HRMS (EI) calcd for $C_{23}H_{17}{}^{79}BrN_4O_2$ $[M + H]^+$ 461.0608, found 461.0604. UV: $\lambda_{max}(CH_2Cl_2)$/nm (ε / mol^{-1}cm^{-1}dm^3) 358 (20486), 343 (23859), 327 (15782).

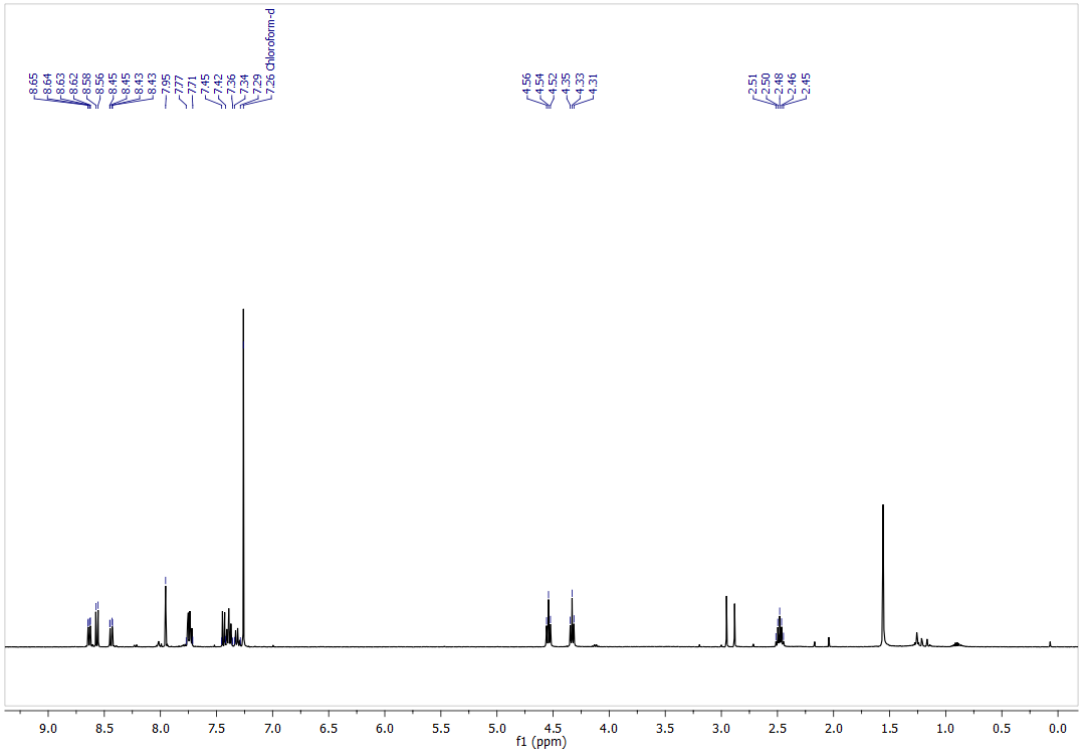
8.65
8.64
8.63
8.62
8.58
8.56
8.45
8.45
8.43
8.43
7.95
7.77
7.71
7.45
7.42
7.36
7.34
7.29
7.26 Chloroform-d
4.56
4.54
4.52
4.35
4.33
4.31
2.51
2.50
2.48
2.46
2.45
9.0
8.5
8.0
7.5
7.0
6.5
6.0
5.5
5.0
4.5
4.0
3.5
3.0
2.5
2.0
1.5
1.0
0.5
0.0
f1 (ppm)

*6-Azido-2-(3-(4-phenyl-1H-1,2,3-triazol-1-yl)propyl)-1H-benzo[de]isoquinoline-1,3(2H)-dione (**78**):*

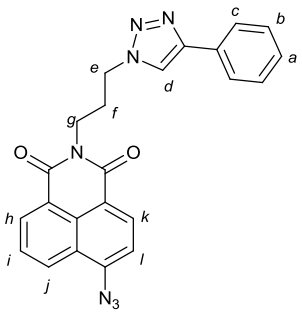

Bromo-triazole **77** (50 mg, 0.11 mmol), and NaN_3 (9.0 mg, 1.2 equiv., 0.13 mmol) were combined in a sealed CEM microwave vial which was purged with N_2 and wrapped in foil. Anhydrous NMP (0.54 mL) was added, and the reaction stirred at r.t. for 24 h. The reaction mixture was diluted with H_2O (5 mL) and stirred for 5 min. The resulting precipitate was collected by suction filtration and purified by flash column chromatography (1:1 Petrol/EtOAc) to yield azide **78** as a yellow powder (35 mg, 76%). ^{1}H NMR (400 MHz, $CDCl_3$) δ_H 8.63 (d, *J* = 7.3, 1H, H_h), 8.56 (d, *J* = 8.0, 1H, H_k), 8.44 (d, *J* = 8.4, 1H, H_j), 7.96 (s, 1H, H_d), 7.77-7.71 (m, 2H, H_i and H_l), 7.45-7.35 (m, 4H, H_b and H_c), 7.34-7.28 (m, 1H, H_a), 4.54 (t, *J* = 7.0, 2H, H_g), 4.33 (t, *J* = 6.6, 2H, H_e), 2.48 (app. quint, *J* = 6.8, 2H, H_f). Due to the instability of **78** we were unable to obtain further characterisation data and it as used in subsequent reactions immediately.

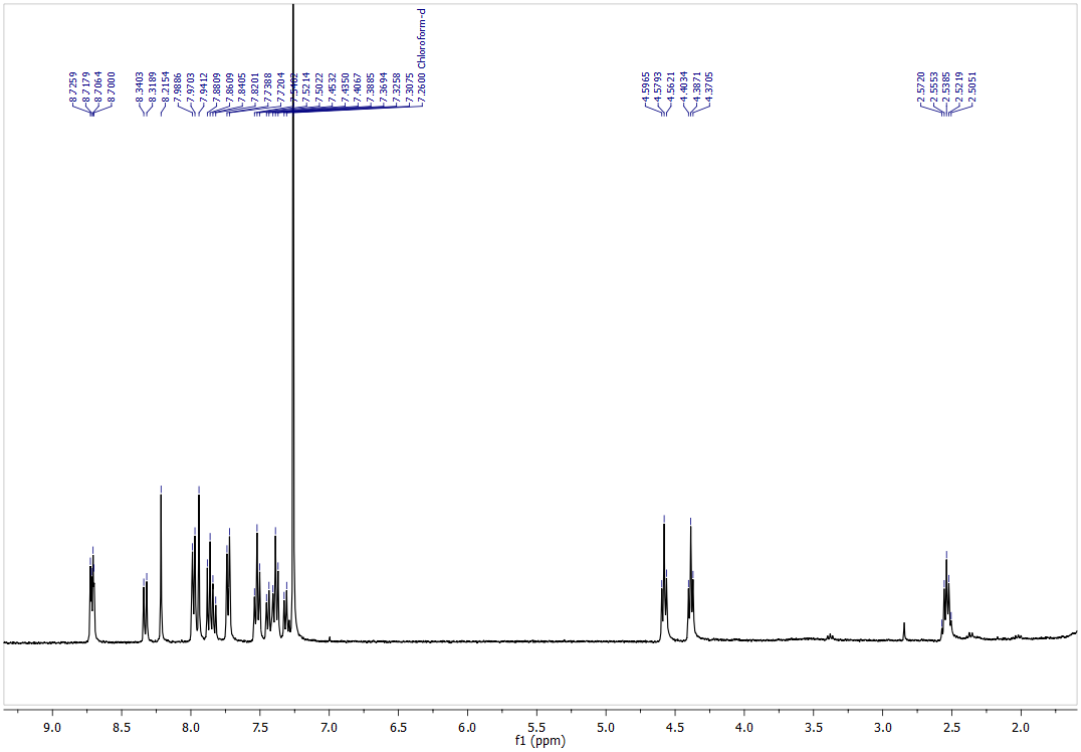
8.7259
8.7179
8.7064
8.7000
8.3403
8.3189
8.3154
8.2896
7.9703
7.9412
7.8809
7.8609
7.8405
7.8201
7.7388
7.7204
7.5402
7.5214
7.5022
7.4852
7.4630
7.4067
7.3885
7.3694
7.3258
7.3075
7.2600 Chloroform-d
4.5965
4.5793
4.5621
4.4034
4.3871
4.3705
2.5720
2.5553
2.5385
2.5219
2.5051
9.0
8.5
8.0
7.5
7.0
6.5
6.0
5.5
5.0
4.5
4.0
3.5
3.0
2.5
2.0
f1 (ppm)

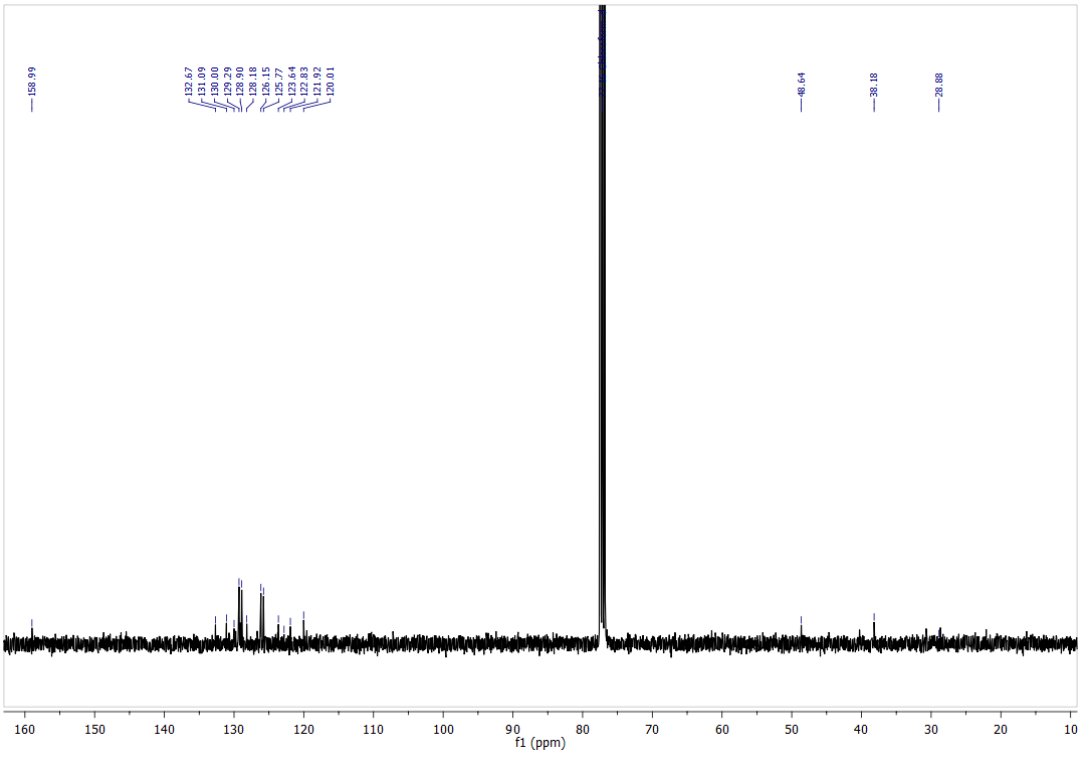
158.99
132.67
131.09
130.00
129.29
128.90
128.18
126.15
125.77
123.64
122.83
121.92
120.01
48.64
38.18
28.88
160
150
140
130
120
110
100
90
80
70
60
50
40
30
20
10
f1 (ppm)

*6-(4-Phenyl-1H-1,2,3-triazol-1-yl)-2-(3-(4-phenyl-1H-1,2,3-triazol-1-yl)propyl)-1H-benzo[de]isoquinoline-1,3(2H)-dione (**79**):*

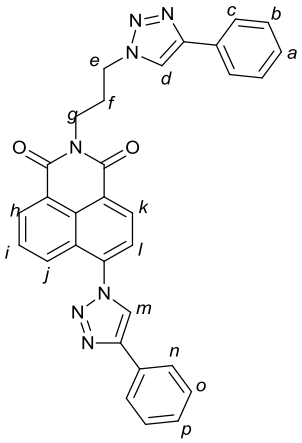

Triazole-azide **78** (64 mg, 0.15 mmol), phenylacetylene (0.02 mL, 0.15 mmol), CuI (2.8 mg, 10 mol%) and NaOAc (1.2 mg, 10 mol%) were combined in a sealed CEM microwave vial which was purged with N_2. Anhydrous NMP (0.76 mL) was added, and the reaction stirred at r.t. for 16 h. The reaction mixture was diluted with a saturated solution of EDTA in 17.5% aqueous NH_3 (10 mL) and stirred for 5 min. The resulting precipitate was collected by suction filtration and purified by flash column chromatography (100% CH_2Cl_2 to 1:1 CH_2Cl_2/EtOAc) to yield bis-triazole **79** as a pale yellow powder (64 mg, 81%). ^{1}H NMR (400 MHz, $CDCl_3$) δ_H 8.72 (d, *J* = 7.8, 1H, H_k), 8.71 (d, *J* = 7.2, 1H, H_h), 8.32 (d, *J* = 8.5, 1H, H_j), 8.21 (s, 1H, H_m), 7.97 (d, *J* = 7.3, 2H, H_n), 7.94 (s, 1H, H_d), 7.89-7.81 (m, 2H, H_i and H_l), 7.73 (d, *J* = 7.3, 2H, H_b), 7.55-7.49 (m, 2H, H_o), 7.47-7.35 (m, 3H, H_c and H_p), 7.34-7.28 (m, 1H, H_a), 4.57 (t, *J* = 6.8, 2H, H_g), 4.38 (t, *J* = 6.6, 2H, H_e), 2.53 (app. quint, *J* = 6.6, 2H, H_f). ^{13}C NMR (101 MHz, $CDCl_3$) δ_C 158.9, 158.9, 132.7, 131.1, 130.0, 129.7, 129.3, 129.1, 128.9, 128.8, 128.2, 126.2, 125.7, 123.6, 121.9, 120.0, 48.6, 38.2, 28.7. IR: (ν_{max}/cm^{-1}) 3126, 3064, 2923, 2112, 1698, 1654, 1583, 1517, 1465, 1432, 1400, 1348, 1232, 1188, 1152, 1057, 976, 898, 783. M.p. (°C) 185-188. HRMS (EI) calcd for $C_{31}H_{23}N_7O_2$ $[M + H]^+$ 526.1986, found 526.1979. UV: $\lambda_{max}(CH_2Cl_2)$/nm (ε / mol^{-1}cm^{-1}dm^3) 345 (30104).

*One-pot: 2-((1-Benzyl-1H-1,2,3-triazol-4-yl)methyl)-6-(4-phenyl-1H-1,2,3-triazol-1-yl)-1H-benzo[de]isoquinoline-1,3(2H)-dione (**73**):*

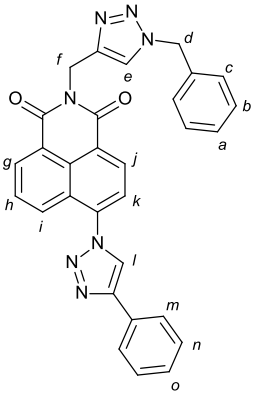

General procedure A was employed with **69** (0.31 g, 1.0 mmol), benzyl azide (0.13 g, 1.0 mmol) in NMP (3.33 mL), followed by phenylacetylene (0.11 mL, 1.0 mmol) and EtOH (3.33 mL). The crude product was obtained obtained *via* precipitation with a saturated solution of EDTA in 17.5% aqueous NH_3 (20 mL) and purified by flash column chromatography (100% CH_2Cl_2 to CH_2Cl_2/EtOAc 1:1) to yield bis-triazole **73** as a pale yellow powder (0.43 g, 85%). All spectroscopic data in accordance with double triazole **73** *vide supra*.

*One-pot: 6-(4-Phenyl-1H-1,2,3-triazol-1-yl)-2-(3-(4-phenyl-1H-1,2,3-triazol-1-yl)propyl)-1H-benzo[de]isoquinoline-1,3(2H)-dione (**79**):*

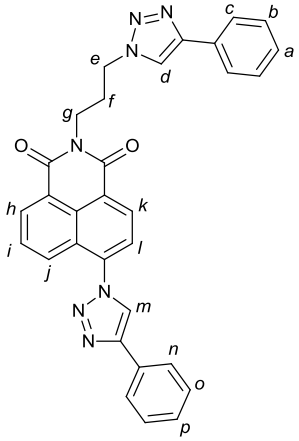

General procedure B was employed with **70** (0.36 g, 1.0 mmol)**,** phenylacetylene (0.11 mL, 1.0 mmol) in NMP (3.33 mL), followed by a second portion of phenylacetylene (0.11 mL, 1.0 mmol) and EtOH (3.33 mL). The crude product was obtained obtained *via* precipitation with a saturated solution of EDTA in 17.5% aqueous NH_3 (20 mL) and purified by flash column chromatography (100% CH_2Cl_2 to CH_2Cl_2/EtOAc 1:1) to yield bis-triazole **79** a pale yellow powder (0.37 g, 72%). All spectroscopic data in accordance with double triazole **79** *vide supra*.

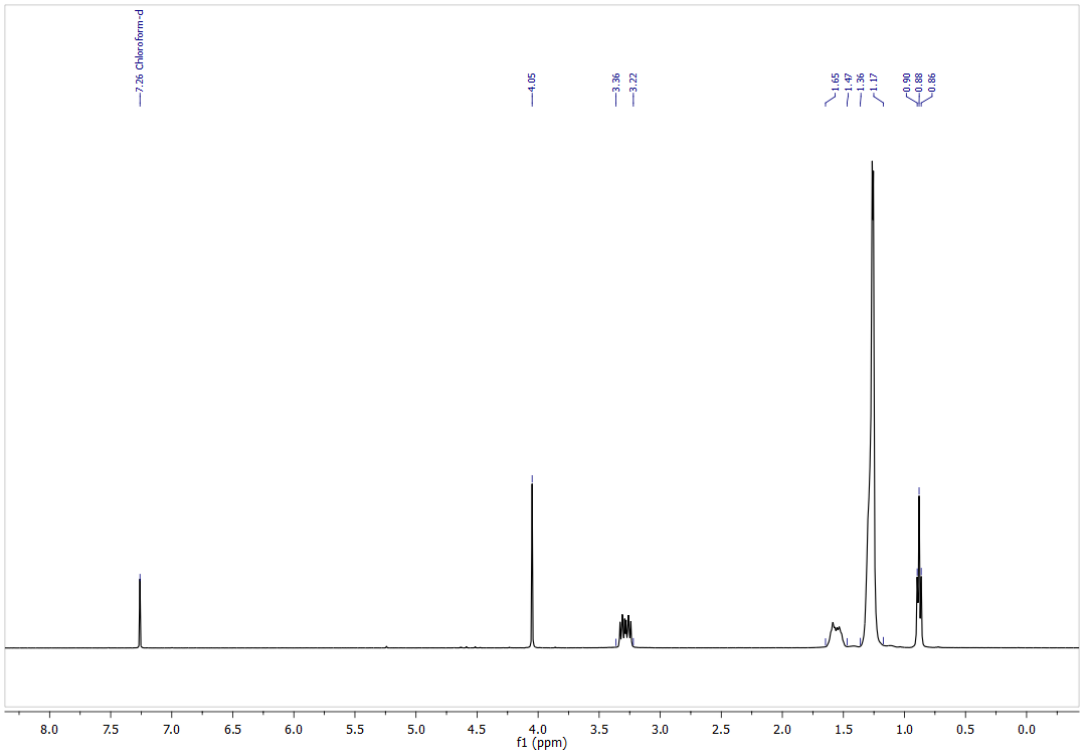
7.26 Chloroform-d
4.05
3.36
3.22
1.65
1.47
1.36
1.17
0.90
0.88
0.86
f1 (ppm)

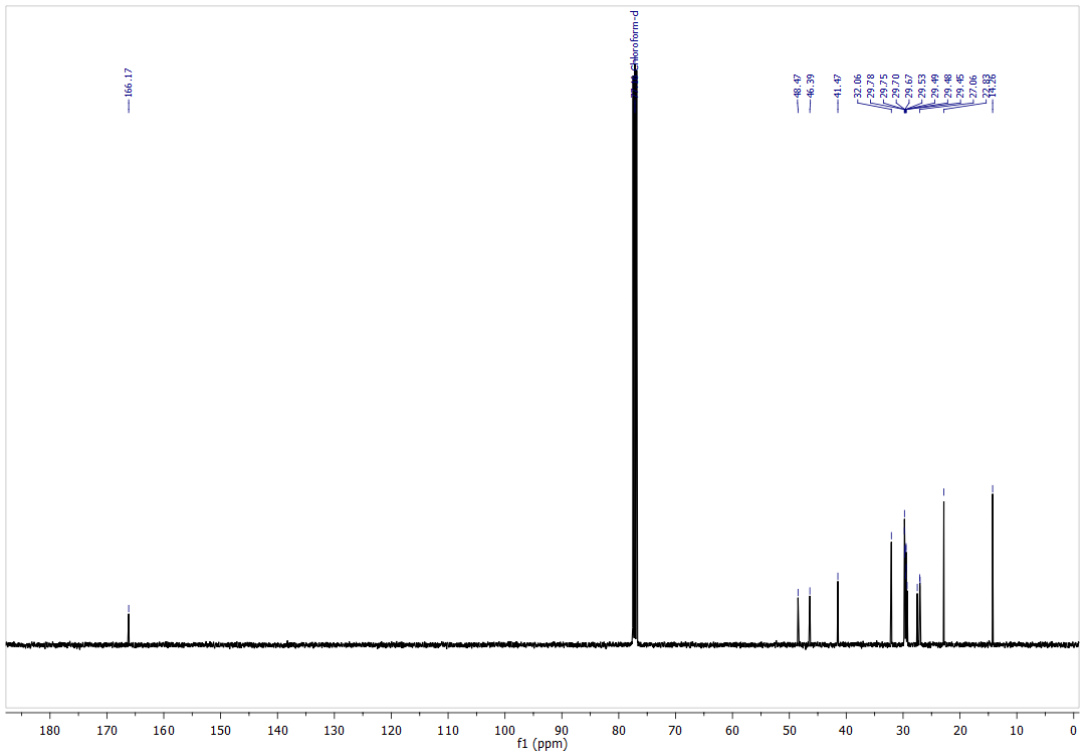
166.17
77.16 Chloroform-d
48.47
46.39
41.47
32.06
29.78
29.75
29.70
29.67
29.53
29.49
29.48
29.45
27.06
22.83
14.26
f1 (ppm)

*2-Chloro-N,N-didodecylacetamide (**81**):*

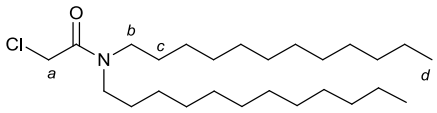

A solution of didodecylamine (2.00 g, 5.65 mmol) and NEt_3 (1.97 mL, 14.1 mmol) in dry CH_2Cl_2 (100 mL) was added in a slow dropwise manner to a solution of chloroacetyl chloride (0.54 mL, 6.79 mmol) in anhydrous CH_2Cl_2 (50 mL) at 0 °C under N_2. When the addition was complete, the red solution was warmed to r.t. and stirred for 24 h. The solution was filtered and the solid washed with chloroform (30 mL). The filtrate was further diluted with chloroform and washed with H_2O (2 x 200 mL), Na_2CO_3 solution (1 M, 2 x 200 mL), HCl solution (1 M, 2 x 200 mL) and brine (2 x 200 mL). The organic phase was dried over $MgSO_4$ and the solvent was removed *in vacuo*. The crude oil was purified by flash column chromatography (4:1 CH_2Cl_2/EtOAc) to yield chloride **81** as a clear oil (1.86 g, 76%). ^{1}H NMR (400 MHz, $CDCl_3$) δ_H 4.05 (s, 2H, H_a), 3.36-3.22 (m, 4H, H_b), 1.65-1.47 (m, 4H, H_c), 1.36-1.17 (m, 36H, alkyl-H), 0.92-0.84 (m, 6H, H_d). ^{13}C NMR (101 MHz, $CDCl_3$) δ_C 166.2, 48.4, 46.3, 41.5, 32.0, 29.8, 29.7, 29.7, 29.6, 29.5, 29.5, 29.4, 29.4, 29.3, 27.5, 27.1, 27.0, 22.8, 14.3. IR: (ν_{max}/cm^{-1}) 2921, 2852, 1653, 1458, 1376, 1302, 1122, 925, 790. HRMS (EI) calcd for $C_{26}H_{52}ClNO$ $[M + H]^+$ 430.3810, found 430.3810.

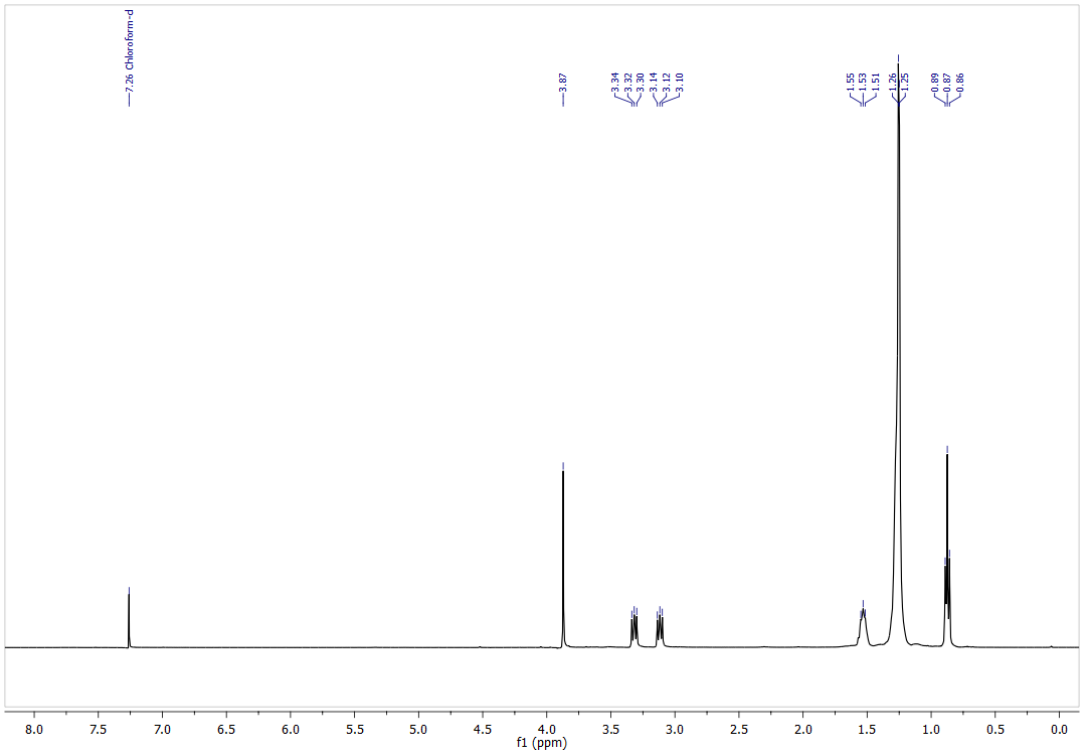
7.26 Chloroform-d
3.87
3.34
3.32
3.30
3.14
3.12
3.10
1.55
1.53
1.51
1.26
1.25
0.89
0.87
0.86
8.0 7.5 7.0 6.5 6.0 5.5 5.0 4.5 4.0 3.5 3.0 2.5 2.0 1.5 1.0 0.5 0.0
f1 (ppm)

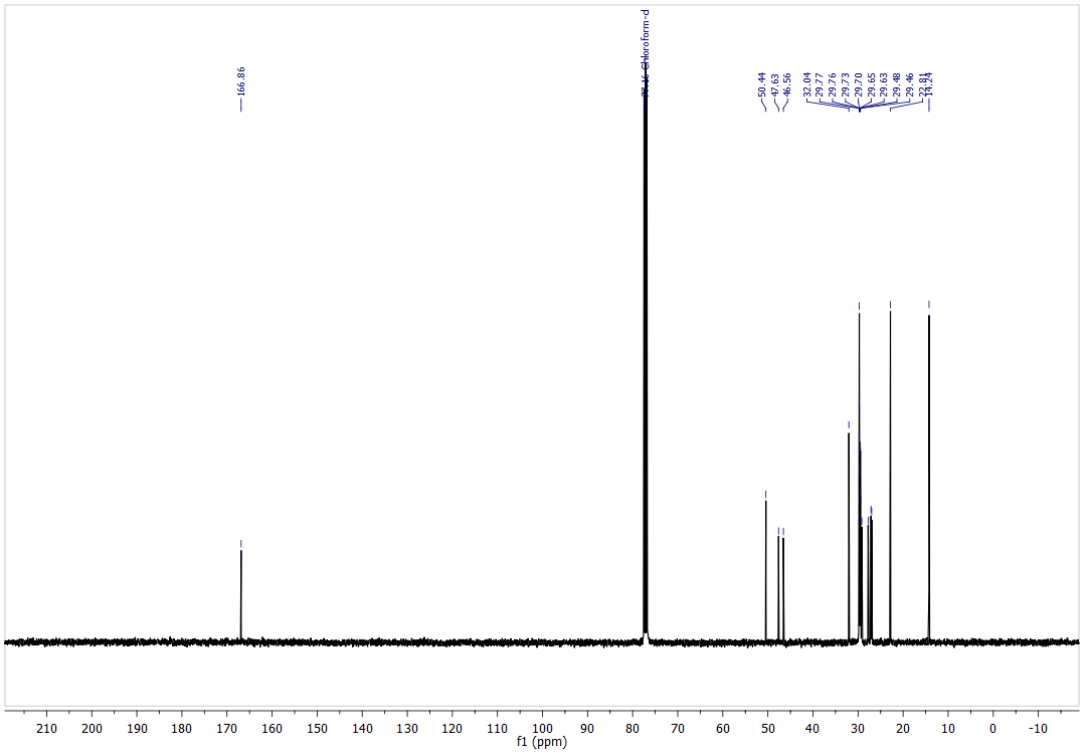
166.86
77.16 Chloroform-d
50.44
47.63
46.56
32.04
29.77
29.76
29.73
29.70
29.65
29.63
29.48
29.46
22.81
14.24
210 200 190 180 170 160 150 140 130 120 110 100 90 80 70 60 50 40 30 20 10 0 -10
f1 (ppm)

*2-Azido-N,N-didodecylacetamide (**82**):*

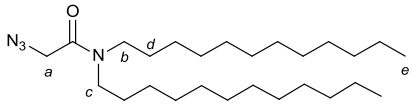

Chloride **81** (1.86 g, 4.31 mmol) and NaN_3 (1.68 g, 25 mmol) were combined in a flask purged with N_2, dissolved in dry DMF (60 mL) and stirred for 24 h at 65 °C. After cooling to r.t, the reaction mixture was slowly poured into icy H_2O (200 mL). The resulting precipitate was extracted with EtOAc (3 x 100 mL), the organic extracts combined and washed with saturated $NaHCO_3$ solution (2 x 200 mL), brine (2 x 200 mL) and H_2O (2 x 100 mL). The organic phase was dried over $MgSO_4$ and the solvent was removed *in vacuo* to give azide **82** as a viscous yellow oil (1.90 g, 98%). ^{1}H NMR (400 MHz, $CDCl_3$) δ_H 3.87 (s, 2H, H_a), 3.31 (t, *J* = 7.6, 2H, H_b), 3.11 (t, *J* = 7.6, 2H, H_c), 1.58-1.48 (m, 4H, H_d), 1.35-1.20 (m, 36H, alkyl-H), 0.91-0.84 (m, 6H, H_e). ^{13}C NMR (101 MHz, $CDCl_3$) δ_C 166.9, 50.4, 47.6, 46.6, 32.0, 29.7, 29.7, 29.7, 29.7, 29.6, 29.6, 29.5, 29.5, 29.4, 29.4, 29.2, 27.8, 27.1, 26.9, 22.8, 14.2. IR: (ν_{max}/cm^{-1}) 2921, 2852, 2103, 1654, 1458, 1425, 1376, 1273, 720. HRMS (EI) calcd for $C_{26}H_{53}N_4O$ $[M + H]^+$ 437.4214, found 437.4215.

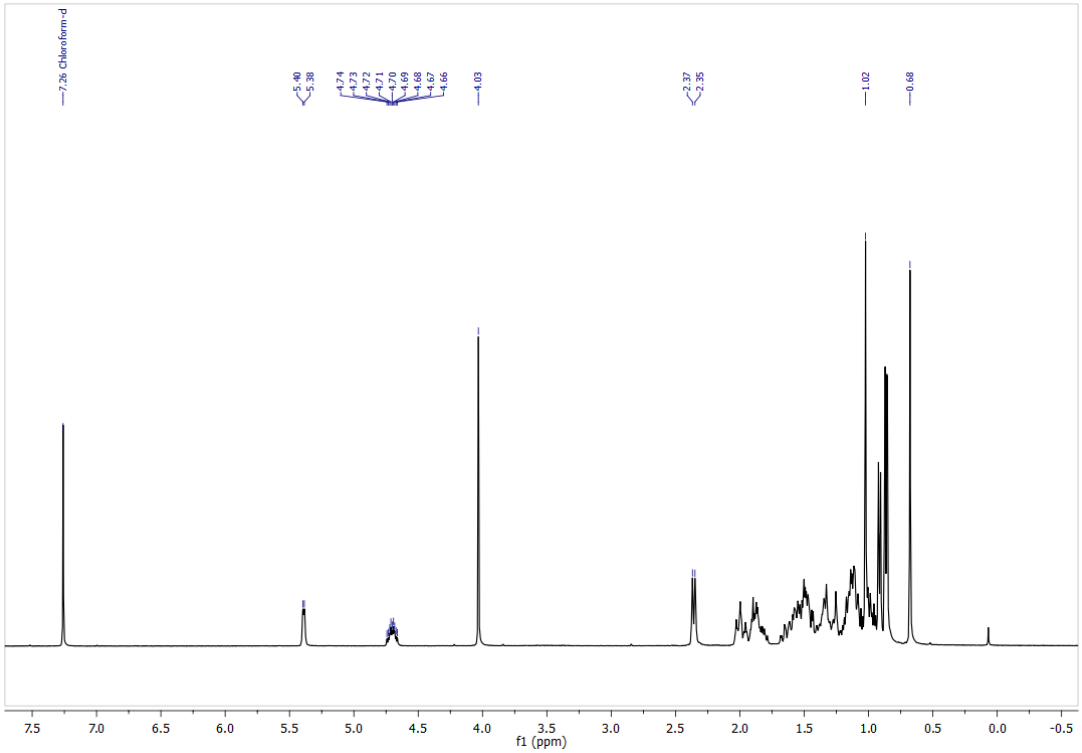
7.26 Chloroform-d
5.40
5.38
4.74
4.73
4.72
4.71
4.70
4.69
4.68
4.67
4.66
4.03
2.37
2.35
1.02
0.68
f1 (ppm)

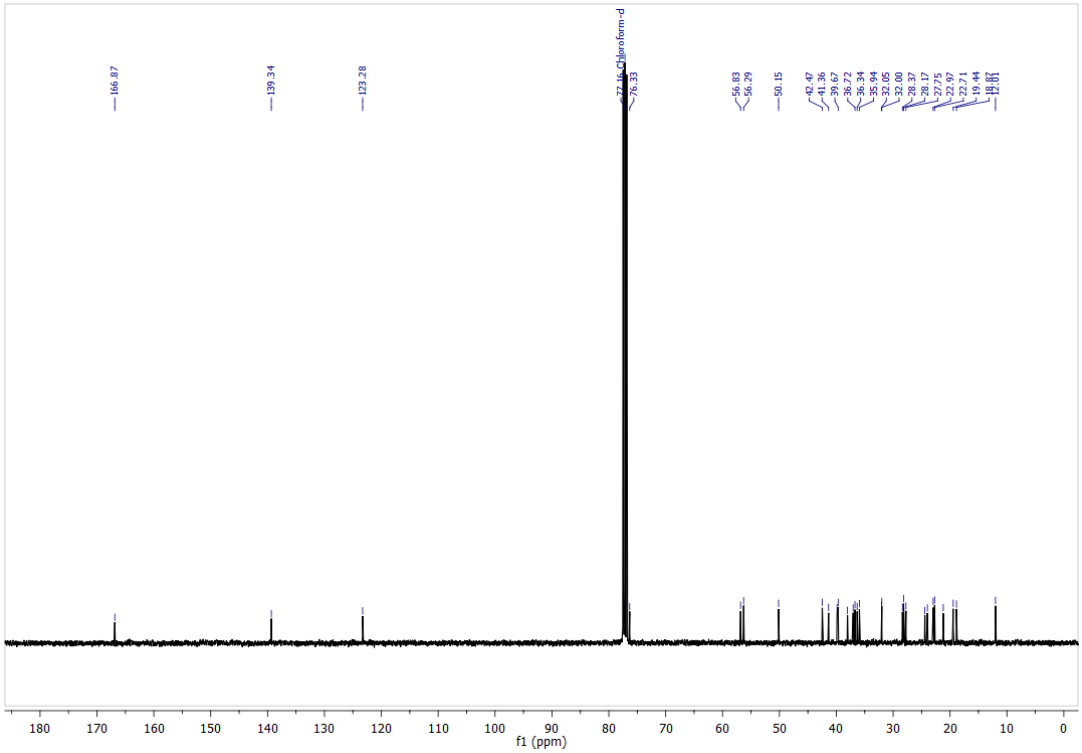
166.87
139.34
123.28
77.16 Chloroform-d
76.33
56.83
56.29
50.15
42.47
41.36
39.67
38.72
36.34
35.94
32.05
32.00
28.37
28.17
27.75
22.97
22.71
19.44
f1 (ppm)

*Cholesterol 2-chloroacetate (**84**):*

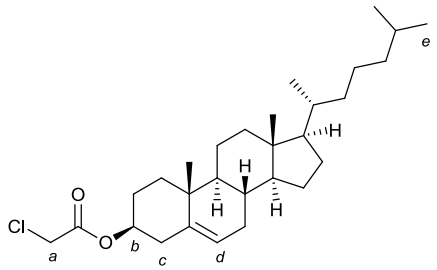

A solution of chloroacetyl chloride (0.25 mL, 3.10 mmol) in anhydrous CH2CL2 (25 mL) was added dropwise to a solution of cholesterol (1.00 g, 2.58 g) and NEt_3 (0.54 mL, 3.88 mmol) in anhydrous CH2CL2 (50 mL) at 0 ^{o}C under N_2. When the addition was complete, the solution was warmed to r.t. and stirred for 24 h. The reaction mixture was washed with aqueous HCl solution (1M, 2 x 100 mL). The organic phase was dried over $MgSO_4$ and the solvent was removed *in vacuo*. The crude solid was purified by flash column chromatography (Petrol/CH2CL2 1:1) to yield chloride **84** as a white powder (1.10 g, 92%). ^{1}H NMR (400 MHz, $CDCl_3$) δ_H 5.39 (d, *J* = 4.4, 1H, H_d), 4.75-4.65 (m, 1H, H_b), 4.03 (s, 2H, H_a), 2.35 (d, *J* = 7.8, 2H, H_c), 2.05-0.80 (m, 38H, Cholesterol-H), 0.67 (s, 3H, H_e). ^{13}C NMR (101 MHz, $CDCl_3$) δ_C 166.8, 139.3, 123.3, 76.3, 56.8, 56.3, 50.1, 42.4, 41.3, 39.9, 39.7, 38.0, 37.0, 36.7, 36.3, 35.9, 32.1, 32.0, 28.3, 28.1, 27.7, 24.4, 23.9, 22.9, 22.7, 21.2, 19.4, 18.8, 12.0. IR: (ν_{max}/cm^{-1}) 2936, 2859, 1750, 1463, 1411, 1311, 1191, 1006, 803, 786, 691. M.p. (^{o}C) 157-159. UV: λ_{max}(CH2CL2)/nm (ε / mol^{-1}cm^{-1}dm^{3}) 275 (43).

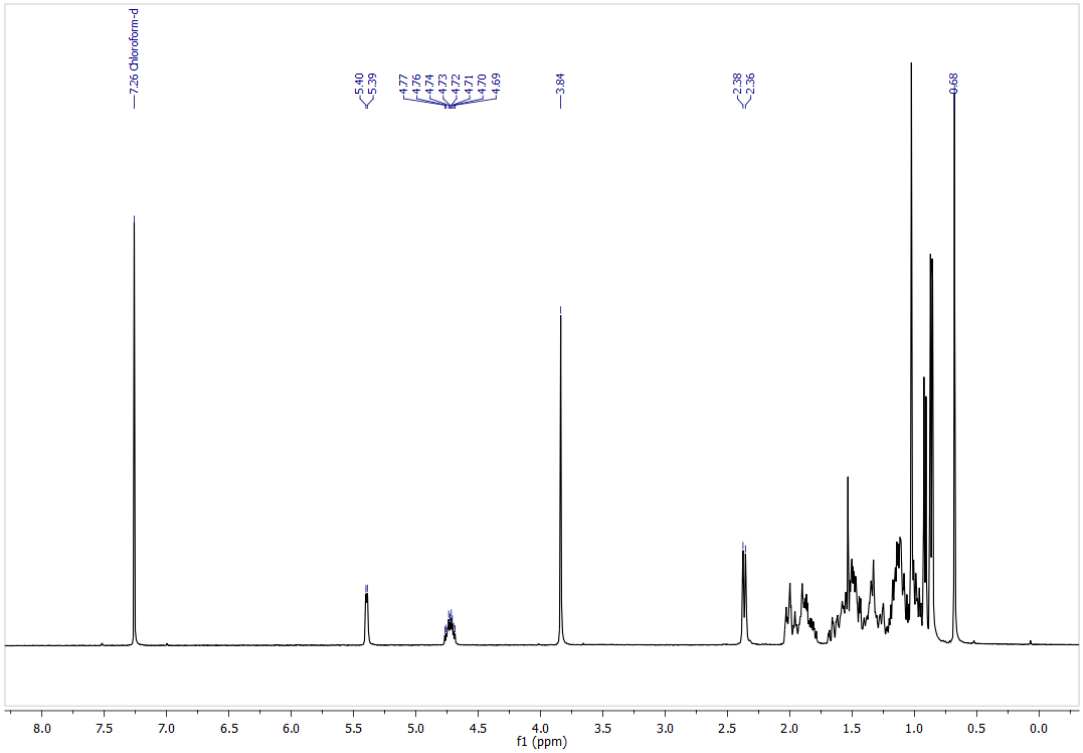
7.26 Chloroform-d
5.40
5.39
4.77
4.76
4.74
4.73
4.72
4.71
4.70
4.69
3.84
2.38
2.36
0.68
f1 (ppm)

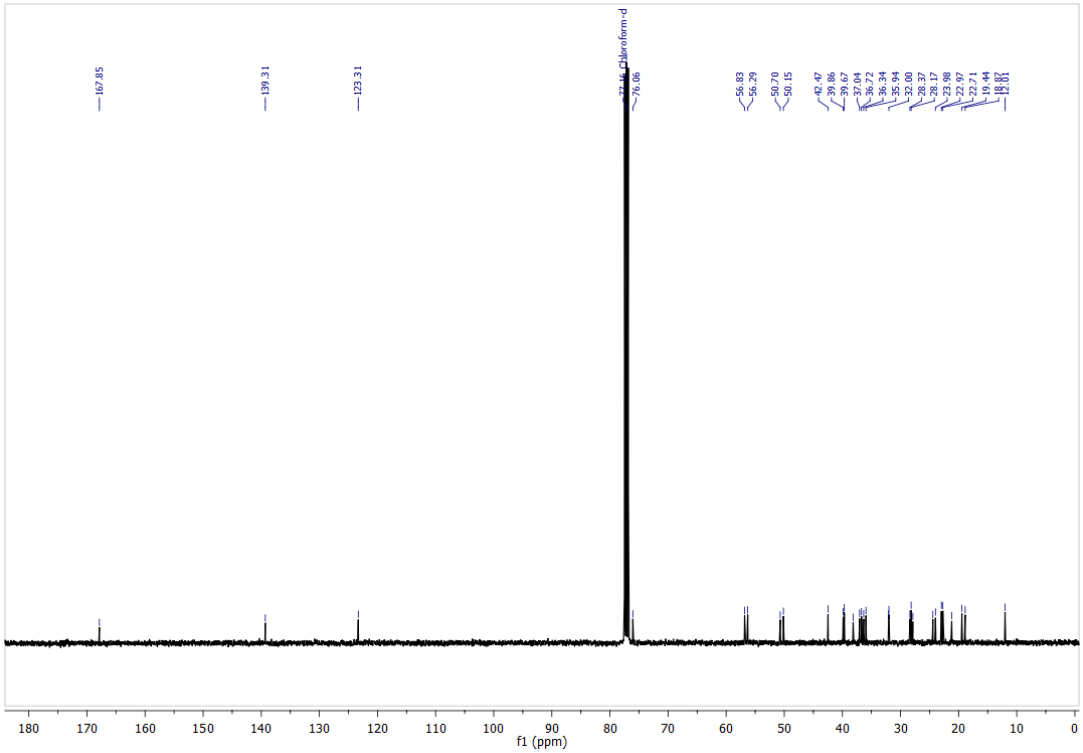
167.85
139.31
123.31
77.46 Chloroform-d
76.06
56.83
56.29
50.70
50.15
42.47
39.86
39.67
37.04
36.72
36.34
35.94
32.00
28.37
28.17
23.98
22.97
22.71
19.44
18.87
12.01
f1 (ppm)

*Cholesterol 2-azido acetate (**85**):*

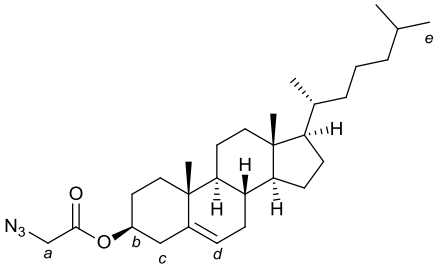

Chloride **84** (1.00 g, 2.15 mmol) and NaN_3 (0.84 g, 12.9 mmol) were combined in a flask purged with N_2, dissolved in anhydrous DMF (60 mL), heated to 65 ^oC and stirred for 24 h. After cooling to r.t, the reaction mixture was slowly poured into iced water (200 mL). The resulting precipitate was extracted with EtOAc (3 x 200 mL), the organic extracts combined and washed with saturated $NaHCO_3$ solution (2 x 100 mL), brine (2 x 100 mL) and H_2O (2 x 100 mL). The organic phase was dried over $MgSO_4$ and the solvent was removed *in vacuo*. The crude oil was purified by flash column chromatography (100% CH2CL2) to give azide **85** as a cream powder (0.68 g, 65%). ^1H NMR (400 MHz, $CDCl_3$) δ_H 5.39 (d, *J* = 4.4, 1H, H_d), 4.76-4.68 (m, 1H, H_b), 3.83 (s, 2H, H_a), 2.36 (d, *J* = 7.8, 2H, H_c), 2.07-0.79 (m, 38H, Cholesterol-H), 0.67 (s, 3H, H_e). ^{13}C NMR (101 MHz, $CDCl_3$) δ_C167.8, 139.3, 123.3, 76.1, 56.8, 56.3, 50.7, 50.2, 42.5, 39.8, 39.6, 38.1, 37.0, 36.7, 36.3, 35.9, 32.0, 32.0, 28.3, 28.2, 27.8, 24.4, 23.9, 22.9, 22.7, 21.2, 19.4, 18.8, 12.0. IR: (ν_{max}/cm^{-1}) 2934, 2866, 2105, 1741, 1465, 1438, 1363, 1209, 1002, 924, 801. M.p. (^oC) 122-123. HRMS (EI) calcd for $C_{29}H_{48}N_3O_2$ $[M + H]^+$ 470.3741, found 470.3731. UV: λ_{max}(CH2CL2)/nm (ε/ $mol^{-1}cm^{-1}dm^3$) 275 (84) .

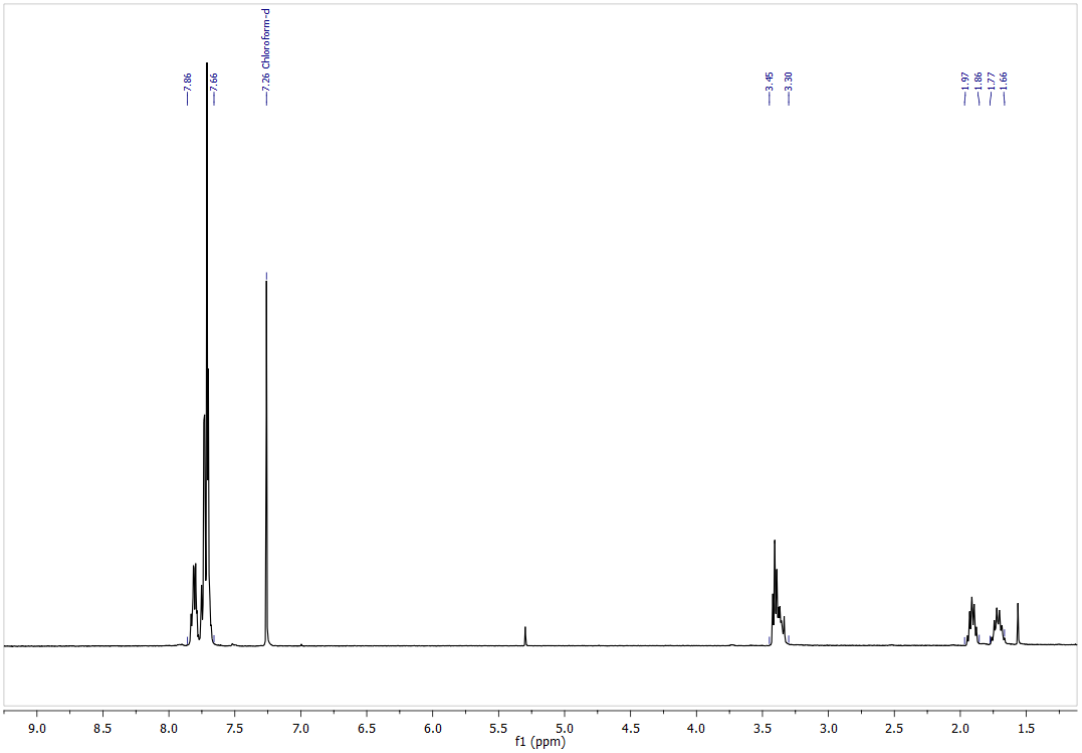
7.86
7.66
7.26 Chloroform-d
3.45
3.30
1.97
1.86
1.77
1.66
f1 (ppm)

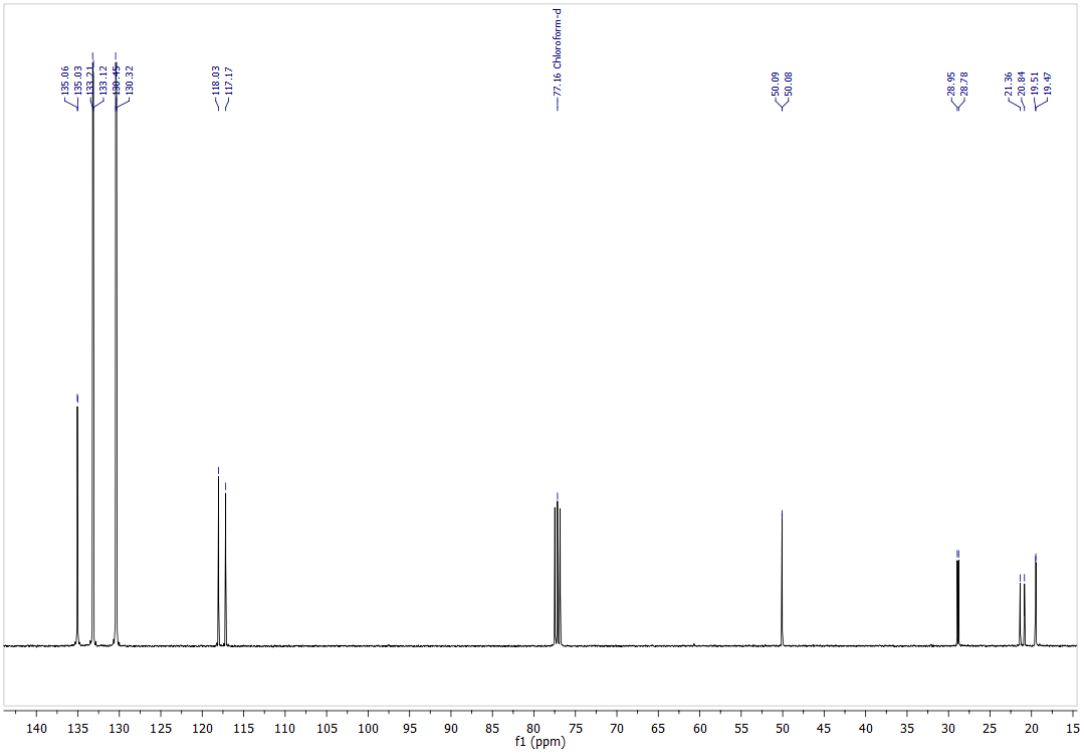
135.06
135.03
133.21
133.12
130.45
130.32
118.03
117.17
77.16 Chloroform-d
50.09
50.08
28.95
28.78
21.36
20.84
19.51
19.47
f1 (ppm)

*(4-Azidobutyl)triphenylphosphonium tetrafluoroborate (**89**):*

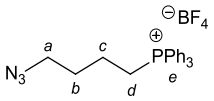

(4-Azidobutyl)triphenylphosphonium bromide **88** (2.27 g, 5.15 mmol) was dissolved in CH_2Cl_2 (40 mL). This solution was thoroughly washed with a saturated aqueous solution of ammonium tetrafluoroborate (50 mL). The organic phase was dried over $MgSO_4$ and the solvent was removed *in vacuo* to yield tetrafluoroborate **89** as a white solid (2.18 g, 95%)**.** ^{1}H NMR (400 MHz, $CDCl_3$) δ_H 7.86-7.65 (m, 15H, H_e), 3.46-3.28 (m, 4H, H_a and H_d), 1.96-1.85 (m, 2H, H_b), 1.78-1.63 (m, 2H, H_c). ^{13}C NMR (101 MHz, $CDCl_3$) δ_C 135.0 ($J_{C\text{-}P}$ = 2.9), 133.2 ($J_{C\text{-}P}$ = 9.9), 130.4 ($J_{C\text{-}P}$ = 12.7), 117.9 ($J_{C\text{-}P}$ = 86.4), 50.1, 28.8 ($J_{C\text{-}P}$ = 16.9), 21.2 ($J_{C\text{-}P}$ = 52.0), 19.5 ($J_{C\text{-}P}$ = 3.9). IR: (ν_{max}/cm^{-1}) 2943, 2923, 2877, 2098, 1588, 1486, 1438, 1342, 1276, 1239, 1025, 749, 722, 689. M.p. (°C) 115-118. HRMS (EI) calcd for $C_{22}H_{23}N_3P_1$ $[M - BF_4]^+$ 360.1624, found 360.1627.

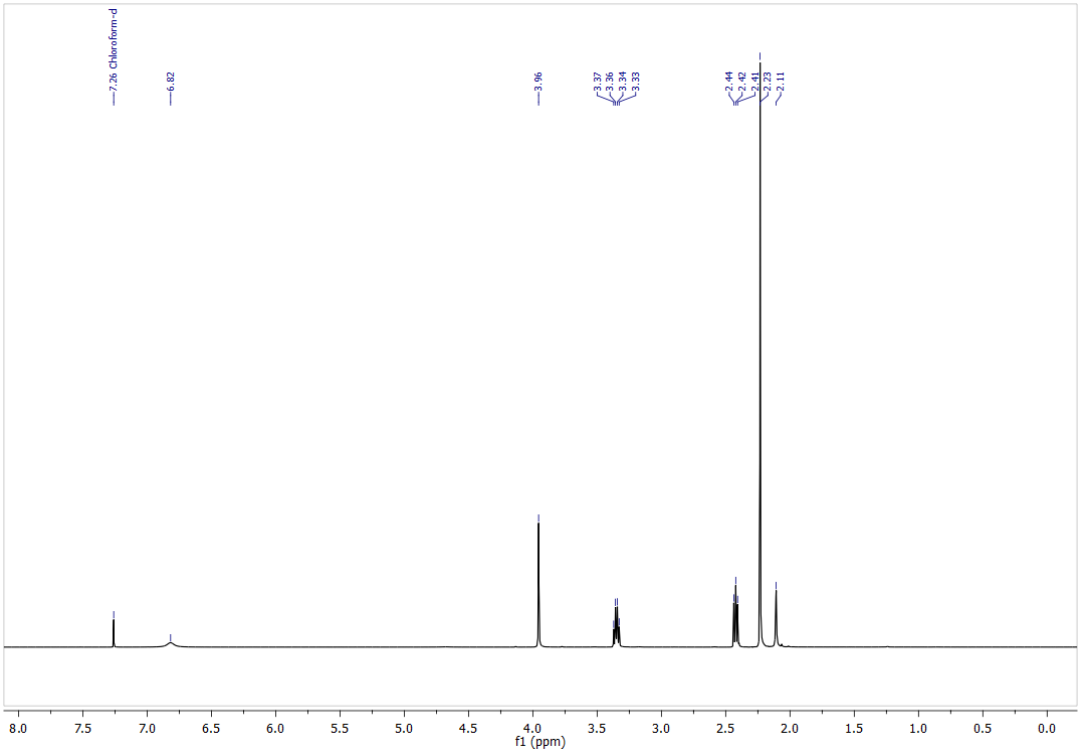
7.26 Chloroform-d
6.82
3.96
3.37
3.36
3.34
3.33
2.44
2.42
2.41
2.23
2.11
8.0 7.5 7.0 6.5 6.0 5.5 5.0 4.5 4.0 3.5 3.0 2.5 2.0 1.5 1.0 0.5 0.0
f1 (ppm)

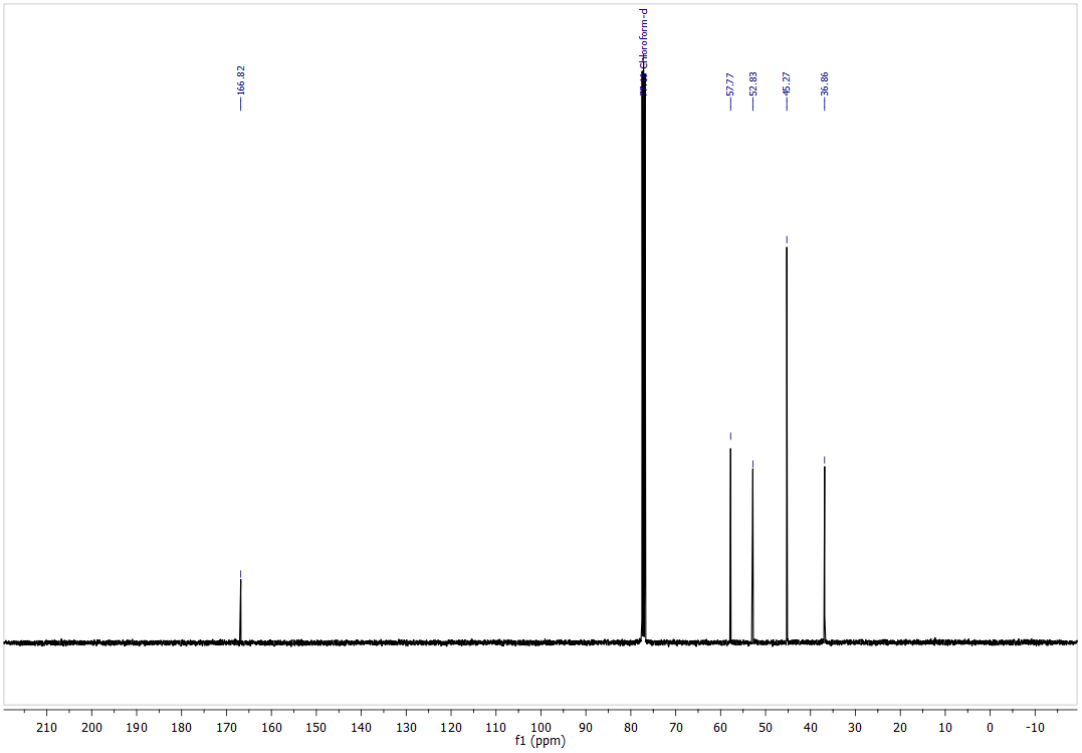
166.82
77.00 Chloroform-d
57.77
52.83
45.27
36.86
210 200 190 180 170 160 150 140 130 120 110 100 90 80 70 60 50 40 30 20 10 0 -10
f1 (ppm)

*2-Azido-N-(2-diethylamino-ethyl)acetamide (**92**):*

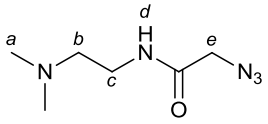

2-Chloro-*N*-(2-diethylamino-ethyl)acetamide hydrochloride **91** (0.83 g, 2.50 mmol) was dissolved in H_2O (12.5 mL), NaN_3 (1.61 g, 15.0 mmol) was added to the flask, and the reaction mixture stirred for 48 h at 65 °C. After cooling, the solution was adjusted to pH 10 using aqueous $NaHCO_3$ (1.0 M), and extracted with EtOAc (3 x 20 mL). The remaining aqueous layer was adjusted to pH 14 with aqueous NaOH (1.0 M), and extracted with EtOAc (3 x 20 mL). All organic extracts were combined, dried over $MgSO_4$ and the solvent was removed *in vacuo* (400 mbar – volatile product) to give azide **92** as a pale yellow oil (0.31 g, 72%). ^{1}H NMR (400 MHz, $CDCl_3$) δ_H 6.82 (br s, 1H, H_d), 3.96 (s, 2H, H_e), 3.34 (q, *J* = 5.9, 2H, H_c), 2.42 (t, *J* = 6.0, 2H, H_b), 2.23 (s, 6H, H_a). ^{13}C NMR (101 MHz, $CDCl_3$) δ_C 166.8, 57.8, 52.8, 45.3, 36.9. IR: (ν_{max}/cm^{-1}) 3292 (b), 3079, 2978, 2948, 2872, 2783, 2101, 1658, 1541, 1461, 1252, 1189, 1166, 1040, 906, 849, 776, 645. HRMS (EI) calcd for $C_6H_{13}N_5O$ $[M + H]^+$ 172.1193, found 172.1191.

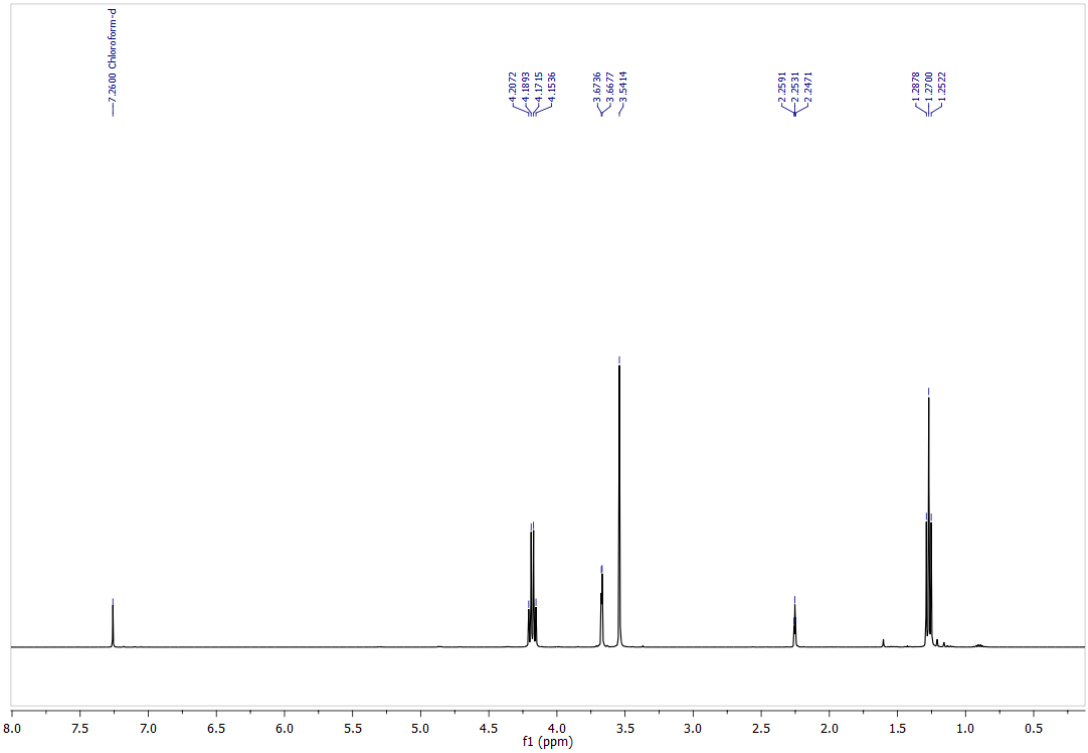
7.2600 Chloroform-d
4.2072
4.1893
4.1715
4.1536
3.6736
3.6677
3.5414
2.2591
2.2531
2.2471
1.2878
1.2700
1.2522
f1 (ppm)

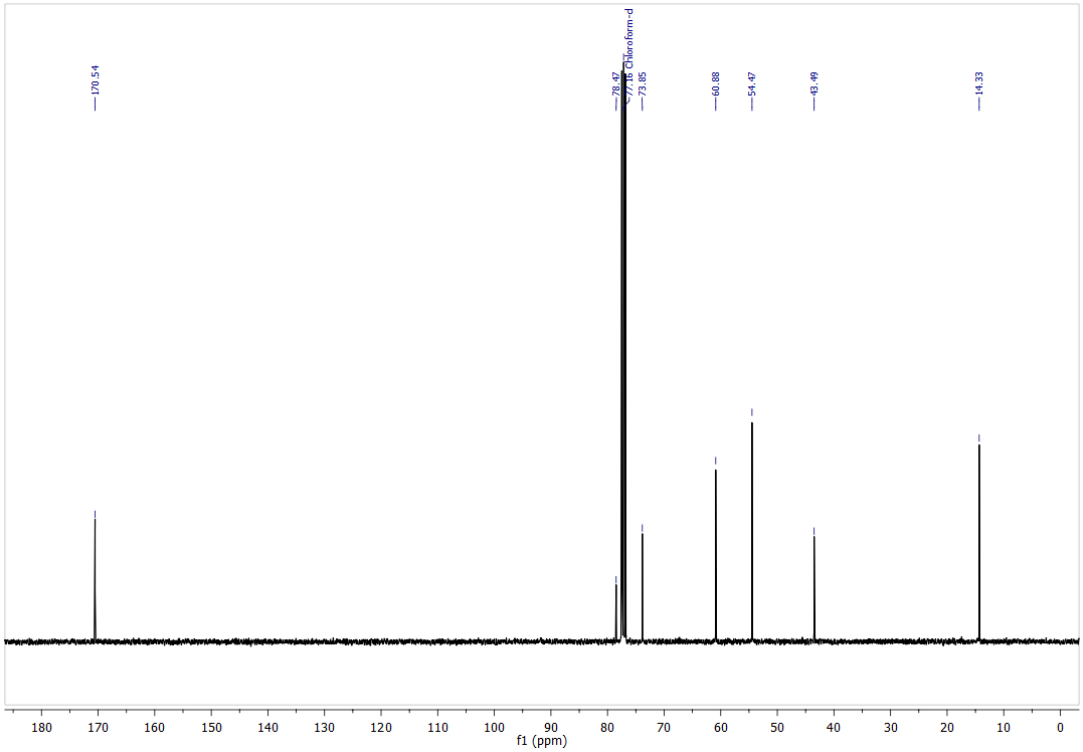
170.54
78.47
77.16 Chloroform-d
73.85
60.88
54.47
43.49
14.33
f1 (ppm)

*Diethyl 2,2'-(prop-2-yn-1-ylazanediyl)diacetate (**104**):*

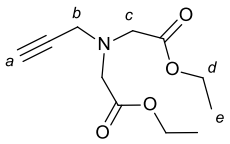

Diethyl iminodiacetate **103** (1.00 g, 5.28 mmol) was dissolved in MeCN (30 mL). K_2CO_3 (1.46 g, 10.5 mmol) was added, and propargyl bromide (0.94 mL, 6.34 mmol) was added slowly to the stirring reaction mixture and refluxed for 16 h. After cooling, the suspension was filtered, and the solvent removed *in vacuo*. The crude oil was purified by flash column chromatography (2:8 EtOAc/Petrol) to yield alkyne **104** as a colourless oil (0.71 g, 58%). ^{1}H NMR (400 MHz, $CDCl_3$) δ_H 4.17 (q, *J* = 7.1, 4H, H_d), 3.66 (d, *J* = 2.3, 2H, H_b), 3.54 (s, 4H, H_c), 2.25 (t, *J* = 2.4, 1H, H_a), 1.27 (t, *J* = 7.1, 6H, H_e). ^{13}C NMR (101 MHz, $CDCl_3$) δ_C 170.5, 78.4, 73.8, 60.8, 54.4, 43.4, 14.3.IR: (ν_{max}/cm^{-1}) 3278, 2978, 2870, 2105, 1733, 1444, 1372, 1190, 1027, 990. HRMS (EI) calcd for $C_{11}H_{18}N_1O_4$ $[M + H]^+$ 228.1230, found 228.1224.

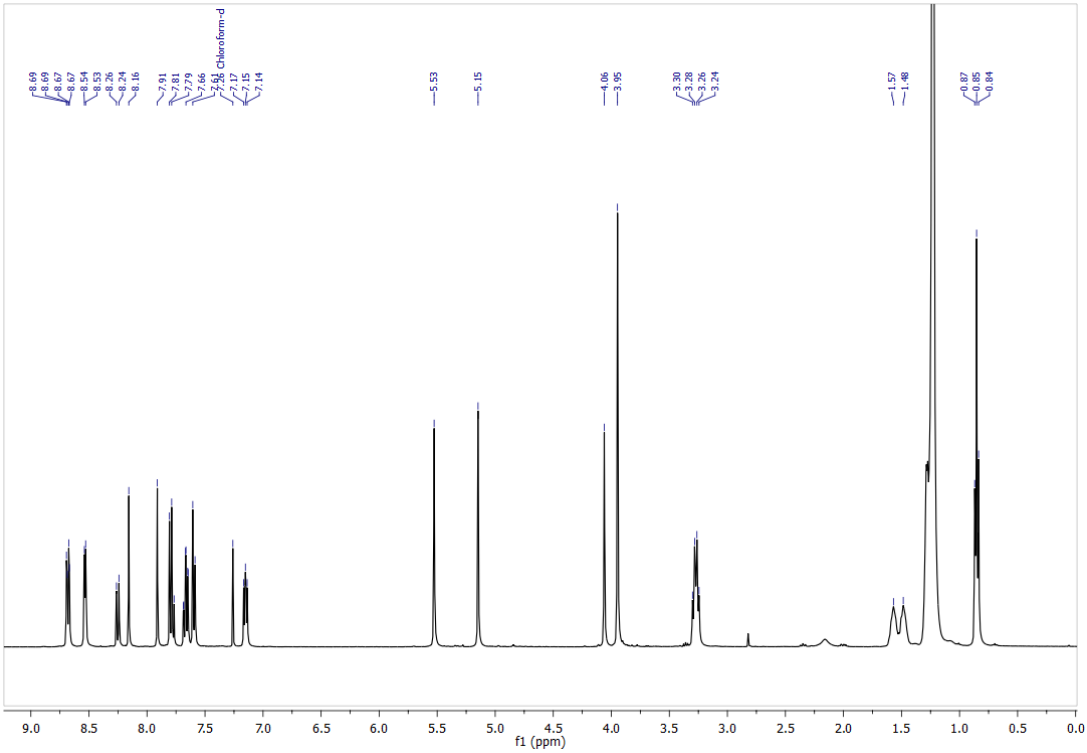
8.69
8.69
8.67
8.67
8.54
8.53
8.26
8.24
8.16
7.91
7.81
7.79
7.66
7.61
Chloroform-d
7.28
7.17
7.15
7.14
5.53
5.15
4.06
3.95
3.30
3.28
3.26
3.24
1.57
1.48
0.87
0.85
0.84
9.0
8.5
8.0
7.5
7.0
6.5
6.0
5.5
5.0
4.5
4.0
3.5
3.0
2.5
2.0
1.5
1.0
0.5
0.0
f1 (ppm)

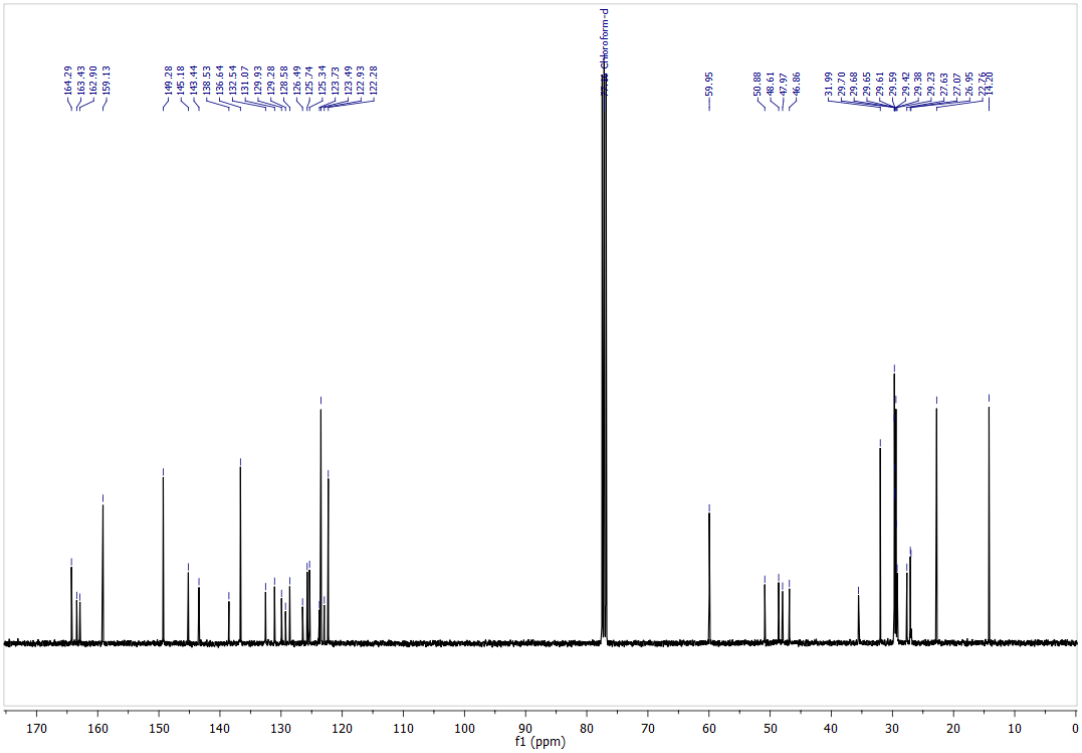
164.29
163.43
157.90
159.13
149.28
145.18
143.44
138.53
136.44
132.54
131.07
129.93
129.28
128.58
126.49
125.74
125.34
123.73
123.49
122.93
122.28
Chloroform-d
59.95
50.88
48.61
47.97
46.86
31.99
29.70
29.68
29.65
29.61
29.59
29.53
29.38
29.23
27.63
27.07
26.95
22.76
14.20
170
160
150
140
130
120
110
100
90
80
70
60
50
40
30
20
10
0
f1 (ppm)

*2-(4-((6-(4-((bis(Pyridin-2-ylmethyl)amino)methyl)-1H-1,2,3-triazol-1-yl)-1,3-dioxo-1H-benzo[de]isoquinolin-2(3H)-yl)methyl)-1H-1,2,3-triazol-1-yl)-N,N-didodecylacetamide (**105**):*

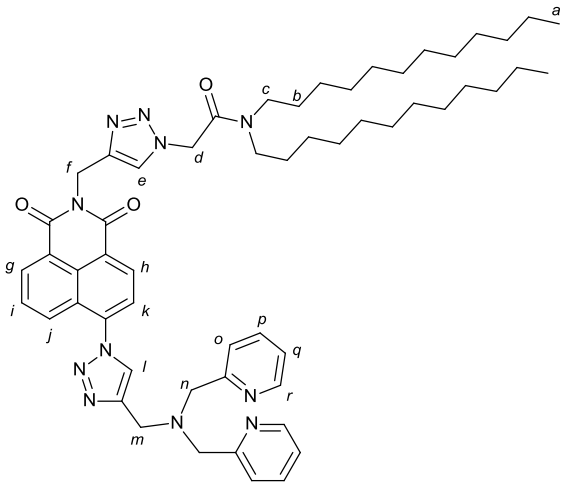

General procedure A was employed with **69** (314 mg, 1.00 mmol)**,** azide **82** (0.48 g, 1.0 mmol) in NMP (3.33 mL), followed by propargyl dipicolylamine **96** (0.29 g, 1.1 mmol) and EtOH (3.33 mL). Crude product obtained after dilution of the reaction mixture with CH_2Cl_2 (10 mL), and washing the organic mixture with a saturated solution of EDTA in 17.5% aqueous NH_3 (3 x 15 mL). The organic phase was dried over $MgSO_4$, concentrated *in vacuo* and purified by flash column chromatography on alumina (99:1 CH_2Cl_2/MeOH) to yield sensor **105** as a brown oil (0.78 g, 82%). ^{1}H NMR (400 MHz, $CDCl_3$) δ_H 8.68 (d, *J* = 7.8, 1H, H_h), 8.67 (d, *J* = 7.1, 1H, H_g), 8.55-8.51 (m, 2H, H_r), 8.25 (d, *J* = 8.5, 1H, H_j), 8.15 (s, 1H, H_l), 7.91 (s, 1H, H_e), 7.82-7.75 (m, 2H, H_i and H_k), 7.66 (app. td, *J* = 7.7, 1.6, 2H, H_p), 7.62-7.57 (m, 2H, H_o), 7.18-7.12 (m, 2H, H_q), 5.52 (s, 2H, H_f), 5.14 (s, 2H, H_d), 4.06 (s, 2H, H_m), 3.94 (s, 4H, H_n), 3.31-3.23 (m, 4H, H_c), 1.64-1.43 (m, 4H, H_b), 1.34-1.12 (m, 36H, alkyl-H), 0.85 (app. t, 6H, H_a). ^{13}C NMR (101 MHz, $CDCl_3$) δ_C 164.3, 163.4, 162.9, 159.1, 149.3, 145.2, 143.4, 138.5, 136.6, 132.5, 131.1, 129.9, 129.3, 128.5, 126.5, 125.7, 125.3, 123.7, 123.5, 122.9, 122.3, 59.9, 50.8, 48.6, 47.9, 46.8, 35.5, 31.9, 29.7, 29.7, 29.6, 29.6, 29.5, 29.4, 29.3, 29.2, 27.6, 27.1, 26.9, 22.8, 14.2. IR: (ν_{max}/cm^{-1}) 2922, 2852, 1703, 1661, 1587, 1467, 1430, 1369, 1233, 1040, 995, 783. HRMS (EI) calcd for $C_{56}H_{76}N_{11}O_3$ $[M + H]^+$ 950.6127, found 950.6117. UV: $\lambda_{max}(CH_2Cl_2)$/nm (ε / mol^{-1}cm^{-1}dm^3) 344 (20365)

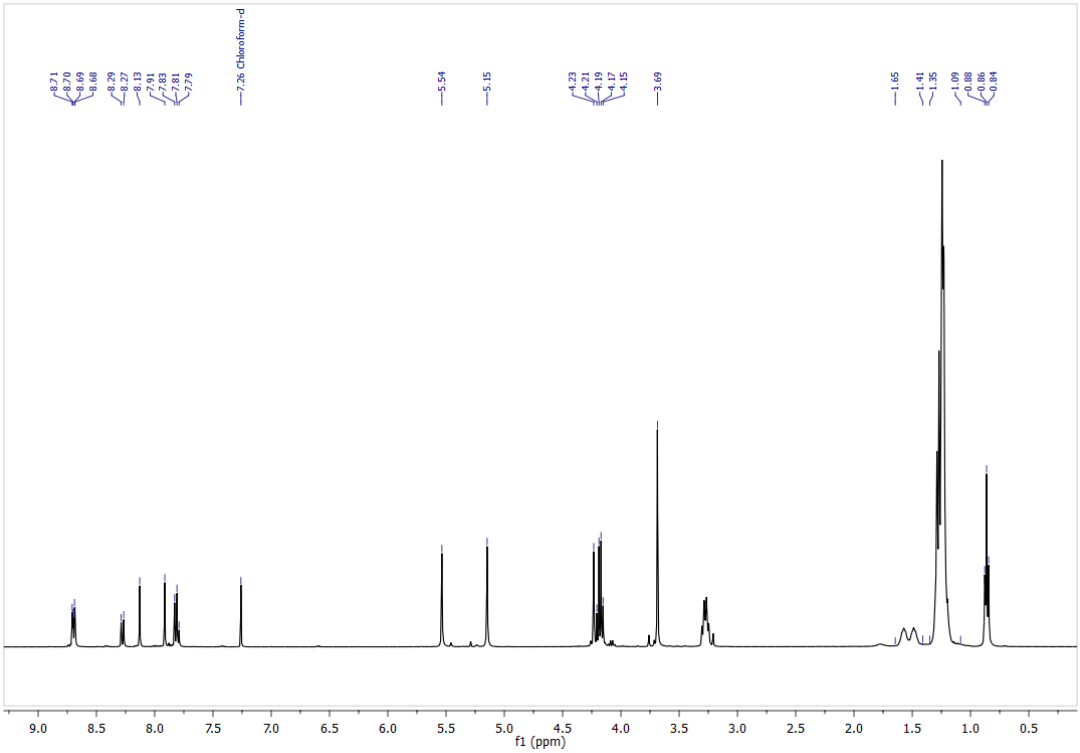
8.71
8.70
8.69
8.68
8.29
8.27
8.13
7.91
7.88
7.81
7.79
7.26 Chloroform-d
5.54
5.15
4.23
4.21
4.19
4.17
4.15
3.69
1.65
1.41
1.35
1.09
0.88
0.86
0.84
9.0
8.5
8.0
7.5
7.0
6.5
6.0
5.5
5.0
4.5
4.0
3.5
3.0
2.5
2.0
1.5
1.0
0.5
f1 (ppm)

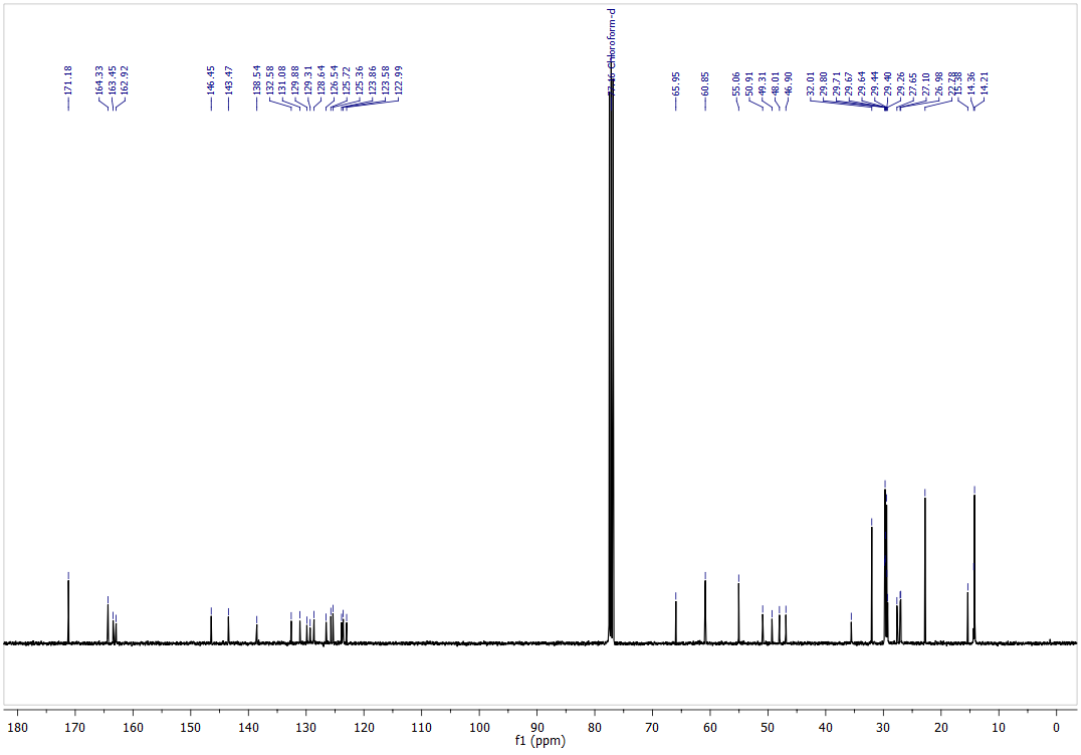
171.18
164.33
163.45
162.92
146.45
143.47
138.54
132.58
131.08
129.88
129.31
128.64
126.54
125.72
125.36
123.86
123.58
122.99
77.16 Chloroform-d
65.95
60.85
55.06
50.91
49.31
48.01
46.90
32.01
29.80
29.71
29.62
29.44
29.40
29.26
27.65
27.10
26.98
22.58
22.38
14.36
14.21
180
170
160
150
140
130
120
110
100
90
80
70
60
50
40
30
20
10
0
f1 (ppm)

*Diethyl 2,2'-(((1-(2-((1-(2-(didodecylamino)-2-oxoethyl)-1H-1,2,3-triazol-4-yl)methyl)-1,3-dioxo-2,3-dihydro-1H-benzo[de]isoquinolin-6-yl)-1H-1,2,3-triazol-4-yl)methyl)azanediyl)diacetate (**106**):*

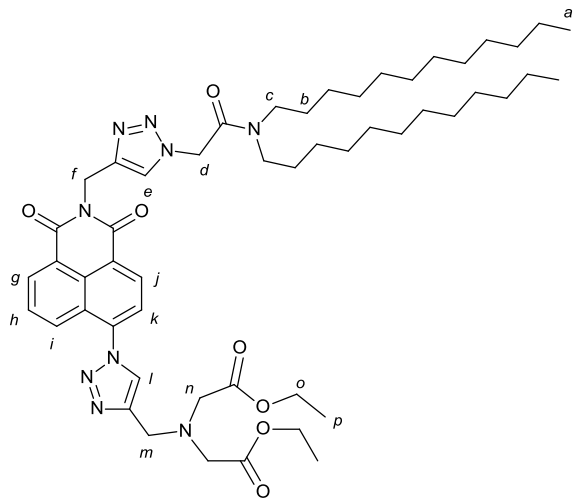

General procedure A was employed with **69** (314 mg, 1.00 mmol), azide **82** (0.48 g, 1.0 mmol) in NMP (3.33 mL), followed by acetylene **104** (0.59 g, 1.1 mmol) and EtOH (3.33 mL). Crude product obtained after dilution of the reaction mixture with CH_2Cl_2 (10 mL), and washing the organic mixture with a saturated solution of EDTA in 17.5% aqueous NH_3 (3 x 15 mL). The organic phase was dried over $MgSO_4$, concentrated *in vacuo* and purified by flash column chromatography (4:1 CH_2Cl_2/EtOAc to EtOAc to 4:1 EtOAc/MeOH) to yield **106** as an orange foam (0.72 g, 76%). ^{1}H NMR (400 MHz, $CDCl_3$) δ_H 8.70 (d, *J* = 7.8, 1H, H_j), 8.69 (d, *J* = 7.2, 1H, H_g), 8.28 (d, *J* = 8.6, 1H, H_i), 8.13 (s, 1H, H_l), 7.91 (s, 1H, H_e), 7.92-7.78 (m, 2H, H_h and H_k), 5.54 (s, 2H, H_f), 5.15 (s, 2H, H_d), 4.23 (s, 2H, H_m), 4.18 (q, *J* = 7.1, H_o), 3.69 (s, 4H, H_n), 3.33-3.22 (m, 4H, H_c), 1.65-1.41 (m, 4H, H_b), 1.35-1.14 (m, 42H, H_p (6H) and alkyl-H (36H)), 0.90-0.80 (m, 6H, H_a). ^{13}C NMR (101 MHz, $CDCl_3$) δ_C 171.2, 164.3, 163.4, 162.9, 146.4, 143.5, 138.5, 132.6, 131.1, 129.9, 129.3, 128.6, 126.5, 125.7, 125.4, 123.9, 123.6, 122.9, 65.9, 60.8, 55.1, 50.9, 49.3, 48.0, 46.9, 35.6, 32.0, 29.8, 29.7, 29.7, 29.6, 29.4, 29.4, 29.3, 27.6, 27.1, 26.9, 22.8, 15.4, 14.4, 14.2. IR: (ν_{max}/cm^{-1}) 3145, 2921, 2852, 1739, 1704, 1659, 1585, 1465, 1369, 1232, 1184, 1026, 949, 783. M.p. (°C) 48-51. HRMS (EI) calcd for $C_{52}H_{78}N_9O_7$ $[M + H]^+$ 940.6019, found 940.6010. UV: $\lambda_{max}(CH_2Cl_2)$/nm (ε / mol^{-1}cm^{-1}dm^3) 344 (18804) .

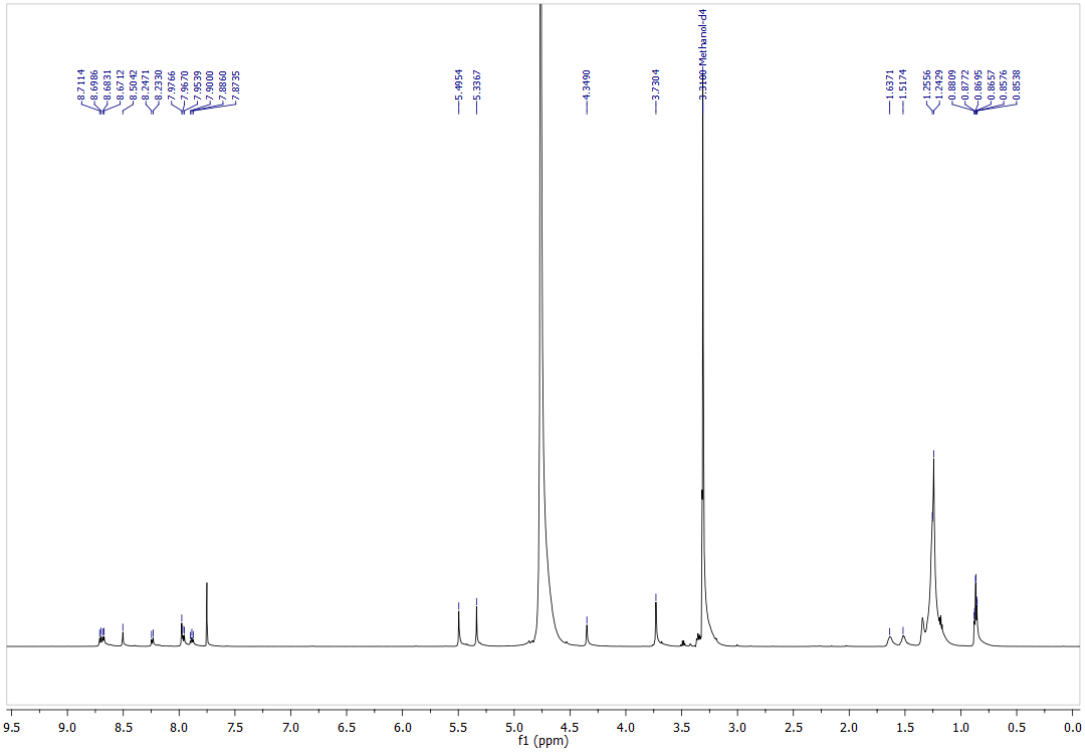
8.7114
8.6986
8.6831
8.6712
8.5042
8.2471
8.2330
7.9766
7.9670
7.9539
7.8900
7.8866
7.8735
5.4954
5.3367
4.3490
3.7304
3.3166 Methanol-d4
1.6371
1.5174
1.2556
1.1429
0.8999
0.8772
0.8695
0.8657
0.8576
0.8538
f1 (ppm)

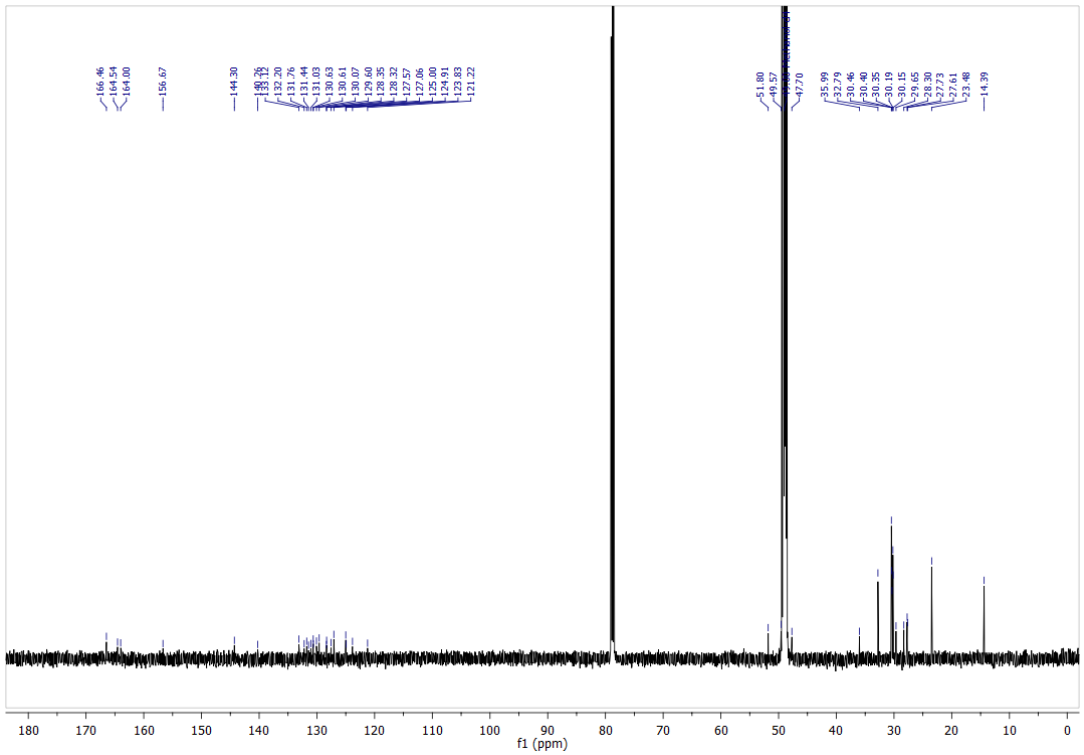
166.46
164.54
164.00
156.67
144.30
133.12
132.20
131.76
131.44
131.03
130.63
130.61
130.07
129.60
128.35
128.32
127.57
127.06
125.00
124.91
123.83
121.22
51.80
49.57
47.70
35.99
32.79
30.46
30.40
30.35
30.19
30.15
29.65
28.30
27.73
27.61
23.48
14.39
f1 (ppm)

*2,2'-(((1-(2-((1-(2-(Didodecylamino)-2-oxoethyl)-1H-1,2,3-triazol-4-yl)methyl)-1,3-dioxo-2,3-dihydro-1H-benzo[de]isoquinolin-6-yl)-1H-1,2,3-triazol-4-yl)methyl)azanediyl)diacetic acid (**107**):*

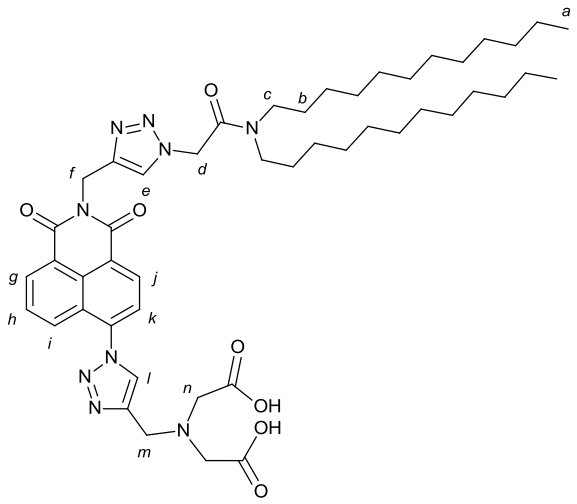

To a stirred solution of **106** (28 mg, 0.030 mmol) in THF (0.15 mL) was added an aqueous solution of LiOH (2 equiv., 0.15 mL). The reaction mixture was stirred for 18 h at r.t., and the solvent removed *in vacuo*. The residue was re-suspended in $CHCl_3$ (5 mL), washed with aqueous citric acid solution (5% w/v, 5 mL), the organic phase dried over $MgSO_4$ and the solvent removed *in vacuo* to yield deprotected sensor **107** as an orange residue (14.0 mg, 53%). ^{1}H NMR (400 MHz, MeOD) δ_H 8.72-8.66 (m, 2H, H_g and H_j), 8.50 (s, 1H, H_l), 8.24 (d, J = 5.6, 1H, H_i), 7.98 (s, 1H, H_e), 7.96 (d, J = 5.2, 1H, H_k), 7.91-7.86 (m, 1H, H_h), 5.49 (s, 2H, H_f), 5.34 (s, 2H, H_d), 4.35 (s, 2H, H_m), 3.73 (s, 4H, H_n), 3.39-3.11 (m, 2H, H_c – obscured by solvent peak), 1.68-1.46 (m, 4H, H_b), 1.37-1.13 (m, 36H, alkyl-H), 0.89-0.84 (m, 6H, H_a). ^{13}C NMR (101 MHz, MeOD) δ_C 166.5, 164.5, 164.0, 156.7, 144.3, 140.3, 133.1, 132.2, 131.8, 131.4, 131.0, 130.6, 130.6, 130.1, 129.6, 128.4, 128.3, 127.6, 127.1, 125.0, 124.9, 123.8, 121.2, 51.8, 49.6, 47.7, 35.9, 32.8, 30.5, 30.4, 30.4, 30.2, 30.1, 29.6, 28.3, 27.7, 27.6, 23.5, 14.4. IR: (ν_{max}/cm^{-1}) 3357 (broad), 2923, 2854, 1705, 1661, 1588, 1465, 1423, 1377, 1235, 1120, 1052, 952, 785. HRMS (EI) calcd for $C_{48}H_{69}N_9O_7$ $[M + H]^+$ 884.5393, found 884.5391. UV: $\lambda_{max}(CH_2Cl_2)$/nm (ε / mol^{-1}cm^{-1}dm^3) 344 (9173)

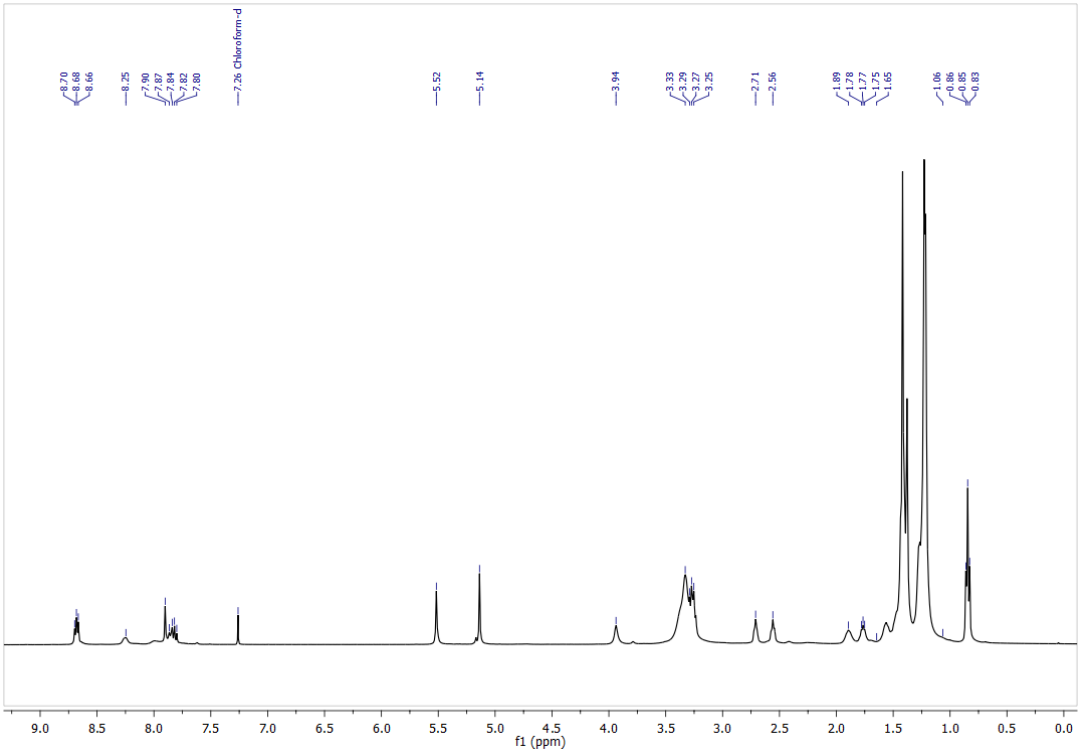
8.70
8.68
8.66
8.25
7.90
7.87
7.84
7.82
7.80
7.26 Chloroform-d
5.52
5.14
3.94
3.33
3.29
3.27
3.25
2.71
2.56
1.89
1.78
1.77
1.75
1.65
1.06
0.86
0.85
0.83
f1 (ppm)

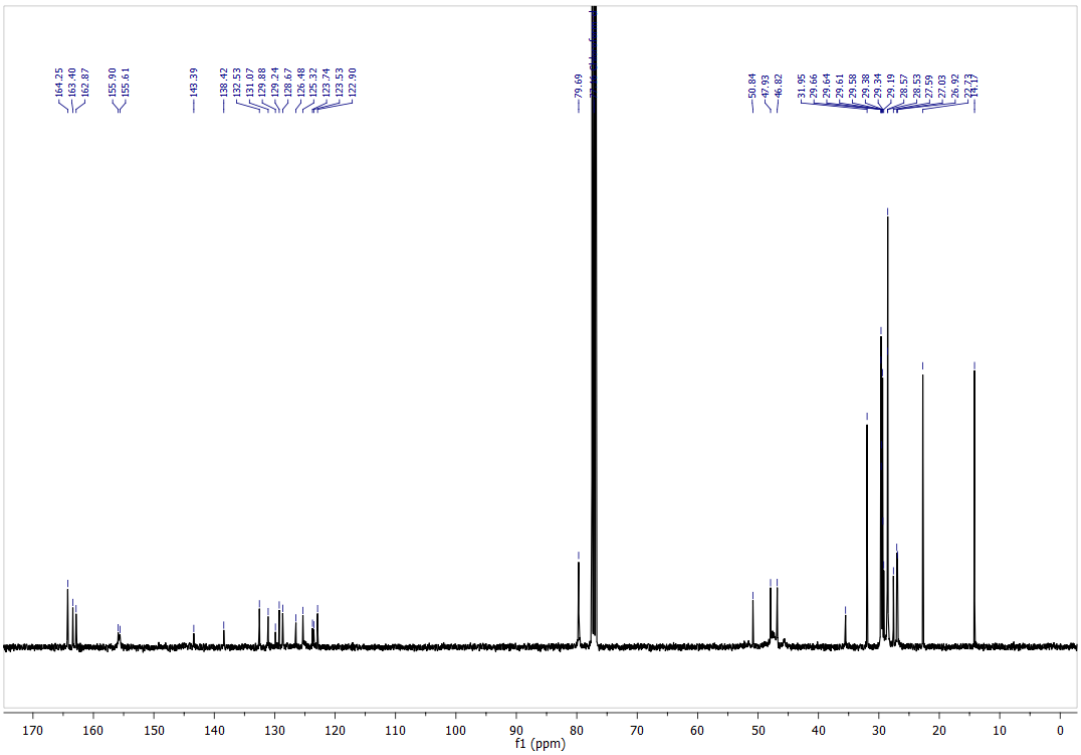
164.25
163.40
162.87
155.90
155.61
143.39
138.42
132.53
131.07
130.88
129.24
126.48
125.32
123.74
123.53
122.90
79.69
50.84
47.93
46.82
31.95
29.66
29.64
29.61
29.58
29.38
29.34
29.19
28.57
28.53
27.59
27.03
26.92
f1 (ppm)

*Tri-tert-butyl 11-((1-(2-((1-(2-(didodecylamino)-2-oxoethyl)-1H-1,2,3-triazol-4-yl)methyl)-1,3-dioxo-2,3-dihydro-1H-benzo[de]isoquinolin-6-yl)-1H-1,2,3-triazol-4-yl)methyl)-1,4,8,11-tetraazacyclotetradecane-1,4,8-tricarboxylate (**108**):*

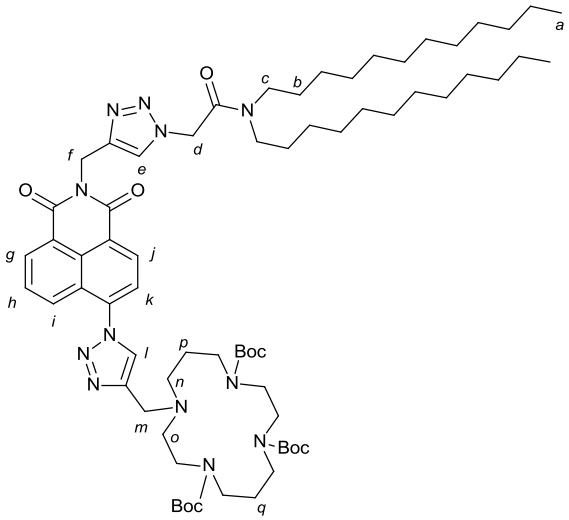

General procedure A was employed with **69** (314 mg, 1.00 mmol)**,** azide **82** in NMP (3.33 mL), followed by cyclam acetylene **65** (0.59 g, 1.1 mmol) and EtOH (3.33 mL). Crude product was obtained by dilution of the reaction mixture with CH_2Cl_2 (10 mL), and washing the organic mixture with a saturated solution of EDTA in 17.5% aqueous NH_3 (3 x 15 mL). The organic phase was dried over $MgSO_4$, concentrated *in vacuo* and purified by flash column chromatography (4:1 CH_2Cl_2/EtOAC to EtOAc to 4:1 EtOAc/MeOH) to yield **108** as a brown oil (0.93 g, 75%). ^{1}H NMR (400 MHz, $CDCl_3$) δ_H 8.67-8.59 (m, 2H, H_g and H_j), 8.20 (app. br s, 1H, H_i), 7.98-7.72 (m, 4H, H_e and H_h, H_l and H_k), 5.47 (s, 2H, H_f), 5.09 (s, 2H, H_d), 3.89 (br s, 2H, H_m), 3.50-3.08 (m, 16H, H_c and Cyclam-H (12H)), 2.70-2.62 (m, 2H, H_o), 2.54-2.48 (m, 2H, H_n), 1.92-1.78 (m, 2H, H_q), 1.76-1.66 (m, 2H, H_p), 1.60-0.93 (m, 67H, H_b (4H), ^{t}Bu (27H) and alkyl-H (36H)), 0.86-0.72 (m, 6H, H_a). ^{13}C NMR (101 MHz, $CDCl_3$) δ_C 164.2, 163.4, 162.8, 155.9, 155.6, 143.4, 138.4, 132.5, 131.1, 129.8, 129.2, 128.7, 126.5, 125.3, 123.7, 123.5, 122.9, 79.7, 50.8, 47.9, 46.8, 35.5, 31.9, 29.7, 29.6, 29.6, 29.5, 29.4, 29.3, 29.2, 28.6, 28.5, 27.6, 27.0, 26.9, 22.7, 14.2. IR: (ν_{max}/cm^{-1}) 2927, 2855, 1691, 1588, 1466, 1414, 1365, 1236, 1166, 782. HRMS (EI) calcd for $C_{29}H_{48}N_3O_2$ $[M + H]^+$ 1251.8149, found 1251.8577. UV: $\lambda_{max}(CH_2Cl_2)$/nm (ε/ mol^{-1}cm^{-1}dm^3) 344 (25178).

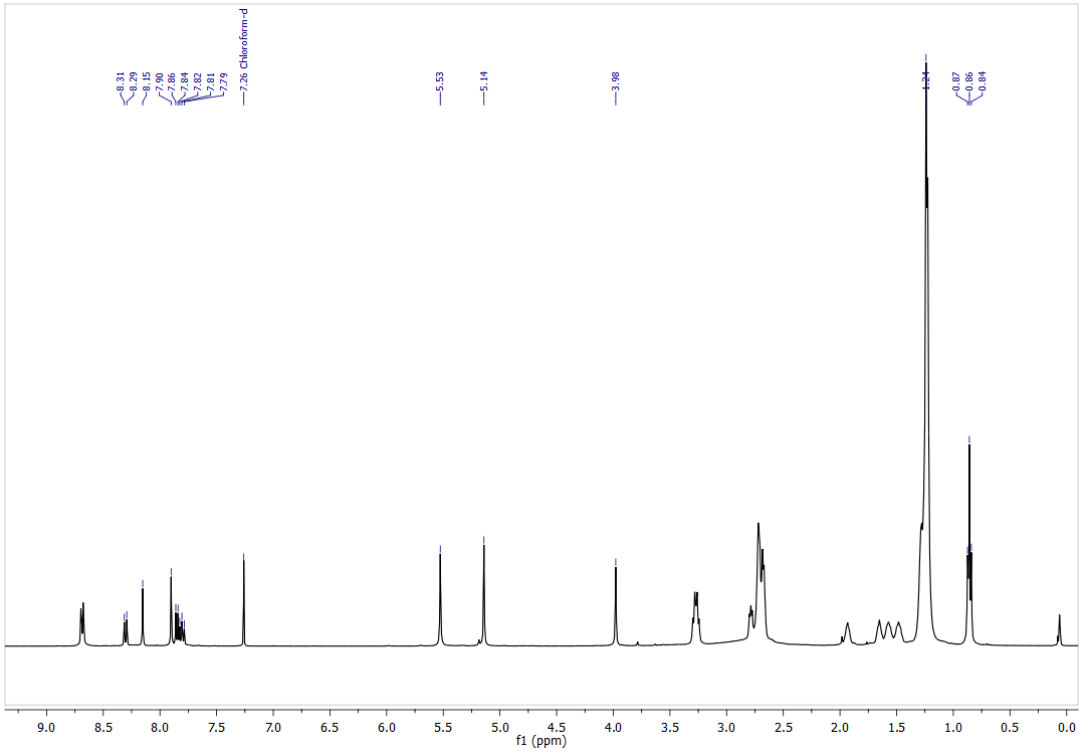
8.31
8.29
8.15
7.90
7.86
7.84
7.82
7.81
7.79
7.26 Chloroform-d
5.53
5.14
3.98
1.24
0.87
0.86
0.84
f1 (ppm)

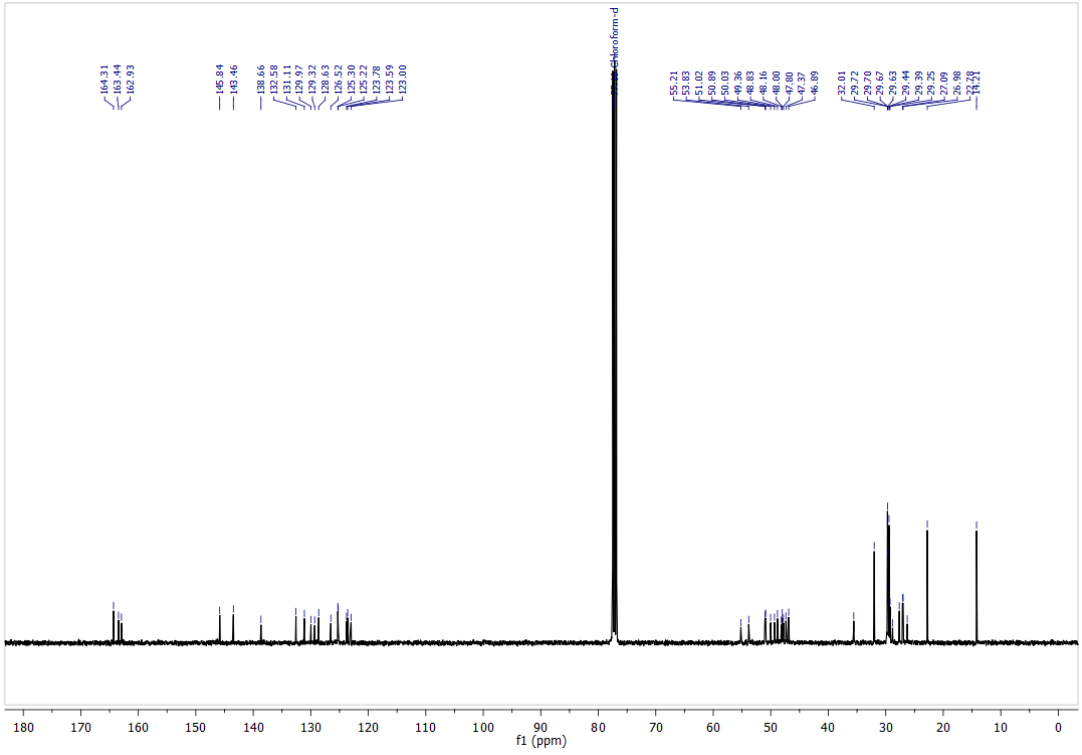
164.31
163.44
162.93
145.84
143.46
138.66
132.58
131.11
129.97
129.32
128.63
126.52
125.30
125.22
123.78
123.59
123.00
77.16 Chloroform-d
55.21
53.83
51.02
50.89
50.03
49.36
48.83
48.16
48.00
47.80
47.37
46.89
32.01
29.72
29.70
29.67
29.63
29.44
29.39
29.25
27.09
26.98
14.21
f1 (ppm)

*2-(4-((6-(4-((1,4,8,11-Tetraazacyclotetradecan-1-yl)methyl)-1H-1,2,3-triazol-1-yl)-1,3-dioxo-1H-benzo[de]isoquinolin-2(3H)-yl)methyl)-1H-1,2,3-triazol-1-yl)-N,N-didodecylacetamide (**109**):*

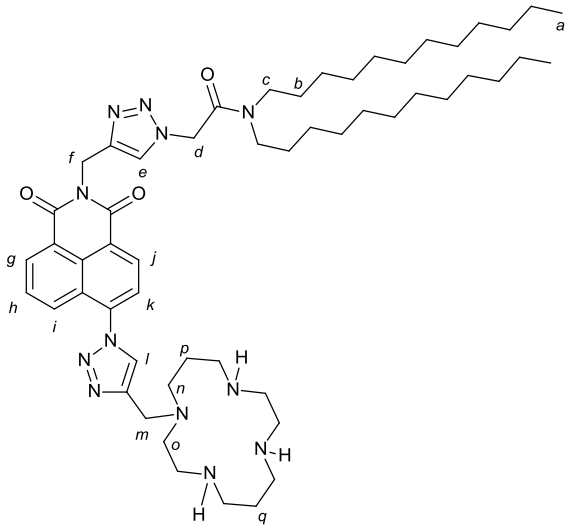

Compound **108** (50 mg, 0.040 mmol) was dissolved in a solution of TFA (20%) in CH_2Cl_2 (1 mL), and for 6 h at r.t. The reaction mixture was concentrated *in vacuo*, re-suspended in $CHCl_3$ (5 mL) and washed with aqueous NaOH (1 M, 5 mL). The organic phase was dried over $MgSO_4$ and the solvent was removed *in vacuo* to yield deprotected sensor **109** as a yellow residue (34.0 mg, 89%). ^{1}H NMR (400 MHz, $CDCl_3$) δ_H 8.72-8.64 (m, 2H, H_g and H_j), 8.30 (d, *J* = 8.5, 1H, H_i), 8.15 (s, 1H, H_l), 7.90 (s, 1H, H_e), 7.85 (d, J = 7.8, 1H, H_k), 7.83-7.78 (m, 1H, H_h), 5.52 (s, 2H, H_f), 5.14 (s, 2H, H_d), 3.98 (s, 2H, H_m), 3.33-3.20 (m, 4H, H_c), 2.84-2.62 (m, 12H, cyclam-H), 2.00-1.87 (m, 2H, H_o), 1.70-1.42 (m, 6H, H_n, H_q, H_p), 1.36-1.12 (m, 40H, H_b (4H), and alkyl-H (36H)), 0.90-0.82 (m, 6H, H_a). ^{13}C NMR (101 MHz, $CDCl_3$) δ_C 164.3, 163.4, 162.9, 145.8, 143.5, 138.6, 132.5, 131.1, 129.9, 129.3, 128.6, 126.5, 125.3, 125.2, 123.8, 123.6, 123.0, 55.2, 53.8, 51.0, 50.9, 50.0, 49.4, 48.8, 48.2, 48.0, 47.8, 47.4, 46.9, 35.6, 32.0, 29.7, 29.7, 29.7, 29.6, 29.4, 29.3, 29.2, 28.8, 27.6, 27.1, 26.9, 26.3, 22.8, 14.2. IR: (ν_{max}/cm^{-1}) 2927, 2850, 1695, 1578, 1460, 1403, 1368, 1244, 1156, 807, 782. HRMS (EI) calcd for $C_{54}H_{86}N_{12}O_3$ $[M + H]^+$ 951.7019, found 951.7022. UV: $\lambda_{max}(CH_2Cl_2)$/nm (ε / mol^{-1}cm^{-1}dm^3) 345 (8389)

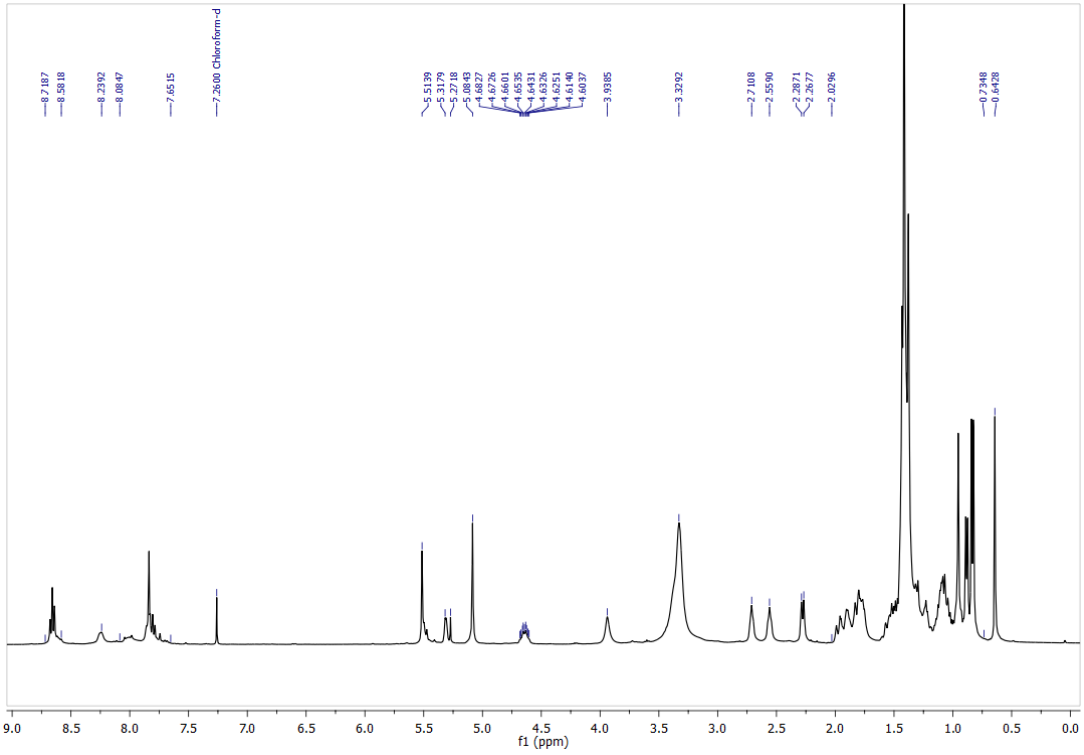
8.7187
8.5818
8.2392
8.0847
7.6515
7.2600 Chloroform-d
5.5139
5.3179
5.2718
5.0843
4.6827
4.6726
4.6601
4.6535
4.6431
4.6326
4.6251
4.6140
4.6037
3.9385
3.3292
2.7108
2.5590
2.2871
2.2677
2.0296
0.7348
0.6428
f1 (ppm)

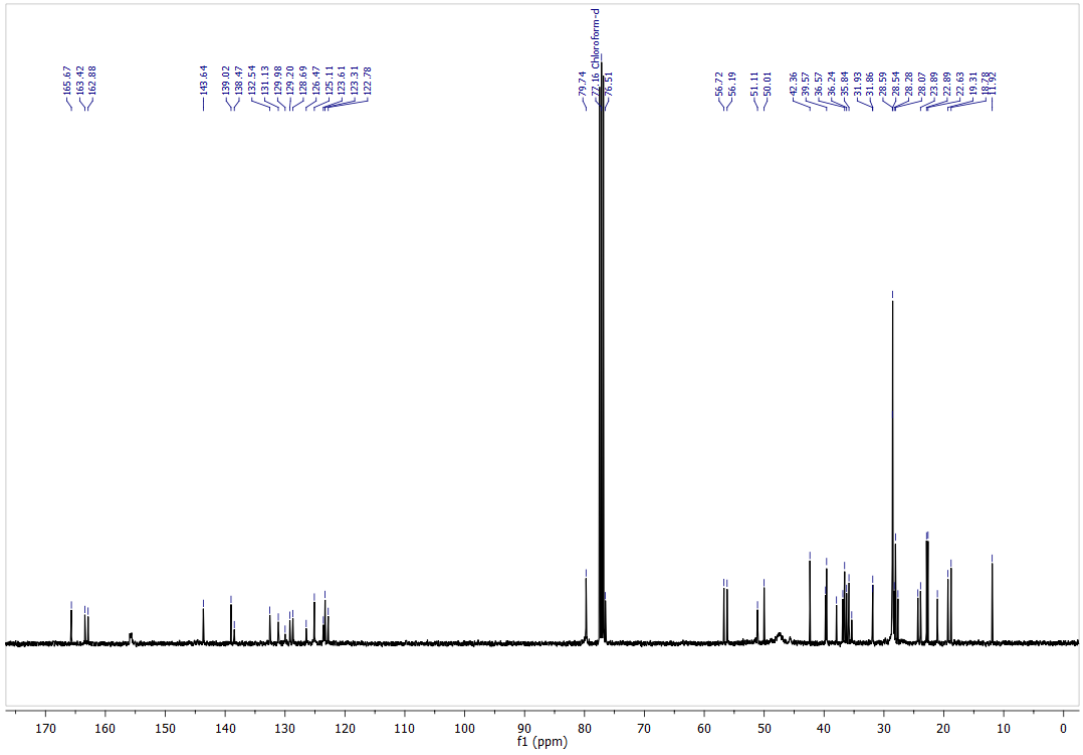
165.67
163.42
162.88
143.64
139.02
138.47
132.54
131.13
129.98
129.20
128.69
126.47
125.11
123.61
123.31
122.78
79.74
77.16 Chloroform-d
76.51
56.72
56.19
51.11
50.01
42.36
39.57
36.57
36.24
35.84
31.93
31.86
28.59
28.54
28.28
28.07
23.89
22.89
22.65
19.31
18.78
11.92
f1 (ppm)

*Tri-tert-butyl 11-((1-(2-((1-(2-cholesterol)-2-oxoethyl)-1H-1,2,3-triazol-4-yl)methyl)-1,3-dioxo-2,3-dihydro-1H-benzo[de]isoquinolin-6-yl)-1H-1,2,3-triazol-4-yl)methyl)-1,4,8,11-tetraazacyclotetradecane-1,4,8-tricarboxylate (**110**):*

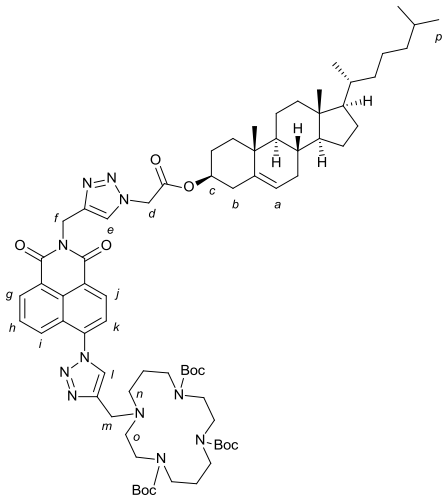

Sensor **13** was prepared according to **General Procedure A** albeit at 0.05 M reaction concentration, using central building block **69** (0.31 g, 1.0 mmol), azide **85** and cyclam acetylene **65**. Reaction times for each stage take longer due to dilution; 6 h, 48 h and 24 h respectively. The crude product was obtained obtained *via* precipitation with a saturated solution of EDTA in 17.5% aqueous NH_3 (20 mL) and purified by flash column chromatography (1:1 Petrol:EtOAc) to yield protected sensor **110** as a yellow foam (0.36 g, 28%). ^{1}H NMR (400 MHz, $CDCl_3$) δ_H 8.70-8.58 (m, 2H, H_g and H_j), 8.24 (bs, 1H, H_l), 7.92-7.62 (m, 4H, H_e and H_h, H_i and H_k), 5.51 (s, 2H, H_m), 5.34-5.29 (m, 1H, H_a), 5.08 (s, 2H, H_f), 4.62 (m, 1H, H_c), 3.93 (bs, 2H, H_d), 3.50-3.15 (m, 12H, Cyclam-H), 2.74-2.68 (m, 2H, H_o), 2.60-2.52 (m, 2H, H_n), 2.27 (d, J = 7.8, 2H, H_b), 2.27-0.75 (m, 71H, Cholesterol-H (40H), tBu (27H), cyclam (4H)), 0.64 (s, 3H, H_p). ^{13}C NMR (101 MHz, $CDCl_3$) δ_C 165.6, 163.4, 162.8, 143.6, 139.0, 138.4, 132.5, 131.1, 129.9, 129.2, 128.7, 126.4, 125.1, 123.6, 123.3, 122.7, 79.7, 76.5, 56.7, 56.2, 51.1, 50.0, 42.3, 39.7, 39.5, 37.9, 36.8, 36.5, 36.2, 35.8, 35.3, 31.9, 31.8, 28.5, 28.5, 28.2, 28.0, 27.6, 24.3, 23.9, 22.9, 22.6, 21.1, 19.3, 18.8, 11.9.IR: (ν_{max}/cm^{-1}) 2934 (broad), 1751, 1677, 1588, 1465, 1410, 1365, 1232, 1159, 732. M.p. (^{o}C) 122-125. HRMS (EI) calcd for $C_{72}H_{106}N_{11}O_{10}$ $[M + H]^+$ 1284.8119, found 1284.8101. UV: $\lambda_{max}(CH_2Cl_2)$/nm (ε / mol^{-1}cm^{-1}dm^3) 344 (74038).

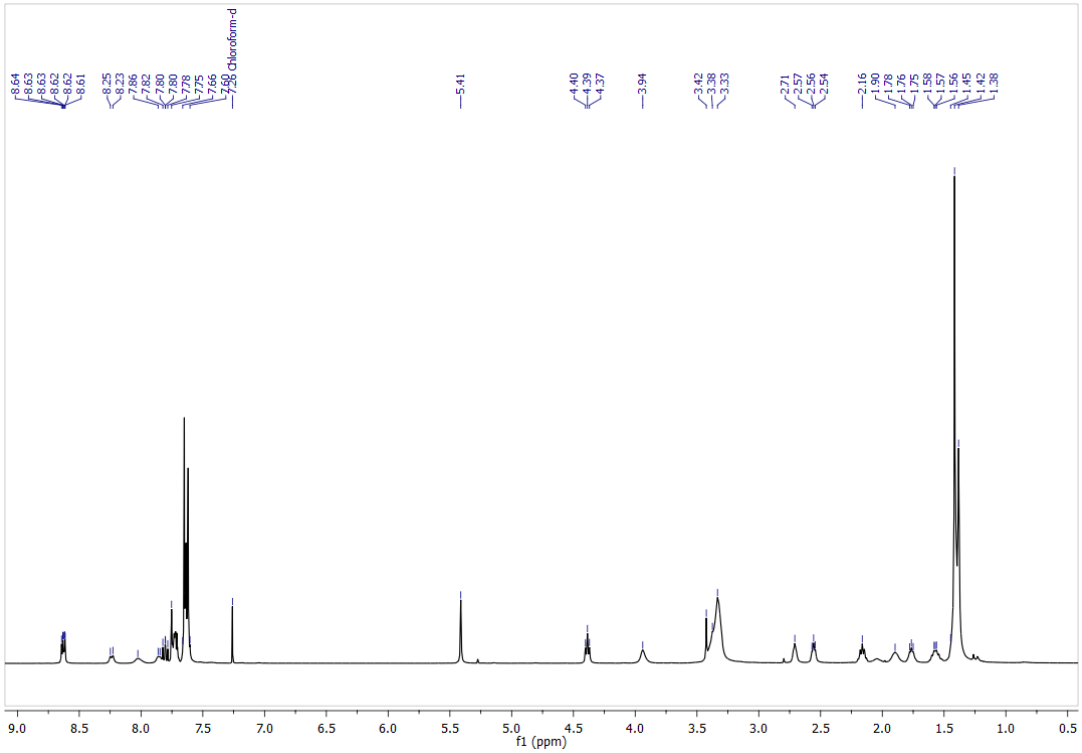
8.64
8.63
8.63
8.62
8.62
8.61
8.25
8.23
7.86
7.82
7.80
7.80
7.78
7.75
7.66
7.60
7.26 Chloroform-d
5.41
4.40
4.39
4.37
3.94
3.42
3.38
3.33
2.71
2.57
2.56
2.54
2.16
1.90
1.78
1.76
1.75
1.58
1.57
1.56
1.45
1.42
1.38
9.0 8.5 8.0 7.5 7.0 6.5 6.0 5.5 5.0 4.5 4.0 3.5 3.0 2.5 2.0 1.5 1.0 0.5
f1 (ppm)

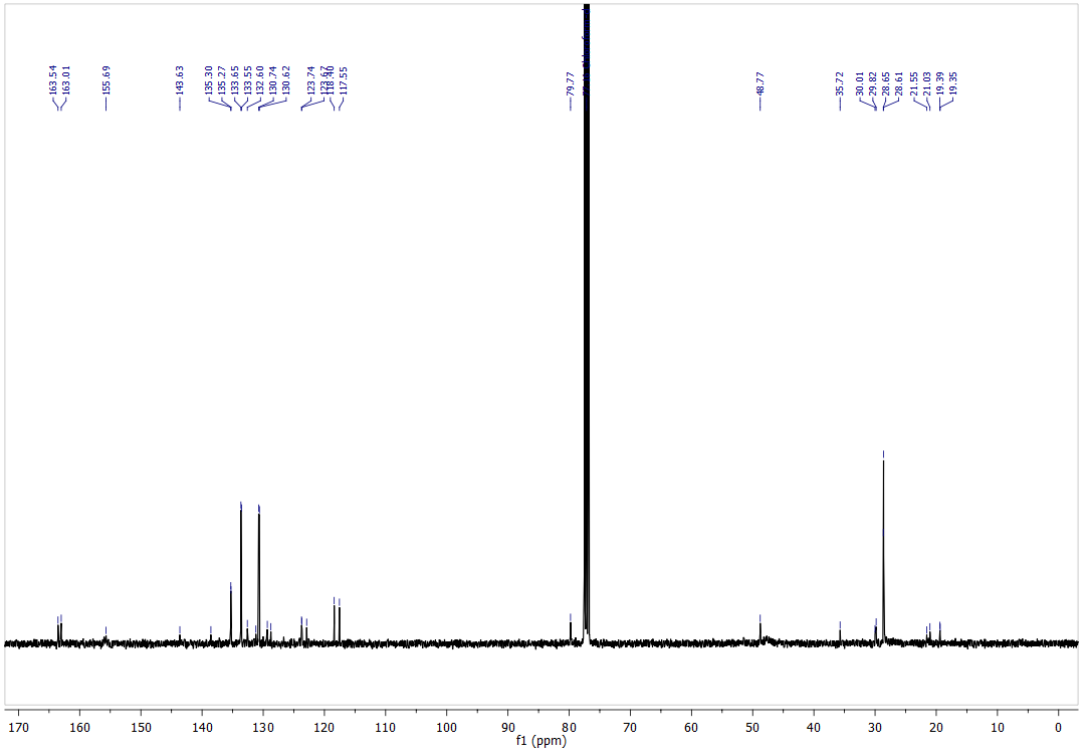
163.54
163.01
155.69
149.63
135.30
135.27
133.65
133.55
132.60
130.74
130.62
123.74
117.55
79.77
48.77
35.72
30.01
29.82
28.65
28.61
21.55
21.03
19.39
19.35
170 160 150 140 130 120 110 100 90 80 70 60 50 40 30 20 10 0
f1 (ppm)

*(4-(4-((1,3-Dioxo-6-(4-((4,8,11-tris(tert-butoxycarbonyl)-1,4,8,11-tetraazacyclotetradecan-1-yl)methyl)-1H-1,2,3-triazol-1-yl)-1H-benzo[de]isoquinolin-2(3H)-yl)methyl)-1H-1,2,3-triazol-1-yl)butyl)triphenylphosphonium (**111**):*

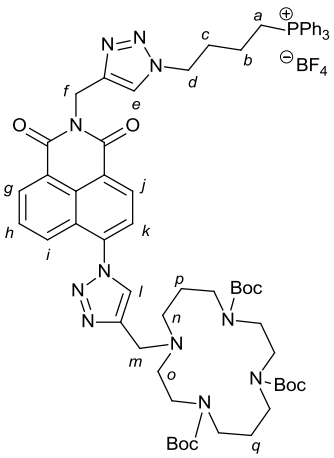

General procedure A was employed with **69** (314 mg, 1.00 mmol)**,** azide **89** (0.45 g, 1.0 mmol) in NMP (5 mL), followed by cyclam acetylene **65** (0.59 g, 1.1 mmol) and EtOH (5 mL). Crude product obtained by dilution of the reaction mixture with CH_2Cl_2 (10 mL), and washing the organic mixture with a saturated solution of EDTA in 17.5% aqueous NH_3 (3 x 15 mL). The organic phase was dried over $MgSO_4$, concentrated *in vacuo* and triturated with EtOAc (3 x 30 mL). The resulting suspension was filtered, the filtrate concentrated *in vacuo* and purified by flash column chromatography (CH_2Cl_2/MeOH 99:1 to 9:1) to yield **111** as a yellow foam (0.84 g, 66%). ^{1}H NMR (400 MHz, $CDCl_3$) δ_H 8.65-8.61 (m, 2H, H_g and H_j), 8.26-8.21 (m, 1H, H_i), 8.02 (br s, 1H, H_l), 7.88-7.83 (m, 1H, H_k), 7.80 (dd, *J* = 7.4, 8.4, 1H, H_h), 7.75 (s, 1H, H_e), 7.75-7.59 (m, 15H, 3 x Ph), 5.41 (s, 2H, H_f), 4.38 (t, *J* = 6.5, 2H, H_d), 3.93 (br s, 2H, H_m), 3.45-3.25 (m, 14H, cyclam-H (12H) and H_c), 2.74-2.68 (m, 2H, H_o), 2.55 (t, *J* = 5.5, 2H, H_n), 2.16 (quint, *J* = 6.7, 2H, H_b), 1.93-1.86 (m, 2H, H_q), 1.80-1.72 (m, 2H, H_p), 1.63-1.51 (m, 2H, H_a), 1.48-1.30 (m, 27H, 3 x Boc). ^{13}C NMR (101 MHz, $CDCl_3$) δ_C 163.5, 163.0, 155.7, 143.6, 138.6, 135.3, 135.3, 133.6, 133.5, 132.6, 131.2, 130.7, 130.6, 129.3, 128.7, 123.7, 123.7, 122.9, 118.4, 117.5, 79.8, 48.8, 35.7, 30.0, 29.8, 28.7, 28.6, 21.5, 21.0, 19.4, 19.3 (overlapping signals). IR: (ν_{max}/cm^{-1}) 2981, 2930, 1684, 1664, 1588, 1478, 1441, 1411, 1364, 1237, 1157, 1111, 1050, 1049, 882. HRMS (EI) calcd for $C_{29}H_{48}N_3O_2$ $[M - BF_4]^+$ 1174.6002, found 1174.5983. UV: $\lambda_{max}(CH_2Cl_2)$/nm (ε / mol^{-1}cm^{-1}dm^3) 344 (3139)

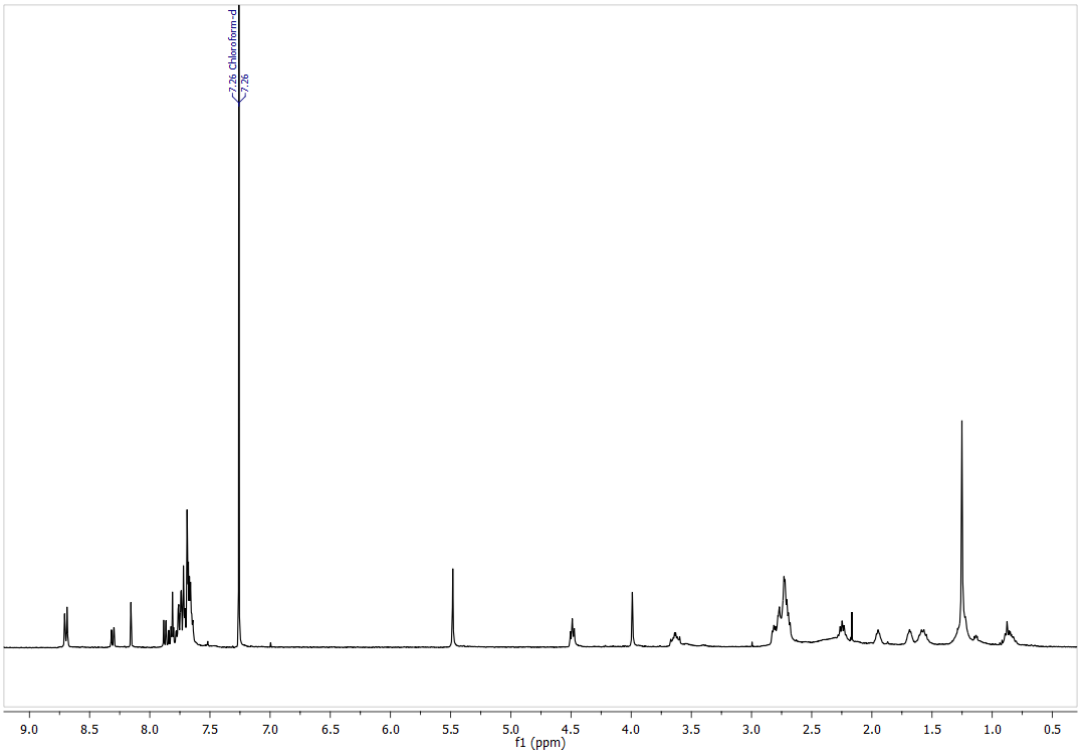
7.26 Chloroform-d
7.26
9.0 8.5 8.0 7.5 7.0 6.5 6.0 5.5 5.0 4.5 4.0 3.5 3.0 2.5 2.0 1.5 1.0 0.5
f1 (ppm)

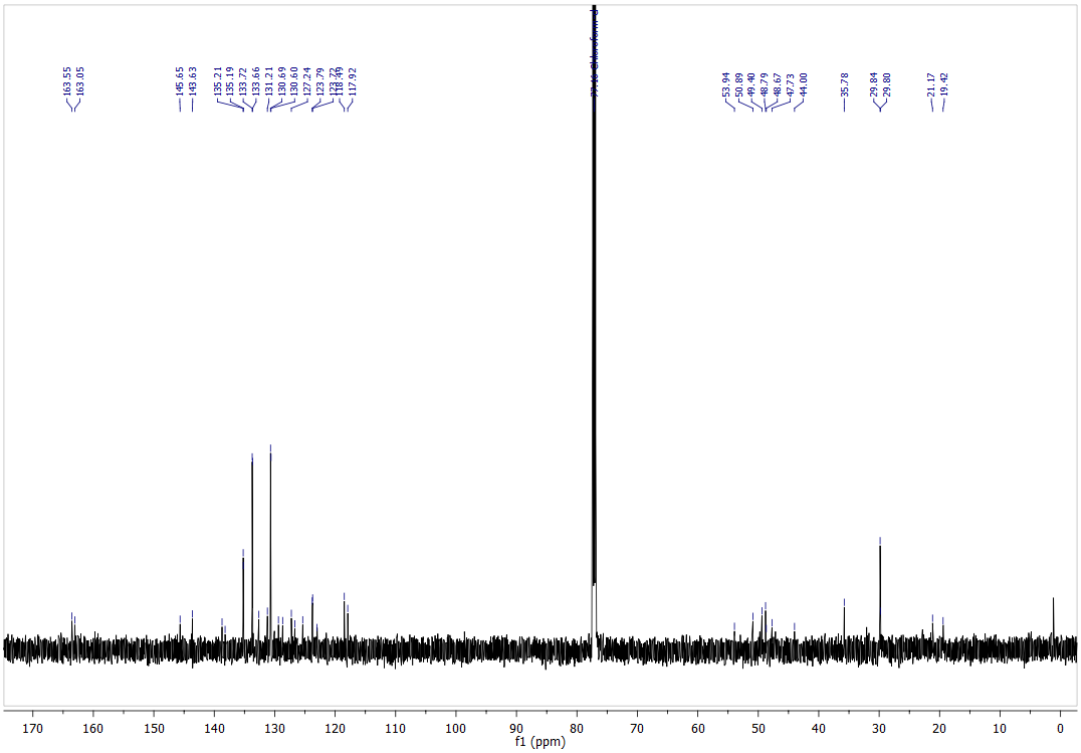
163.55
163.05
146.65
143.63
135.21
135.19
133.72
133.66
131.21
130.69
130.60
129.64
122.24
123.79
123.72
118.49
117.92
77.26 Chloroform-d
53.94
50.89
49.40
48.79
48.67
47.73
44.00
35.78
29.84
29.80
21.17
19.42
170 160 150 140 130 120 110 100 90 80 70 60 50 40 30 20 10 0
f1 (ppm)

*(4-(4-((6-(4-((1,4,8,11-Tetraazacyclotetradecan-1-yl)methyl)-1H-1,2,3-triazol-1-yl)-1,3-dioxo-1H-benzo[de]isoquinolin-2(3H)-yl)methyl)-1H-1,2,3-triazol-1-yl)butyl)triphenylphosphonium trifluoroacetate (**112**):*

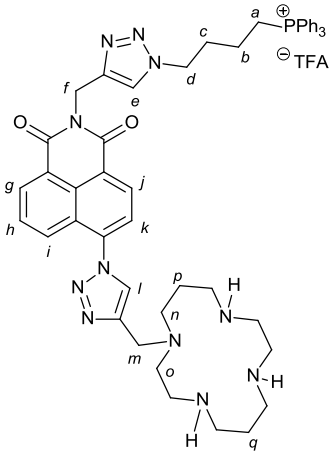

Compound **111** (20 mg, 0.016 mmol) was dissolved in a solution of TFA (20%) in CH_2Cl_2 (1 mL), and for 6 h at r.t. The reaction mixture was concentrated *in vacuo*, re-suspended in $CHCl_3$ (5 mL) and washed with aqueous NaOH (1 M, 5 mL). The organic phase was dried over $MgSO_4$ and the solvent was removed *in vacuo* to yield deprotected sensor **112** as a yellow residue (12.0 mg, 74%) ^{1}H NMR (400 MHz, $CDCl_3$) δ_H 8.71-8.64 (m, 2H, H_g and H_j), 8.30 (dd, *J* = 8.6, 0.9, 1H, H_i), 8.16 (s, 1H, H_l), 7.87 (d, *J* = 7.8, 1H, H_k), 7.83-7.58 (m, 16H, H_h and 3 x Ph), 7.80 (s, 1H, H_e), 5.46 (s, 2H, H_f), 4.47 (t, *J* = 6.3, 2H, H_d), 3.98 (s, 2H, H_m), 3.64-3.55 (m, 2H, H_c), 2.87-2.64 (m, 16H, cyclam-H (12H) and H_n + H_o), 2.22 (app. quint, *J* = 6.6, 2H, H_b), 1.99-1.90 (m, 2H, H_q), 1.74-1.65 (m, 2H, H_p), 1.63-1.52 (m, 2H, H_a). ^{13}C NMR (101 MHz, $CDCl_3$) δ_C 163.5, 163.1, 145.6, 143.6, 138.7, 138.2, 135.2, 135.2, 133.7, 133.7, 132.6, 131.2, 130.7, 130.6, 129.4, 128.7, 127.2, 126.7, 125.4, 123.8, 123.7, 123.0, 118.5, 117.9, 53.9, 50.9, 49.4, 48.8, 48.7, 47.7, 44.0, 35.8, 29.8, 29.8, 21.2, 19.4. ^{19}F NMR (376MHz, $CDCl_3$) δ_F -75.0. ^{31}P NMR (162 MHz, $CDCl_3$) δ_P 24.3. IR: (ν_{max}/cm^{-1}) 3509 (b), 2966, 2943, 1663, 1585, 1482, 1443, 1419, 1363, 1325, 1232, 1167, 1108, 1030, 863, 802. HRMS (EI) calcd for [M – anion]$^+$ 874.4429, found 874.4425. UV: λ_{max}(CH_2Cl_2)/nm (ε/ mol^{-1}cm^{-1}dm^3) 345 (10549)

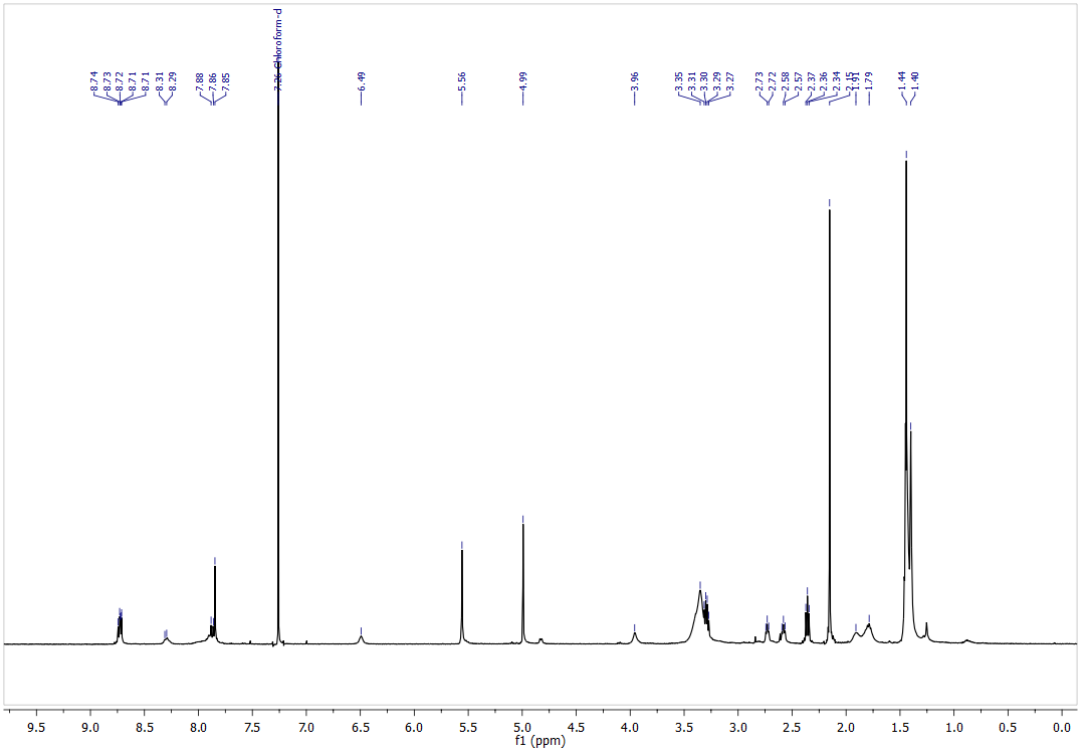
8.74
8.73
8.72
8.71
8.71
8.31
8.29
7.88
7.86
7.85
7.26 Chloroform-d
6.49
5.56
4.99
3.96
3.35
3.31
3.30
3.29
3.27
2.73
2.72
2.58
2.57
2.37
2.36
2.34
1.79
1.44
1.40
f1 (ppm)

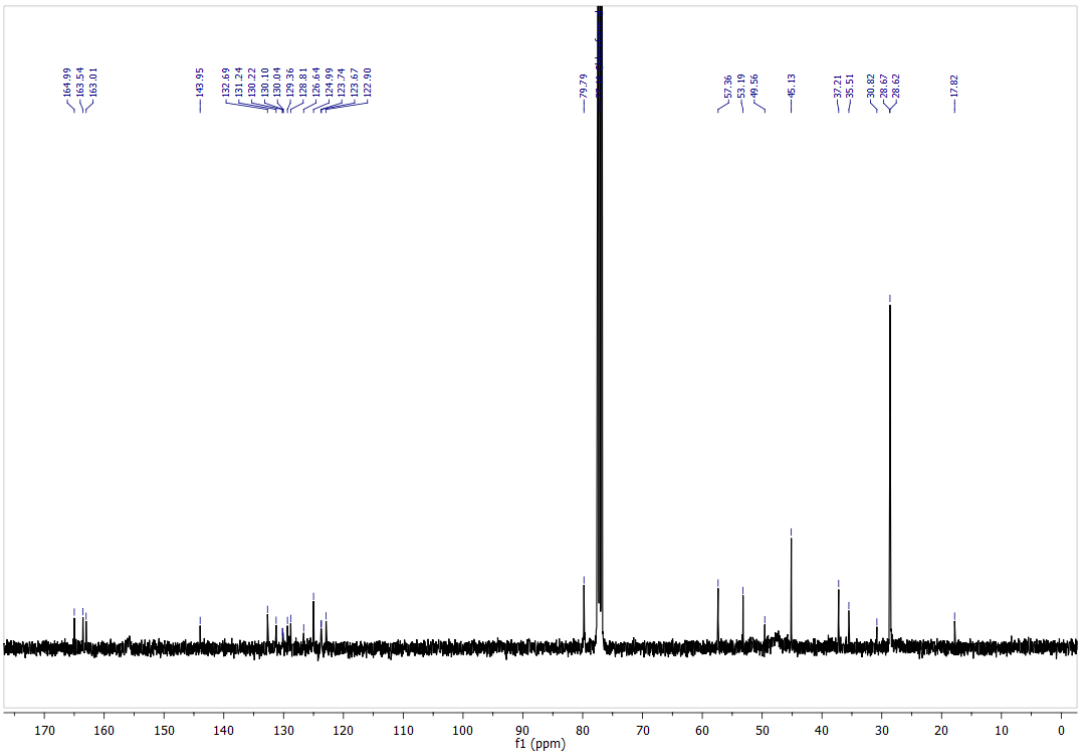
164.99
163.54
160.01
149.95
132.69
131.24
130.22
130.10
130.04
129.36
128.81
126.64
124.99
123.74
123.67
122.90
79.79
57.36
53.19
49.56
45.13
37.21
35.51
30.82
28.67
28.62
17.82
f1 (ppm)

*tri-tert-Butyl 11-((1-(2-((1-(2-((2-(dimethylamino)ethyl)amino)-2-oxoethyl)-1H-1,2,3-triazol-4-yl)methyl)-1,3-dioxo-2,3-dihydro-1H-benzo[de]isoquinolin-6-yl)-1H-1,2,3-triazol-4-yl)methyl)-1,4,8,11-tetraazacyclotetradecane-1,4,8-tricarboxylate (**113**):*

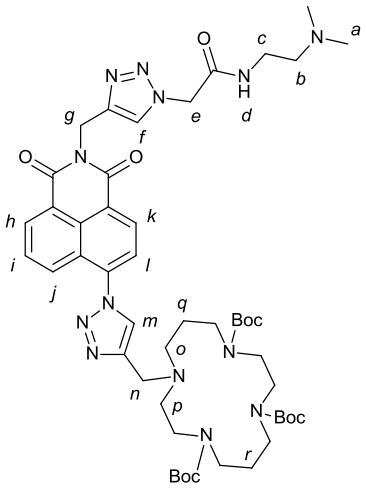

General procedure A was employed with **69** (314 mg, 1.0 mmol)**,** azide **92** (0.17 g, 1.0 mmol) in NMP (5 mL), followed by cyclam acetylene **65** (0.59 g, 1.1 mmol) and EtOH (5 mL). The crude product was obtained by dilution of the reaction mixture with CH_2Cl_2 (10 mL), and washing the organic mixture with a saturated solution of EDTA in 17.5% aqueous NH_3 (3 x 15 mL). The organic phase was dried over $MgSO_4$, concentrated *in vacuo* and purified by flash column chromatography on alumina (EtOAC to 9:1 EtOAc/MeOH) to yield **113** as a brown oil (0.67 g, 68%). ^{1}H NMR (400 MHz, $CDCl_3$) 8.75-8.69 (m, 2H, H_h and H_k), 8.34-8,26 (m, 1H,H_j), 7.98-7.82 (m, 4H, H_f, H_i, H_l and H_m), 6.49 (br s, 1H, H_d), 5.56 (s, 2H, H_g), 4.99 (s, 2H, H_e), 3.96 (br s, 2H, H_n), 3.49-3.25 (m, 12H, cyclam-H), 3.29 (q, *J* = 5.8, 2H, H_c), 2.70 (t, *J* = 5.2, 2H, H_p), 2.58 (t, *J* = 5.8, 2H, H_o), 2.35 (t, *J* = 6.0, 2H, H_b), 2.15 (s, 6H, H_a (2 x CH_3), 1.95-1.70 (m, 4H, H_p + H_q), 1.49-1.35 (m, 27H, 3 x ^{t}Bu). δ_H ^{13}C NMR (101 MHz, $CDCl_3$) δ_C 164.9, 163.5, 163.0, 143.9, 132.7, 131.2, 130.2, 130.1, 130.0, 129.4, 128.8, 126.6, 124.9, 123.7, 123.7, 122.9, 79.8, 57.4, 53.2, 49.6, 45.1, 37.2, 35.5, 30.8, 28.7, 28.6, 17.8 (overlapping signals). IR: (ν_{max}/cm^{-1}) 3409, 2966, 2919, 2850, 1691, 1688, 1593, 1476, 1420, 1369, 1260, 1165, 1096, 1017, 864, 801. HRMS (EI) calcd for $C_{49}H_{71}N_{13}O_9$ $[M + H]^+$ 986.5570, found 986.5562. UV: $\lambda_{max}(CH_2Cl_2)$/nm (ε / mol^{-1}cm^{-1}dm^3) 344 (43812).

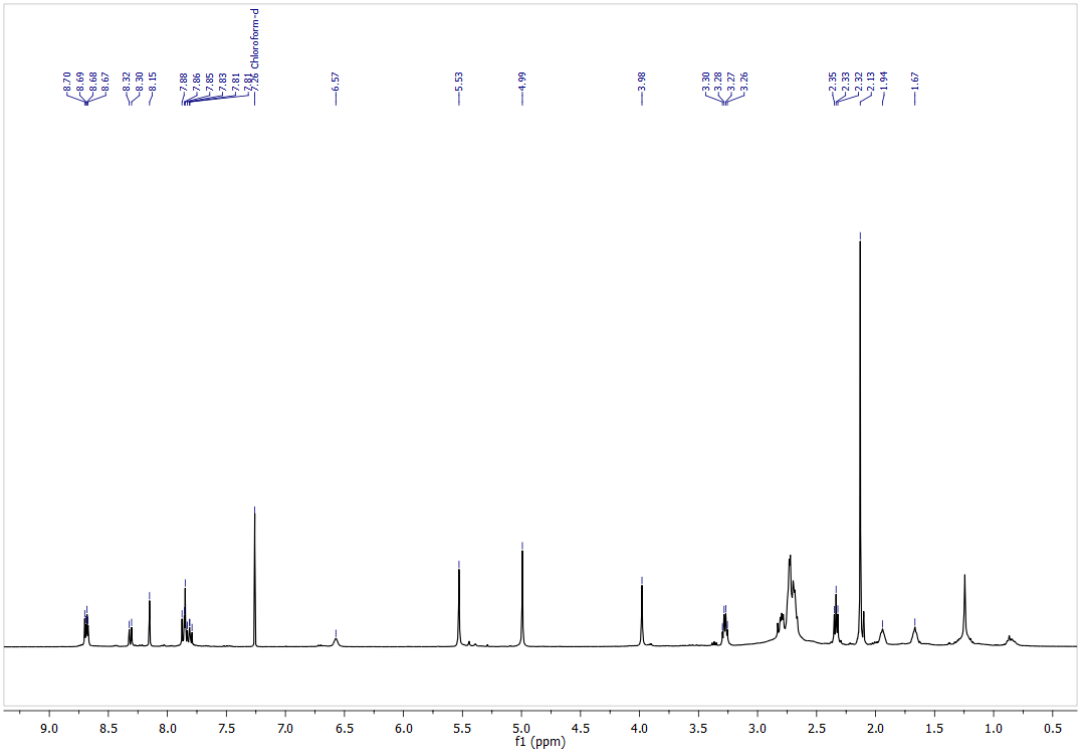
8.70
8.69
8.68
8.67
8.32
8.30
8.15
7.88
7.86
7.85
7.83
7.81
7.26 Chloroform-d
6.57
5.53
4.99
3.98
3.30
3.28
3.27
3.26
2.35
2.33
2.32
2.13
1.94
1.67
9.0 8.5 8.0 7.5 7.0 6.5 6.0 5.5 5.0 4.5 4.0 3.5 3.0 2.5 2.0 1.5 1.0 0.5
f1 (ppm)

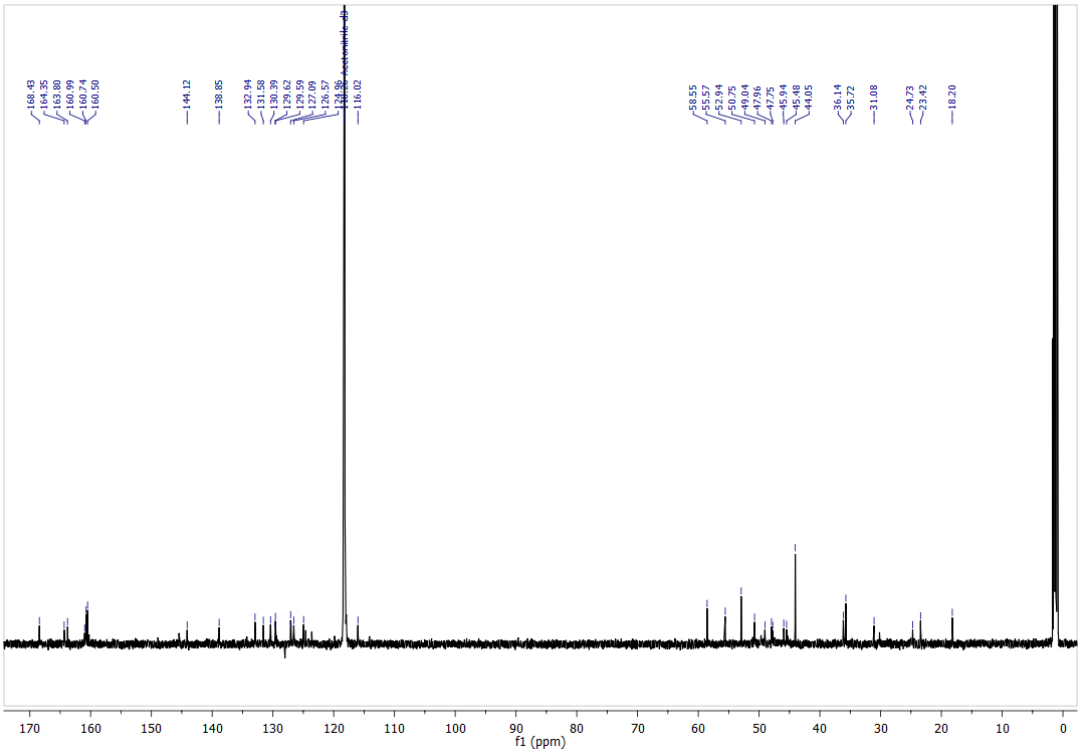
168.43
164.35
163.80
160.99
160.74
160.50
144.12
138.85
132.94
131.58
130.39
129.62
129.59
127.09
126.57
116.02
68.55
55.57
52.94
50.75
49.04
47.96
47.75
45.94
45.48
44.05
36.14
35.72
31.08
24.73
23.42
18.20
170 160 150 140 130 120 110 100 90 80 70 60 50 40 30 20 10 0
f1 (ppm)

*2-(4-((6-(4-((1,4,8,11-Tetraazacyclotetradecan-1-yl)methyl)-1H-1,2,3-triazol-1-yl)-1,3-dioxo-1H-benzo[de]isoquinolin-2(3H)-yl)methyl)-1H-1,2,3-triazol-1-yl)-N-(2-(dimethylamino)ethyl)acetamide (**114**):*

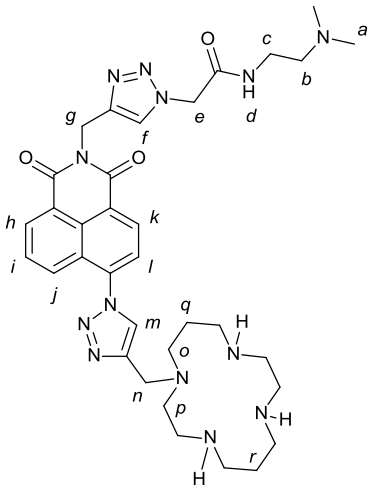

Compound **113** (20.0 mg, 0.016 mmol) was dissolved in a solution of TFA (20%) in CH_2Cl_2 (1 mL), and for 6 h at r.t.. The reaction mixture was concentrated *in vacuo*, re-suspended in $CHCl_3$ (5 mL) and washed with aqueous NaOH (1 M, 5 mL). The organic phase was dried over $MgSO_4$ and the solvent was removed *in vacuo* to yield deprotected sensor **114** as a yellow residue (8.9 mg, 63%) ^{1}H NMR (400 MHz, $CDCl_3$) δ_H 8.72-8.66 (m, 2H, H_h + H_k), 8.31 (d, *J* = 6.5, 1H, H_j), 8.15 (s, 1H, H_m), 7.87 (d, *J* = 7.8, 1H, H_l), 7.84 (s, 1H, H_m), 7.81 (dd, *J* = 7.4, 8.5, 1H, H_i and H_l), 6.57 (br s, 1H, H_d), 5.53 (s, 2H, H_g), 4.99 (s, 2H, H_e), 3.98 (s, 2H, H_n), 3.28 (q, *J* = 5.7, 2H, H_c), 2.85-2.60 (m, 16H, H_o and H_p and cyclam-H), 2.33 (t, *J* = 6.0, 2H, H_b), 2.13 (s, 6H, H_a (2 x CH_3)), 1.96-1.89 (m, 2H, H_r), 1.70-1.62 (m, 2H, H_q). ^{13}C NMR (101 MHz, CD_3CN) δ_C 168.4, 164.4, 163.8, 160.9, 160.7, 160.5, 144.1, 138.8, 132.9, 131.6, 130.4, 129.6, 129.6, 127.1, 127.0, 126.6, 124.9, 118.3, 116.0, 58.5, 55.5, 52.9, 50.7, 49.0, 47.9, 47.7, 45.9, 45.5, 44.1, 36.1, 35.7, 31.0, 24.7, 23.4, 18.2. IR: (ν_{max}/cm^{-1}). UV: λ_{max}(CH_2Cl_2)/nm (ε / $mol^{-1}cm^{-1}dm^3$) 345 (11800)

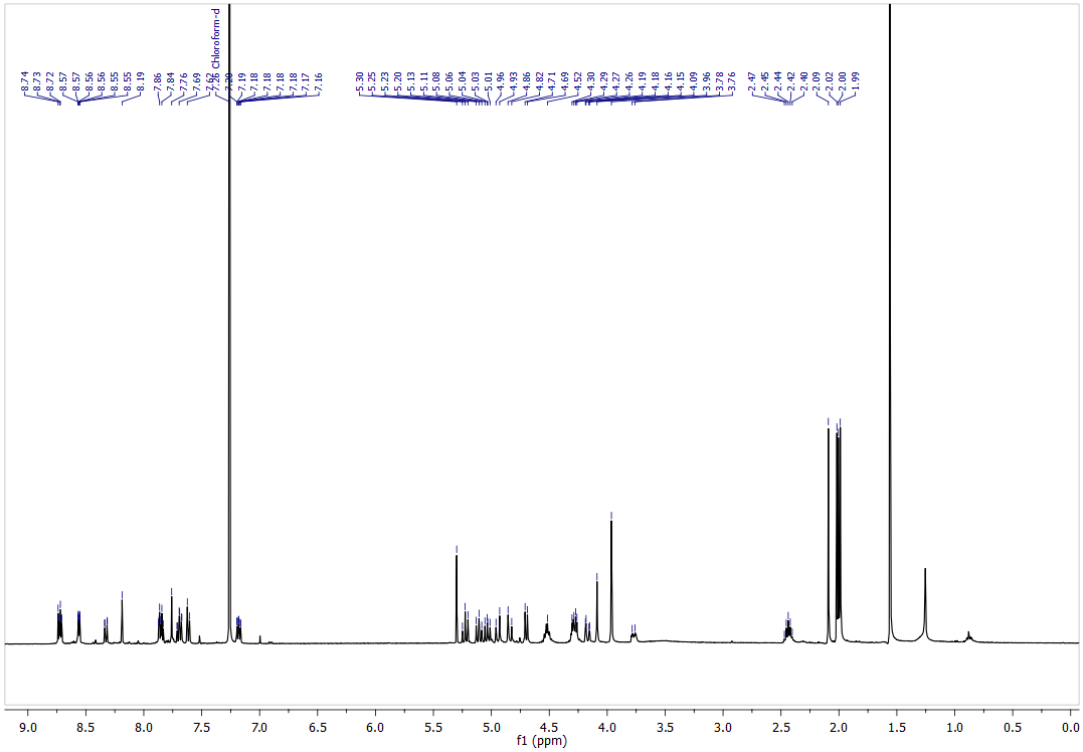
f1 (ppm)

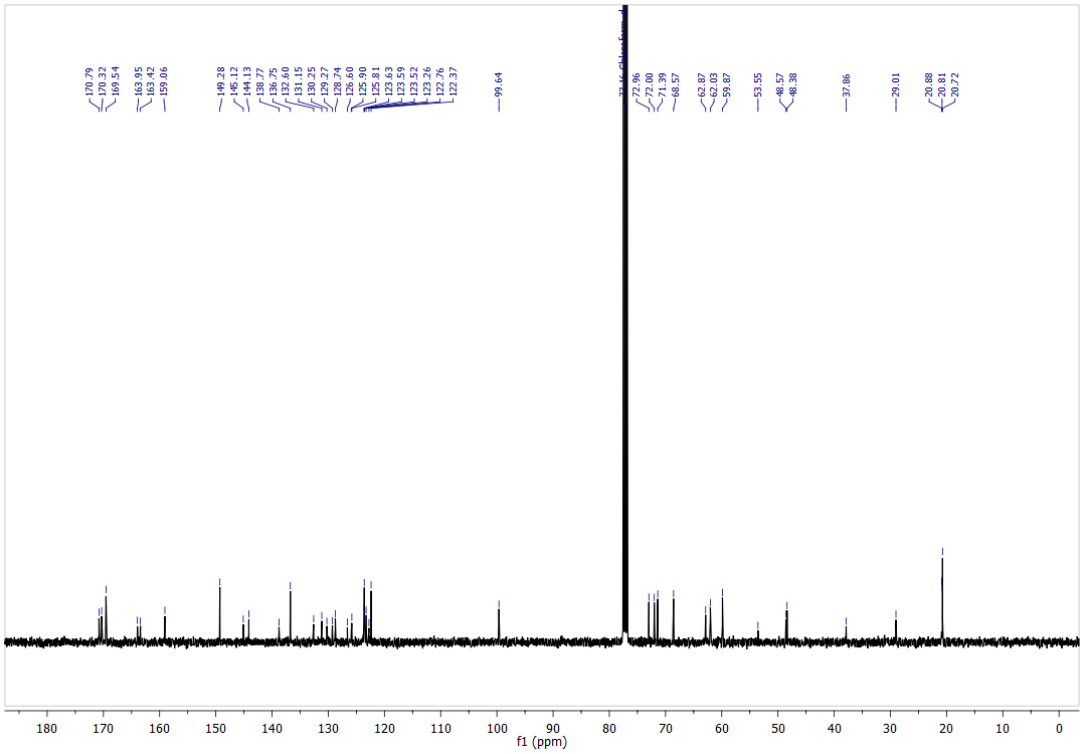
f1 (ppm)

*(2R,3R,4S,5R,6R)-2-(Acetoxymethyl)-6-((1-(3-(6-(4-((bis(pyridin-2-ylmethyl)amino)methyl)-1H-1,2,3-triazol-1-yl)-1,3-dioxo-1H-benzo[de]isoquinolin-2(3H)-yl)propyl)-1H-1,2,3-triazol-4-yl)methoxy)tetrahydro-2H-pyran-3,4,5-triyl triacetate (**115**):*

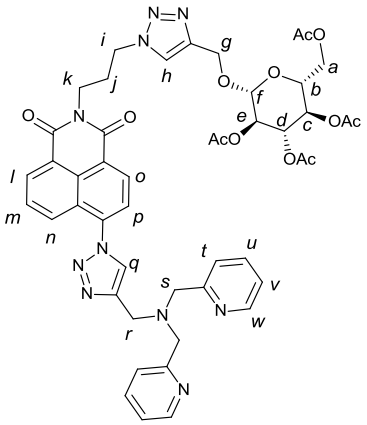

General procedure B was employed with **70** (359 mg, 1.00 mmol)**,** propargyl-glucose **94** (0.36 g, 1.0 mmol) in NMP (3.33 mL), followed by propargyl dipicolylamine **96** (0.26 g, 1.1 mmol) and EtOH (3.33 mL). Crude product obtained by dilution of the reaction mixture with CH_2Cl_2 (10 mL), and washing the organic mixture with a saturated solution of EDTA in 17.5% aqueous NH_3 (3 x 15 mL). The organic phase was dried over $MgSO_4$, concentrated *in vacuo* and purified by flash column chromatography on alumina (gradient from 99:1 to 90:10 CH_2Cl_2/MeOH) to yield **115** as a yellow foam (0.58 g, 61%). ^{1}H NMR (400 MHz, $CDCl_3$) δ_H 8.75-8.70 (m, 2H, H_l + H_o), 8.58-8.54 (m, 2H, H_w), 8.32 (dd, *J* = 8.6, 1.0, 1H, H_n), 8.19 (s, 1H, H_q), 7.88-7.82 (m, 2H, H_m + H_p), 7.76 (s, 1H, H_h), 7.69 (td, *J* = 7.7, 1.8, 2H, H_u), 7.63-7.59 (m, 2H, H_t), 7.20-7.16 (m, 2H, H_v), 5.22 (t, *J* = 9.5, 1H, H_d), 5.10 (t, *J* = 9.5, 1H, H_c), 5.03 (dd, *J* = 9.5, 8.0, 1H, H_e), 4.94 (d, *J* = 12.7, 1H, one of H_g), 4.84 (d, *J* = 12.7, 1H, one of H_g), (4.69 (d, *J* = 7.9, 1H, H_f), 4.56-4.48 (m, 2H, H_k), 4.33-4.24 (m, 3H, H_i and one of H_a), 4.17 (dd, *J* = 12.2, 2.2, 1H, one of H_a), 4.08 (s, 2H, H_r), 3.96 (s, 4H, H_s), 3.80-3.74 (m, 1H, H_b), 2.43 (app. quint, *J* = 6.5, 2H, H_j), 2.09 (s, 3H, Ac), 2.02 (s, 3H, Ac), 2.00 (s, 3H, Ac), 1.99 (s, 3H, Ac). ^{13}C NMR (101 MHz, $CDCl_3$) δ_C 170.8, 170.3, 169.5, 163.9, 163.4, 159.1, 149.3, 145.1, 144.1, 138.8, 136.7, 132.6, 131.2, 130.3, 129.3, 128.7, 126.6, 125.8, 123.6, 123.6, 123.5, 123.3, 122.7, 122.4, 99.6, 72.9, 72.0, 71.4, 68.6, 62.9, 62.0, 59.9, 53,5, 48.6, 48.4, 37.9, 29.0, 20.9, 20.8, 20.7 (overlapping signals). IR: (ν_{max}/cm^{-1}) 3454 (weak), 3138, 3006, 2958, 1753, 1704, 1660, 1588, 1435, 1361, 1218, 1038, 995, 905, 785, 755. HRMS (EI) calcd for $C_{47}H_{48}N_{10}O_{12}$ $[M + H]^+$ 945.3526**,** found 945.3517. UV: $\lambda_{max}(CH_2Cl_2)$/nm (ε/ mol^{-1}cm^{-1}dm^3) 344 (16280)

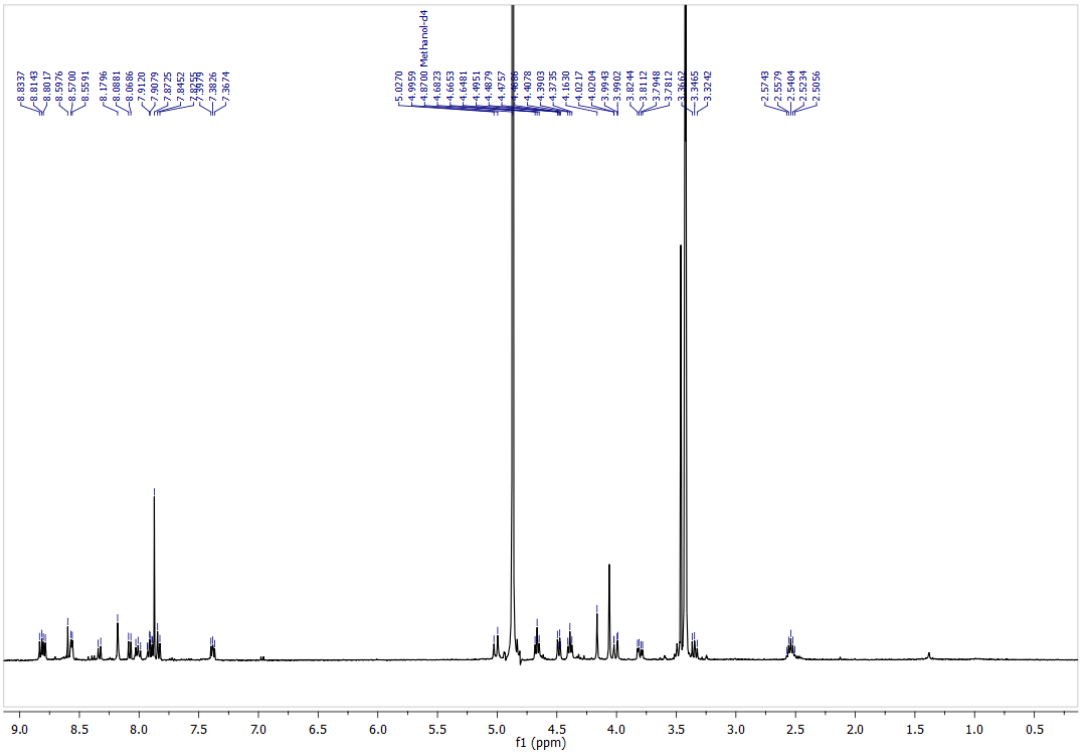
8.8337
8.8143
8.8017
8.5976
8.5700
8.5591
8.1796
8.0881
8.0686
7.9120
7.9079
7.8725
7.8455
7.3979
7.3826
7.3674
5.0270
4.9959
Methanol-d4
4.8700
4.6823
4.6653
4.6481
4.4951
4.4879
4.4757
4.4078
4.3903
4.3735
4.1630
4.0217
4.0204
3.9943
3.9902
3.8244
3.8112
3.7948
3.7812
3.3662
3.3465
3.3242
2.5743
2.5579
2.5404
2.5234
2.5056
f1 (ppm)

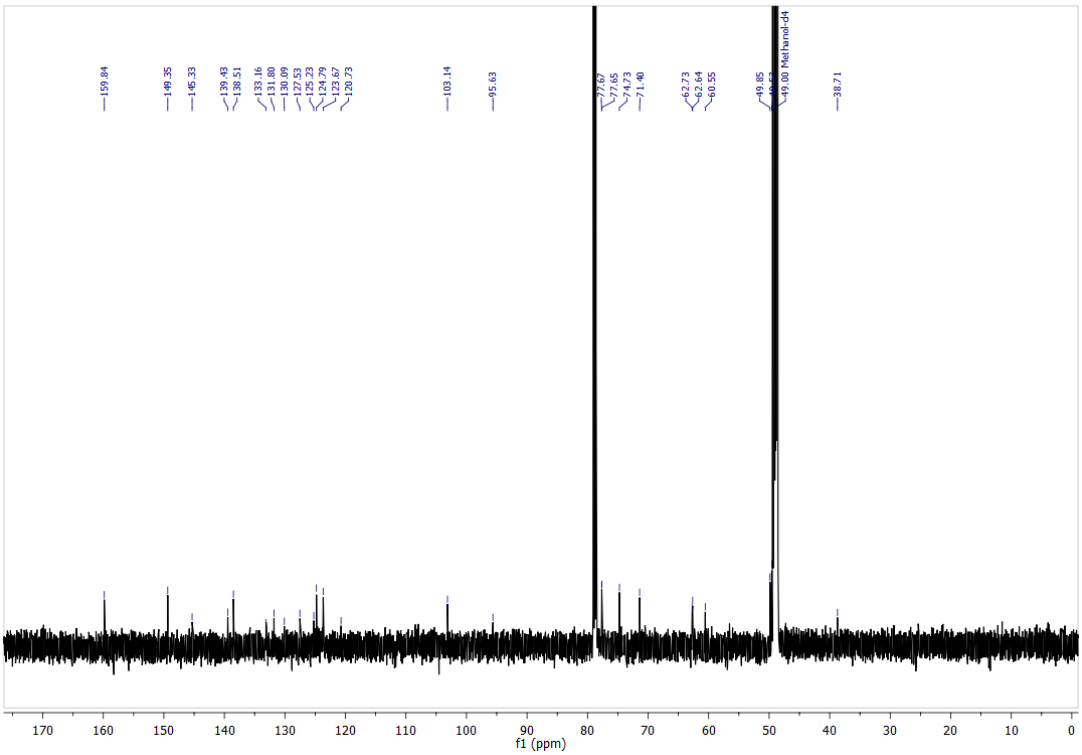
159.84
149.35
145.33
139.43
138.51
133.16
131.80
130.09
127.53
125.23
124.79
123.67
120.73
103.14
95.63
77.67
77.65
74.73
71.40
62.73
62.64
60.55
49.85
49.00
Methanol-d4
38.71
f1 (ppm)

*6-(4-((bis(pyridin-2-ylmethyl)amino)methyl)-1H-1,2,3-triazol-1-yl)-2-(3-(4-((((2R,3R,4S,5S,6R)-3,4,5-trihydroxy-6-(hydroxymethyl)tetrahydro-2H-pyran-2-yl)oxy)methyl)-1H-1,2,3-triazol-1-yl)propyl)-1H-benzo[de]isoquinoline-1,3(2H)-dione (**116**):*

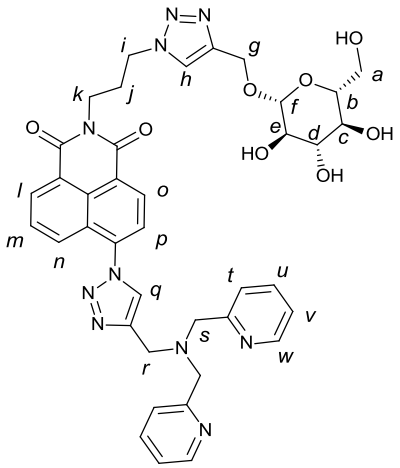

Following a modified literature procedure, sensor **115** (25 mg, 0.026 mmol) was dissolved in MeOH (0.5 mL) and NaOMe (0.3 eq) was added to the solution. The reaction mixture was stirred for 4 h, and evaporated to dryness *in vacuo* to yield deprotected sensor **116** as a yellow residue (16.0 mg, 79%). ^{1}H NMR (400 MHz, MeOD) δ_H 8.84-8.77 (m, 2H, H_l + H_o), 8.60 (s, 1H, H_q), 8.58-8.55 (m, 2H, H_w), 8.33 (d, *J* = 8.6, 1H, H_n), 8.17 (s, 1H, H_h), 8.07 (d, *J* = 7.8, 1H, H_p), 8.04-7.98 (m, 1H, H_m), 7.90 (td, *J* = 7.7, 1.6, 2H, H_u), 7.86-7.81 (m, 2H, H_t), 7.41-7.35 (m, 2H, H_m), 5.01 (d, *J* = 12.5, 1H, one of H_g), 4.86-4.82 (m, 1H, one of H_g – obscured by solvent peak, identified by cross peak on COSY), 4.66 (t, *J* = 6.8, 2H, H_k), 4.48 (d, *J* = 7.7, 1H, H_f), 4.39 (t, *J* = 7.0, 2H, H_i), 4.16 (s, 2H, H_r), 4.06 (s, 4H, H_s), 4.00 (dd, *J* = 12.1, 1.6, 1H, one of H_a), 3.80 (dd, *J* = 11.8, 5.3, 1H, one of H_a), 3.50-3.40 (m, 3H, H_c and H_d and H_e – obscured by solvent peak, identified by cross peak on COSY), 3.34 (dd, *J* = 9.0, 7.8, 1H, H_b), 2.54 (quint, *J* = 7.0, 2H, H_j). ^{13}C NMR (101 MHz, $CDCl_3$) δ_C 159.8, 149.3, 145.3, 139.4, 138.5, 133.2, 131.8, 130.1, 127.5, 125.2, 124.8, 123.7, 120.7, 103.1, 95.6, 77.7, 77.6, 74.7, 71.4, 62.7, 62.6, 60.5, 49.8, 49.6, 38.7. IR: (ν_{max}/cm^{-1}) 3378 (broad), 2929, 2831, 1699, 1659, 1623, 1592, 1476, 1434, 1394, 1352, 1268, 1233, 1103, 1082, 1046, 996, 842. HRMS (EI) calcd for $C_{39}H_{40}N_{10}O_8$ $[M + H]^+$ 777.3103, found 777.3104. UV: λ_{max}(CH_2Cl_2)/nm (ε/ mol^{-1}cm^{-1}dm^3) 345 (13126).

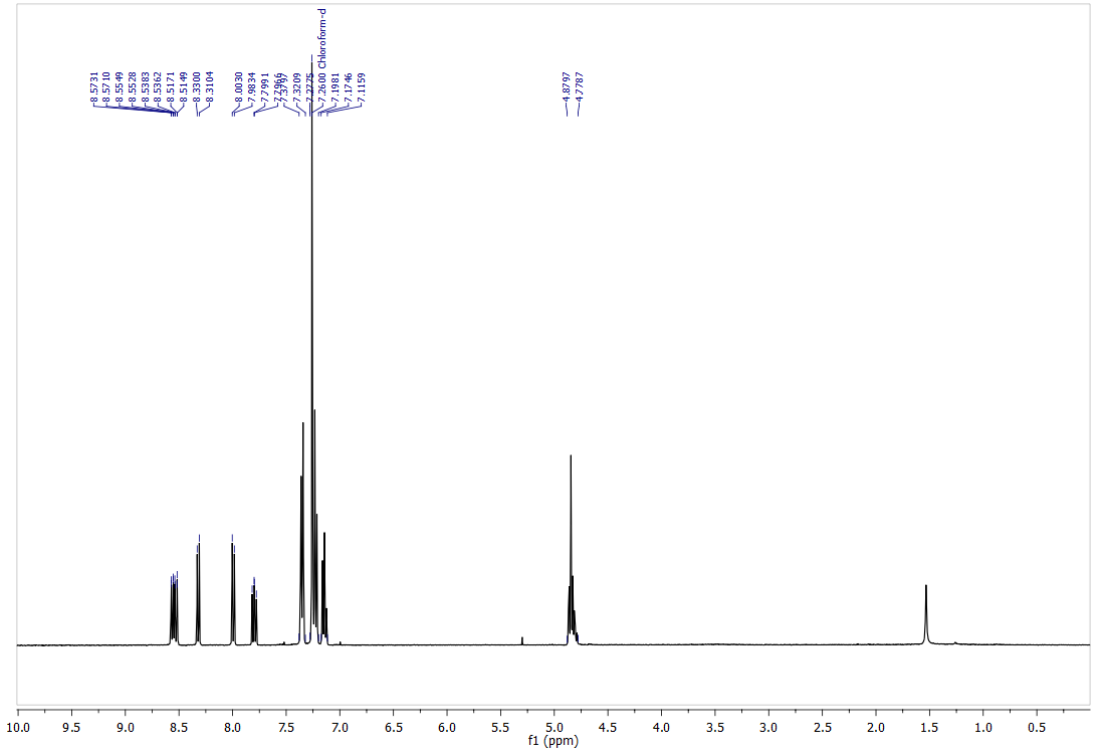
8.5731
8.5710
8.5549
8.5528
8.5383
8.5362
8.5171
8.5149
8.3300
8.3104
8.0030
7.9834
7.7991
7.7969
7.3209
7.2775
Chloroform-d
7.2600
7.1981
7.1746
7.1159
4.8797
4.7787
10.0 9.5 9.0 8.5 8.0 7.5 7.0 6.5 6.0 5.5 5.0 4.5 4.0 3.5 3.0 2.5 2.0 1.5 1.0 0.5
f1 (ppm)

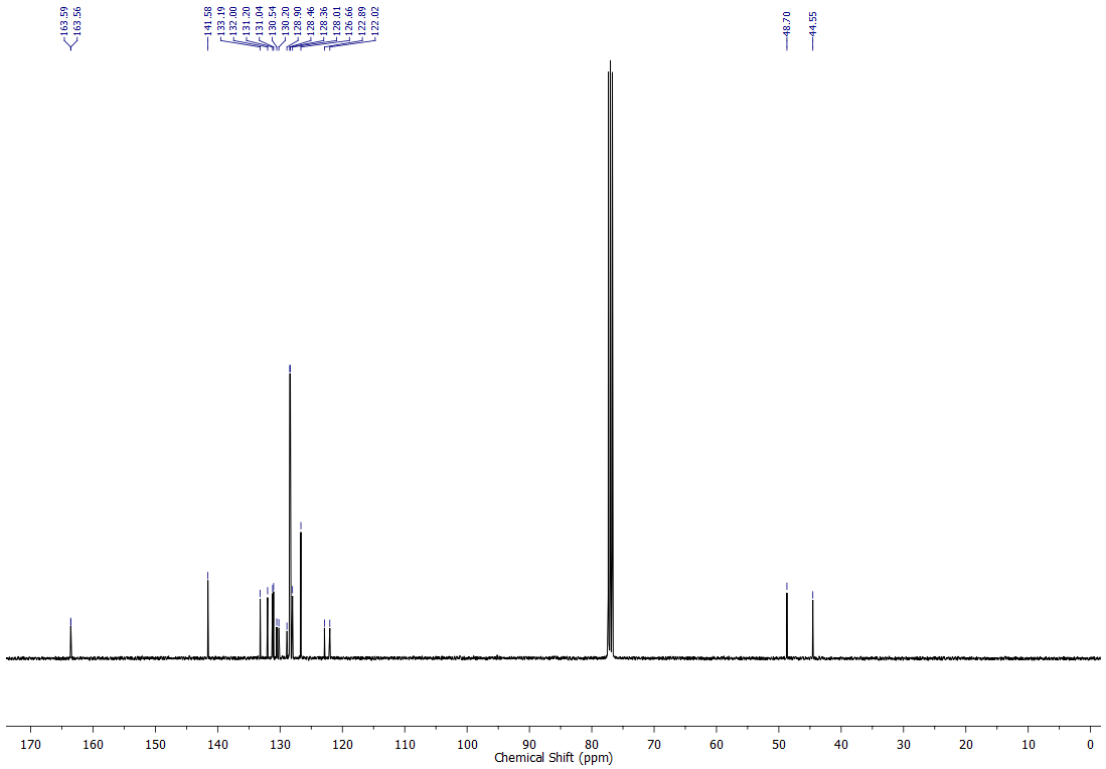
163.59
163.56
141.58
133.19
132.00
131.20
131.04
130.54
130.20
128.90
128.46
128.36
128.01
126.66
122.89
122.02
48.70
44.55
170 160 150 140 130 120 110 100 90 80 70 60 50 40 30 20 10 0
Chemical Shift (ppm)

*6-bromo-2-(2,2-diphenylethyl)-1H-benzo[de]isoquinoline-1,3(2H)-dione (**138**)*

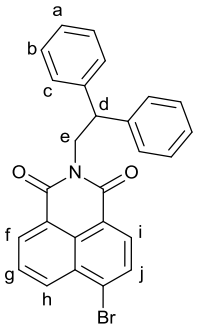

4-bromo-1,8-naphthalic anhydride (1.5 g, 5.4 mmol) was dissolved in EtOH (45 mL). Diphenyl ethylamine (1.3 g, 6.5 mmol) was added to the solution and refluxed at 80 °C for 18 h. After cooling the reaction mixture to r.t., and then on ice, the resulting precipitate was collected by suction filtration and dried *in vacuo* to give bromide **138** as a light brown solid (2.4 g, 97%). ^{1}H NMR (400 MHz, $CDCl_3$) δ_H 8.56 (dd, *J* = 7.4, 0.8, 1H, H_f) 8.52 (dd, *J* = 8.4, 0.8, 1H, H_h), 8.32 (d, *J* = 7.8, 1H, H_i), 7.99 (d, *J* = 7.8, 1H, H_j), 7.79 (dd, *J* = 8.4, 7.4, 1H, H_g), 7.38-7.32 (m, 4H, H_c), 7.28-7.20 (m, 4H, H_b), 7.17-7.12 (m, 2H, H_c), 4.88-4.78 (m, 3H, H_d and H_e). ^{13}C NMR (101 MHz, $CDCl_3$) δ_C 163.6, 163.6, 141.6, 133.2, 132.0, 131.2, 131.0, 130.5, 128.9, 128.5, 128.4, 128.0 126.7, 122.9, 122.0, 48.7, 44.6. IR: (ν_{max}/cm^{-1}) 3120, 1704, 1650, 1570, 1320, 1009, 960, 740. M.p. (°C) 136-140. LRMS (ES$^+$) 456. UV: λ_{max}(MeCN)/nm (ε / mol^{-1}cm^{-1}dm^3) 341 (11395).

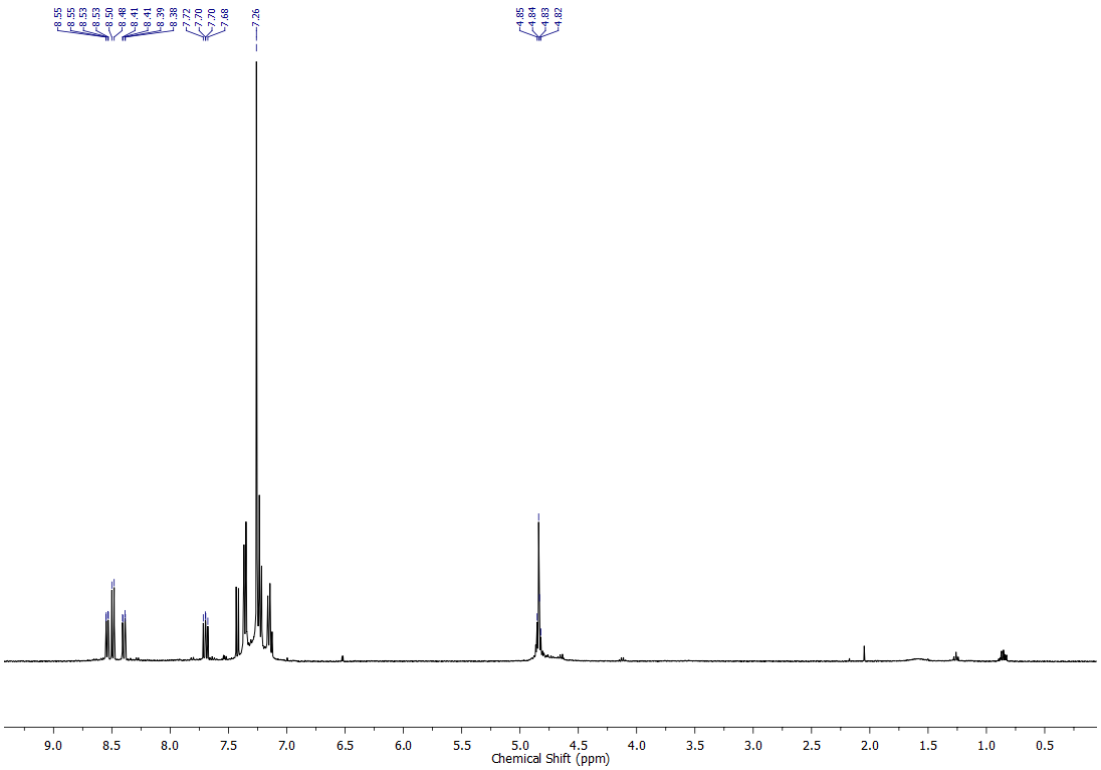
8.55
8.55
8.53
8.53
8.50
8.48
8.41
8.41
8.39
8.38
7.72
7.70
7.70
7.68
7.26
4.85
4.84
4.83
4.82
9.0
8.5
8.0
7.5
7.0
6.5
6.0
5.5
5.0
4.5
4.0
3.5
3.0
2.5
2.0
1.5
1.0
0.5
Chemical Shift (ppm)

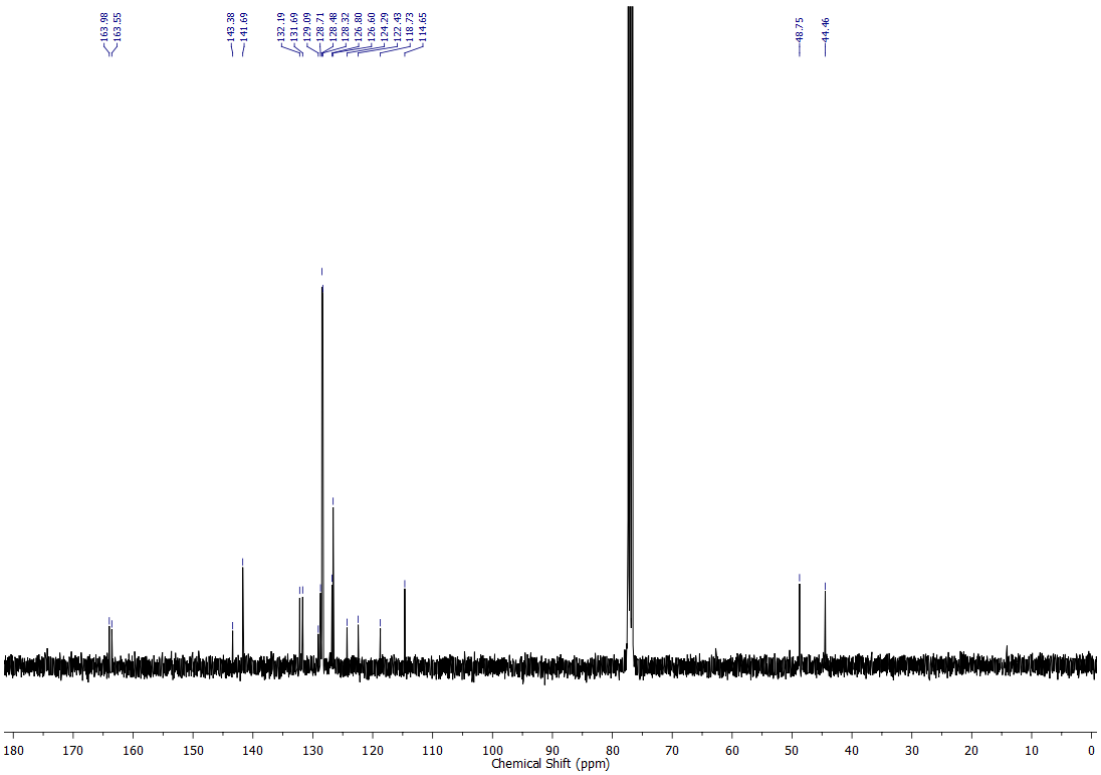
163.98
163.55
143.38
141.69
132.19
131.69
130.09
129.71
128.48
128.32
126.80
126.60
124.29
122.43
118.73
114.65
48.75
44.46
180
170
160
150
140
130
120
110
100
90
80
70
60
50
40
30
20
10
0
Chemical Shift (ppm)

*6-azido-2-(2,2-diphenylethyl)-1H-benzo[de]isoquinoline-1,3(2H)-dione (**139**)*

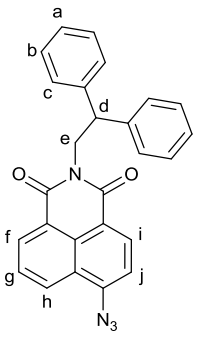

Bromide **138** (0.82 g, 1.8 mmol) was stirred with NaN_3 (0.23 g, 3.6 mmol) in NMP (20 mL) at r.t. for 24 h. After reducing the volume to ~5 mL *in vacuo*, the reaction was diluted with EtOAc (30 mL) and washed with brine (3 x 30 mL). The organic layer was dried with $MgSO_4$, filtered and concentrated *in vacuo*. The crude product was purified by flash column chromatography (8:2 Petrol/EtOAc) to yield azide **139** as a brown solid (0.45 g, 59%). ^{1}H NMR (400 MHz, $CDCl_3$) δ_H 8.54 (dd, *J* = 7.3, 0.9, 1H, H_f), 8.49 (d, *J* = 8.0, 1H, H_i), 8.39 (dd, *J* = 8.4, 0.9, 1H, H_h), 7.69 (dd, *J* = 8.2, 7.5, 1H, H_g), 7.42 (d, *J* = 8.0, 1H, H_j), 7.38-7.33 (m, 4H, H_c), 7.27-7.20 (m, 4H, H_b), 7.17-7.11 (m, 2H, H_a), 4.87-4.78 (m, 3H, H_d and H_e). ^{13}C NMR (101 MHz, $CDCl_3$) δ_C ^{13}C NMR (101 MHz, $CDCl_3$) δ 164.9, 164.4, 158.9, 158.7, 155.6, 151.4, 142.3, 137.8, 130.6, 129.1, 128.7, 128.3, 126.5, 123.5, 122.3, 122.3, 122.2, 121.2, 120.1, 115.0, 73.1, 70.9, 66.7, 49.0, 44.2, 42.6, 35.0, 31.5, 24.8. IR: (ν_{max}/cm^{-1}) 3140, 2923, 2110, 1650, 1560, 1290, 1233, 1046. M.p. (°C) 162-165. HRMS (EI) calcd for $C_{26}H_{18}N_4O_2$ $[M + Na]^+$ 491.1133, found 491.1121. UV: λ_{max}(MeCN)/nm (ε / mol^{-1}cm^{-1}dm^3) 364 (3937).

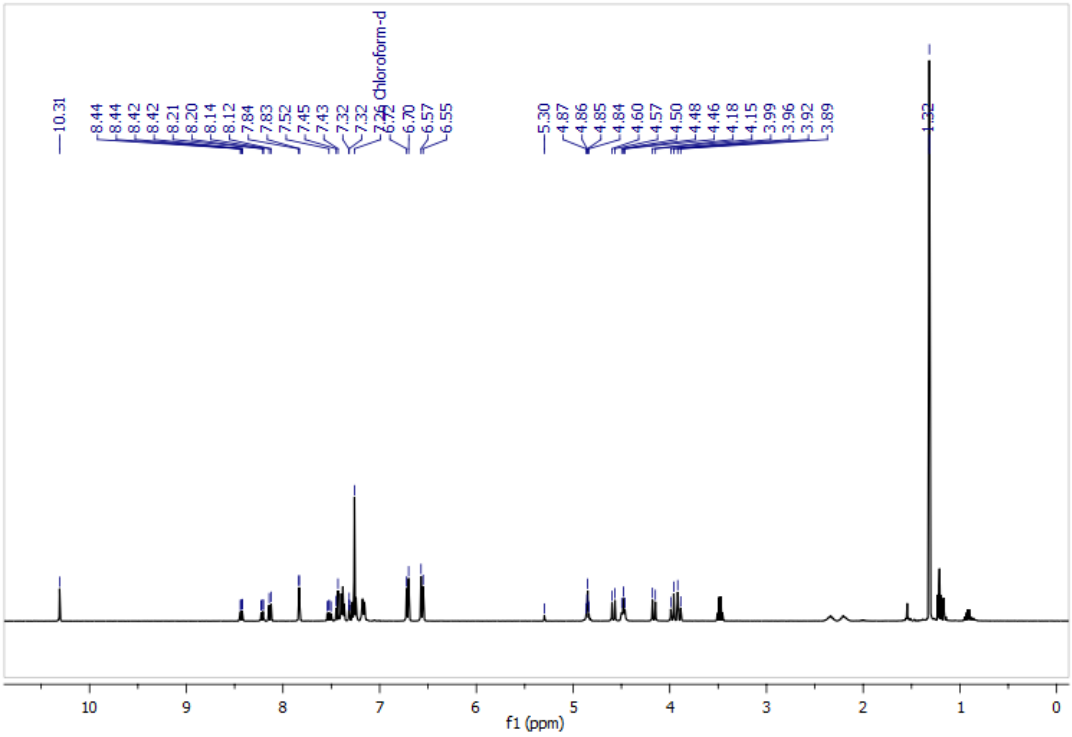
10.31
8.44
8.44
8.42
8.42
8.21
8.20
8.14
8.12
7.84
7.83
7.52
7.45
7.43
7.32
7.32
7.26 Chloroform-d
6.72
6.70
6.57
6.55
5.30
4.87
4.86
4.85
4.84
4.60
4.57
4.50
4.48
4.46
4.18
4.15
3.99
3.96
3.92
3.89
1.32
f1 (ppm)

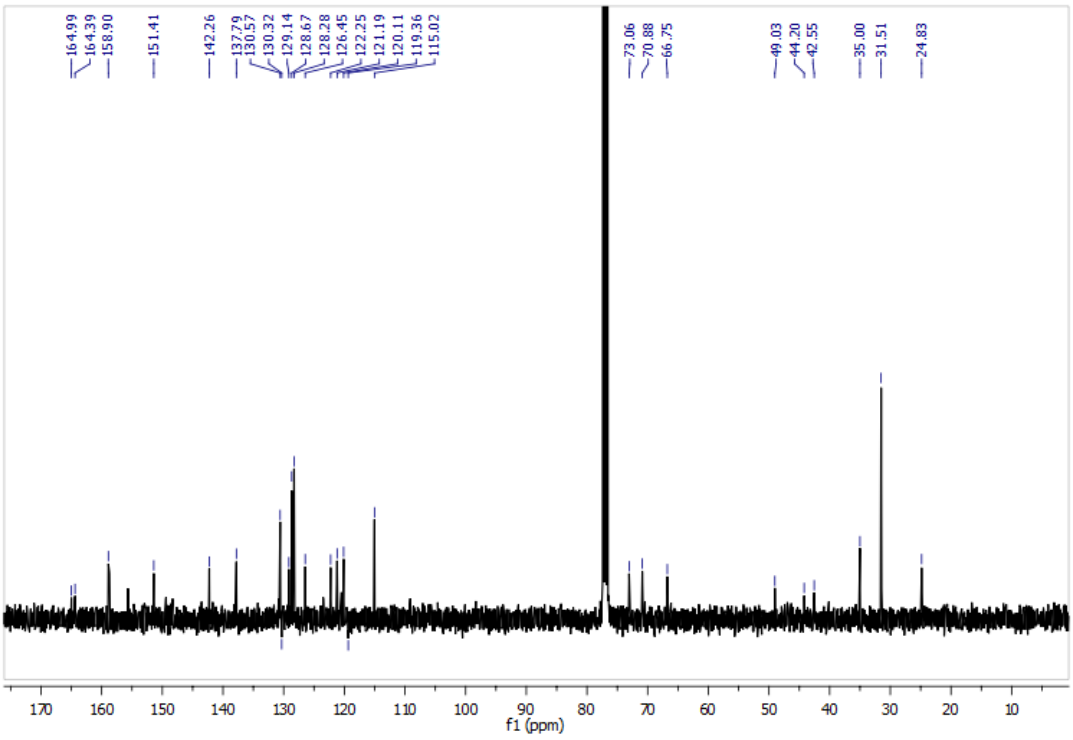
164.99
164.39
158.90
151.41
142.26
137.79
130.57
130.32
129.14
128.67
128.28
126.45
122.25
121.19
120.11
119.36
115.02
73.06
70.88
66.75
49.03
44.20
42.55
35.00
31.51
24.83
f1 (ppm)

*Rotaxane **140***

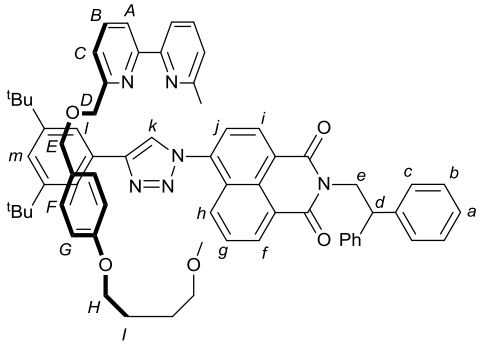

General procedure C was employed with macrocyle **136** (0.20 g, 0.41 mmol) acetylene **123** (0.09 g, 0.41 mmol), azide **139** (0.19 g, 0.41 mmol), $[Cu(MeCN)_4]PF_6$ (0.15 g, 0.40 mmol), and DIPEA (72 µL, 0.41 mmol) in EtOH (20 mL). Purification as noted gave rotaxane **150** as a light brown foam (0.41 g, 88%). ^{1}H NMR (400 MHz, $CDCl_3$) δ_H 10.30 (s, 1H, H_k), 8.43 (dd, *J* = 7.3, 1.0, 1H, H_f), 8.21 (dd, *J* = 8.5, 1.0, 1H, H_h), 8.13 (d, *J* = 7.9, 1H, H_i), 7.84 (d, *J* = 1.8, 2H, H_l), 7.52 (dd, *J* = 8.5, 7.3, 1H, H_g), 7.46-7.36 (m, 7H, H_h, H_B and H_c), 7.31 (t, *J* = 1.8,1H, H_m), 7.29-7.23 (m, 6H, two of H_A/H_C and H_b), 7.20-7.14 (m, 4H, two of H_A/H_C and H_a), 6.71 (d, *J* = 8.5, 4H, H_F), 6.56 (d, *J* = 8.5, 4H, H_G), 4.88-4.82 (m, 3H, H_d and H_e), 4.57 (d, *J* = 12.1, 2H, two of H_E), 4.47 (ap. t, *J* = 6.6, 4H, H_H), 4.16 (d, *J* = 12.1, 2H, two of H_E), 3.97 (d, *J* = 12.3, 2H, two of H_D), 3.90 (d, *J* = 12.3, 2H, two of H_D), 2.40-2.30 (m, 2H, two of H_l), 2.25-2.13 (m, 2H, two of H_l), 1.32 (s, 18H, 2 x ^{t}Bu). ^{13}C NMR (101 MHz, $CDCl_3$) δ_C ^{13}C NMR (101 MHz, $CDCl_3$) δ 164.9, 164.4, 158.9, 158.7, 155.6, 151.4, 142.3, 137.8, 130.6, 129.1, 128.7, 128.3, 126.5, 122.2, 121.2, 120.1, 115.0, 49.0, 44.2, 42.5, 35.0, 31.5, 24.8. IR: (ν_{max}/cm^{-1}) 2965, 2902, 2840, 2347, 1713, 1679, 1598, 1253, 1079, 990. M.p. (°C) 45-50. HRMS (EI) calcd for $C_{72}H_{70}N_6O_6$ [M + H]$^+$ 1115.5430, found 1115.5429. UV: λ_{max}(MeCN)/nm (ε / mol^{-1}cm^{-1}dm^3) 345 (9874).

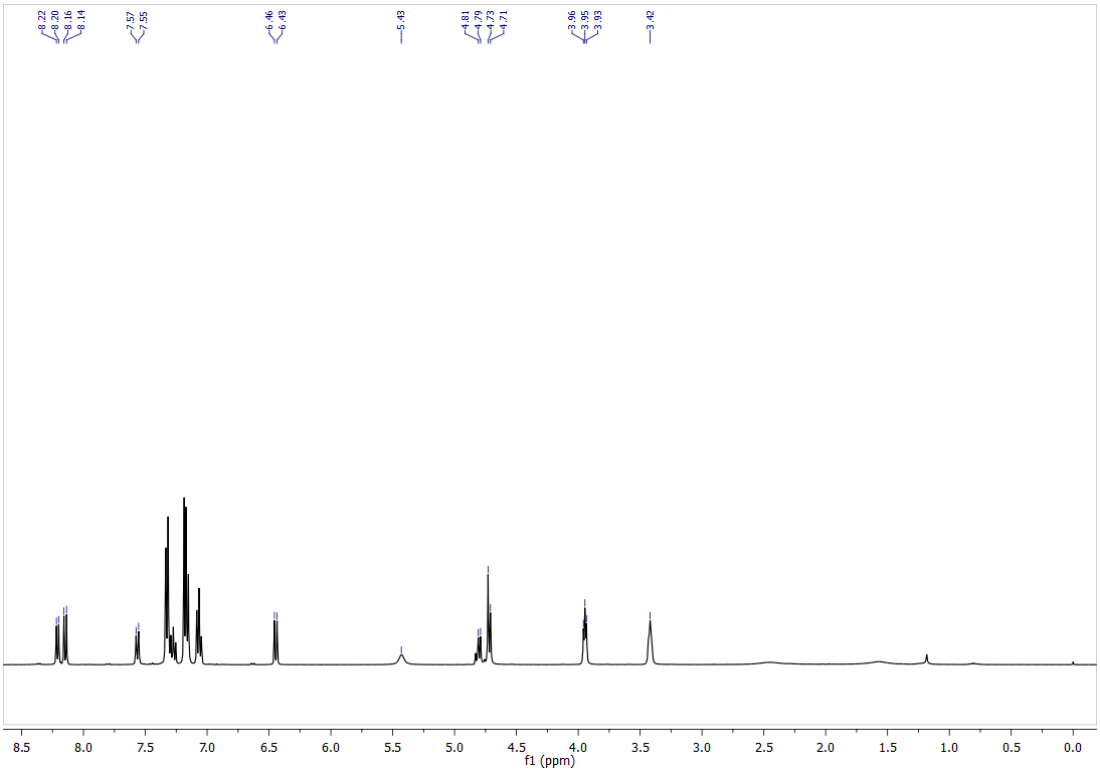
8.22
8.20
8.16
8.14
7.57
7.55
6.46
6.43
5.43
4.81
4.79
4.73
4.71
3.96
3.95
3.93
3.42
f1 (ppm)

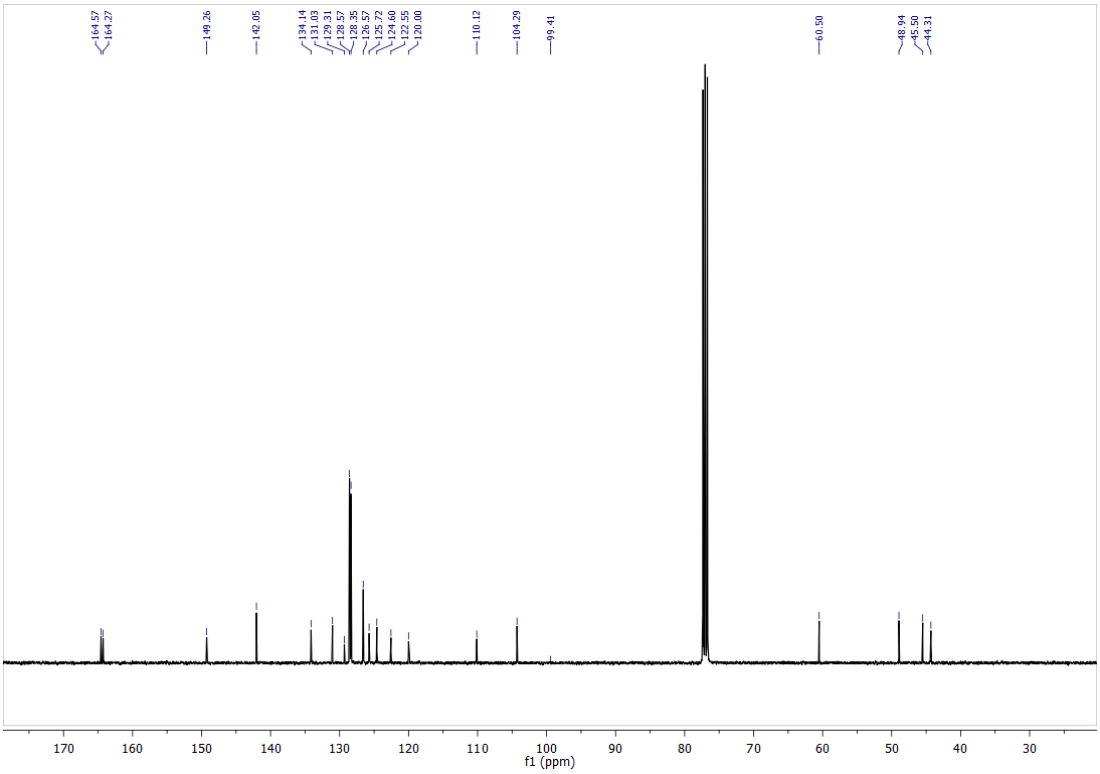
164.57
164.27
149.26
142.05
134.14
131.03
129.31
128.57
128.35
126.57
125.72
124.60
122.55
120.00
110.12
104.29
99.41
60.50
48.94
45.50
44.31
f1 (ppm)

2-(2,2-diphenylethyl)-6-((2-hydroxyethyl)amino)-1H-benzo[de]isoquinoline-1,3(2H)-dione ***(144)***

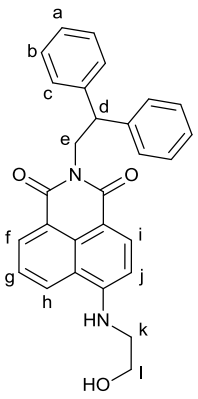

To a solution of bromide **138** (0.3 g, 0.64 mmol) in DMSO (10 mL) was added Cu_2O (1.8 mg, 0.013 mmol) , K_2CO_3 (18.0 mg, 0.13 mmol) and ethanolamine (0.39 mL, 6.4 mmol), and was heated at 90oc overnight. The reaction mixture was diluted with brine (40 mL), and the aqueous portion extracted with EtOAc (2 x 40 mL). The organic phase was dried with $MgSO_4$, filtered and concentrated *in vacuo*. The resulting oil was purified by flash column chromatography (CH_2Cl_2 to 7:3 CH_2Cl_2/EtOAc) to give alcohol **144** as an orange foam (0.27 g, 96%). ^{1}H NMR (400 MHz, $CDCl_3$) δ_H 8.21 (d, *J* = 7.2, 1H, H_f), 8.14 (d, *J* = 8.4, 1H, H_i), 7.56 (d, *J* = 8.4, 1H, H_h), 7.35-7.30 (m, 4H, H_c), 7.27 (ap. t, *J* = 7.8, 1H, H_g), 7.20-7.14 (m, 4H, H_b), 7.09-7.03 (m, 2H, H_a), 6.44 (d, *J* = 8.4, 1H, H_j), 5.43 (bs, 1H, -*NH*-), 4.83-4.78 (m, 1H, H_d), 4.75-4.69 (m, 2H, H_e), 3.94 (t, *J* = 4.9, 2H, H_l), 3.41 (t (broad), *J* = 4.4, 2H, H_k).^{13}C NMR (101 MHz, $CDCl_3$) δ_C 164.7, 164.4, 149.4, 142.2, 134.3, 131.2, 129.5, 128.7, 128.5, 126.7, 125.8, 124.7, 122.7, 120.1, 110.2, 104.4, 60.6, 49.1, 45.6, 44.5. IR: (ν_{max}/cm^{-1}) 3505, 2950, 2350, 1699, 1635, 1589, 1380, 1340, 1180. M.p. (°C) 43-45. LRMS (ES$^+$) 437 [M + H$^+$]. UV: λ_{max}(MeCN)/nm (ε / mol^{-1}cm^{-1}dm^3) 432 (2347).

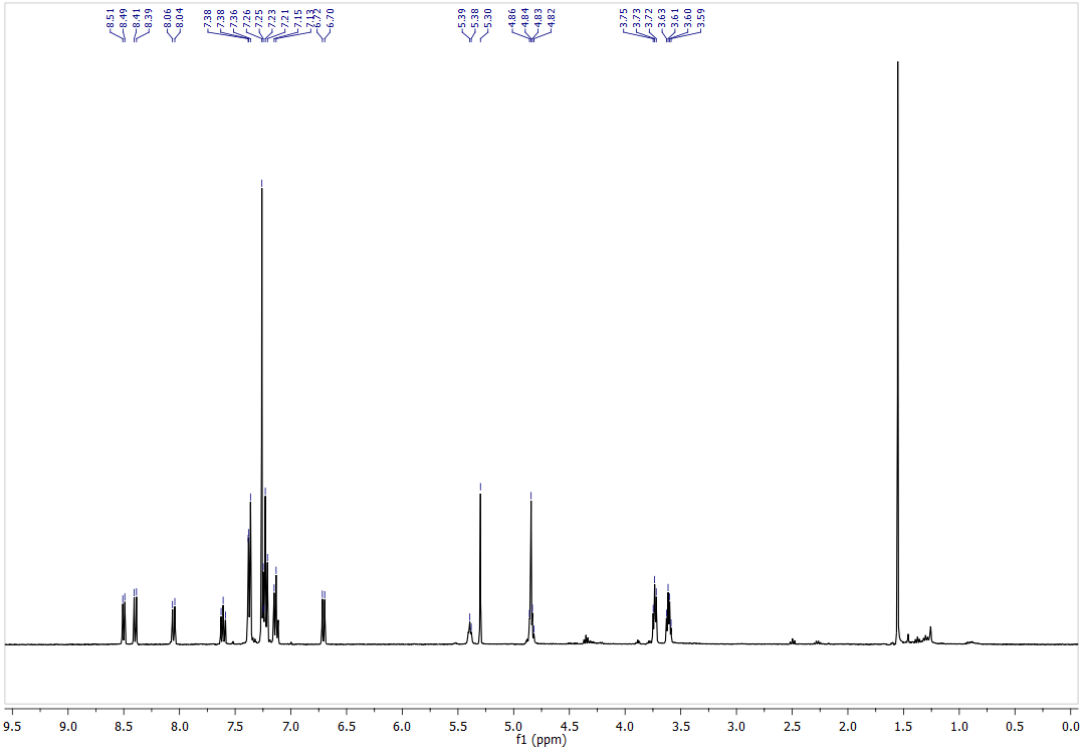
8.51
8.49
8.41
8.39
8.06
8.04
7.38
7.38
7.36
7.26
7.25
7.23
7.21
7.15
7.13
6.72
6.70
5.39
5.38
5.30
4.86
4.84
4.83
4.82
3.75
3.73
3.72
3.63
3.61
3.60
3.59
9.5 9.0 8.5 8.0 7.5 7.0 6.5 6.0 5.5 5.0 4.5 4.0 3.5 3.0 2.5 2.0 1.5 1.0 0.5 0.0
f1 (ppm)

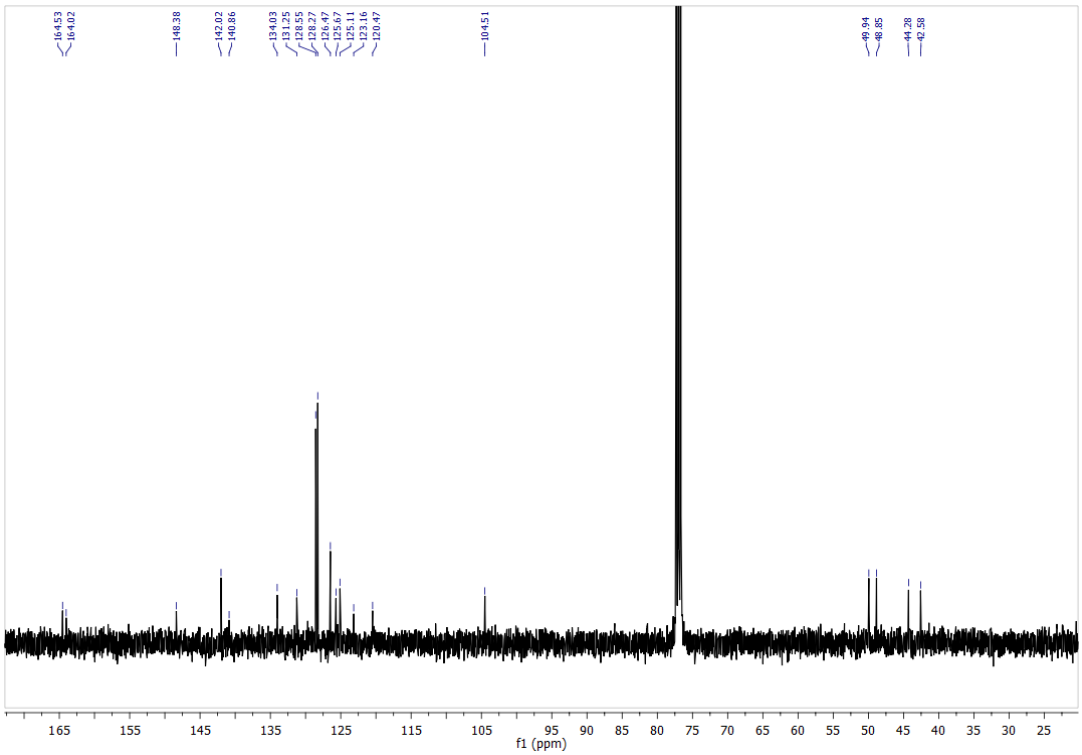
164.53
164.02
148.38
142.02
140.86
134.03
131.25
128.55
128.27
126.47
125.67
125.11
123.16
120.47
104.51
49.94
48.85
44.28
42.58
165 155 145 135 125 115 105 95 90 85 80 75 70 65 60 55 50 45 40 35 30 25
f1 (ppm)

*6-((2-azidoethyl)amino)-2-(2,2-diphenylethyl)-1H-benzo[de]isoquinoline-1,3(2H)-dione (**141**)*

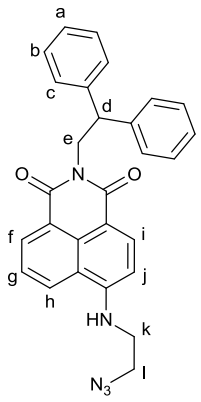

Alcohol **144** (0.13 g, 0.29 mmol) and triphenylphosphine (0.23 g, 0.87 mmol) were combined in a sealed flask which was purged with N_2. Anhydrous THF (15 mL) was added, and the stirring solution was cooled to 0 °C. DEAD (0.14 mL, 0.87 mmol) was added to the reaction, followed by diphenyl phosphoryl azide (0.20 mL, 0.87 mmol), and stirred for 15 mins. The reaction was then stirred at rt for 2 h, and then concentrated *in vacuo*. The resulting oil was purified by flash column chromatography (1:1 Petrol/ CH_2Cl_2 to CH_2Cl_2 to 7:3 CH_2Cl_2/EtOAc) to give azide **141** as an orange solid (0.085 g, 61%). ^{1}H NMR (400 MHz, $CDCl_3$) δ_H 8.50 (d, *J* = 7.2, 1H, H_f), 8.40 (d, *J* = 8.3, 1H, H_i), 8.05 (d, *J* = 8.4, 1H, H_h), 7.61 (ap. t, *J* = 7.4, 1H, H_g), 7.42-7.34 (m, 4H, H_c), 7.28-7.20 (m, 4H, H_b), 7.16-7.11 (m, 2H, H_a), 6.70 (d, *J* = 8.4, 1H, H_j), 5.39 (br s, 1H, -*NH*-), 4.89-4.80 (m, 3H, H_d and H_e), 3.73 (t, *J* = 5.1, 2H, H_l), 3.65-3.57 (m, 2H, H_k). ^{13}C NMR (101 MHz, $CDCl_3$) δ_C 164.5, 164.0, 148.4, 142.0, 140.8, 134.0, 131.3, 128.5, 128.3, 126.5, 125.7, 125.1, 123.2, 120.5, 104.5, 49.9, 48.8, 44.3, 42.6. IR: (ν_{max}/cm^{-1}) 3350, 2954, 2101, 1695, 1658, 1580, 1347, 1235, 1120, 1052, 952. M.p. (°C) 90-95. LRMS (ES$^+$) 462 [M + H$^+$], 484 [M + Na]. UV: λ_{max}(MeCN)/nm (ε / mol^{-1}cm^{-1}dm^3) 410 (3856).

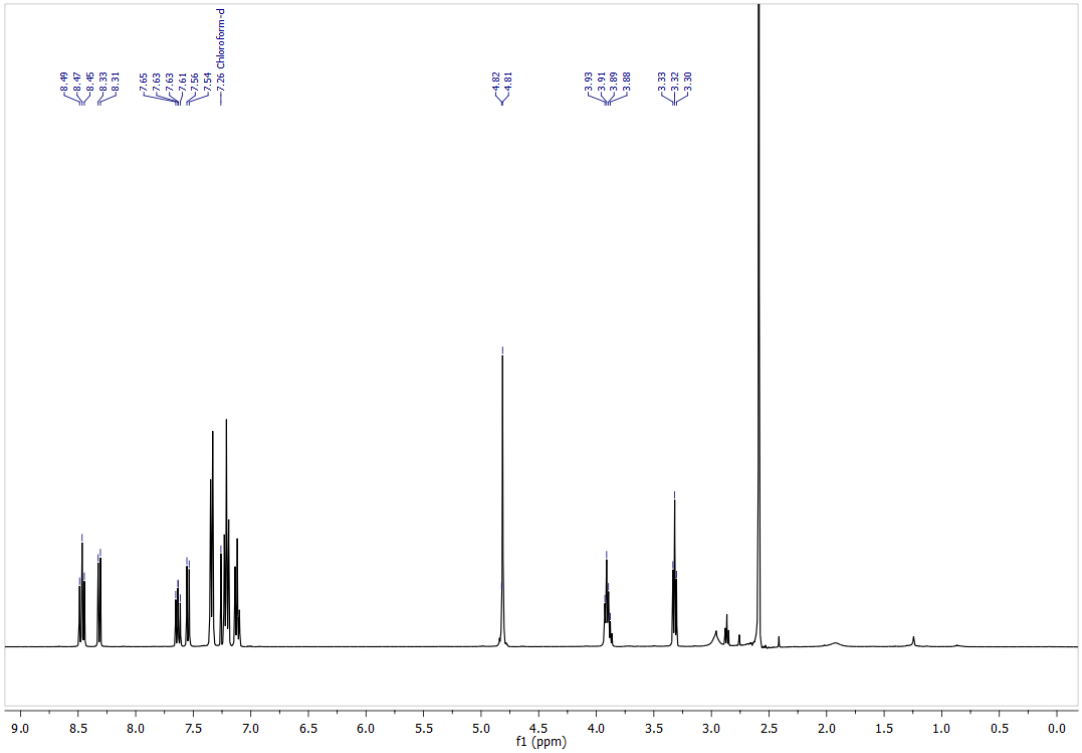
8.49
8.47
8.45
8.33
8.31
7.65
7.63
7.63
7.61
7.56
7.54
7.26 Chloroform-d
4.82
4.81
3.93
3.91
3.89
3.88
3.33
3.32
3.30
9.0
8.5
8.0
7.5
7.0
6.5
6.0
5.5
5.0
4.5
4.0
3.5
3.0
2.5
2.0
1.5
1.0
0.5
0.0
f1 (ppm)

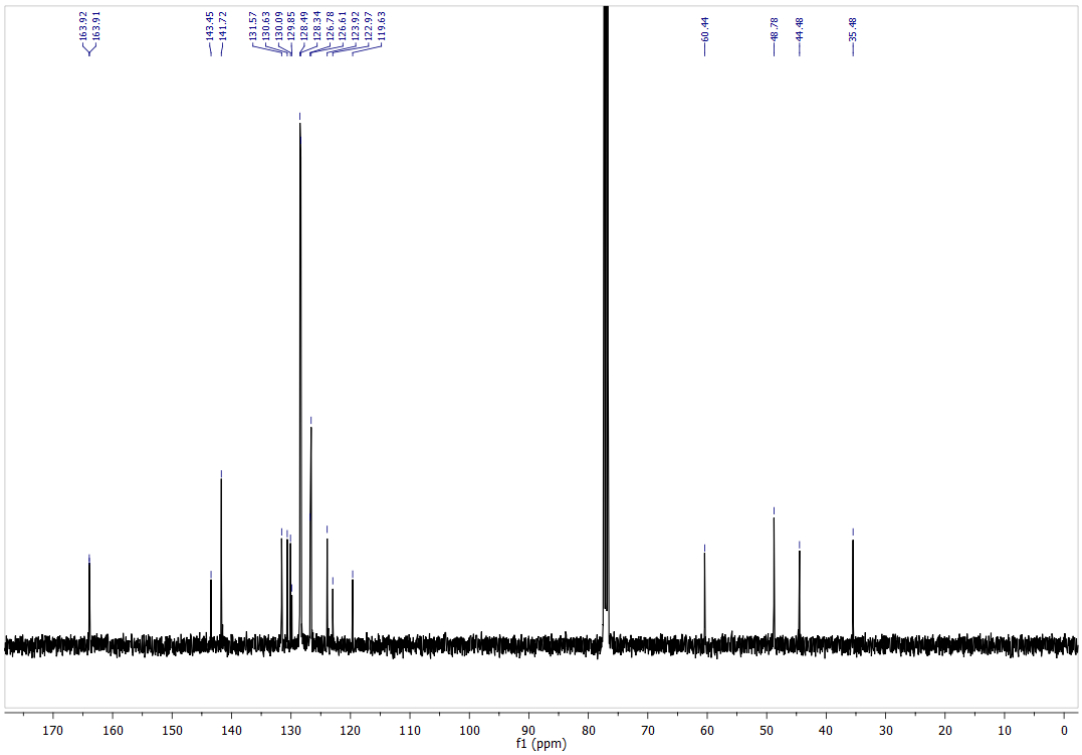
163.92
163.91
143.45
141.72
131.57
130.63
130.09
129.85
128.49
128.34
126.78
126.61
123.92
122.97
119.63
60.44
48.78
44.48
35.48
170
160
150
140
130
120
110
100
90
80
70
60
50
40
30
20
10
0
f1 (ppm)

*2-(2,2-diphenylethyl)-6-((2-hydroxyethyl)thio)-1H-benzo[de]isoquinoline-1,3(2H)-dione (**145**)*

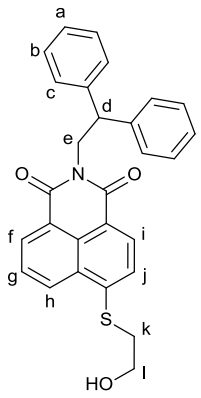

To a solution of bromide **138** (0.3 g, 0.64 mmol) in DMSO (10 mL) was added Cu_2O (1.8 mg, 0.013 mmol) , K_2CO_3 (18.0 mg, 0.13 mmol) and 2-thioethanol (0.46 mL, 6.4 mmol), and was heated at 90oc overnight. The reaction mixture was diluted with brine (40 mL), and the aqueous portion extracted with EtOAc (2 x 40 mL). The organic phase was dried with $MgSO_4$, filtered and concentrated *in vacuo*. The resulting oil was purified by flash column chromatography (CH_2Cl_2 to 8:2 CH_2Cl_2/EtOAc) to give alcohol **145** as an yellow foam (0.24 g, 82%). ^{1}H NMR (400 MHz, $CDCl_3$) δ_H 8.50-8.44 (m, 2H, H_f and H_h), 8.31 (d, *J* = 7.8, 1H, H_i), 7.63 (dd, *J* = 8.3, 7.5, 1H, H_g), 7.54 (d, *J* = 7.9, 1H, H_j), 7.37-7.31 (m, 4H, H_c), 7.24-7.18 (m, 4H, H_b) 7.15-7.09 (m, 2H, H_a), 4.83-4.79 (m, 3H, H_d and H_e), 3.94-3.86 (m, 2H, H_l), 3.31 (t, *J* = 6.2, 2H, H_k). ^{13}C NMR (101 MHz, $CDCl_3$) δ_C 163.9, 163.9, 143.5, 141.7, 131.6, 130.6, 130.01, 129.8, 128.5, 128.4, 128.3, 128.2, 126.8, 126.6, 123.9, 122.9, 119.6, 60.4, 48.8, 44.5, 35.5. IR: (ν_{max}/cm^{-1}) 3505, 2940, 2346, 1695, 1640, 1559, 1352, 1245, 973. . M.p. (°C) 39-41. LRMS (ES$^+$) 454 [M + H$^+$], 476 [M + Na]. UV: λ_{max}(MeCN)/nm (ε / mol^{-1}cm^{-1}dm^3) 389 (5331).

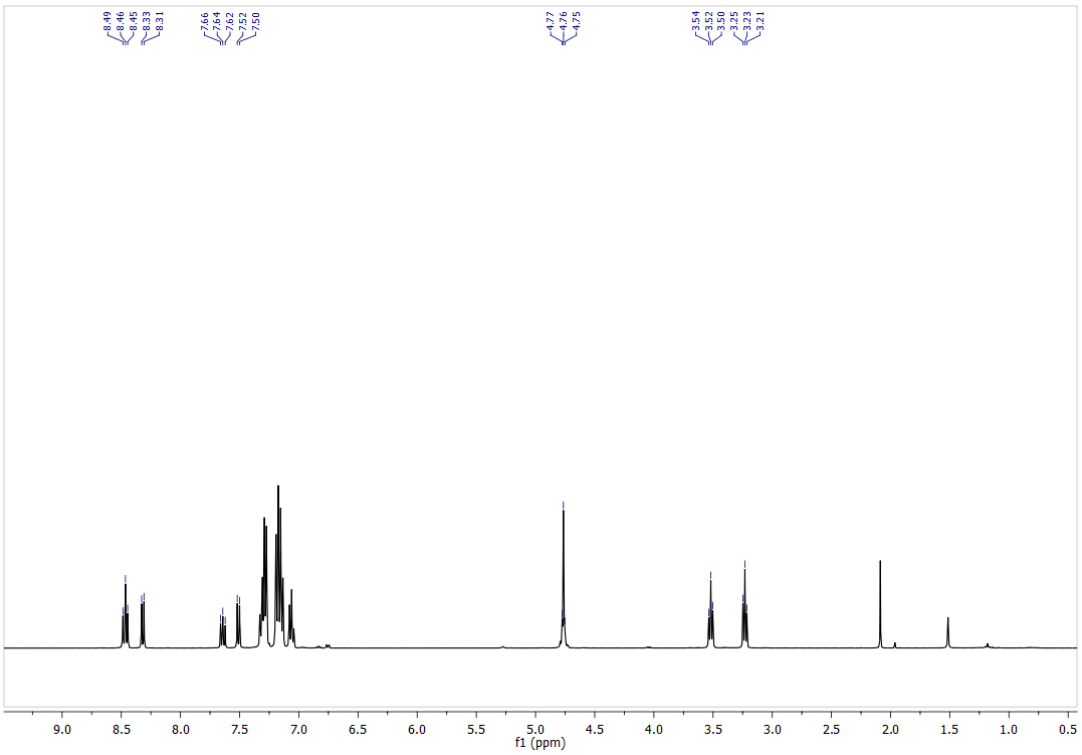
8.49
8.46
8.45
8.33
8.31
7.66
7.64
7.62
7.52
7.50
4.77
4.76
4.75
3.54
3.52
3.50
3.25
3.23
3.21
9.0
8.5
8.0
7.5
7.0
6.5
6.0
5.5
5.0
4.5
4.0
3.5
3.0
2.5
2.0
1.5
1.0
0.5
f1 (ppm)

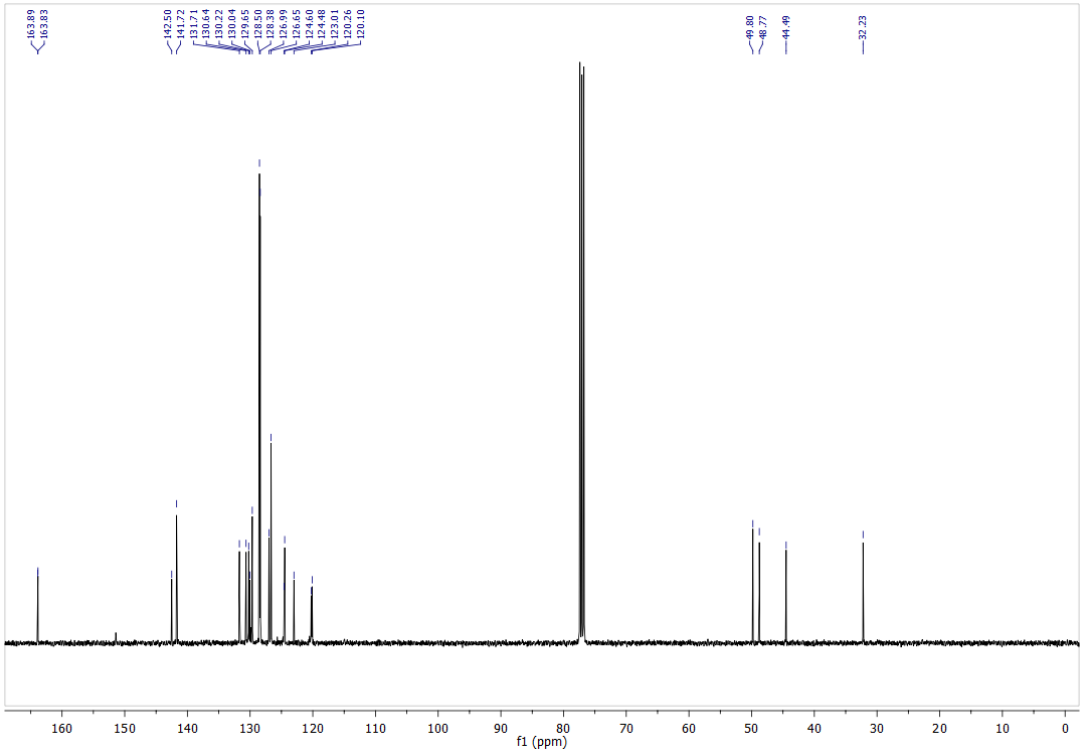
163.89
163.83
142.50
141.72
131.71
130.64
130.22
130.04
129.65
128.50
128.38
126.99
126.65
124.60
124.48
123.01
120.26
120.10
49.80
48.77
44.49
32.23
160
150
140
130
120
110
100
90
80
70
60
50
40
30
20
10
0
f1 (ppm)

*6-((2-azidoethyl)thio)-2-(2,2-diphenylethyl)-1H-benzo[de]isoquinoline-1,3(2H)-dione (**143**)*

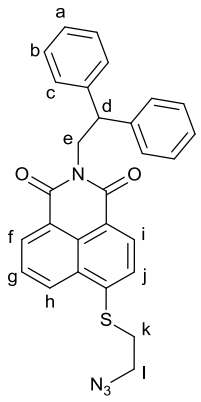

Alcohol **145** (0.13 g, 0.28 mmol) and triphenylphosphine (0.22 g, 0.83 mmol) were combined in a sealed flask which was purged with N_2. Anhydrous THF (12 mL) was added, and the stirring solution was cooled to 0 °C. DEAD (0.13 mL, 0.83 mmol) was added to the reaction, followed by diphenyl phosphoryl azide (0.19 mL, 0.83 mmol), and stirred for 15 mins. The reaction was then stirred at r.t. for 2 h, and then concentrated *in vacuo*. The resulting oil was purified by flash column chromatography (1:1 Petrol/ CH_2Cl_2 to CH_2Cl_2 to 8:2 CH2CL2/EtOAc) to give azide **143** as an orange foam (0.095 g, 72%). ^{1}H NMR (400 MHz, $CDCl_3$) δ_H 8.57-8.49 (m, 2H, H_f and H_h), 8.39 (d, *J* = 7.8, 1H, H_i), 7.71 (dd, *J* = 7.5, 8.2, 1H, H_g), 7.57 (d, *J* = 7.8, 1H, H_j), 7.40-7.31 (m, 4H, H_c), 7.27-7.18 (m, 4H, H_b), 7.16-7.10 (m, 2H, H_a), 4.85-4.80 (m, 3H, H_d and H_e), 3.58 (t, *J* = 6.7, 2H, H_l), 3.30 (t, *J* = 6.7, 2H, H_k).^{13}C NMR (101 MHz, $CDCl_3$) δ_C 163.9, 163.9, 142.6, 141.8, 131.8, 130.7, 130.3, 130.1, 129.8, 129.7, 128.6, 128.5, 127.1, 126.7, 124.7, 124.5, 123.1, 120.4, 120.3, 120.2, 49.8, 48.8, 44.6, 32.3. IR: (ν_{max}/cm^{-1}) 3505, 2950, 2351, 2101, 1705, 1669, 1590, 1379, 1345, 1228. M.p. (°C) 45-48. HRMS (EI) calcd for $C_{28}H_{22}N_4O_2S$ [M +Na]$^+$ 501.1356, found 501.1358.UV: λ_{max}(MeCN)/nm (ε / mol^{-1}cm^{-1}dm^3) 381 (6093).

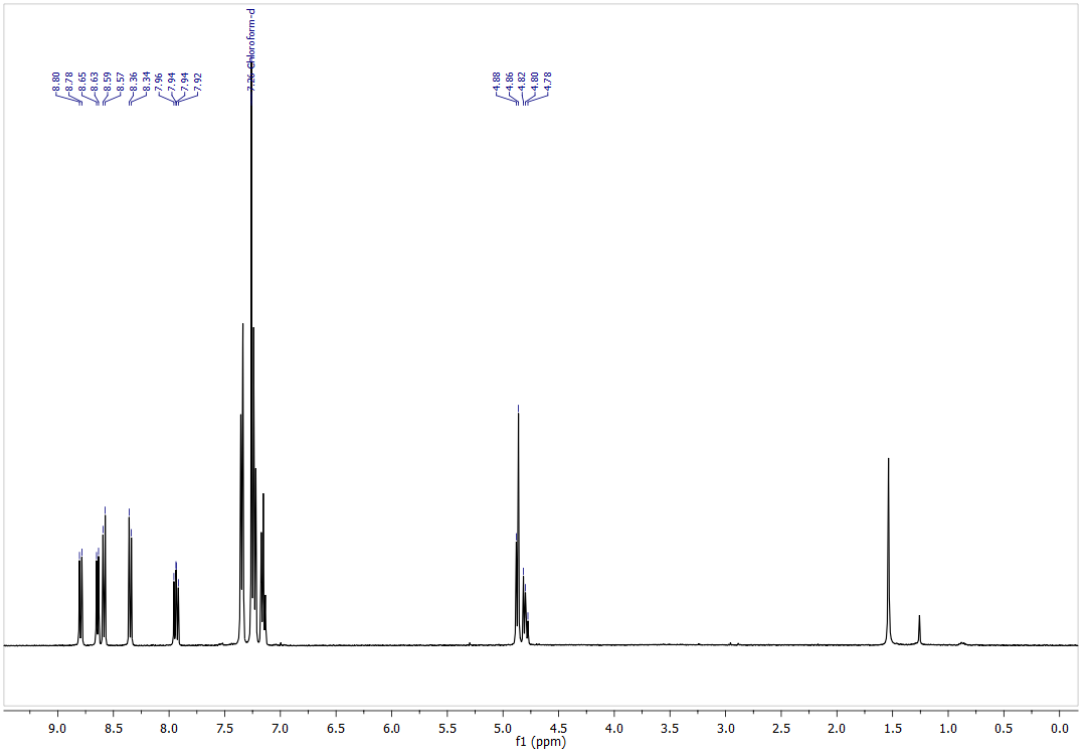
8.80
8.78
8.65
8.63
8.59
8.57
8.36
8.34
7.96
7.94
7.94
7.92
7.26 Chloroform-d
4.88
4.86
4.82
4.80
4.78
9.0 8.5 8.0 7.5 7.0 6.5 6.0 5.5 5.0 4.5 4.0 3.5 3.0 2.5 2.0 1.5 1.0 0.5 0.0
f1 (ppm)

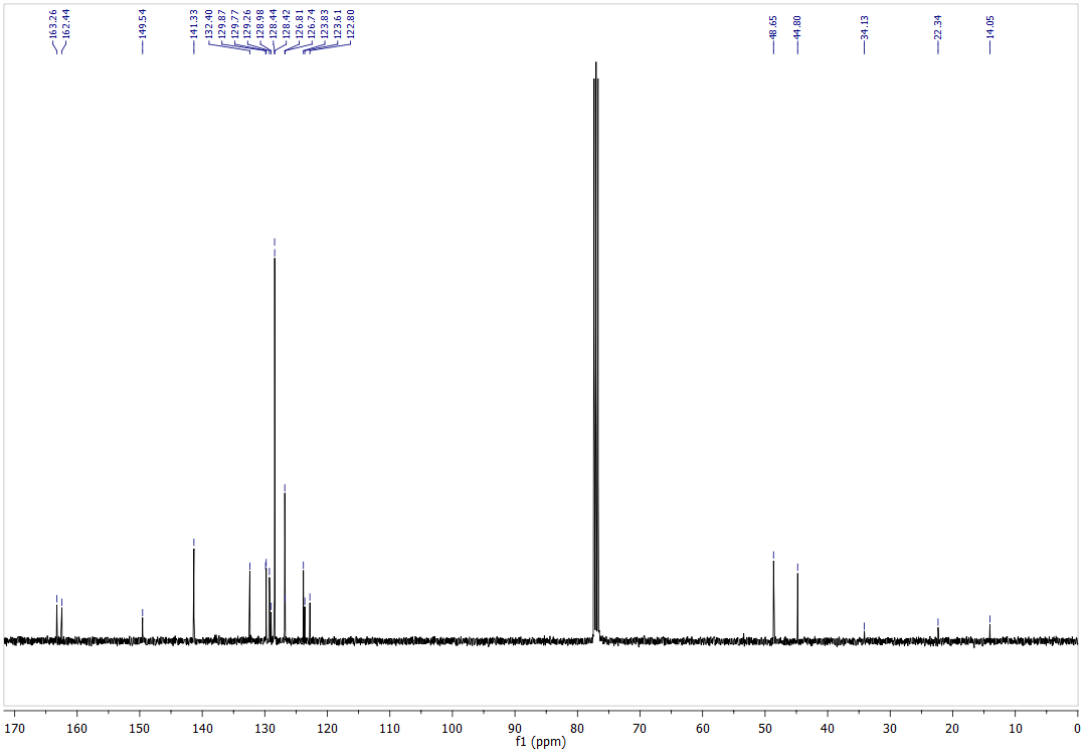
163.26
162.44
149.54
141.33
132.40
129.87
129.77
129.26
128.98
128.44
128.42
126.81
126.74
123.83
123.61
122.80
48.65
44.80
34.13
22.34
14.05
170 160 150 140 130 120 110 100 90 80 70 60 50 40 30 20 10 0
f1 (ppm)

*2-(2,2-diphenylethyl)-6-nitro-1H-benzo[de]isoquinoline-1,3(2H)-dione (**147**)*

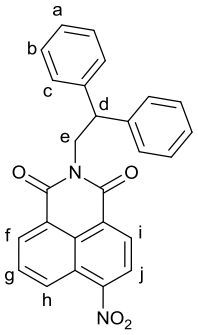

4-nitro-1,8-naphthalic anhydride (0.5 g, 2.1 mmol) was dissolved in EtOH (15 mL). Diphenyl ethylamine (0.49 g, 2.5 mmol) was added to the solution and refluxed at 80 °C for 18 h. After cooling the reaction mixture to r.t., the solvent was removed *in vacuo* and purified by flash column chromatography (1:1 Petrol/ CH_2Cl_2) to give nitro-compound **147** as a yellow foam (0.75 g, 86%). ^{1}H NMR (400 MHz, $CDCl_3$) δ_H 8.79 (dd, *J* = 8.7, 1.0, 1H, H_h), 8.64 (dd, *J* = 7.3, 1.0, 1H, H_f), 8.58 (d, *J* = 8.0, 1H, H_j), 8.34 (d, *J* = 8.0, 1H, H_i), 7.93 (dd, *J* = 8.7, 7.4, 1H, H_g), 7.37-7.32 (m, 4H, H_c), 7.27-7.21 (m, 4H, H_b), 7.18-7.13 (m, 2H, H_a), 4.89-4.85 (m, 2H, H_e), 4.82-4.71 (m, 1H, H_d). ^{13}C NMR (101 MHz, $CDCl_3$) δ_C 163.3, 162.4, 149.5, 141.3, 132.4, 129.9, 129.7, 129.3, 128.9, 128.4, 128.4, 126.8, 126.7, 123.8, 123.6, 122.8, 48.5, 44.8, 34.1, 22.3, 14.1. IR: (ν_{max}/cm^{-1}) 3405, 2905, 1692, 1620, 1577, 1520, 1375, 1313, 1226, 1181, 989. M.p. (°C) 40-43. LRMS (ES$^+$) 423 [M +H$^+$]. UV: λ_{max}(MeCN)/nm (ε / mol^{-1}cm^{-1}dm^3) 347 (10978).

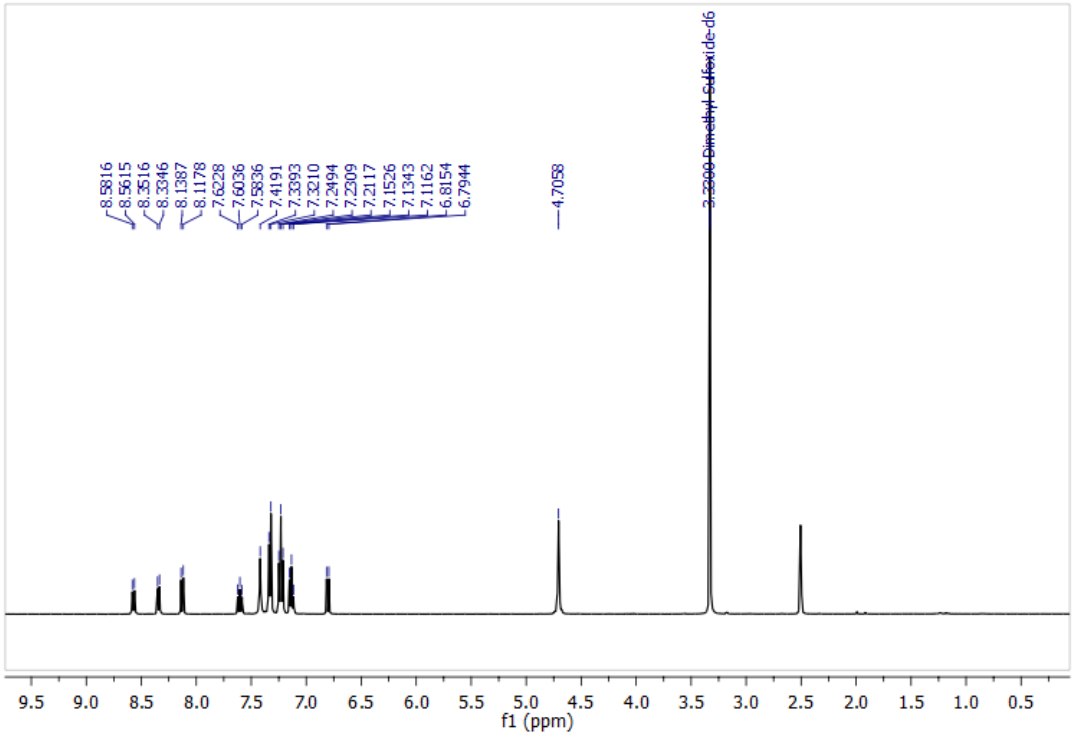
8.5816
8.5615
8.3516
8.3346
8.1387
8.1178
7.6228
7.6036
7.5836
7.4191
7.3393
7.3210
7.2494
7.2309
7.2117
7.1526
7.1343
7.1162
6.8154
6.7944
4.7058
2.7390 Dimethyl Sulfoxide-d6
9.5 9.0 8.5 8.0 7.5 7.0 6.5 6.0 5.5 5.0 4.5 4.0 3.5 3.0 2.5 2.0 1.5 1.0 0.5
f1 (ppm)

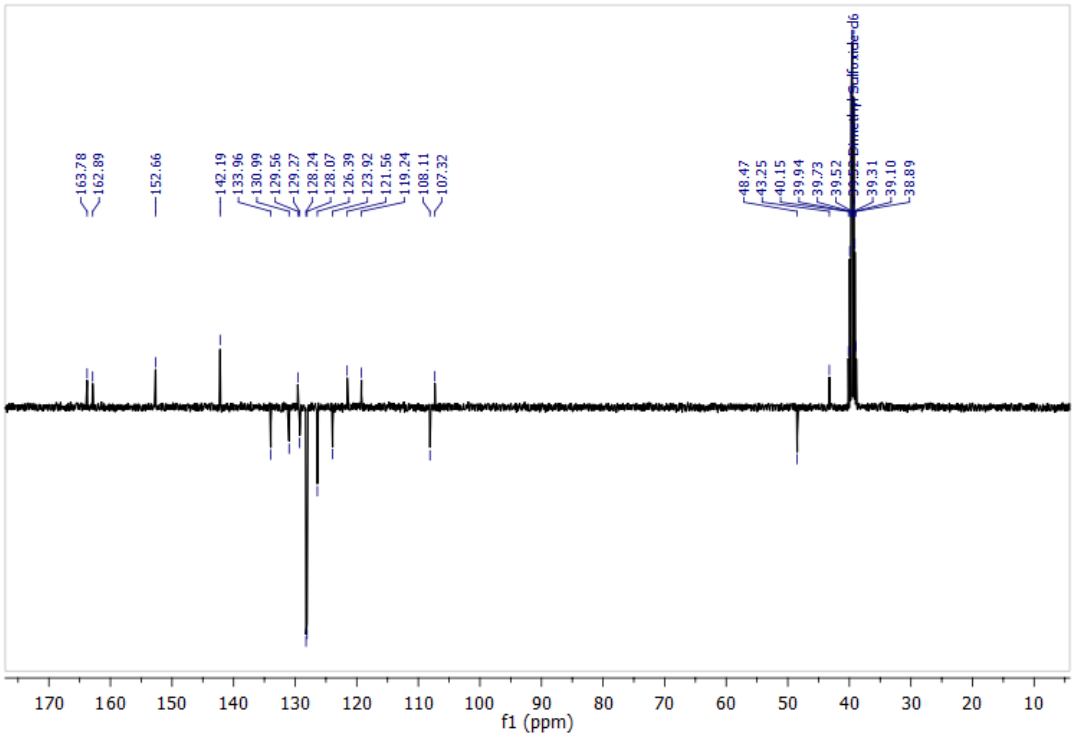
163.78
162.89
152.66
142.19
133.96
130.99
129.56
129.27
128.24
128.07
126.39
123.92
121.56
119.24
108.11
107.32
48.47
43.25
40.15
39.94
39.73
39.52
39.31
39.10
38.89
Dimethyl Sulfoxide-d6
170 160 150 140 130 120 110 100 90 80 70 60 50 40 30 20 10
f1 (ppm)

*2-(2,2-diphenylethyl)-6-amino-1H-benzo[de]isoquinoline-1,3(2H)-dione (**148**)*

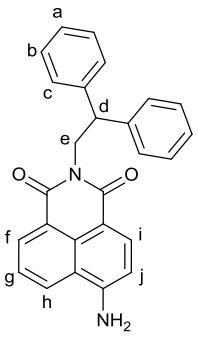

Nitro-compound **147** (0.36 g, 0.95 mmol) was hydrogenated in MeOH/EtOAc (1:1, 20 mL) at r.t. under a hydrogen atmosphere, using a Pd/C catalyst (5%wt, 0.20g, 0.095 mmol,). The reaction was monitored by TLC until all starting material had been consumed (~4 h). The reaction mixture was filtered through Celite, washed with MeOH/EtOAc (1:1), and the solvent evaporated *in vacuo* to yield aniline **148** as a yellow solid (0.36 g, 97%). ^{1}H NMR (400 MHz, DMSO-d_6) δ_H 8.57 (d, *J* = 8.0, 1H, H_h), 8.34 (d, *J* = 6.8, 1H, H_f), 8.12 (d, *J* = 8.4, 1H, H_i), 7.60 (dd, *J* = 7.7, 8.0, 1H, H_g), 7.42 (br s, 1H, -*NH_2*-), 7.35-7.30 (m, 4H, H_c), 7.26-7.20 (m, 4H, H_b), 7.16-7.11 (m, 2H, H_a), 7.80 (d, *J* = 8.4, 1H, H_j), 4.73-4.69 (m, 3H, H_d and H_e).^{13}C NMR (101 MHz, DMSO-d_6) δ_C 163.8, 162.9, 152.6, 142.2, 133.9, 130.9, 129.6, 129.3, 128.2, 128.0, 126.4, 123.9, 121.6, 119.2, 108.1, 107.3, 48.4, 43.3. IR: (ν_{max}/cm^{-1}) 3505, 3349, 3225, 2358, 1648, 1592, 1375, 1246, 1017. 982. M.p. (°C) 95-96. LRMS (ES$^+$) 393 [M +H$^+$]. UV: λ_{max}(MeCN)/nm (ε/ mol^{-1}cm^{-1}dm^3) 428 (3226).

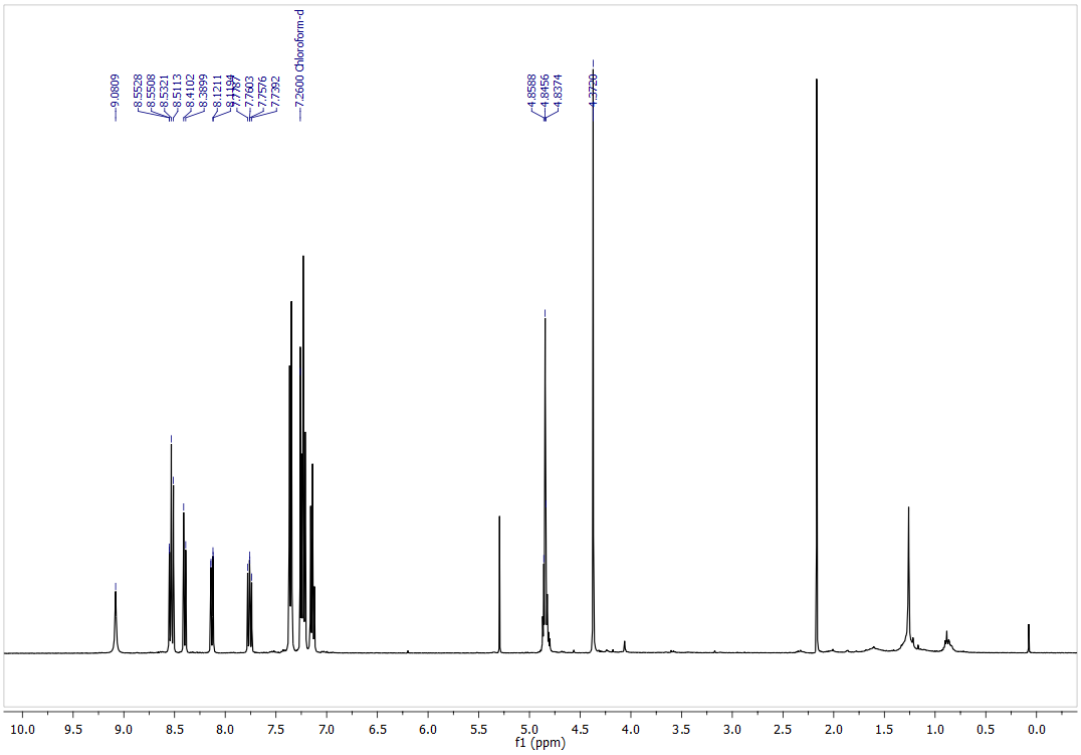
9.0809
8.5528
8.5508
8.5321
8.5113
8.4102
8.3899
8.1211
7.7603
7.7576
7.7392
7.2600 Chloroform-d
4.8588
4.8456
4.8374
4.3720
f1 (ppm)

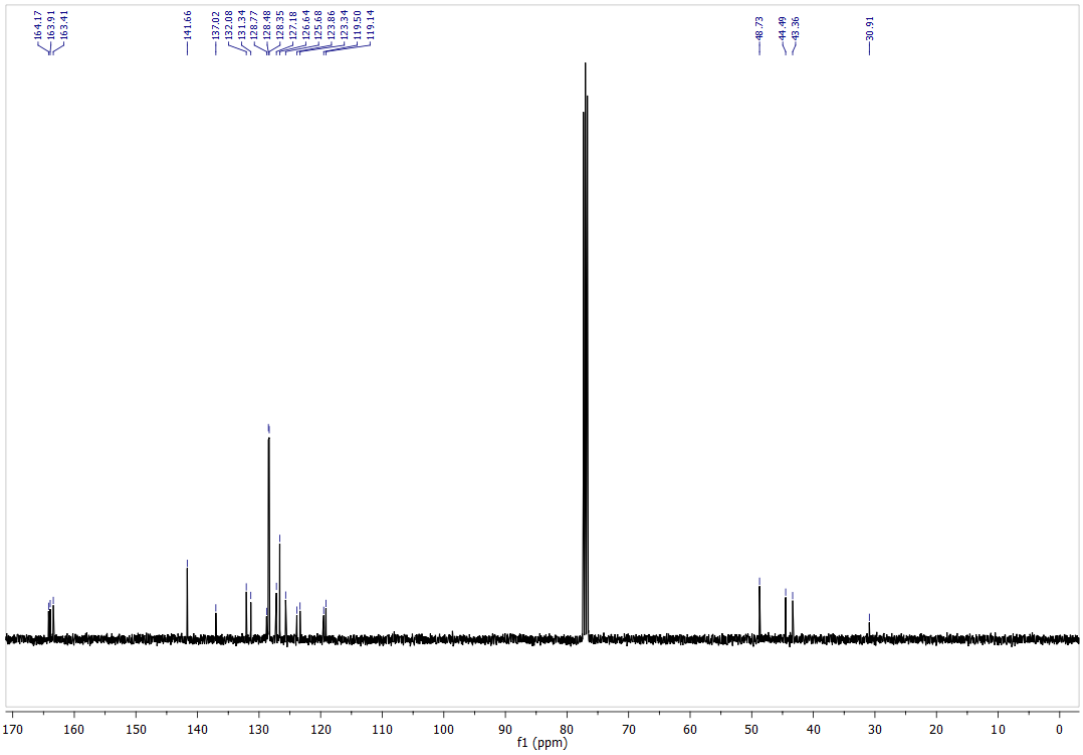
164.17
163.91
163.41
141.66
137.02
132.08
131.34
128.77
128.46
128.35
127.18
126.64
125.68
123.86
123.34
119.50
119.14
48.73
44.49
43.36
30.91
f1 (ppm)

*2-chloro-N-(2-(2,2-diphenylethyl)-1,3-dioxo-2,3-dihydro-1H-benzo[de]isoquinolin-6-yl)acetamide (**149**)*

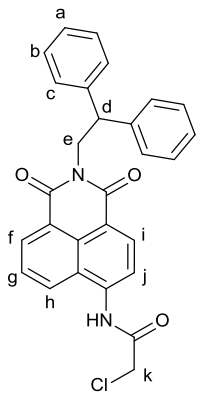

Aniline **148** (0.36 g, 0.92 mmol) and DMAP (56 mg, 0.46 mmol) were combined in a sealed flask which was purged with N_2. Anhydrous THF (15 mL) was added, and the stirring solution was cooled to 0 °C. A solution of 2-chloroacetyl chloride (0.12 mL, 1.4 mmol) in anhydrous THF (10 mL) was added to the cold stirring solution dropwise over 20 min. The solution was then stirred at r.t. for 6 h. The reaction mixture was diluted with H_2O (30 mL) and stirred vigorously, then extracted with EtOAc (3 x 30 mL). The combined organic phase was washed with brine (30 mL) and saturated aqueous $NaHCO_3$ (2 x 30 mL), dried using $MgSO_4$, filtered and concentrated *in vacuo* to yield amide **149** without further purification as a yellow solid (0.42 g, 98%).^{1}H NMR (400 MHz, $CDCl_3$) δ_H 9.08 (s, 1H, -*NH*-), 8.56-8.50 (m, 2H, H_f and H_i), 8.40 (d, *J* = 8.1, 1H, H_j), 8.13 (dd, *J* = 8.5, 0.7, 1H, H_h), 7.76 (dd, *J* = 8.4, 7.4, 1H, H_g), 7.38-7.33 (m, 4H, H_c), 7.26-7.20 (m, 4H, H_b), 7.17-7.11 (m, 2H, H_a), 4.88-4.80 (m, 3H, H_d and H_e), 4.37 (s, 2H, H_k).^{13}C NMR (101 MHz, $CDCl_3$) δ_C 164.2, 163.9, 163., 141.66, 137.0, 132.1, 131.3, 128.7, 128.5, 128.4, 127.18, 126.6, 125.7, 123.8, 123.3, 119.5, 119.1, 48.7, 44.5, 43.4, 30.9. IR: (ν_{max}/cm^{-1}) 3465, 3202, 2965, 2345, 1729, 1690, 1594, 1565, 1293, 1203, 1101, 979.. M.p. (°C) 139-144. LRMS (ES$^+$) 469 [M +H$^+$], 491 [M + Na].. UV: λ_{max}(MeCN)/nm (ε/ mol^{-1}cm^{-1}dm^3) 360 (10571).

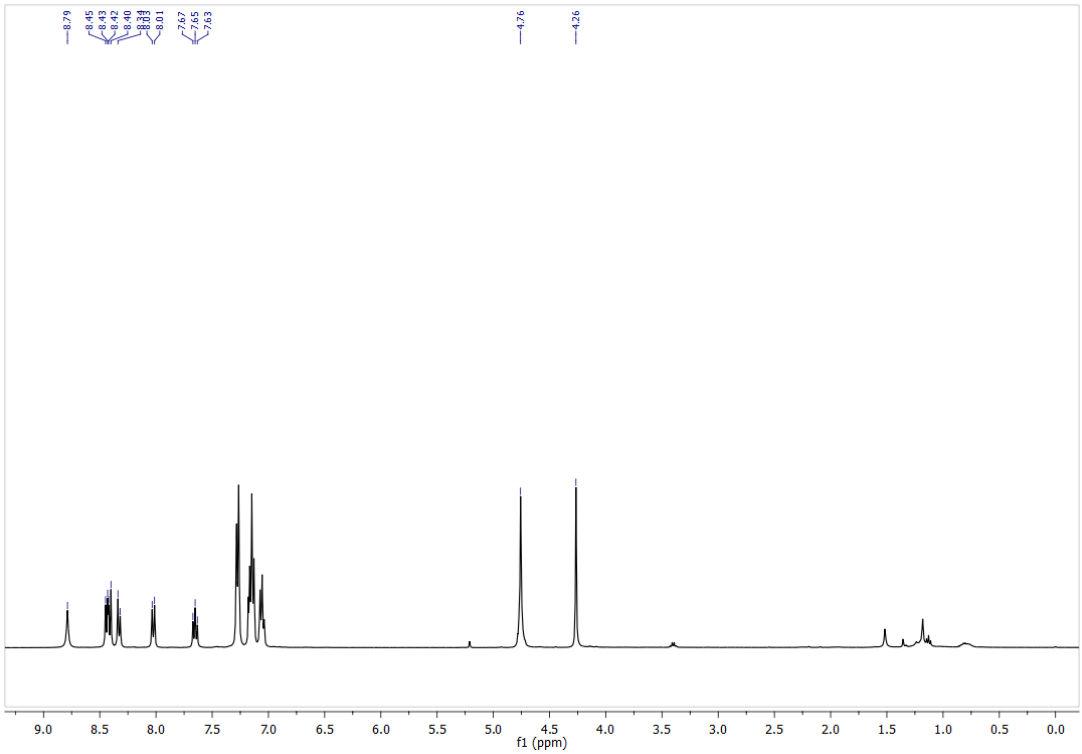
8.79
8.45
8.43
8.42
8.40
8.01
7.67
7.65
7.63
4.76
4.26
9.0 8.5 8.0 7.5 7.0 6.5 6.0 5.5 5.0 4.5 4.0 3.5 3.0 2.5 2.0 1.5 1.0 0.5 0.0
f1 (ppm)

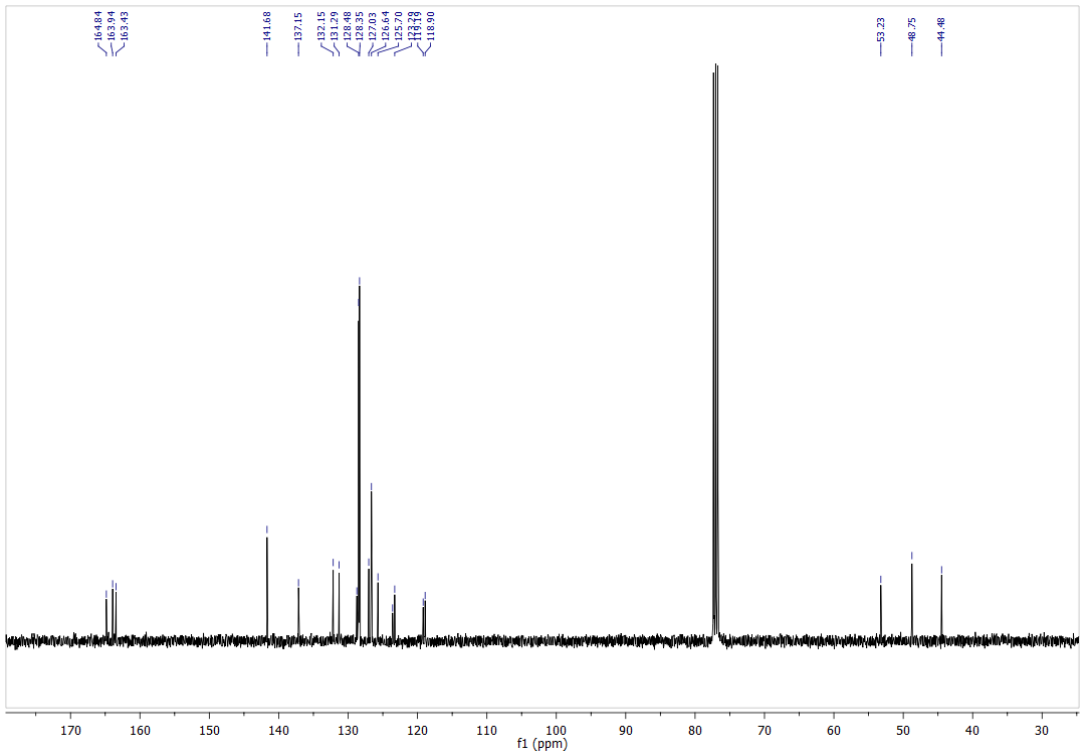
164.84
163.94
163.43
141.68
137.15
132.15
131.49
128.48
128.35
127.03
126.64
125.70
118.90
53.23
48.75
44.48
170 160 150 140 130 120 110 100 90 80 70 60 50 40 30
f1 (ppm)

2-azido-N-(2-(2,2-diphenylethyl)-1,3-dioxo-2,3-dihydro-1H-benzo[de]isoquinolin-6-yl)acetamide (**142**)

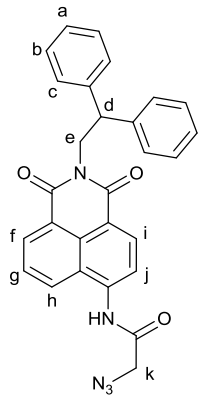

Chloride **149** (0.4 g, 0.85 mmol) and NaN_3 (0.11 g, 1.71 mmol) were dissolved in DMF (60 mL) and stirred at r.t. for 24 h. The mixture was diluted with brine (100 mL) and the aqueous layer was extracted with EtOAc (3 x 100 mL). The organic phases were combined and washed with saturated aqueous $NaHCO_3$ (150 mL), dried with $MgSO_4$, filtered and concentrated *in vacuo*. The resulting residue was purified by flash column chromatography (9:1 CH_2Cl_2/EtOAc) to give azide **142** as a brown solid (0.34 g, 84%). ^{1}H NMR (400 MHz, $CDCl_3$) δ_H 8.87 (s, 1H, -*NH*-), 8.54-8.47 (m, 2H, H_f and H_i), 8.41 (d, *J* = 8.2, 1H, H_j), 8.13 (d, *J* = 8.4, 1H, H_h), 7.76 (ap. t, *J* = 7.8, 1H, H_g), 7.39-7.32 (m, 4H, H_c), 7.27-7.20 (m, 4H, H_b), 7.17-7.10 (m, 2H, H_a), 4.87-4.80 (m, 3H, H_d and H_e), 4.35 (s, 2H, H_k). ^{13}C NMR (101 MHz, $CDCl_3$) δ_C 164.8, 163.9, 163.4, 141.6, 137.1, 132.1, 131.3, 128.7, 128.5, 128.4, 127.0, 126.6, 125.7, 123.6, 123.3, 119.2, 118.9, 53.2, 48.7, 44.5. IR: (ν_{max}/cm^{-1}) 3460, 3207, 2966, 2339, 2105, 1730, 1696, 1588, 1306, 1212, 1089 M.p. (°C) 146-149. HRMS (EI) calcd for $C_{28}H_{21}N_5O_3$ $[M + H]^+$ 476.1717, found 476.1710.UV: λ_{max}(MeCN)/nm (ε / mol^{-1}cm^{-1}dm^3) 361 (10925).

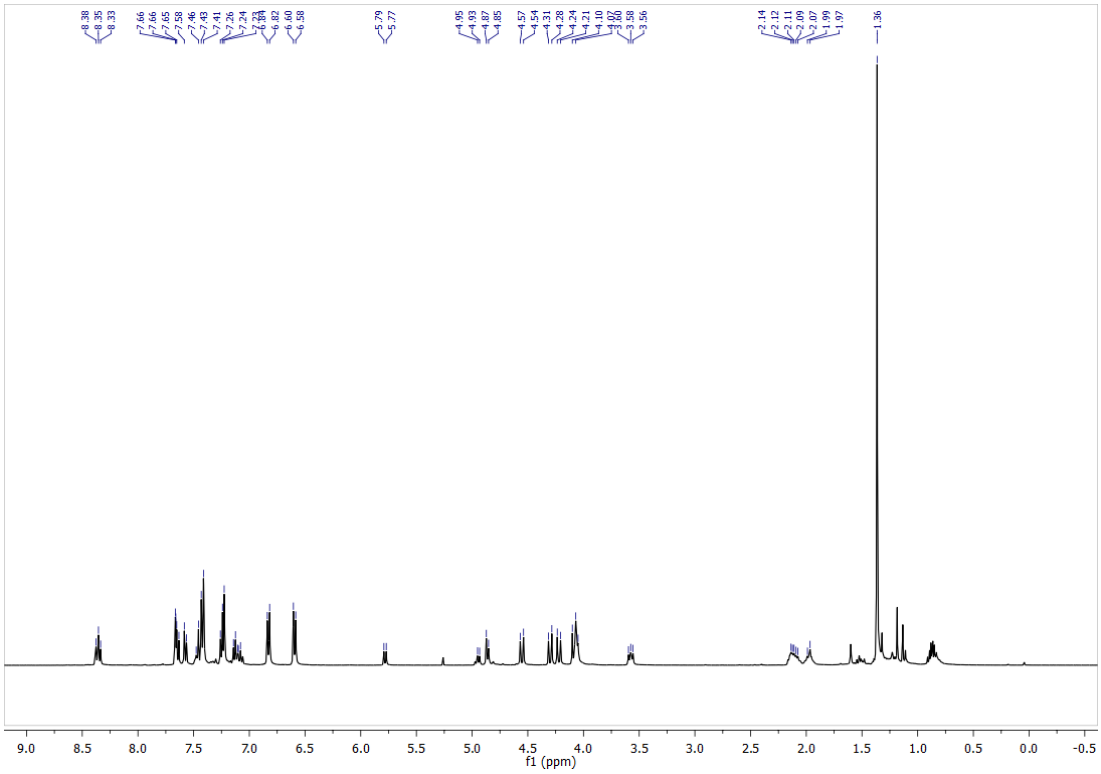
8.38
8.35
8.33
7.66
7.66
7.65
7.58
7.46
7.43
7.41
7.26
7.24
6.82
6.60
6.58
5.79
5.77
4.95
4.93
4.87
4.85
4.57
4.54
4.31
4.28
4.24
4.21
4.10
4.07
3.60
3.58
3.56
2.14
2.12
2.11
2.09
2.07
1.99
1.97
1.36
9.0
8.5
8.0
7.5
7.0
6.5
6.0
5.5
5.0
4.5
4.0
3.5
3.0
2.5
2.0
1.5
1.0
0.5
0.0
-0.5
f1 (ppm)

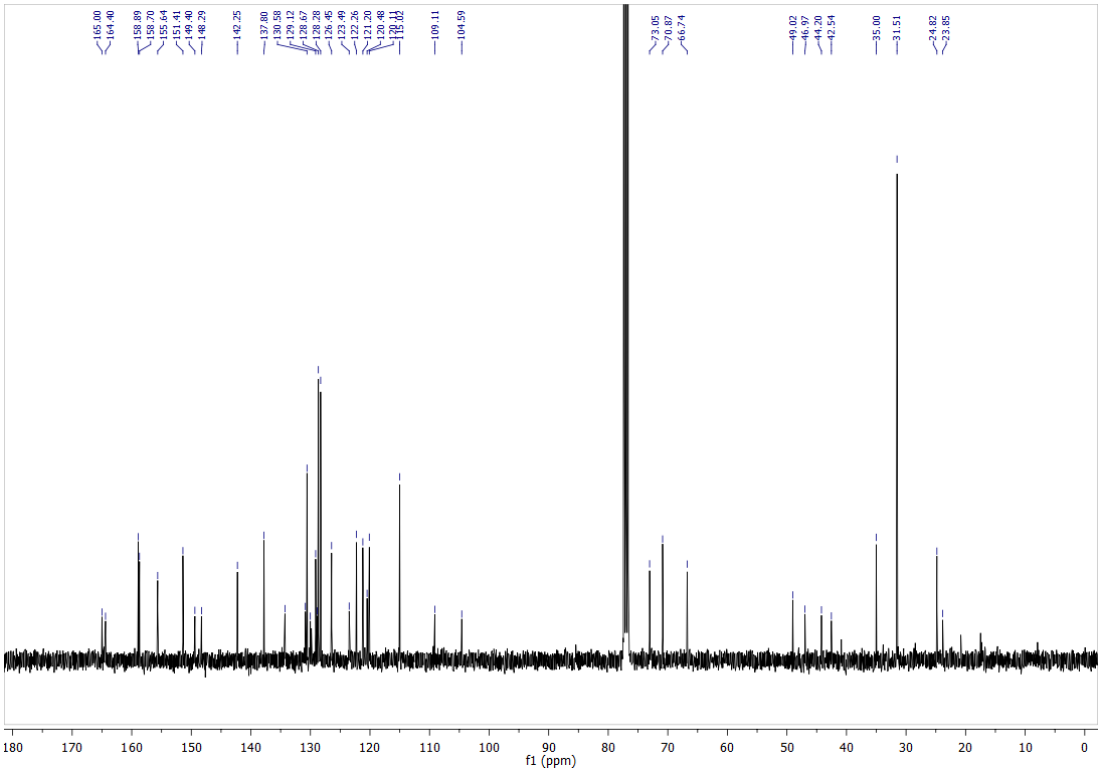
165.00
164.40
159.89
158.70
155.64
151.41
149.40
148.29
142.25
137.80
130.58
129.12
128.67
128.28
126.45
123.49
122.26
121.20
120.48
109.11
104.59
73.05
70.87
66.74
49.02
46.97
44.20
42.54
35.00
31.51
24.82
23.85
180
170
160
150
140
130
120
110
100
90
80
70
60
50
40
30
20
10
0
f1 (ppm)

*Rotaxane **150***

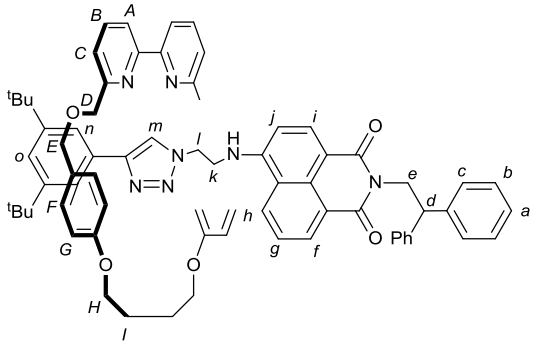

General procedure C was employed with macrocyle **136** (0.20 g, 0.41 mmol) acetylene **123** (0.09 g, 0.41 mmol), azide **141** (0.17 g, 0.41 mmol), $[Cu(MeCN)_4]PF_6$ (0.15 g, 0.40 mmol), and DIPEA (72 µL, 0.41 mmol) in EtOH (20 mL). Purification as noted gave rotaxane **140** as an orange residue (0.35 g, 72%). ^{1}H NMR (400 MHz, $CDCl_3$) δ_H 8.21-8.13 (m, 2H, H_i and H_f), 7.49-7.43 (m, 3H, H_h and H_B), 7.40-7.36 (m, 2H, H_n), 7.28-7.20 (m, 6H, H_c and two of H_A/H_C), 7.08-7.01 (m, 7H, H_b, H_o and two of H_A/H_C), 6.96-6.91 (m, 2H, H_a), 6.89 (dd, *J* = 8.3, 7.5, 1H, H_g), 6.63 (d, *J* = 8.5, 4H, H_F), 6.40 (d, *J* = 8.5, 4H, H_G), 5.58 (d, *J* = 8.6, 1H, H_j), 4.79-4.73 (m, 1H, H_d), 4.70-4.61 (m, 2H, H_e), 4.36 (d, *J* = 11.8, 2H, two of H_E), 4.11 (d, *J* = 12.0, 2H, two of H_D), 4.02 (d, *J* = 11.8, 2H, two of H_E), 3.90 (d, *J* = 12.0, 2H, two of H_D), 3.89-3.83 (m, 4H, H_H), 3.42-3.35 (m, 2H, H_l), 1.98-1.73 (m, 6H, H_k and H_l), 1.17 (s, 18H, 2 x ^{t}Bu).^{13}C NMR (101 MHz, $CDCl_3$) δ_C ^{13}C NMR (101 MHz, $CDCl_3$) δ 159.0, 158.8, 155.8, 151.6, 148.5, 142.4, 137.9, 134.4, 130.7, 130.2, 130.0, 129.3, 128.9, 128.8, 128.4, 126.6, 123.6, 122.5, 122.5, 122.4, 121.4, 120.7, 120.6, 120.3, 115.2, 109.3, 104.7, 73.2, 71.0, 66.9, 49.2, 47.1, 44.3, 42.7, 35.2, 31.7, 24.9. IR: (ν_{max}/cm^{-1}) 2965, 2902, 2840, 2347, 1703, 1660, 1579, 1203, 1191, 1006, 979.. HRMS (EI) calcd for $C_{74}H_{74}N_7O_6$ $[M + H]^+$ 1158.5852, found 1158.5860. UV: λ_{max}(MeCN)/nm (ε / mol^{-1}cm^{-1}dm^3) 436 (15720).

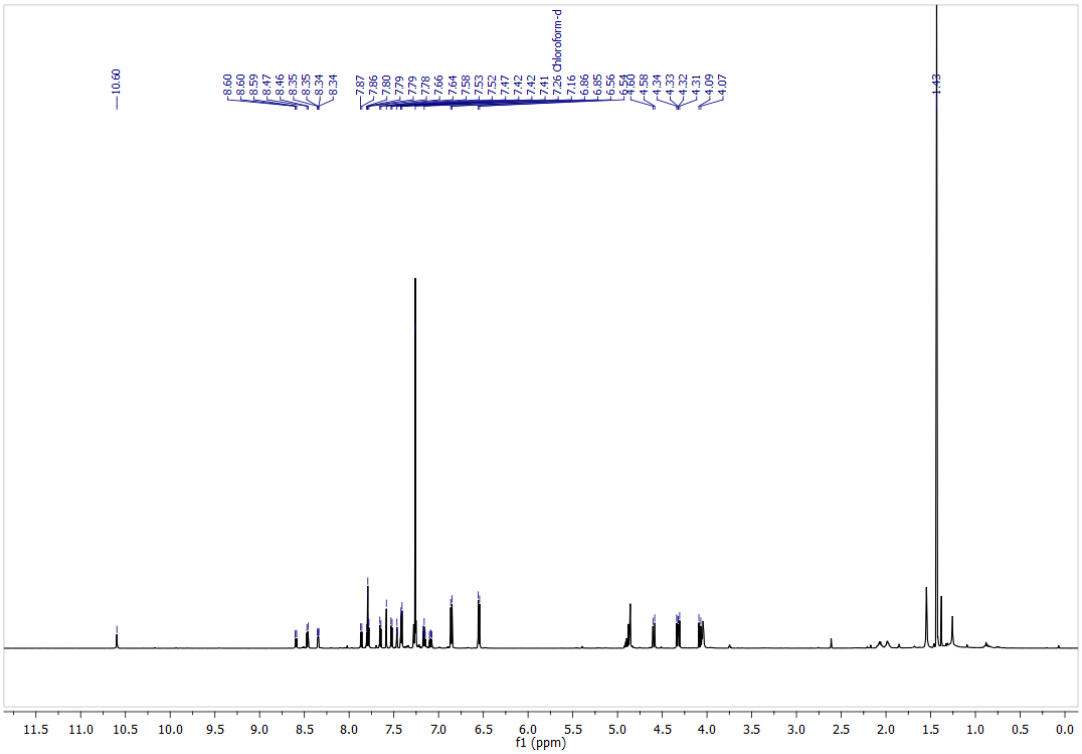
10.60
8.60
8.60
8.59
8.47
8.46
8.35
8.35
8.34
8.34
7.87
7.86
7.80
7.79
7.79
7.78
7.66
7.64
7.58
7.53
7.52
7.47
7.42
7.41
7.26 Chloroform-d
7.16
6.86
6.85
6.56
6.55
4.60
4.58
4.34
4.33
4.32
4.31
4.09
4.07
1.43
11.5 11.0 10.5 10.0 9.5 9.0 8.5 8.0 7.5 7.0 6.5 6.0 5.5 5.0 4.5 4.0 3.5 3.0 2.5 2.0 1.5 1.0 0.5 0.0
f1 (ppm)

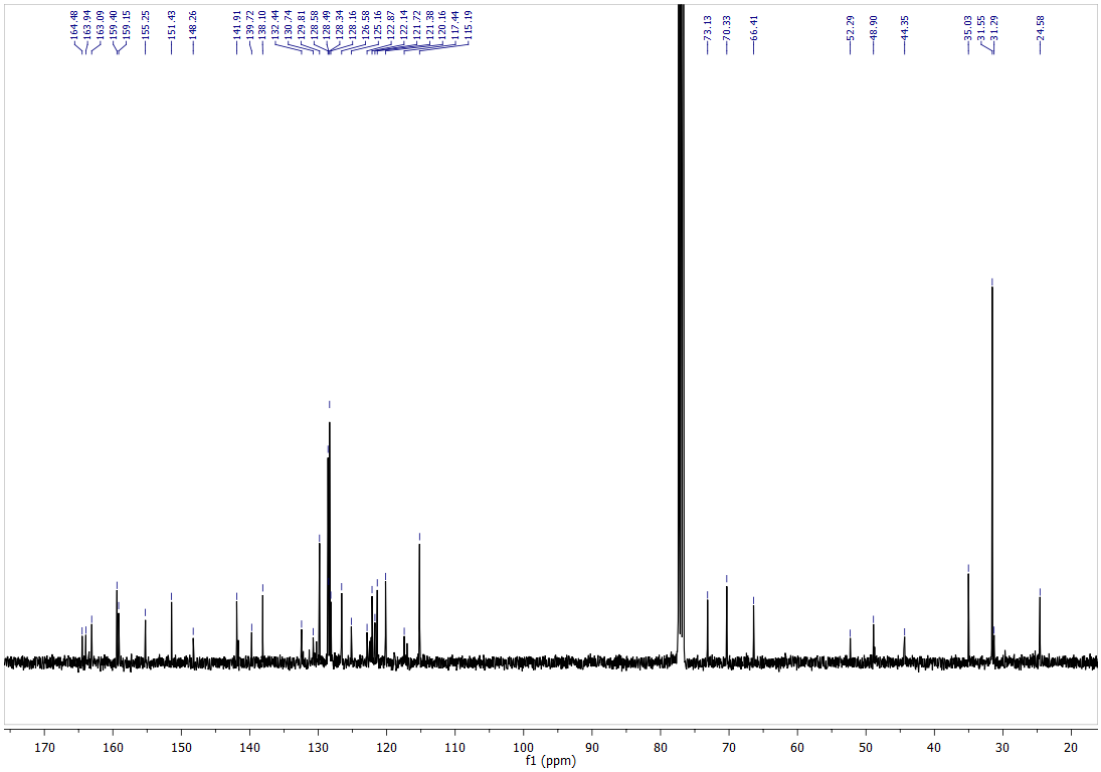
164.48
163.94
163.09
159.40
159.15
155.25
151.43
148.26
141.91
139.72
138.10
132.44
130.74
129.81
128.58
128.49
128.34
128.16
126.58
125.16
122.87
121.74
121.72
121.38
120.16
117.44
115.19
73.13
70.33
66.41
52.29
48.90
44.35
35.03
31.55
31.29
24.58
170 160 150 140 130 120 110 100 90 80 70 60 50 40 30 20
f1 (ppm)

*Rotaxane **152***

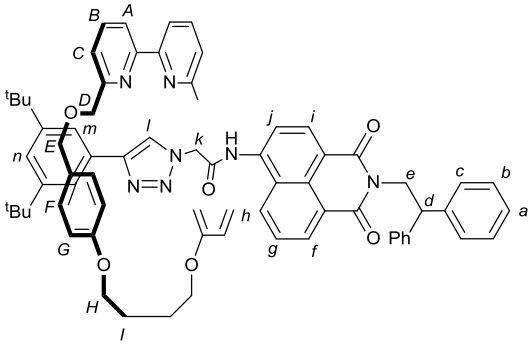

General procedure C was employed with macrocyle **136** (0.20 g, 0.41 mmol) acetylene **123** (0.09 g, 0.41 mmol), azide **142** (0.20 g, 0.41 mmol), $[Cu(MeCN)_4]PF_6$ (0.15 g, 0.40 mmol), and DIPEA (72 µL, 0.41 mmol) in EtOH (20 mL). Purification as noted gave rotaxane **152** as a yellow residue (0.29 g, 60%). ^{1}H NMR (400 MHz, $CDCl_3$) δ_H 10.59 (s, 1H, -*NH*-), 8.59 (dd, *J* = 8.6, 0.8, 1H, H_f), 8.46 (d, *J* = 8.3, 1H, H_i), 8.35 (dd, *J* = 7.3, 0.8, 1H, H_h), 7.86 (d, *J* = 8.4, 1H, H_j), 7.81-7.77 (m, 4H, H_m and H_B), 7.65 (d, *J* = 7.7, 2H, two of H_A/H_C), 7.58 (s, 1H, H_l), 7.52 (d, *J* = 7.7, 2H, two of H_A/H_C), 7.46 (t, *J* = 1.8, 1H, H_n), 7.43-7.40 (m, 4H, H_c), 7.29-7.24 (m, 4H, H_b), 7.18-7.14 (m, 2H, H_a), 7.09 (dd, *J* = 8.5, 7.3, 1H, H_g), 6.85 (d, *J* = 8.6, 4H, H_F), 6.54 (d, *J* = 8.6, 4H, H_G), 4.92-4.84 (m, 5H, H_d, H_e and H_k), 4.59 (d, *J* = 11.8, 2H, two of H_E), 4.33 (d, *J* = 11.8, 2H, two of H_E), 4.31 (d, *J* = 12.8, 2H, two of H_D), 4.07 (d, *J* = 12.8, 2H, two of H_D), 4.06-4.03 (m, 4H, H_H), 2.11-1.93 (m, 4H, H_I), 1.44 (s, 18H,2 x ^{t}Bu) ^{13}C NMR (101 MHz, $CDCl_3$) δ_C 164.5, 163.9, 163.1, 159.4, 159.2, 155.3, 151.4, 148.3, 141.9, 141.7, 139.7, 138.1, 132.4, 130.7, 130.3, 129.8, 128.6, 128.5, 128.3, 128.1, 126.5, 125.1, 122.8, 122.5, 122.2, 122.1, 121.7, 121.4, 120.1, 117.4, 117.0, 115.2, 73.1, 70.3, 66.4, 52.3, 48.9, 44.3, 35.0, 31.5, 31.3, 24.6. IR: (ν_{max}/cm^{-1}) 3207, 2966, 2857, 2339, 1730, 1696, 1588, 1306, 1212, 1093, 983. HRMS (EI) calcd for $C_{74}H_{72}N_7O_7$ $[M + H]^+$ 1172.5644, found 1172.5648. UV: λ_{max}(MeCN)/nm (ε / mol^{-1}cm^{-1}dm^3) 380 (11905).

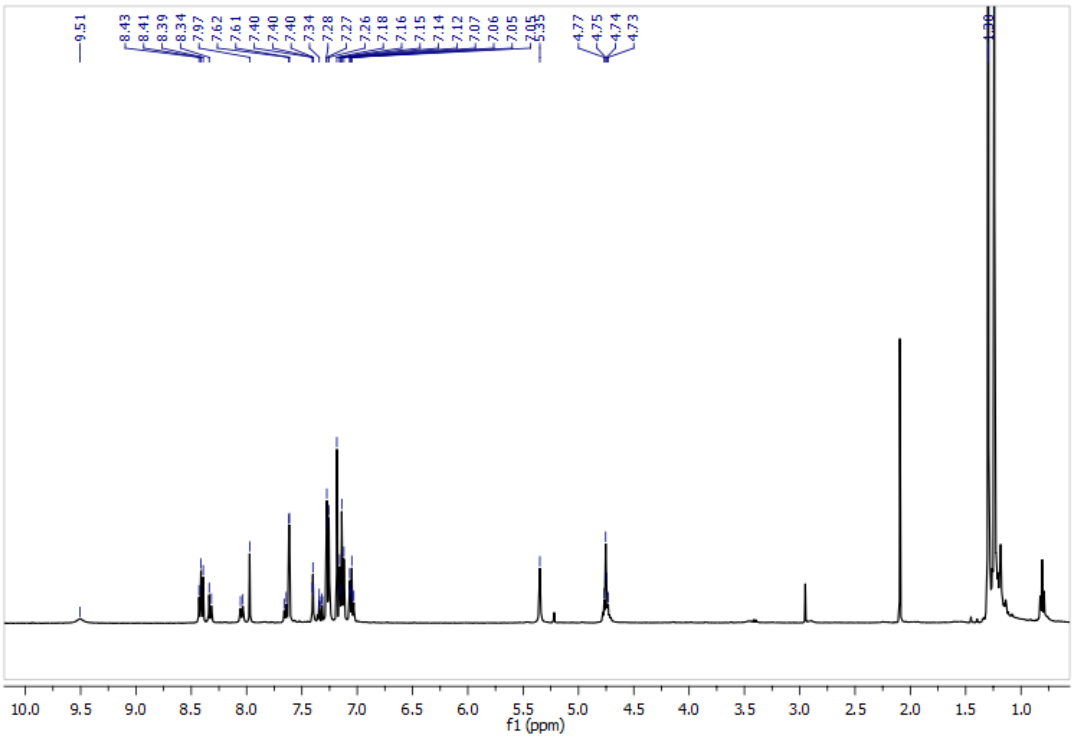
9.51
8.43
8.41
8.39
8.34
7.97
7.62
7.61
7.40
7.40
7.40
7.34
7.28
7.27
7.26
7.18
7.16
7.15
7.14
7.12
7.07
7.06
7.05
5.35
4.77
4.75
4.74
4.73
1.38
10.0 9.5 9.0 8.5 8.0 7.5 7.0 6.5 6.0 5.5 5.0 4.5 4.0 3.5 3.0 2.5 2.0 1.5 1.0
f1 (ppm)

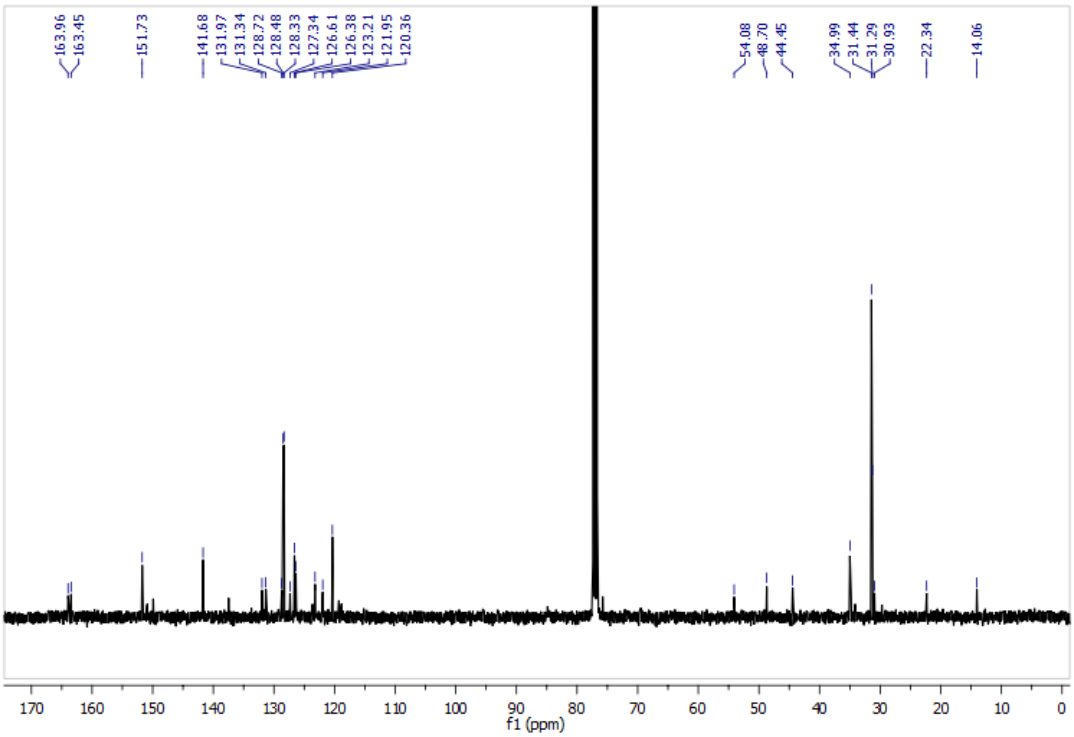
163.96
163.45
151.73
141.68
131.97
131.34
128.72
128.48
128.33
127.34
126.61
126.38
123.21
121.95
120.36
54.08
48.70
44.45
34.99
31.44
31.29
30.93
22.34
14.06
170 160 150 140 130 120 110 100 90 80 70 60 50 40 30 20 10 0
f1 (ppm)

*Thread **153***

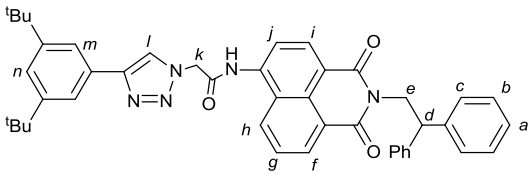

Azide **142** (44 mg, 0.093 mmol), alkyne **123** (20 mg, 0.093 mmol) and $[Cu(MeCN)_4]PF_6$ (8.7 mg, 0.023 mmol) were weighed dry into a sealed flask and purged with N_2. CH_2Cl_2 (1 mL) was added, followed by DIPEA (1 drop) and the mixture stirred at r.t. for 4 h. The solvent was diluted with CH_2Cl_2 (4 mL) and washed with 16% aqueous EDTA tetrasodium-saturated ammonia solution (5 mL). The organic layer was retained and the aqueous layer extracted twice further with CH_2Cl_2. The organic extracts were combined, dried over $MgSO_4$, filtered and dried in vacuo. The crude mixture was purified by flash column chromatography (1:1 Petrol/CH2CL2 to 10% MeCN/1:1 Petrol-CH2CL2) to yield the product **153** as a yellow residue (57 mg, 89%). ^{1}H NMR (400 MHz, $CDCl_3$) δ_H 9.56 (br s, 1H, -*NH*-), 8.53-8.46 (m, 2H, H_f and H_i), 8.41 (d, *J* = 8.2, 1H, H_j), 8.12 (d, *J* = 8.4, 1H, H_h), 8.05 (s, 1H, H_l), 7.73 (ap. t, *J* = 8.0, 1H, H_g), 7.69 (d, *J* = 1.7, 2H, H_m), 7.47 (t, J = 1.7, 1H, H_n), 7.37-7.30 (m, 4H, H_c), 7.25-7.18 (m, 4H, H_b), 7.16-7.09 (m, 2H, H_a), 5.43 (s, 2H, H_k), 4.87-4.79 (m, 3H, H_d and H_e), 1.37 (s, 18H, 2 x ^{t}Bu) ^{13}C NMR (101 MHz, $CDCl_3$) δ_C 163.9, 163. 5, 160.8, 151.7, 150.8, 149.9, 141.6, 137.4, 131.9, 131.3, 128.7, 128.5, 128.33, 127.3, 126.6, 126.3, 123.6, 123.2, 123.0, 121.9, 120.3, 119.2, 118.8, 54.0, 48.7, 44.5, 34.9, 31. 4, 31.2, 30.9, 22.3, 14.0. IR: (ν_{max}/cm^{-1}) 3202, 2956, 2851, 2347, 1740, 1689, 1591, 1313, 1201, 1012. HRMS (EI) calcd for $C_{44}H_{43}N_5O_3$ $[M + H]^+$ 690.3439, found 690.3436 UV: λ_{max}(MeCN)/nm (ε / mol^{-1}cm^{-1}dm^3) 361 (14285).

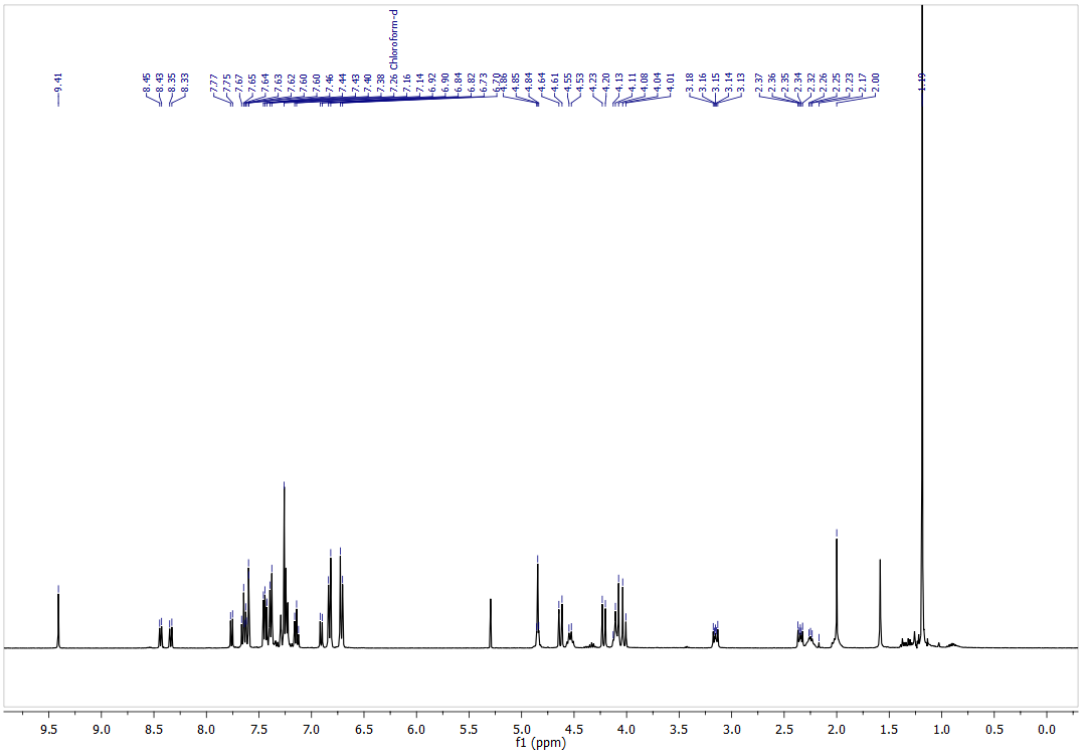
9.41
8.45
8.43
8.35
8.33
7.77
7.75
7.67
7.65
7.64
7.63
7.62
7.60
7.60
7.46
7.44
7.43
7.40
7.38
7.26 Chloroform-d
7.16
7.14
6.92
6.90
6.84
6.82
6.73
4.90
4.86
4.85
4.84
4.64
4.61
4.55
4.53
4.23
4.20
4.13
4.11
4.08
4.04
4.01
3.18
3.16
3.15
3.14
3.13
2.37
2.36
2.35
2.34
2.32
2.26
2.25
2.23
2.17
2.00
1.49
f1 (ppm)

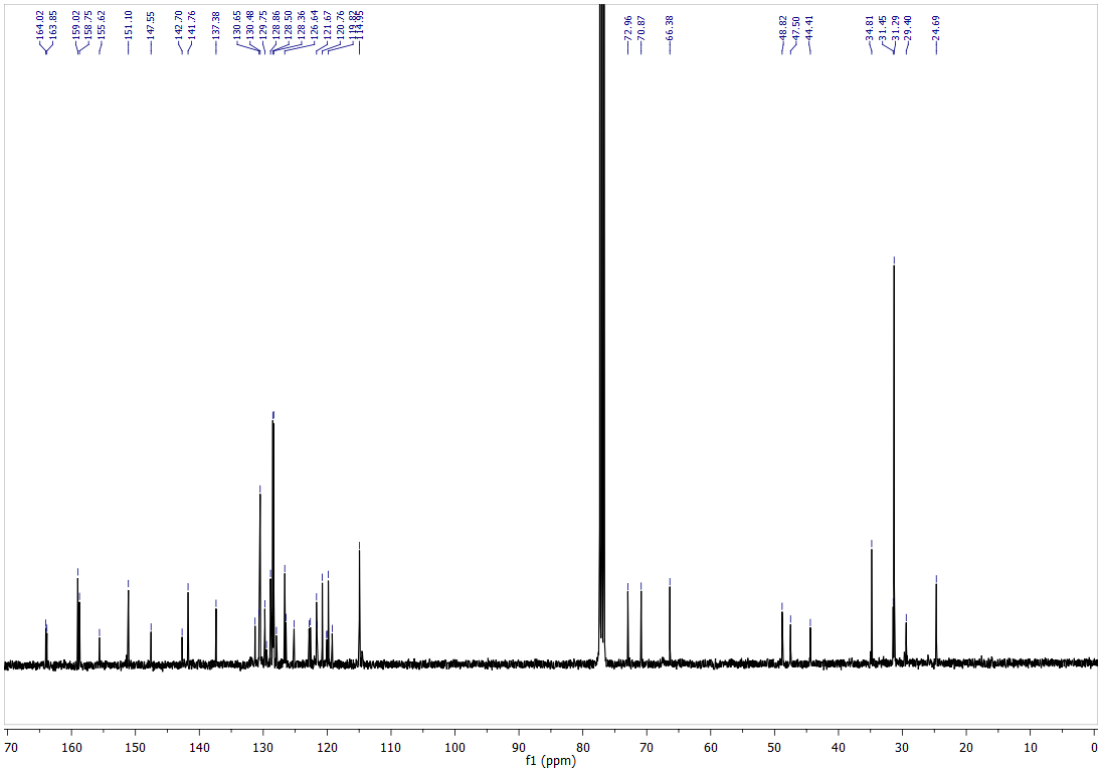
164.02
163.85
159.02
158.75
155.62
151.10
147.55
142.70
141.76
137.38
130.65
130.48
129.75
128.86
128.50
128.36
126.64
121.67
120.76
72.96
70.87
66.38
48.82
47.50
44.41
34.81
31.45
31.29
29.40
24.69
f1 (ppm)

*Rotaxane **154***

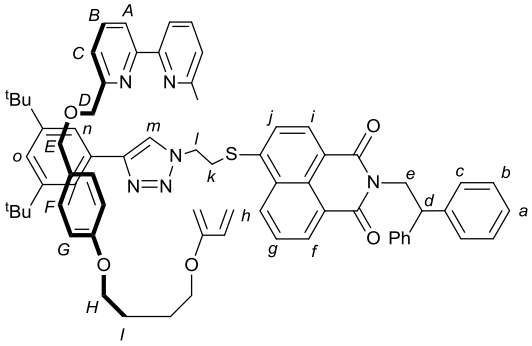

General procedure C was employed with macrocyle **136** (0.25 g, 0.52 mmol) acetylene **123** (0.11 g, 0. 52 mmol), azide **143** (0.25 g, 0. 52 mmol), $[Cu(MeCN)_4]PF_6$ (0.18 g, 0.50 mmol), and DIPEA (90 µL, 0. 52 mmol) in EtOH (25 mL). Purification as noted gave rotaxane **154** as a pale yellow foam (0.52 g, 86%). ^{1}H NMR (400 MHz, $CDCl_3$) δ_H 9.41 (s, 1H, H_m), 8.43 (d, *J* = 7.2, 1H, H_f), 8.33 (d, *J* = 8.3, 1H, H_h), 7.76 (d, *J* = 7.8, 1H, H_i), 7.67-7.61 (m, 3H, H_g and H_B), 7.61-7.59 (m, 2H, two of H_C/H_A), 7.47-7.42 (m, 4H, H_n and two of H_C/H_A), 7.41-7.37 (m, 4H, H_c), 7.27 (t, *J* = 1.6, 1H, H_o), 7.27-7.22 (m, 4H, H_b), 7.17-7.11 (m, 2H, H_a), 6.90 (d, *J* = 7.8, 1H, H_j), 6.82 (d, *J* = 8.5, 4H, H_F), 6.71 (d, *J* = 8.5, 4H, H_G), 4.87-4.83 (m, 3H, H_d and H_e), 4.62 (d, *J* = 11.8, 2H, two of H_E), 4.58-4.50 (m, 2H, two of H_H), 4.21 (d, *J* = 11.8, 2H, two of H_E), 4.14-4.07 (m, 2H, two of H_H), 4.09 (d, *J* = 12.2, 2H, two of H_D), 4.01 (d, *J* = 12.2, 2H, two of H_D), 3.18-3.12 (m, 2H, H_l), 2.38-2.23 (m, 2H, H_k), 2.30-2.19 (m, 2H, two of H_l), 2.06-1.94 (m, 2H, two of H_l), 1.85 (s, 18H, 2 x ^{t}Bu). ^{13}C NMR (101 MHz, $CDCl_3$) δ_C 164.0, 163.8, 159.0, 158.7, 155.6, 151.1, 147.5, 142.7, 141.7, 137.4, 131.3, 130.6, 130.5, 129.7, 129.5, 128.8, 128.5, 128.4, 127.9, 126.6, 126.5, 125.3, 125.3, 125.2, 122.8, 122.6, 121.7, 121.6, 120.7, 120.1, 120.0, 120.0, 119.8, 119.2, 114.9, 72.9, 70.8, 66.4, 48.8, 47.5, 44.4, 34.8, 31.5, 31.3, 29.4, 24.7. IR: (ν_{max}/cm^{-1}) 2970, 2901, 2839, 2353, 1711, 1656, 1569, 1202, 1186, 1112, 1093. M.p. (°C) 50-52. HRMS (EI) calcd for $C_{74}H_{73}N_6O_6S$ $[M + H]^+$ 1175.5463, found 1175.5479. UV: λ_{max}(MeCN)/nm (ε/ mol^{-1}cm^{-1}dm^3) 381 (10674).

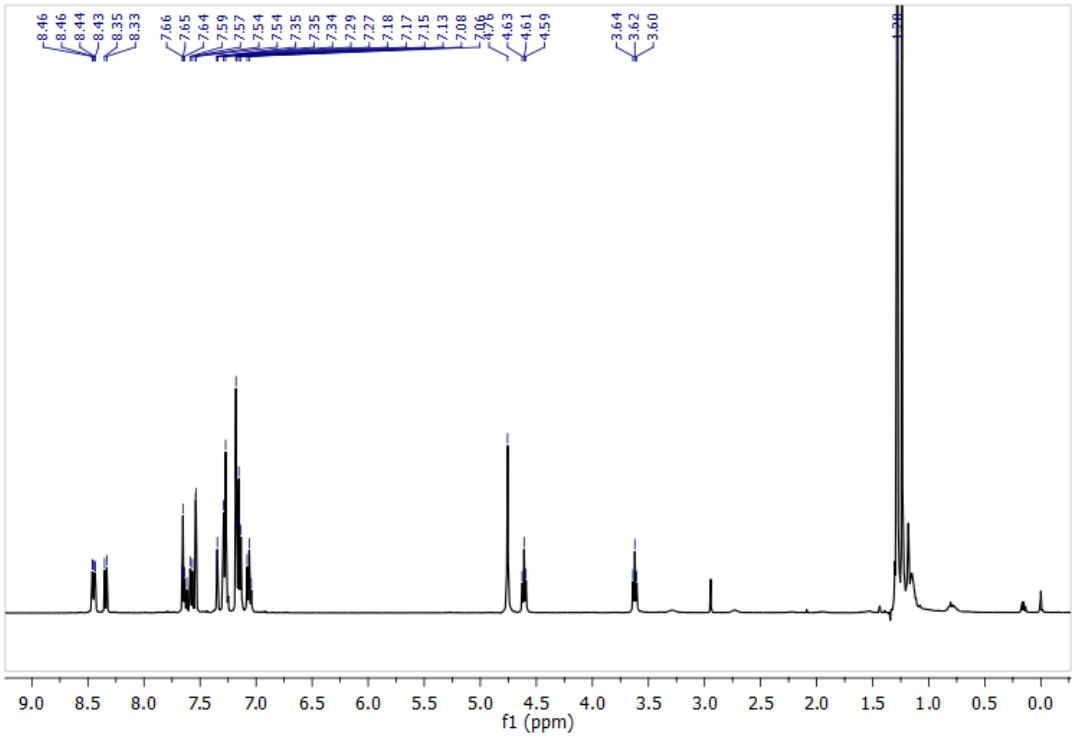
8.46
8.46
8.44
8.43
8.35
8.33
7.66
7.65
7.64
7.59
7.57
7.54
7.54
7.35
7.35
7.34
7.29
7.27
7.18
7.17
7.15
7.13
7.08
4.63
4.61
4.59
3.64
3.62
3.60
9.0 8.5 8.0 7.5 7.0 6.5 6.0 5.5 5.0 4.5 4.0 3.5 3.0 2.5 2.0 1.5 1.0 0.5 0.0
f1 (ppm)

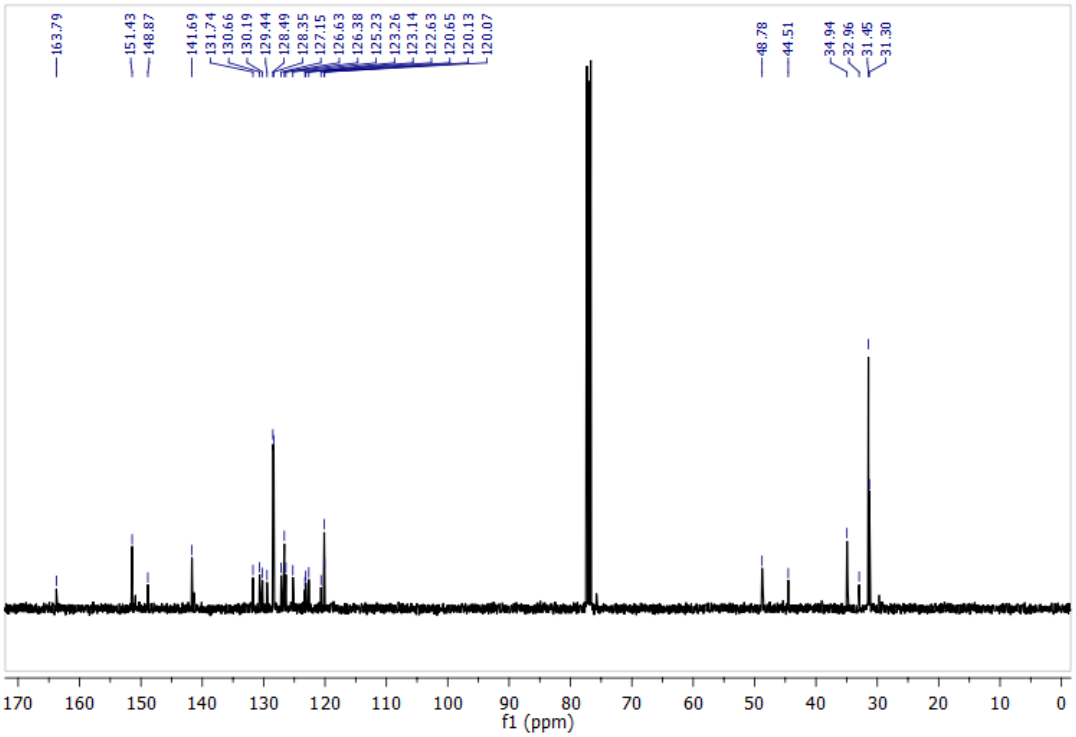
163.79
151.43
148.87
141.69
131.74
130.66
130.19
129.44
128.49
128.35
127.15
126.63
126.38
125.23
123.26
123.14
122.63
120.65
120.13
120.07
48.78
44.51
34.94
32.96
31.45
31.30
170 160 150 140 130 120 110 100 90 80 70 60 50 40 30 20 10 0
f1 (ppm)

Thread ***155***

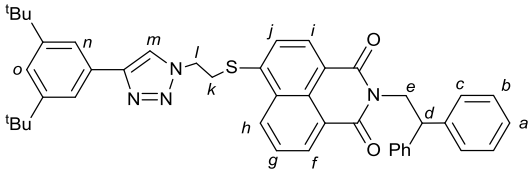

Azide **143** (45 mg, 0.093 mmol), alkyne **123** (20 mg, 0.093 mmol) and $[Cu(MeCN)_4]PF_6$ (8.7 mg, 0.023 mmol) were weighed dry into a sealed flask and purged with N_2. CH_2Cl_2 (1 mL) was added, followed by DIPEA (1 drop) and the mixture stirred at r.t. for 4 h. The solvent was diluted with CH_2Cl_2 (4 mL) and washed with 16% aqueous EDTA tetrasodium-saturated ammonia solution (5 mL). The organic layer was retained and the aqueous layer extracted twice further with CH_2Cl_2. The organic extracts were combined, dried over $MgSO_4$, filtered and dried in vacuo. The crude mixture was purified by flash column chromatography (1:1 Petrol/CH2CL2 to 10% MeCN/1:1 Petrol-CH2CL2) to yield the product **155** as a pale yellow residue (62 mg, 96%). ^{1}H NMR (400 MHz, $CDCl_3$) δ_H 8.53 (d, *J* = 7.2, 1H, H_f), 8.51 (d, *J* = 8.5, 1H, H_h), 8.42 (d, *J* = 7.8, 1H, H_i), 7.73 (s, 1H, H_m) 7.71 (dd, *J* = 8.1, 7.3, 1H, H_g), 7.65 (d, *J* = 1.7, 2H, H_j), 7.92 (d, *J* = 1.7, 2H, H_n), 7.43 (t, *J* = 1.7, 1H, H_o), 7.39-7.31 (m, 4H, Hc), 7.26-7.20 (m, 4H, Hb), 7.17-7.13 (m, 2H, Ha), 4.86-4.82 (m, 3H, Hd and He), 4.69 (t, *J* = 6.7, 2H, H_k), 3.70 (t, *J* = 6.7, 2H, H_l), 1.28 (s, 18H, 2 x ^{t}Bu). ^{13}C NMR (101 MHz, $CDCl_3$) δ_C 163.8, 151.4, 148.8, 141.7, 131.7, 130.6, 130.2, 129.4, 128.5, 128.4, 127.2, 126.6, 126.4, 125.2, 123.2, 123.1, 122.6, 120.6, 120.1, 120.0, 48. 8, 44.5, 34.9, 32.9, 31.4, 31.3. IR: (ν_{max}/cm^{-1}) 2970, 2901, 2839, 2353, 1711, 1656, 1569, 1202, 1186, 1112, 1093. HRMS (EI) calcd for $C_{44}H_{44}N_4O_2S$ [M + H]$^+$ 693.3258, found 693.3255 UV: λ_{max}(MeCN)/nm (ε / mol^{-1}cm^{-1}dm^3) 378 (12228).

Chapter 6: Supplementary Data

6.1. Aggregation Studies of Sensor **105**

6.1.1. Effect of Probe Concentration of the Fluorescence Response of Probe **105**

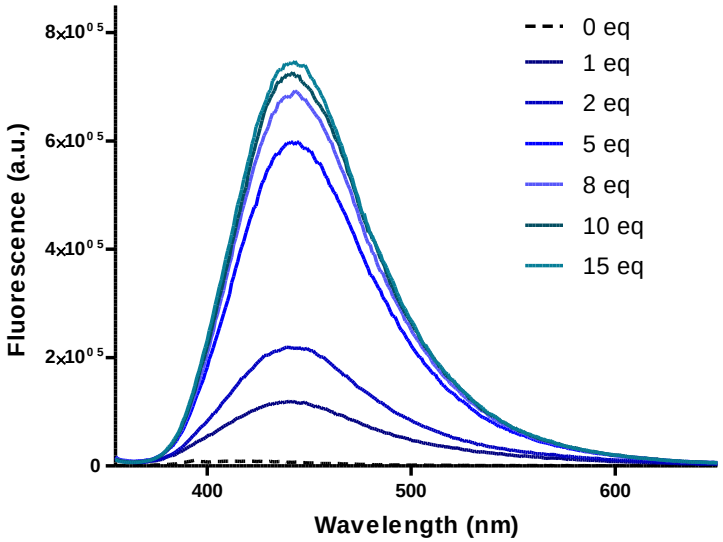

Fig. S1 Fluorescence response of the titration of sensor **105** (100 μM) with increasing amounts of Zn^{2+} in aqueous buffer (0.1 mM HEPES, pH 7.4, ambient temperature, λ_{ex} = 347 nm.

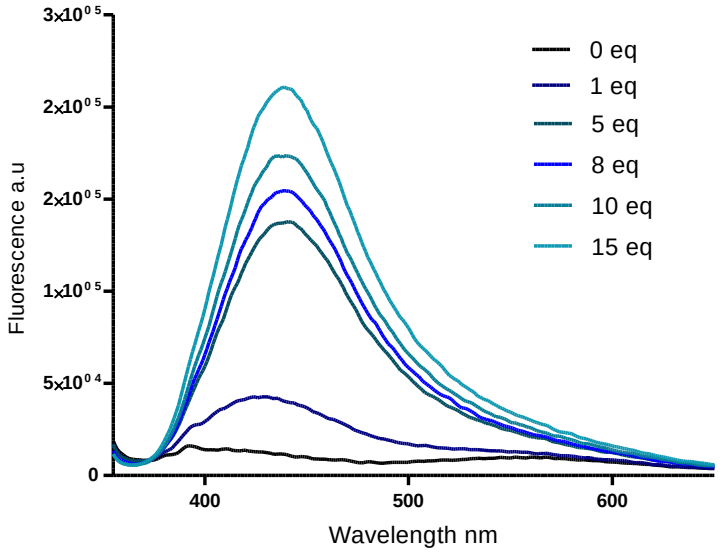

Fig. S2 Fluorescence response of the titration of sensor **105** (50 μM) with increasing amounts of Zn^{2+} in aqueous buffer (0.1 mM HEPES, pH 7.4, ambient temperature, λ_{ex} = 347 nm).

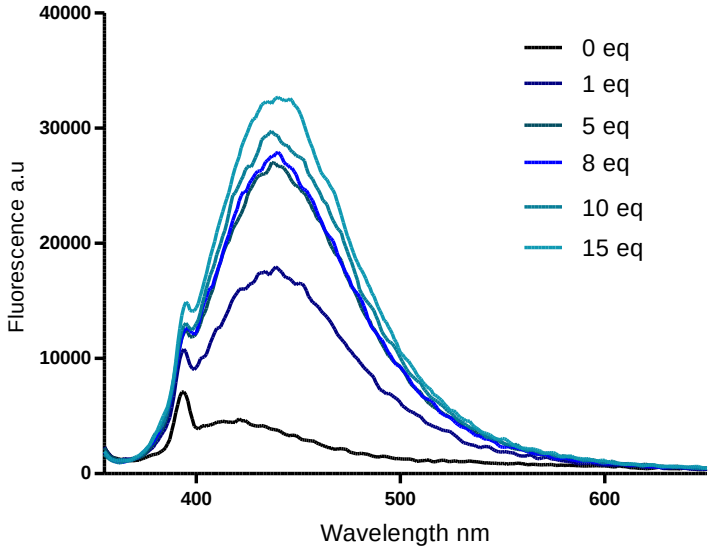

Fig. S3 Fluorescence response of the titration of sensor **105** (10 μM) with increasing amounts of Zn^{2+} in aqueous buffer (0.1 mM HEPES, pH 7.4, ambient temperature, λ_{ex} = 347 nm).

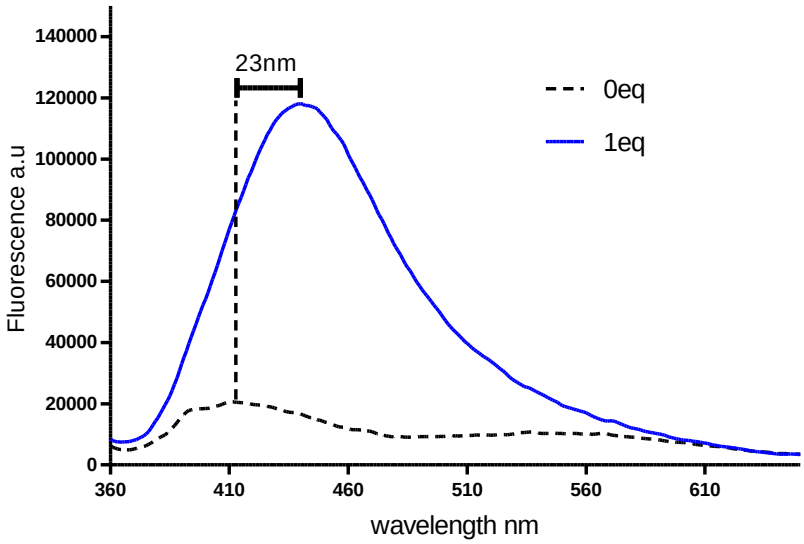

Fig. S4 Graphical representation of the red-shift in λ_{em} upon binding of 1 equiv. Zn^{2+} with sensor **105** (100 μM) in aqueous buffer (0.1 mM HEPES, pH 7.4, ambient temperature, λ_{ex} = 347 nm).

6.1.2. Effect of Solvent Composition on the Fluorescence Response of Probe 105

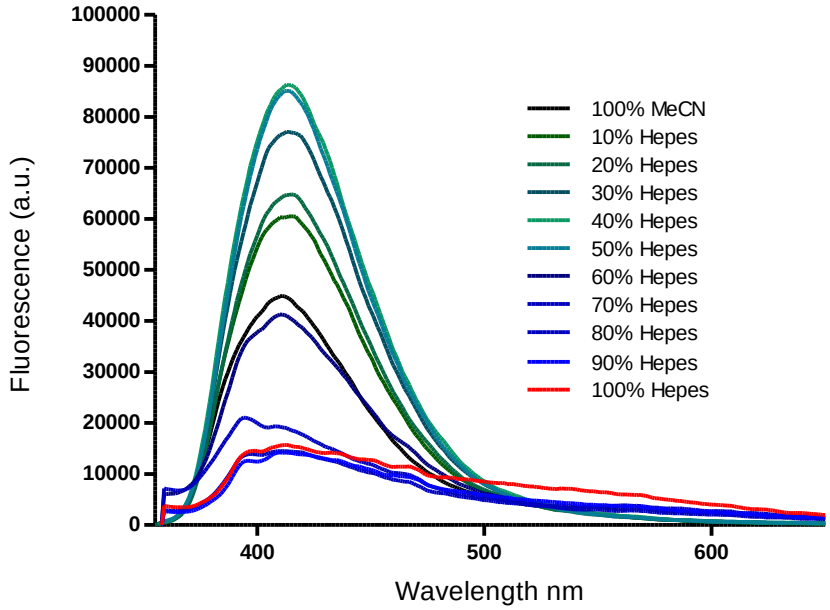

Fig. S5 HEPES/MeCN titration of sensor **105** (100 μM) (0.1 mM HEPES, pH 7.4, ambient temperature, λ_{ex} = 347 nm).

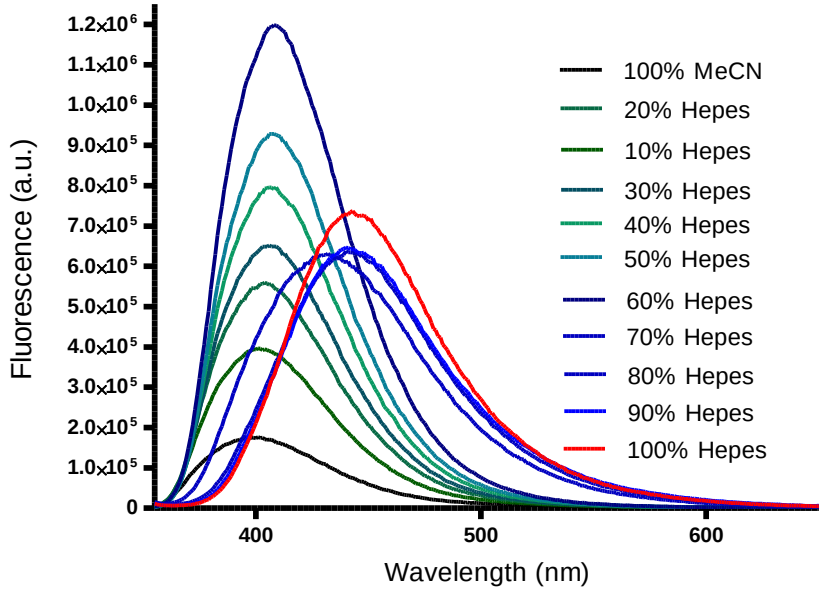

Fig. S6 HEPES/MeCN titration of sensor **105** (100 μM) with 5 equiv. of Zn^{2+} (0.1 mM HEPES, pH 7.4, ambient temperature, λ_{ex} = 347 nm).

6.1.3. Dynamic Light Scattering Study

Dynamic light scattering (DLS) experiments were performed at a sensor concentration of 30 μM in HEPES buffer (1% DMSO). Sensor **105** demonstrates aggregation phenomena in aqueous solution, as demonstrated by the large particle size observed in these samples. The aggregates are at their largest with no Zn^{2+} present; in the presence of Zn^{2+} the particle size decreases greatly, coinciding with an increase in fluorescence emission upon addition of Zn^{2+} to the sensor. Samples containing **116** on the other hand, structurally similar to **6** but with a different biological targeting unit, show no significant aggregation as demonstrated by the low degree of scattering and poor signal quality, demonstrating the difference small structural changes can have on the behaviour of these probes.

- Sensor **105**

Size Distribution Report by Intensity

v2.2

Malvern

Sample Details

Sample Name:	JP2107 Water 30uM 0 1
SOP Name:	mansettings.nano
General Notes:	Average result created from record number(s): 1 2 3

File Name:	ZET0002884.dts	Dispersant Name:	Water
Record Number:	16	Dispersant RI:	1.330
Material RI:	1.59	Viscosity (cP):	0.8872
Material Absorbtion:	0.010	Measurement Date and Time:	04 October 2013 10:15:43

System

Temperature (℃):	25.0	Duration Used (s):	50
Count Rate (kcps):	155.5	Measurement Position (mm):	1.25
Cell Description:	Disposable sizing cuvette	Attenuator:	7

Results

			Size (d.nm):	% Intensity:	St Dev (d.n...
Z-Average (d.nm):	772.6	Peak 1:	732.1	98.6	222.7
PdI:	0.250	Peak 2:	5011	1.4	603.9
Intercept:	0.972	Peak 3:	0.000	0.0	0.000

Result quality : Refer to quality report

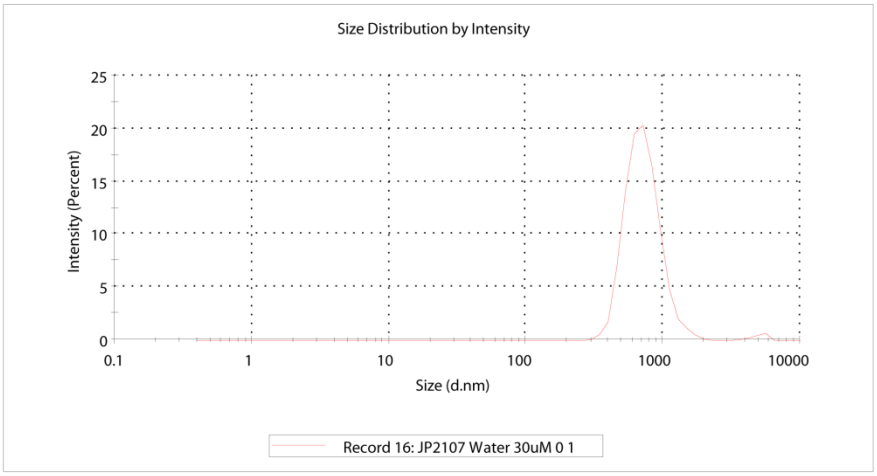

Malvern Instruments Ltd
www.malvern.com

Zetasizer Ver. 7.02
Serial Number : MAL500457

File name: ZET0002884.dts
Record Number: 16
04 Oct 2013 10:17:13

- Sensor **105** + 1 equiv. Zn^{2+}:

Size Distribution Report by Intensity

v2.2

Malvern

Sample Details

Sample Name:	JP2-107 30uM 1 zinc 1
SOP Name:	mansettings.nano
General Notes:	

File Name:	ZET0002894.dts	Dispersant Name:	Water
Record Number:	2	Dispersant RI:	1.330
Material RI:	1.59	Viscosity (cP):	0.9781
Material Absorbtion:	0.010	Measurement Date and Time:	17 October 2013 14:38:36

System

Temperature (℃):	21.0	Duration Used (s):	70
Count Rate (kcps):	191.6	Measurement Position (mm):	4.65
Cell Description:	Disposable sizing cuvette	Attenuator:	7

Results

			Size (d.nm):	% Intensity:	St Dev (d.n...
Z-Average (d.nm):	260.6	Peak 1:	290.0	100.0	113.5
PdI:	0.165	Peak 2:	0.000	0.0	0.000
Intercept:	0.968	Peak 3:	0.000	0.0	0.000

Result quality : Good

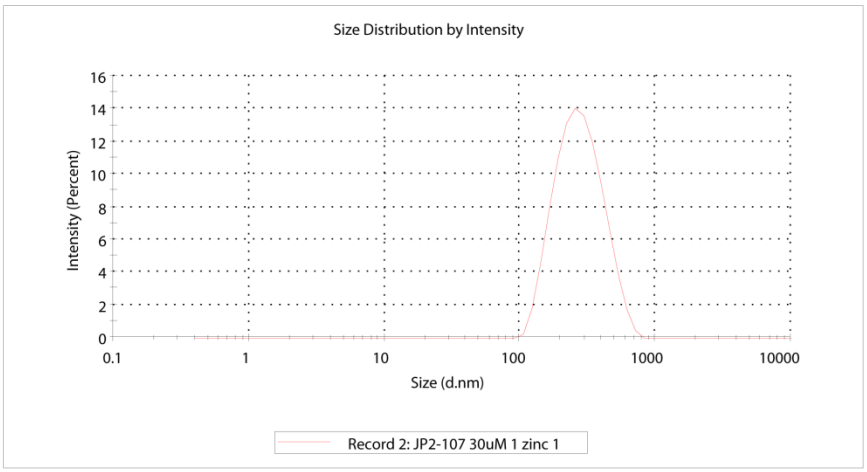

- Sensor **105** + 5 equiv. Zn^{2+}:

Size Distribution Report by Intensity

v2.2

Malvern

Sample Details

Sample Name:	JP2-107 30uM 5 zinc 1
SOP Name:	mansettings.nano
General Notes:	

File Name:	ZET0002894.dts	Dispersant Name:	Water
Record Number:	3	Dispersant RI:	1.330
Material RI:	1.59	Viscosity (cP):	0.9781
Material Absorbtion:	0.010	Measurement Date and Time:	17 October 2013 14:45:15

System

Temperature (℃):	21.0	Duration Used (s):	80
Count Rate (kcps):	150.6	Measurement Position (mm):	4.65
Cell Description:	Disposable sizing cuvette	Attenuator:	7

Results

			Size (d.nm):	% Intensity:	St Dev (d.n...
Z-Average (d.nm):	226.1	Peak 1:	243.2	96.6	94.35
PdI:	0.210	Peak 2:	4769	3.4	737.7
Intercept:	0.969	Peak 3:	0.000	0.0	0.000

Result quality : Good

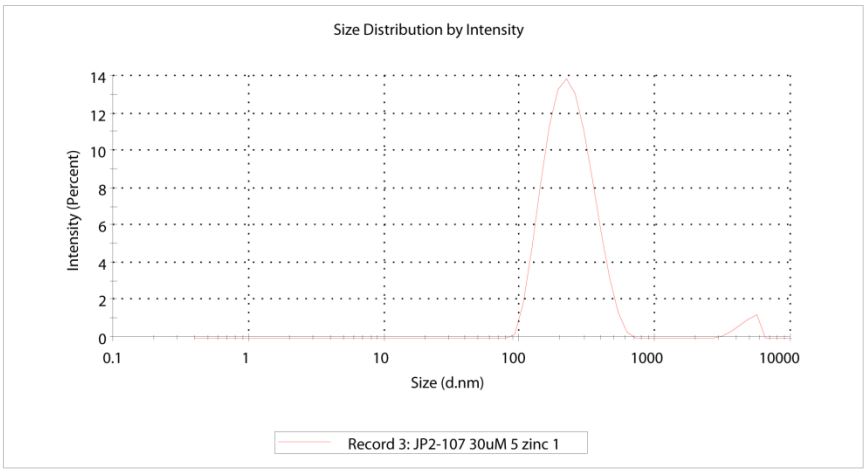

- Sensor **105** + 15 equiv. Zn^{2+}:

Size Distribution Report by Intensity

v2.2

Malvern

Sample Details

Sample Name:	JP2-107 30uM 15 zinc 1
SOP Name:	mansettings.nano
General Notes:	

File Name:	ZET0002894.dts	Dispersant Name:	Water
Record Number:	4	Dispersant RI:	1.330
Material RI:	1.59	Viscosity (cP):	0.9781
Material Absorbtion:	0.010	Measurement Date and Time:	17 October 2013 14:50:33

System

Temperature (℃):	21.0	Duration Used (s):	70
Count Rate (kcps):	185.7	Measurement Position (mm):	4.65
Cell Description:	Disposable sizing cuvette	Attenuator:	7

Results

			Size (d.nm):	% Intensity:	St Dev (d.n...
Z-Average (d.nm):	247.2	Peak 1:	279.7	100.0	116.4
PdI:	0.187	Peak 2:	0.000	0.0	0.000
Intercept:	0.972	Peak 3:	0.000	0.0	0.000

Result quality : Good

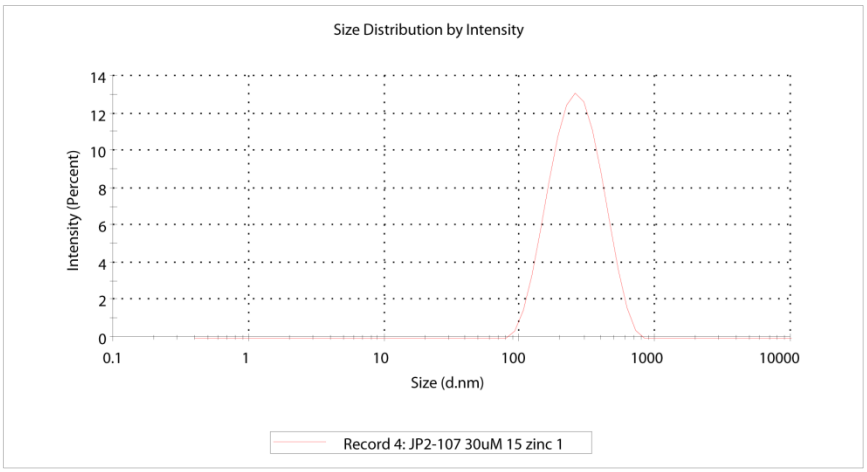

Malvern Instruments Ltd
www.malvern.com

Zetasizer Ver. 7.02
Serial Number : MAL500457

File name: ZET0002894
Record Number: 4
23 Oct 2013 09:51:30

- Sensor **116** blank:

Size Distribution Report by Intensity

v2.2

Malvern

Sample Details

Sample Name:	JP2-156D 30uM 0 zinc 1
SOP Name:	mansettings.nano
General Notes:	

File Name:	ZET0002894.dts	Dispersant Name:	Water
Record Number:	5	Dispersant RI:	1.330
Material RI:	1.59	Viscosity (cP):	0.9781
Material Absorbtion:	0.010	Measurement Date and Time:	17 October 2013 14:56:37

System

Temperature (℃):	21.0	Duration Used (s):	70
Count Rate (kcps):	116.7	Measurement Position (mm):	4.65
Cell Description:	Disposable sizing cuvette	Attenuator:	10

Results

			Size (d.nm):	% Intensity:	St Dev (d.n...
Z-Average (d.nm):	552.7	Peak 1:	144.9	91.5	15.18
PdI:	0.638	Peak 2:	16.53	8.5	1.176
Intercept:	1.03	Peak 3:	0.000	0.0	0.000

Result quality : Refer to quality report

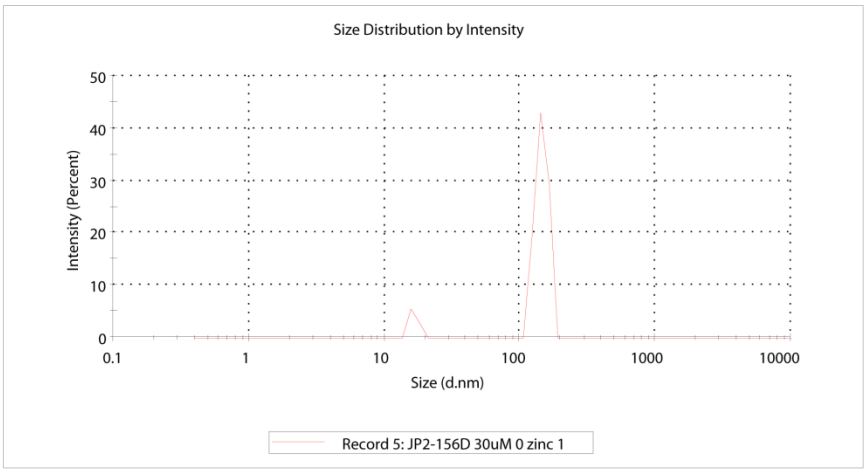

Malvern Instruments Ltd
www.malvern.com

Zetasizer Ver. 7.02
Serial Number : MAL500457

File name: ZET0002894
Record Number: 5
23 Oct 2013 09:52:30

- Sensor **116** + 1 equiv. Zn^{2+}:

Size Distribution Report by Intensity

v2.2

Malvern

Sample Details

Sample Name:	JP2-156D 30uM 1 zinc 1
SOP Name:	mansettings.nano
General Notes:	

File Name:	ZET0002894.dts	Dispersant Name:	Water
Record Number:	6	Dispersant RI:	1.330
Material RI:	1.59	Viscosity (cP):	0.9781
Material Absorbtion:	0.010	Measurement Date and Time:	17 October 2013 15:02:53

System

Temperature (℃):	21.0	Duration Used (s):	60
Count Rate (kcps):	337.7	Measurement Position (mm):	4.65
Cell Description:	Disposable sizing cuvette	Attenuator:	10

Results

			Size (d.nm):	% Intensity:	St Dev (d.n...
Z-Average (d.nm):	452.2	Peak 1:	226.4	100.0	27.00
PdI:	0.468	Peak 2:	0.000	0.0	0.000
Intercept:	1.01	Peak 3:	0.000	0.0	0.000

Result quality : Refer to quality report

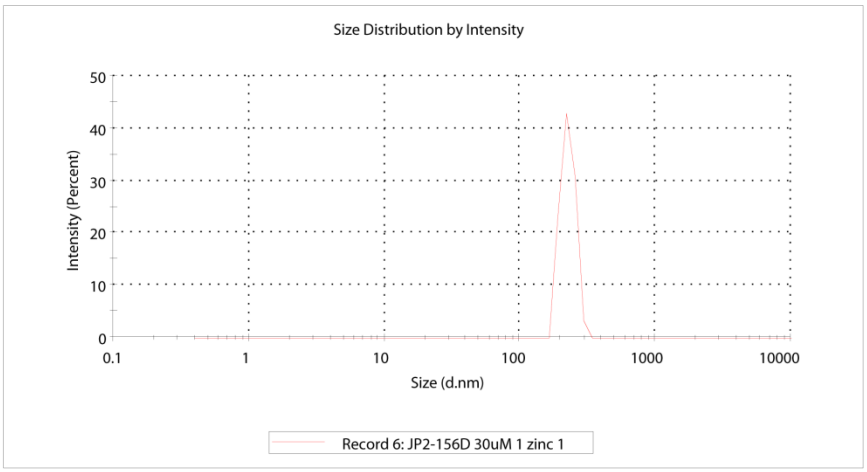

Malvern Instruments Ltd
www.malvern.com

Zetasizer Ver. 7.02
Serial Number : MAL500457

File name: ZET0002894
Record Number: 6
23 Oct 2013 09:52:51

- Sensor **116** + 5 equiv. Zn^{2+}:

Size Distribution Report by Intensity

v2.2

Malvern

Sample Details

Sample Name:	JP2-156D 30uM 5 zinc 1
SOP Name:	mansettings.nano
General Notes:	

File Name:	ZET0002894.dts	Dispersant Name:	Water
Record Number:	7	Dispersant RI:	1.330
Material RI:	1.59	Viscosity (cP):	0.9781
Material Absorbtion:	0.010	Measurement Date and Time:	17 October 2013 15:08:06

System

Temperature (℃):	21.0	Duration Used (s):	60
Count Rate (kcps):	302.3	Measurement Position (mm):	4.65
Cell Description:	Disposable sizing cuvette	Attenuator:	10

Results

			Size (d.nm):	% Intensity:	St Dev (d.n...
Z-Average (d.nm):	1791	Peak 1:	214.1	100.0	12.08
PdI:	1.000	Peak 2:	0.000	0.0	0.000
Intercept:	1.25	Peak 3:	0.000	0.0	0.000

Result quality : Refer to quality report

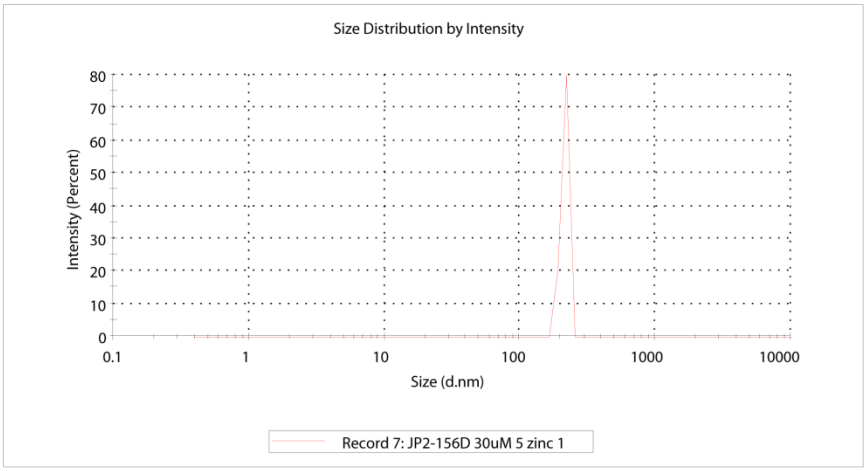

Malvern Instruments Ltd
www.malvern.com

Zetasizer Ver. 7.02
Serial Number : MAL500457

File name: ZET0002894
Record Number: 7
23 Oct 2013 09:53:06

- Sensor **116** + 15 equiv. Zn^{2+}:

Size Distribution Report by Intensity

v2.2

Malvern

Sample Details

Sample Name:	JP2-156D 30uM 15 zinc 1
SOP Name:	mansettings.nano
General Notes:	

File Name:	ZET0002894.dts	Dispersant Name:	Water
Record Number:	8	Dispersant RI:	1.330
Material RI:	1.59	Viscosity (cP):	0.9781
Material Absorbtion:	0.010	Measurement Date and Time:	17 October 2013 15:14:23

System

Temperature (℃):	21.0	Duration Used (s):	60
Count Rate (kcps):	279.3	Measurement Position (mm):	4.65
Cell Description:	Disposable sizing cuvette	Attenuator:	10

Results

			Size (d.nm):	% Intensity:	St Dev (d.n...
Z-Average (d.nm):	1679	Peak 1:	216.2	100.0	10.22
PdI:	1.000	Peak 2:	0.000	0.0	0.000
Intercept:	1.29	Peak 3:	0.000	0.0	0.000

Result quality : Refer to quality report

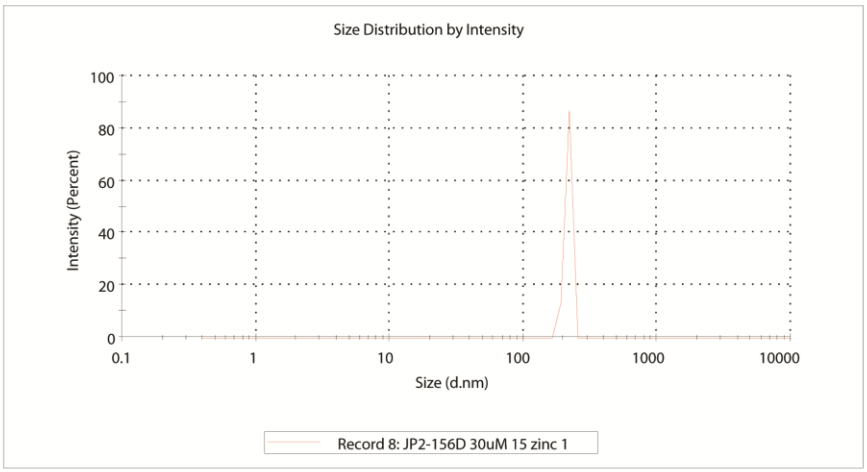

Malvern Instruments Ltd
www.malvern.com

Zetasizer Ver. 7.02
Serial Number : MAL500457

File name: ZET0002894
Record Number: 8
23 Oct 2013 09:53:20

6.2. Experimental Procedures for the Evaluation of Sensors in Pancreatic Islets

Female CD1 mice (8-12 weeks of age) were housed under specific pathogen free conditions with *ad libitum* access to food and water. Animals were euthanized by cervical dislocation before isolation of islets by collagenase digestion, as previously described (PMID: 20204627). Animal procedures were approved by the Home Office according to the Animals (Scientific Procedures) Act 1986 of the United Kingdom (PPL 70/7349). Following 24-48 h culture, islets were incubated for 60 min. with the sensor under study before imaging using a Zeiss Axiovert 200 inverted widefield stereomicroscope. Illumination was delivered through a 20× 0.4NA objective (LD Plan Neofluar) using a halogen light source and a DAPI filter set (λ_{ex} = 365/12, λ_{em} = 447/60). Emitted signals were detected using a highly-sensitive 1344 x 1024 CCD camera (Hamamatsu ORCA-ER). Throughout, islets were incubated at 36 ^{o}C and irrigated with HEPES-bicarbonate buffer (120 mM NaCl, 4.8 mM KCl, 24 mM $NaHCO_3$, 0.5 mM Na_2HPO_4, 5 mM HEPES, 2.5 mM $CaCl_2$ and 1.2 mM $MgCl_2$) saturated with 95% O_2/5% CO_2 and adjusted to pH 7.4. Offline signal analysis was performed using Volocity (Perkin Elmer) and Igor Pro (Wavemetrics) softwares. For two-photon imaging of probe distribution, islets were incubated with sensor as above before imaging using a Leica SP5 multiphoton microscope equipped with a 25× 0.95NA water-dipping objective adjusted for infrared wavelengths (HCX IRAPO). Two-photon excitation was achieved using a Spectraphysics Mai Tai femtosecond-pulsed laser (λ_{ex} = 850 nm) and emitted signals were collected using a PMT (λ_{em} = 400-550 nm). Image analysis was performed using Image J (NIH).

6.2.1. Cytotoxicity Assay

Islets were incubated with 3 µM calcein-AM (Life Technologies) and 2.5 µM propidium iodide (PI; Sigma-Aldrich) before detection of absorbance/emission at 491/525nm and 561/620nm, respectively. Calcein AM is a vital stain and requires cleavage by intracellular esterases for fluorescence. Conversely, PI is a necrosis stain which only enters the nucleus in membrane-compromised cells. The islet area occupied by dead cells was expressed as a unitary ratio versus that occupied by live cells. Non-multifactorial pairwise comparisons were performed using Student's t-test. Interactions between multiple treatments were assessed using Kruskal-Wallis test followed by pairwise comparisons using Dunn's post-hoc test. In all cases, analysis was performed using Graphpad Prism (Graphpad Software) and results considered significant at $P<0.05$.

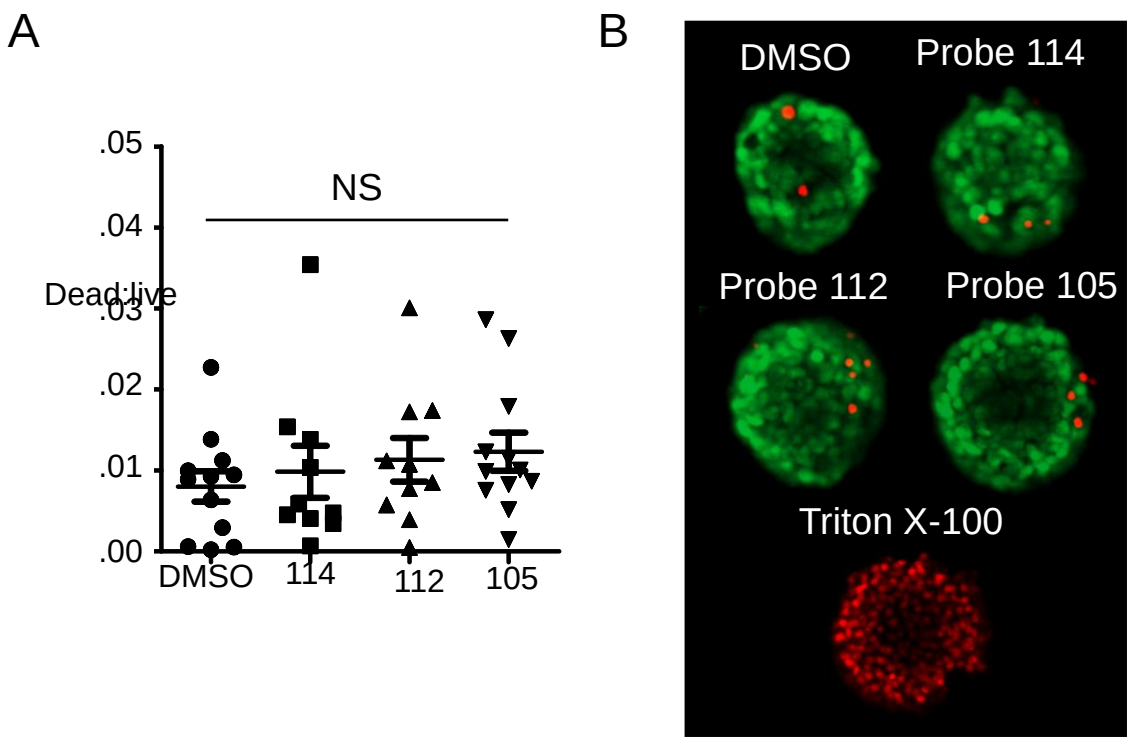

Fig. S7 Cytotoxicity assays for probes **105**, **112** and **114**. A. Incubation of mouse islets with probes **6**, **112** and **114** does not significantly induce cell death (necrosis) versus DMSO-alone (1:333) (NS, non-significant; P<0.54). B. Representative images showing calcein and PI staining in islets treated with DMSO and probes **105**, **112** and **114**. Below is a positive control (Triton X-100; to permeabilise the membrane).

6.2.2. Live Imaging of Dye Co-localisation

MIN6 beta cells were incubated for 1-2 h with each Zn^{2+}-binding probe (30 µM for probes **105** and **112**; 300 µM for probe **114** before 30 min incubation with either 200 nM Mitotracker Red FM or 200 nM Lysotracker DND-99 (both Life Technologies). Cells were washed three times with PBS before live-imaging using a confocal microscope equipped with an acousto optical beam splitter (AOBS) and spectral detectors (Leica TCS SP5). The Zn^{2+}-binding probes were excited using a 405 nm diode laser and emissions collected at 460/70 nm (63 x oil-immersion objective; NA 1.4). The organelle-specific dyes were excited using a 543 HeNe laser and emitted light captured using PMTs centred on 650/50 nm and 595/50 nm for Mitotracker and Lysotracker, respectively. Analysis of co-localisation was performed after background fluorescence correction using the Pearson's correlation coefficient embedded within the Intensity Correlation Analysis (ICA) plugin for ImageJ (NIH). Uniform linear adjustments were applied to contrast/brightness to improve image quality for analysis/presentation purposes.

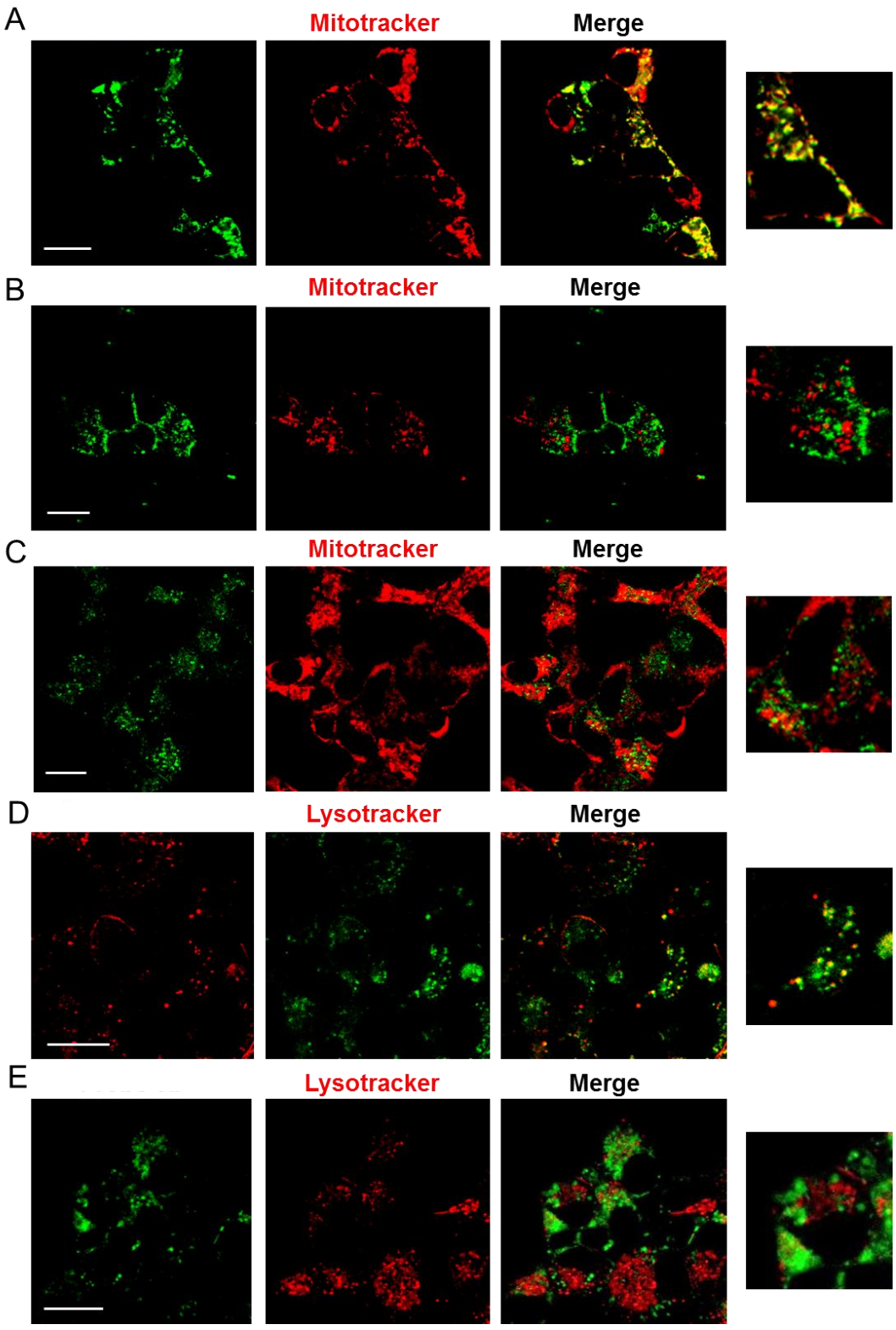

Fig. S8 Cellular distribution of probes **105**, **112** and **114**. A. Probe **112**, expected to sequester in mitochondria, is co-localised with Mitotracker. B. Probe **115**, expected to aggregate at the plasma membrane, does not co-localise with Mitotracker. C. Probe **114**, expected to aggregate in lysosomes, does not co-localise with Mitotracker. D. Probe **114**

co-localises with Lysotracker, a marker of acidic organelles. E. Probe **112** does not co-localise with Lysotracker, further confirming its mitochondrial specificity. Scale bar represents 10 µm.

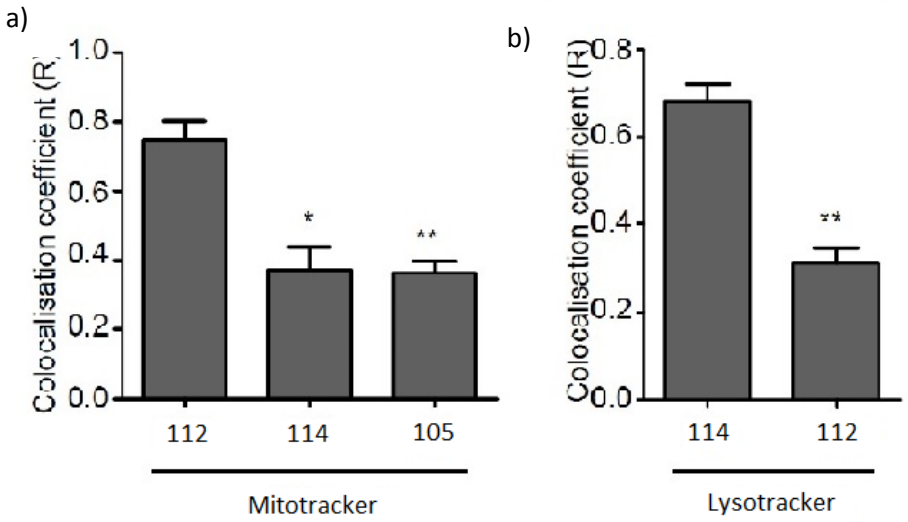

Fig. S9 Statistical analysis of probe localisation with a) mito- and b) lyso-tracker.

Image analysis demonstrates that the signals from probe **112** and Mitotracker are strongly correlated. By contrast, fluorescence from both probe **114** and probe **105** poorly correlates with that of the organelle-specific dye (*P<0.05 and **P<0.01 versus probe **112**) (Kruskal-Wallis test). Note that some co-localisation is still apparent due to the inability to fully resolve sub-cellular structures close to the diffraction limit. We also observe a strong correlation between probe **114** and Lysotracker DND-99, but not probe **112** and the organelle-specific dye (**P<0.001 probe 112 versus probe **114**) (Student's t-test).

6.3. Supplementary Spectroscopic Data for compounds **89**, **111** and **112**.

^{31}P NMR of **89**

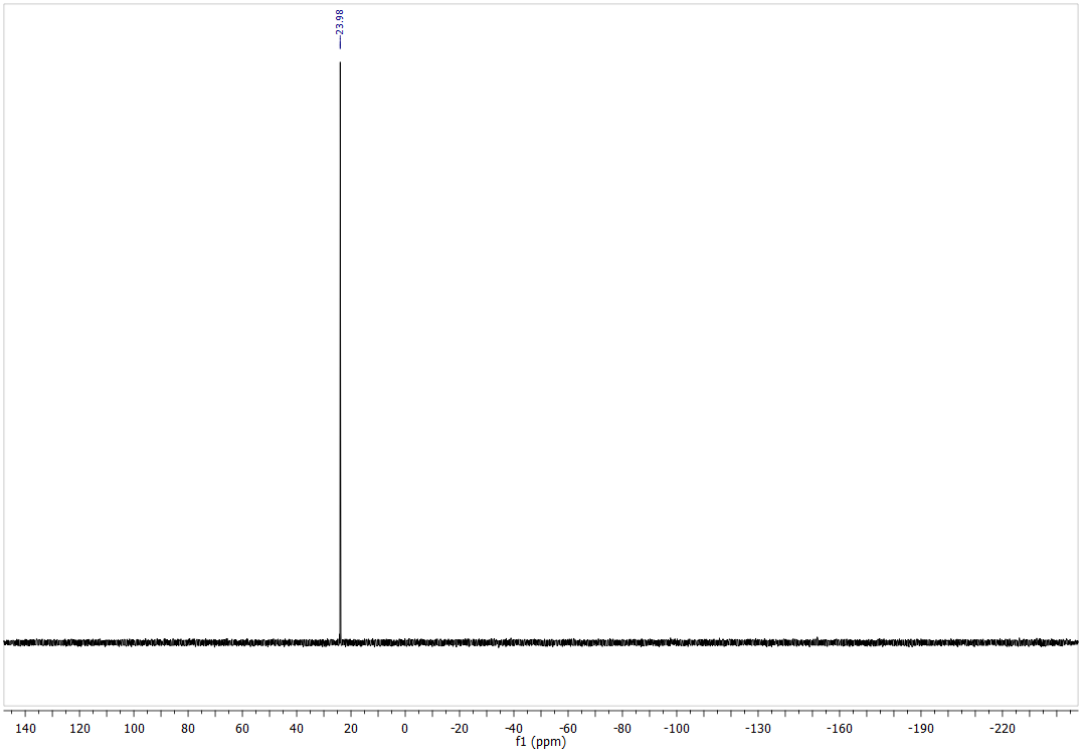

F NMR of **89**

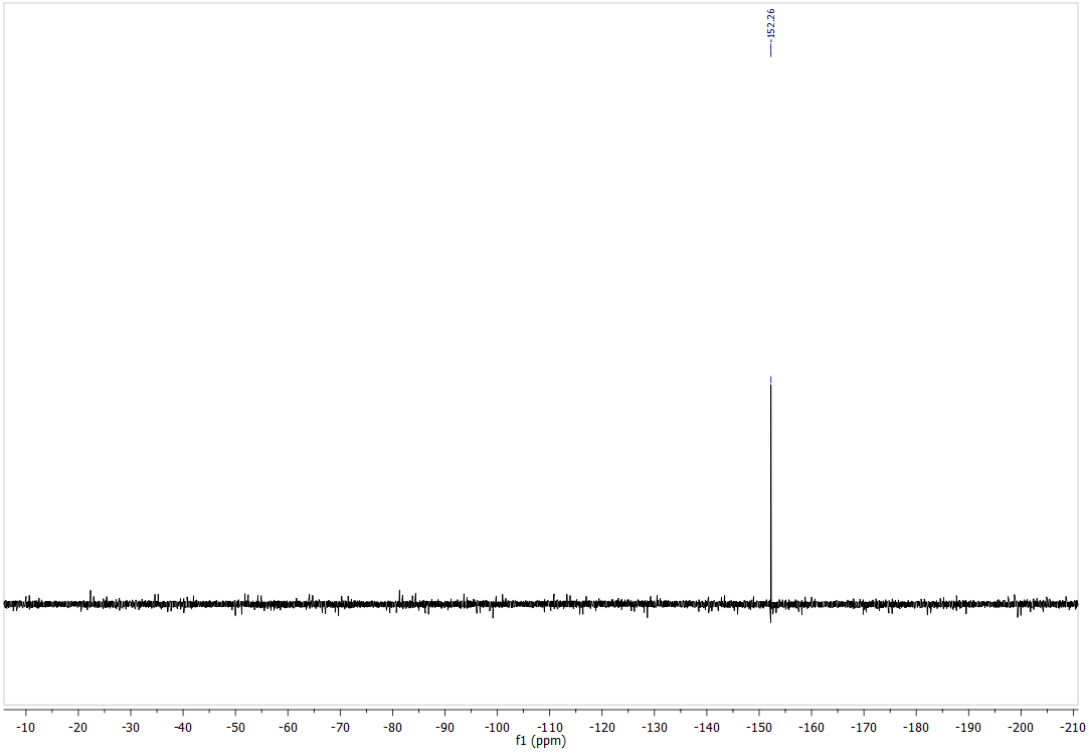

^{31}P NMR of **111**

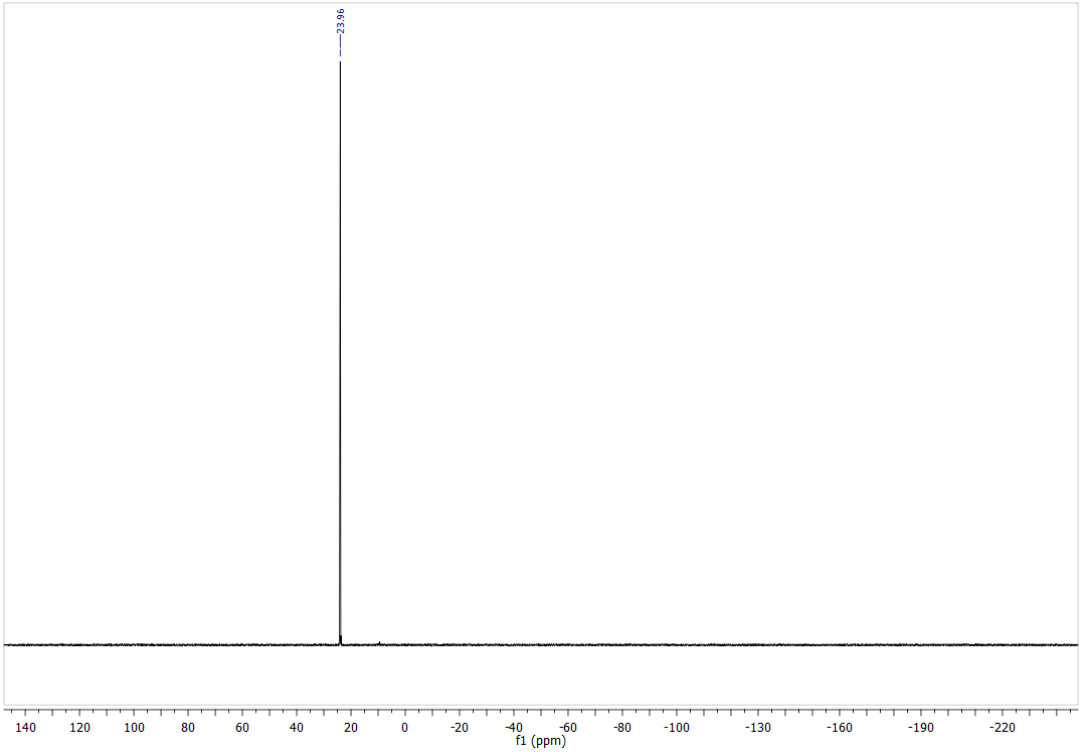

F NMR of **111**

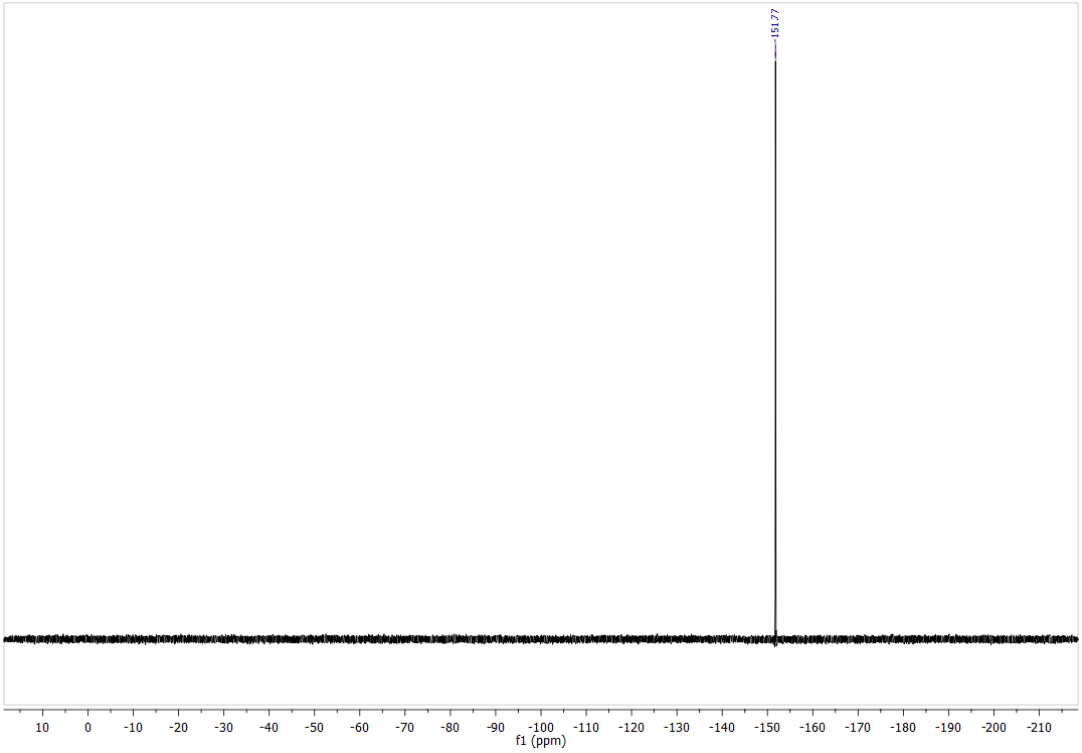

^{31}P of **112**

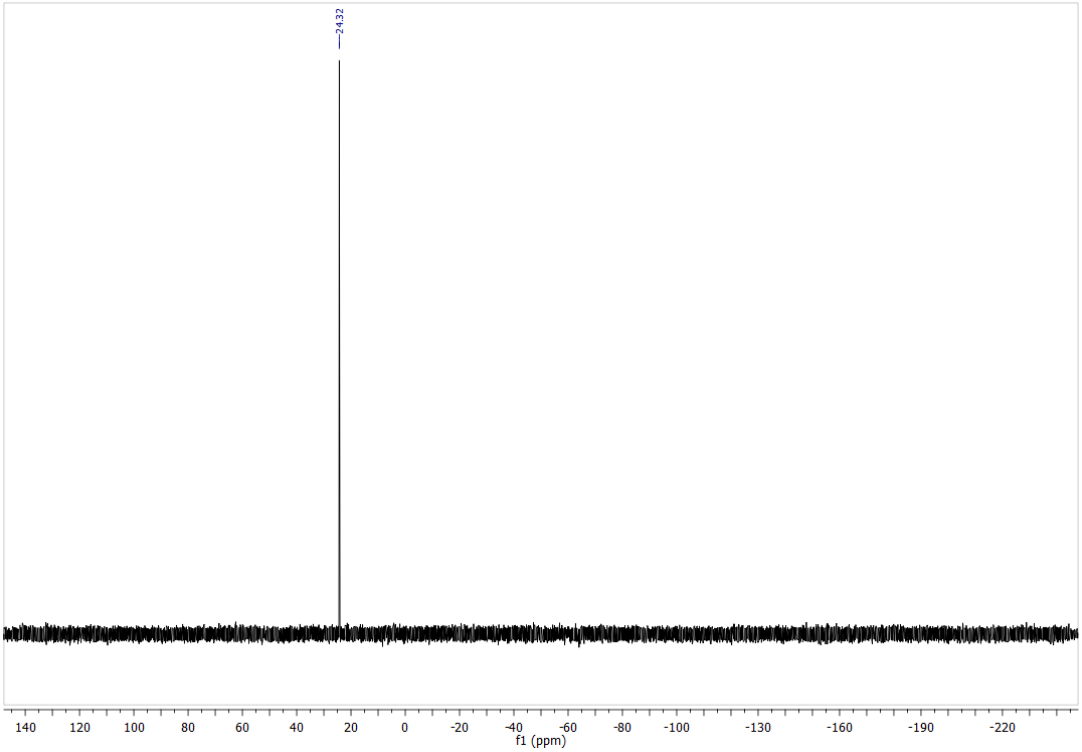

F NMR of **112**

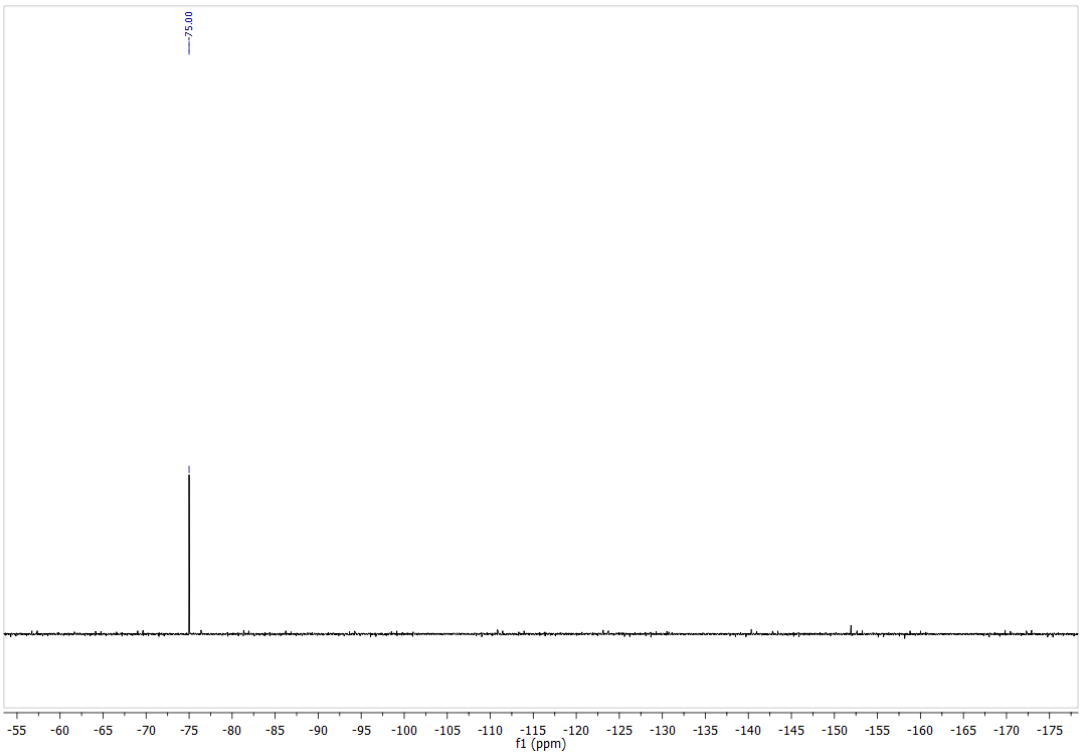

Chapter 7: References

1 O. S. Wolfbeis, *Angew. Chemie Int. Ed.*, 2013, **52**, 9864–9865.

2 J. M. Berg and Y. Shi, *Science*, 1996, **271**, 1081–1085.

3 W. Maret, *Zinc and zinc ions in biological systems: roles, Encyclopedia of Metalloproteins*, Springer, New York, 2013.

4 E. Tomat and S. J. Lippard, *Curr. Opin. Chem. Biol.*, 2010, 14, 225–230.

5 U. Diabetes, *Diabetes: Stats and Facts*, 2014.

6 K. J. Barnham and A. I. Bush, *Curr. Opin. Chem. Biol.*, 2008, **12**, 222–228.

7 P. Paoletti, a. M. Vergnano, B. Barbour and M. Casado, *Neuroscience*, 2009, **158**, 126–136.

8 J.-Y. Koh, S. W. Suh, B. J. Gwag, Y. Y. He, C. Y. Hsu and D. W. Choi, *Science (80-.).*, 1996, **272**, 1013–1016.

9 C. L. Fischer Walker and R. E. Black, *Int. J. Epidemiol.*, 2010, **39**.

10 C. Fischer Walker and R. E. Black, *Annu. Rev. Nutr.*, 2004, **24**, 255–275.

11 I. Lengyel, J. M. Flinn, T. Peto, D. H. Linkous, K. Cano, A. C. Bird, A. Lanzirotti, C. J. Frederickson and F. J. G. M. van Kuijk, *Exp. Eye Res.*, 2007, **84**, 772–780.

12 S. K. Ghosh, P. Kim, X. Zhang, S.-H. Yun, A. Moore, S. J. Lippard and Z. Medarova, *Cancer Res.*, 2010, **70**, 6119–6127.

13 E. L. Que, D. W. Domaille and C. J. Chang, *Chem. Rev.*, 2008, **108**, 1517–1549.

14 D. W. Christianson and J. D. Cox, *Annu. Rev. Biochem.*, 1999, **68**, 33–57.

15 L. Zhu, Z. Yuan, T. J. Simmons and K. Sreenath, *RSC Adv.*, 2014, **4**, 1–74.

16 Z. Xu, J. Yoon and D. R. Spring, *Chem. Soc. Rev.*, 2010, **39**, 1996–2006.

17 D. W. Domaille, E. L. Que and C. J. Chang, *Nat. Chem. Biol.*, 2008, **4**, 168–175.

18 K. P. Carter, A. M. Young and A. E. Palmer, *Chem. Rev.*, 2014, **114**, 4564–4601.

19 P. Jiang and Z. Guo, *Coord. Chem. Rev.*, 2004, 248, 205–229.

20 a P. De Silva, H. Q. N. Gunaratne, T. Gunnlaugsson, A. J. M. Huxley, C. P. McCoy, J. T. Rademacher and T. E. Rice, *Chem. Rev.*, 1997, **97**, 1515–1566.

21 S. a. De Silva, A. Zavaleta, D. E. Baron, O. Allam, E. V. Isidor, N. Kashimura and J. M. Percarpio, *Tetrahedron Lett.*, 1997, **38**, 2237–2240.

22 S. Huang, R. J. Clark and L. Zhu, *Org. Lett.*, 2007, **9**, 4999–5002.

23 T. Hirano, K. Kikuchi, Y. Urano, T. Higuchi and T. Nagano, *Angew. Chemie*, 2000, **112**, 1094–1096.

24 Y. Wu, X. Peng, B. Guo, J. Fan, Z. Zhang, J. Wang, A. Cui and Y. Gao, *Org. Biomol. Chem.*, 2005, **3**, 1387.

25 S. Maruyama, K. Kikuchi, T. Hirano, Y. Urano and T. Nagano, *J. Am. Chem. Soc.*, 2002, **124**, 10650–10651.

26 C. W. MacDiarmid, M. a. Milanick and D. J. Eide, *J. Biol. Chem.*, 2003, **278**, 15065–15072.

27 Z. Liu, C. Zhang, Y. Chen, F. Qian, Y. Bai, W. He and Z. Guo, *Chem. Commun. (Camb).*, 2014, **50**, 1253–5.

28 J. F. Zhu, H. Yuan, W. H. Chan and A. W. M. Lee, *Tetrahedron Lett.*, 2010, **51**, 3550–3554.

29 G. Sivaraman, T. Anand and D. Chellappa, *Anal. Methods*, 2014, **6**, 2343.

30 P. J. Dittmer, J. G. Miranda, J. a. Gorski and A. E. Palmer, *J. Biol. Chem.*, 2009, **284**, 16289–16297.

31 Y. Qin, P. J. Dittmer, J. G. Park, K. B. Jansen and A. E. Palmer, *Proc. Natl. Acad. Sci. U. S. A.*, 2011, **108**, 7351–7356.

32 E. Tomat, E. M. Nolan, J. Jaworski and S. J. Lippard, *J. Am. Chem. Soc.*, 2008, **130**, 15776–15777.

33 E. M. Nolan and S. J. Lippard, *Acc. Chem. Res.*, 2009, **42**, 193–203.

34 R. J. Radford, W. Chyan and S. J. Lippard, *Chem. Sci.*, 2013, **4**, 3080–3084.

35 K. M. Dean, Y. Qin and A. E. Palmer, *Biochim. Biophys. Acta - Mol. Cell Res.*, 2012, **1823**, 1406–1415.

36 J. L. Vinkenborg, T. J. Nicolson, E. a Bellomo, M. S. Koay, G. a Rutter and M. Merkx, *Nat. Methods*, 2009, **6**, 737–740.

37 S. L. Sensi, P. Paoletti, A. I. Bush and I. Sekler, *Nat. Rev. Neurosci.*, 2009, **10**, 780–791.

38 S. L. Sensi, D. Ton-That, J. H. Weiss, A. Rothe and K. R. Gee, *Cell Calcium*, 2003, **34**, 281–284.

39 M. C. Frantz and P. Wipf, *Environ. Mol. Mutagen.*, 2010, **51**, 462–475.

40 L. Xue, G. Li, C. Yu and H. Jiang, *Chem. - A Eur. J.*, 2012, **18**, 1050–1054.

41 G. Masanta, C. S. Lim, H. J. Kim, J. H. Han, H. M. Kim and B. R. Cho, *J. Am. Chem. Soc.*, 2011, **133**, 5698–5700.

42 G. R. Rosania, J. W. Lee, L. Ding, H. S. Yoon and Y. T. Chang, *J. Am. Chem. Soc.*, 2003, **125**, 1130–1131.

43 M. P. Murphy and R. A. J. Smith, *Annu. Rev. Pharmacol. Toxicol.*, 2007, **47**, 629–656.

44 H. M. Kim and B. R. Cho, *Chem. Rev.*, 2015, **115**, 5014–5055.

45 N. Y. Baek, C. H. Heo, C. S. Lim, G. Masanta, B. R. Cho and H. M. Kim, *Chem. Commun.*, 2012, **48**, 4546–4548.

46 K. Rathore, C. S. Lim, Y. Lee and B. R. Cho, *Org. Biomol. Chem.*, 2014, **12**, 3406–12.

47 Z. Liu, C. Zhang, Y. Chen, W. He and Z. Guo, *Chem. Commun.*, 2012, **48**, 8365.

48 W. Chyan, D. Y. Zhang, S. J. Lippard and R. J. Radford, *Proc. Natl. Acad. Sci. U. S. A.*, 2014, **111**, 143–8.

49 S. Iyoshi, M. Taki and Y. Yamamoto, *Org. Lett.*, 2011, **13**, 4558–4561.

50 D. Li, S. Chen, E. A. Bellomo, A. I. Tarasov, C. Kaut, G. A. Rutter and W. -h. Li, *Proc. Natl. Acad. Sci.*, 2011, 108, 21063–21068.

51 K. Rathore, C. S. Lim, Y. Lee, H. J. Park and B. R. Cho, *Asian J. Org. Chem.*, 2014, **3**, 1070–1073.

52 S.-J. Lee, K. S. Cho and J.-Y. Koh, *Glia*, 2009, **57**, 1351–1361.

53 L. Xue, G. Li, D. Zhu, Q. Liu and H. Jiang, *Inorg. Chem.*, 2012, **51**, 10842–10849.

54 H. M. Kim, M. J. An, J. H. Hong, B. H. Jeong, O. Kwon, J.-Y. Hyon, S.-C. Hong, K. J. Lee and B. R. Cho, *Angew. Chemie Int. Ed.*, 2008, **47**, 2231–2234.

55 J. H. Son, C. S. Lim, J. H. Han, I. A. Danish, H. M. Kim and B. R. Cho, *J. Org. Chem.*, 2011, **76**, 8113–8116.

56 T. Liu, Z. Xu, D. R. Spring and J. Cui, *Org. Lett.*, 2013, **15**, 2310–2313.

57 H. Zhu, J. Fan, S. Zhang, J. Cao, K. Song, D. Ge, H. Dong, J. Wang and X. Peng, *Biomater. Sci.*, 2014, **2**, 89–97.

58 Y. Mikata, A. Ugai, K. Yasuda, S. Itami, S. Tamotsu, H. Konno and S. Iwatsuki, *Chem. Biodivers.*, 2012, **9**, 2064–2075.

59 R. Daly, G. Vaz, A. M. Davies, M. O. Senge and E. M. Scanlan, *Chem. - A Eur. J.*, 2012, **18**, 14671–14679.

60 L. Dong, Y. Zang, D. Zhou, X.-P. He, G.-R. Chen, T. D. James and J. Li, *Chem. Commun.*, 2015, **51**, 11852–11855.

61 W. Lin, D. Buccella and S. J. Lippard, *J. Am. Chem. Soc.*, 2013, **135**, 13512–13520.

62 L. E. McQuade and S. J. Lippard, *Inorg. Chem.*, 2010, **49**, 9535–9545.

63 H. C. Kolb, M. G. Finn and K. B. Sharpless, *Angew. Chemie Int. Ed.*, 2001, **40**, 2004–2021.

64 V. V. Rostovtsev, L. G. Green, V. V. Fokin and K. B. Sharpless, *Angew. Chemie - Int. Ed.*, 2002, **41**, 2596–2599.

65 C. W. Tornøe, C. Christensen and M. Meldal, *J. Org. Chem.*, 2002, **67**, 3057–3064.

66 J. E. Hein and V. V Fokin, *Chem. Soc. Rev.*, 2010, **39**, 1302–1315.

67 B. T. Worrell, J. a Malik and V. V Fokin, *Science (80-.).*, 2013, **340**, 457–460.

68 L. Jin, D. R. Tolentino, M. Melaimi and G. Bertrand, *Sci. Adv.*, 2015, **1**, e1500304–e1500304.

69 H. C. Kolb and K. B. Sharpless, *Drug Discov. Today*, 2003, **8**, 1128–1137.

70 L. Liang and D. Astruc, *Coord. Chem. Rev.*, 2011, **255**, 2933–2945.

71 Y. H. Lau, P. J. Rutledge, M. Watkinson and M. H. Todd, *Chem. Soc. Rev.*, 2011, **40**, 2848–2866.

72 E. Tamanini, A. Katewa, L. M. Sedger, M. H. Todd and M. Watkinson, *Inorg. Chem.*, 2009, **48**, 319–324.

73 S. Ast, P. J. Rutledge and M. H. Todd, *Eur. J. Inorg. Chem.*, 2012, **2012**, 5611–5615.

74 S. Ast, S. Kuke, P. J. Rutledge and M. H. Todd, *Eur. J. Inorg. Chem.*, 2015, **2015**, 58–66.

75 M. Yu, S. Ast, Q. Yu, A. T. S. Lo, R. Flehr, M. H. Todd and P. J. Rutledge, *PLoS One*, 2014, **9**, e100761.

76 M. Yu, Q. Yu, P. J. Rutledge and M. H. Todd, *ChemBioChem*, 2013, **14**, 224–229.

77 R. K. Pathak, V. K. Hinge, M. Mondal and C. P. Rao, *J. Org. Chem.*, 2011, **76**, 10039–10049.

78 L.-N. Zhu, S.-L. Gong, S.-L. Gong, C.-L. Yang and J.-G. Qin, *Chinese J. Chem.*, 2008, **26**, 1424–1430.

79 R. K. Pathak, K. Tabbasum, A. Rai, D. Panda and C. P. Rao, *Anal. Chem.*, 2012, **84**, 5117–5123.

80 S. A. Ingale and F. Seela, *J. Org. Chem.*, 2012, **77**, 9352–9356.

81 S. Kotha, D. Goyal (née Bansal), S. Banerjee and A. Datta, *Analyst*, 2012, **137**, 2871.

82 E. Hao, T. Meng, M. Zhang, W. Pang, Y. Zhou and L. Jiao, *J. Phys. Chem. A*, 2011, **115**, 8234–8241.

83 N. V. Sokolova and V. G. Nenajdenko, *RSC Adv.*, 2013, **3**, 16212.

84 Y. L. Angell and K. Burgess, *Chem. Soc. Rev.*, 2007, **36**, 1674–1689.

85 T.-F. Niu, C. Cai and L. Yi, *Helv. Chim. Acta*, 2012, **95**, 87–99.

86 K. Lörincz, P. Kele and Z. Novák, *Synthesis (Stuttg).*, 2009, 3527–3532.

87 F. Friscourt and G. J. Boons, *Org. Lett.*, 2010, **12**, 4936–4939.

88 E. Merkul, F. Klukas, D. Dorsch, U. Grädler, H. E. Greiner and T. J. J. Müller, *Org. Biomol. Chem.*, 2011, **9**, 5129–5136.

89 K. Brahma, B. Achari and C. Chowdhury, *Synthesis (Stuttg).*, 2013, **45**, 545–555.

90 S. Hwang, H. Bae, S. Kim and S. Kim, *Tetrahedron*, 2012, **68**, 1460–1465.

91 S. Bräse, C. Gil, K. Knepper and V. Zimmermann, *Angew. Chemie - Int. Ed.*, 2005, **44**, 5188–5240.

92 A. K. Feldman, B. Colasson and V. V. Fokin, *Org. Lett.*, 2004, **6**, 3897–3899.

93 P. Appukkuttan, W. Dehaen, V. V Fokin and E. Van der Eycken, *Org. Lett.*, 2004, **6**, 4223–4225.

94 T. R. Chan, R. Hilgraf, K. B. Sharpless and V. V. Fokin, *Org. Lett.*, 2004, **6**, 2853–2855.

95 J. Andersen, S. Bolvig and X. Liang, *Synlett*, 2005, 2941–2947.

96 K. Kacprzak, *Synlett*, 2005, 943–946.

97 K. Odlo, E. A. Høydahl and T. V. Hansen, *Tetrahedron Lett.*, 2007, **48**, 2097–2099.

98 J. D. Crowley, P. H. Bandeen and L. R. Hanton, *Polyhedron*, 2010, **29**, 70–83.

99 J. D. Crowley and P. H. Bandeen, *Dalton Trans.*, 2010, 612–623.

100 F. Alonso, Y. Moglie, G. Radivoy and M. Yus, *Adv. Synth. Catal.*, 2010, **352**, 3208–3214.

101 H. Sharghi, R. Khalifeh and M. M. Doroodmand, *Adv. Synth. Catal.*, 2009, **351**, 207–218.

102 R. B. Nasir Baig and R. S. Varma, *Green Chem.*, 2012, **14**, 625.

103 J. A. Shin, Y. G. Lim and K. H. Lee, *J. Org. Chem.*, 2012, **77**, 4117–4122.

104 B. S. P. Anil Kumar, K. Harsha Vardhan Reddy, B. Madhav, K. Ramesh and Y. V. D. Nageswar, *Tetrahedron Lett.*, 2012, **53**, 4595–4599.

105 N. Mukherjee, S. Ahammed, S. Bhadra and B. C. Ranu, *Green Chem.*, 2013, **15**, 389.

106 Y. Chen, Z. J. Zhuo, D. M. Cui and C. Zhang, *J. Organomet. Chem.*, 2014, **749**, 215–218.

107 C. Z. Tao, X. Cui, J. Li, A. X. Liu, L. Liu and Q. X. Guo, *Tetrahedron Lett.*, 2007, **48**, 3525–3529.

108 G. Ilyashenko, R. Al-Safadi, R. Donnan, R. Dubrovka, J. Pancholi, M. Watkinson and A. Whiting, *RSC Adv.*, 2013, **3**, 17081.

109 B. Sreedhar, P. S. Reddy and V. R. Krishna, *Tetrahedron Lett.*, 2007, **48**, 5831–5834.

110 P. Surendra Reddy, V. Ravi and B. Sreedhar, *Tetrahedron Lett.*, 2010, **51**, 4037–4041.

111 P. E. Eaton, A. M. Fisher and R. E. Hormann, *Synlett*, 1990, **1990**, 737–738.

112 P. T. Nyffeler, C. H. Liang, K. M. Koeller and C. H. Wong, *J. Am. Chem. Soc.*, 2002, **124**, 10773–10778.

113 P. B. Alper, S. C. Hung and C. H. Wong, *Tetrahedron Lett.*, 1996, **37**, 6029–6032.

114 Q. Liu and Y. Tor, *Org. Lett.*, 2003, **5**, 2571–2572.

115 A. Titz, Z. Radic, O. Schwardt and B. Ernst, *Tetrahedron Lett.*, 2006, **47**, 2383–2385.

116 J. Raushel, S. M. Pitram and V. V. Fokin, *Org. Lett.*, 2008, **10**, 3385–3388.

117 N. G. Angelo and P. S. Arora, *J. Am. Chem. Soc.*, 2005, **127**, 17134–17135.

118 N. G. Angelo and P. S. Arora, *J. Org. Chem.*, 2007, **72**, 7963–7967.

119 C. J. Cavender and V. J. Shiner, *J. Org. Chem.*, 1972, **37**, 3567–3569.

120 H. S. G. Beckmann and V. Wittmann, *Org. Lett.*, 2007, **9**, 1–4.

121 S. Higashiya, C. Kaibara, K. Fukuoka, F. Suda, M. Ishikawa, M. Yoshida and T. Hata, *Bioorganic Med. Chem. Lett.*, 1996, **6**, 39–42.

122 T. Wada, A. Mochizuki, S. Higashiya, H. Tsuruoka, S. I. Kawahara, M. Ishikawa and M. Sekine, *Tetrahedron Lett.*, 2001, **42**, 9215–9219.

123 M. Jafarzadeh, *Synlett*, 2007, 2144–2145.

124 K. Barral, A. D. Moorhouse and J. E. Moses, *Org. Lett.*, 2007, **9**, 1809–1811.

125 E. D. Goddard-Borger and R. V. Stick, *Org. Lett.*, 2007, **9**, 3797–3800.

126 N. M. Smith, M. J. Greaves, R. Jewell, M. W. D. Perry, M. J. Stocks and J. P. Stonehouse, *Synlett*, 2009, 1391–1394.

127 S. Maisonneuve and J. Xie, *Synlett*, 2009, 2977–2981.

128 V. Aucagne and D. a. Leigh, *Org. Lett.*, 2006, **8**, 4505–4507.

129 J. a. Opsteen and J. C. M. Van Hest, *J. Polym. Sci. Part A Polym. Chem.*, 2007, **45**, 2913–2924.

130 R. M. Meudtner, M. Ostermeier, R. Goddard, C. Limberg and S. Hecht, *Chem. - A Eur. J.*, 2007, **13**, 9834–9840.

131 P. M. E. Gramlich, S. Warncke, J. Gierlich and T. Carell, *Angew. Chemie - Int. Ed.*, 2008, **47**, 3442–3444.

132 I. E. Valverde, A. F. Delmas and V. Aucagne, *Tetrahedron*, 2009, **65**, 7597–7602.

133 S. Ladouceur, A. M. Soliman and E. Zysman-Colman, *Synthesis (Stuttg).*, 2011, 3604–3611.

134 A. Kolarovič, M. Schnürch and M. D. Mihovilovic, *J. Org. Chem.*, 2011, **76**, 2613–2618.

135 A. Kolarovič and Z. Fáberová, *J. Org. Chem.*, 2009, **74**, 7199–7202.

136 Y. Li and A. H. Flood, *J. Am. Chem. Soc.*, 2008, **130**, 12111–12122.

137 J. M. Spruell, W. R. Dichtel, J. R. Heath and J. F. Stoddart, *Chem. - A Eur. J.*, 2008, **14**, 4168–4177.

138 B. H. M. Kuijpers, S. Groothuys, C. Hawner, J. ten Dam, P. J. L. M. Quaedflieg, H. E. Schoemaker, F. L. van Delft and F. P. J. T. Rutjes, *Org. Process Res. Dev.*, 2008, **12**, 503–511.

139 V. Hornillos, F. Amat-Guerri and a. U. Acuña, *J. Photochem. Photobiol. A Chem.*, 2012, **243**, 56–60.

140 R. Lucas, R. Zerrouki, R. Granet, P. Krausz and Y. Champavier, *Tetrahedron*, 2008, **64**, 5467–5471.

141 H. Elamari, F. Meganem, J. Herscovici and C. Girard, *Tetrahedron Lett.*, 2011, **52**, 658–660.

142 D. C. Kennedy, C. S. McKay, M. C. B. Legault, D. C. Danielson, J. a. Blake, A. F. Pegoraro, A. Stolow, Z. Mester and J. P. Pezacki, *J. Am. Chem. Soc.*, 2011, **133**, 17993–18001.

143 D. M. Beal, V. E. Albrow, G. Burslem, L. Hitchen, C. Fernandes, C. Lapthorn, L. R. Roberts, M. D. Selby and L. H. Jones, *Org. Biomol. Chem.*, 2012, 10, 548.

144 N. J. Agard, J. a. Prescher and C. R. Bertozzi, *J. Am. Chem. Soc.*, 2004, **126**, 15046–15047.

145 D. M. Beal, V. E. Albrow, G. Burslem, L. Hitchen, C. Fernandes, C. Lapthorn, L. R. Roberts, M. D. Selby and L. H. Jones, *Org. Biomol. Chem.*, 2012, **10**, 548.

146 Z. Yuan, G. C. Kuang, R. J. Clark and L. Zhu, *Org. Lett.*, 2012, **14**, 2590–2593.

147 W. S. Brotherton, H. a Michaels, J. T. Simmons, R. J. Clark, N. S. Dalal and L. Zhu, *Org. Lett.*, 2009, **11**, 4954–4957.

148 G. C. Kuang, H. a. Michaels, J. T. Simmons, R. J. Clark and L. Zhu, *J. Org. Chem.*, 2010, **75**, 6540–6548.

149 C. Uttamapinant, A. Tangpeerachaikul, S. Grecian, S. Clarke, U. Singh, P. Slade, K. R. Gee and A. Y. Ting, *Angew. Chemie - Int. Ed.*, 2012, **51**, 5852–5856.

150 S. a. Ingale and F. Seela, *J. Org. Chem.*, 2013, **78**, 3394–3399.

151 S. S. Pujari, H. Xiong and F. Seela, *J. Org. Chem.*, 2010, **75**, 8693–8696.

152 H. Xiong and F. Seela, *J. Org. Chem.*, 2011, **76**, 5584–5597.

153 S. S. Pujari and F. Seela, *J. Org. Chem.*, 2012, **77**, 4460–4465.

154 K. P. Kaliappan, P. Kalanidhi and S. Mahapatra, *Synlett*, 2009, 2162–2166.

155 T. Koike, T. Watanabe, S. Aoki, E. Kimura and M. Shiro, *J. Am. Chem. Soc.*, 1996, **118**, 12696–12703.

156 K. Jobe, C. H. Brennan, M. Motevalli, S. M. Goldup and M. Watkinson, *Chem. Commun. (Camb).*, 2011, **47**, 6036–6038.

157 D. K. Dalvie, A. S. Kalgutkar, S. C. Khojasteh-Bakht, R. S. Obach and J. P. O'Donnell, *Chem. Res. Toxicol.*, 2002, **15**, 269–299.

158 R. M. Duke, E. B. Veale, F. M. Pfeffer, P. E. Kruger and T. Gunnlaugsson, *Chem. Soc. Rev.*, 2010, **39**, 3936–53.

159 S. Banerjee, E. B. Veale, C. M. Phelan, S. a Murphy, G. M. Tocci, L. J. Gillespie, D. O. Frimannsson, J. M. Kelly and T. Gunnlaugsson, *Chem. Soc. Rev.*, 2013, **42**, 1601–18.

160 W. Yang, Y. Li, J. Zhang, N. Chen, S. Chen, H. Liu and Y. Li, *J. Org. Chem.*, 2011, **76**, 7750–7756.

161 Y. Yu, Y. Li, S. Chen, T. Liu, Z. Qin, H. Liu and Y. Li, *European J. Org. Chem.*, 2012, 4287–4292.

162 K. Varazo, F. Xie, D. Gulledge and Q. Wang, *Tetrahedron Lett.*, 2008, **49**, 5293–5296.

163 T. Gunnlaugsson, T. C. Lee and R. Parkesh, *Org. Biomol. Chem.*, 2003, **1**, 3265–3267.

164 M. Meldal and C. W. Tomøe, *Chem. Rev.*, 2008, **108**, 2952–3015.

165 F. Fazio, M. C. Bryan, O. Blixt, J. C. Paulson and C. H. Wong, *J. Am. Chem. Soc.*, 2002, **124**, 14397–14402.

166 B. H. Lipshutz and B. R. Taft, *Angew. Chemie - Int. Ed.*, 2006, **45**, 8235–8238.

167 L. Y. Wu, Y. X. Xie, Z. S. Chen, Y. N. Niu and Y. M. Liang, *Synlett*, 2009, 1453–1456.

168 Z. Gonda and Z. Novák, *Dalton Trans.*, 2010, **39**, 726–729.

169 A. E. Cohrt, J. F. Jensen and T. E. Nielsen, *Org. Lett.*, 2010, **12**, 5414–5417.

170 V. V. Komnatnyy, M. Givskov and T. E. Nielsen, *Chem. - A Eur. J.*, 2012, **18**, 16793–16800.

171 X. Chen, G. N. Khairallah, R. a J. O'Hair and S. J. Williams, *Tetrahedron Lett.*, 2011, **52**, 2750–2753.

172 T. Gunnlaugsson, D. F. Brougham, A. M. Fanning, M. Nieuwenhuyzen, J. E. O'Brien and R. Viguier, *Org. Lett.*, 2004, **6**, 4805–4808.

173 O. B. Locos, C. C. Heindl, A. Corral, M. O. Senge and E. M. Scanlan, *European J. Org. Chem.*, 2010, **2010**, 1026–1028.

174 E. Tomat and S. J. Lippard, *Curr. Opin. Chem. Biol.*, 2010, 14, 225–230.

175 P. G. M. Wuts and T. W. Greene, *Greene's Protective Groups in Organic Synthesis*, John Wiley & Sons, Inc., Hoboken, NJ, USA, 4th Editio., 2006.

176 Y. C. Lin and R. G. Weiss, *Macromolecules*, 1987, **20**, 414–417.

177 H. Shi, N. Zhao, D. Ding, J. Liang, B. Z. Tang and B. Liu, *Org. Biomol. Chem.*, 2013, **11**, 7289–7296.

178 X. Meng, S. Wang, Y. Li, M. Zhu and Q. Guo, *Chem. Commun.*, 2012, **48**, 4196.

179 P. Thordarson, *Chem. Soc. Rev.*, 2011, **40**, 1305–1323.

180 B. Branchi, G. Bergamini, L. Fiandro, P. Ceroni, A. Alvino, G. Doddi, F. Vögtle and F.-G. Klärner, *Dalton Trans.*, 2011, **40**, 1356–1364.

181 R. Sladek, G. Rocheleau, J. Rung, C. Dina, L. Shen, D. Serre, P. Boutin, D. Vincent, A. Belisle, S. Hadjadj, B. Balkau, B. Heude, G. Charpentier, T. J. Hudson, A. Montpetit, A. V Pshezhetsky, M. Prentki, B. I. Posner, D. J. Balding, D. Meyre, C. Polychronakos and P. Froguel, *Nature*, 2007, **445**, 881–885.

182 T. J. Nicolson, E. a. Bellomo, N. Wijesekara, M. K. Loder, J. M. Baldwin, A. V. Gyulkhandanyan, V. Koshkin, A. I. Tarasov, R. Carzaniga, K. Kronenberger, T. K. Taneja, G. da Silva Xavier, S. Libert, P. Froguel, R. Scharfmann, V. Stetsyuk, P. Ravassard, H. Parker, F. M. Gribble, F. Reimann, R. Sladek, S. J. Hughes, P. R. V. Johnson, M. Masseboeuf, R. Burcelin, S. a. Baldwin, M. Liu, R. Lara-Lemus, P. Arvan, F. C. Schuit, M. B. Wheeler, F. Chimienti and G. a. Rutter, *Diabetes*, 2009, **58**, 2070–2083.

183 G. a. Rutter, *Islets*, 2010, **2**, 49–50.

184 A. R. Sarkar, D. E. Kang, H. M. Kim and B. R. Cho, *Inorg. Chem.*, 2014, **53**, 1794–803.

185 I. T. Harrison and S. Harrison, *J. Am. Chem. Soc.*, 1967, **89**, 5723–5724.

186 C. O. Dietrick-Buchecker, P. a. Marnot and J. P. Sauvage, *Tetrahedron Lett.*, 1982, **23**, 5291–5294.

187 K. D. Hänni and D. a Leigh, *Chem. Soc. Rev.*, 2010, **39**, 1240–1251.

188 J. D. Crowley, S. M. Goldup, A.-L. Lee, D. A. Leigh and R. T. McBurney, *Chem. Soc. Rev.*, 2009, **38**, 1530–1541.

189 V. Aucagne, J. Berná, J. D. Crowley, S. M. Goldup, K. D. Hänni, D. A. Leigh, P. J. Lusby, V. E. Ronaldson, A. M. Z. Slawin, A. Viterisi and D. B. Walker, *J. Am. Chem. Soc.*, 2007, **129**, 11950–11963.

190 V. Aucagne, K. D. Hänni, D. a. Leigh, P. J. Lusby and D. B. Walker, *J. Am. Chem. Soc.*, 2006, **128**, 2186–2187.

191 H. Lahlali, K. Jobe, M. Watkinson and S. M. Goldup, *Angew. Chemie - Int. Ed.*, 2011, **50**, 4151–4155.

192 R. J. Bordoli and S. M. Goldup, *J. Am. Chem. Soc.*, 2014, **136**, 4817–4820.

193 J. Winn, A. Pinczewska and S. M. Goldup, *J. Am. Chem. Soc.*, 2013, **135**, 13318–13321.

194 M. J. Chmielewski, J. J. Davis and P. D. Beer, *Org. Biomol. Chem.*, 2009, **7**, 415–424.

195 M. J. Langton and P. D. Beer, *Acc. Chem. Res.*, 2014, **47**, 1935–1949.

196 X. Ma and H. Tian, *Chem. Soc. Rev.*, 2010, **39**, 70–80.

197 M. J. Langton and P. D. Beer, *Chem. - A Eur. J.*, 2012, **18**, 14406–14412.

198 C. G. Collins, E. M. Peck, P. J. Kramer and B. D. Smith, *Chem. Sci.*, 2013, **4**, 2557.

199 G. T. Spence, M. B. Pitak and P. D. Beer, *Chem. - A Eur. J.*, 2012, **18**, 7100–7108.

200 C. Allain, P. D. Beer, S. Faulkner, M. W. Jones, A. M. Kenwright, N. L. Kilah, R. C. Knighton, T. J. Sørensen and M. Tropiano, *Chem. Sci.*, 2013, **4**, 489–493.

201 S. S. Zhu and T. M. Swager, *J. Am. Chem. Soc.*, 1997, **119**, 12568–12577.

202 K. Hiratani, M. Kaneyama, Y. Nagawa, E. Koyama and M. Kanesato, *J. Am. Chem. Soc.*, 2004, **126**, 13568–13569.

203 Y. Nagawa, J. Suga, K. Hiratani, E. Koyama and M. Kanesato, *Chem. Commun.*, 2005, 749.

204 W. Zhou, J. Li, X. He, C. Li, J. Lv, Y. Li, S. Wang, H. Liu and D. Zhu, *Chem. - A Eur. J.*, 2008, **14**, 754–763.

205 J. M. Baumes, I. Murgu, R. D. Connell, W. J. Culligan, A. G. Oliver and B. D. Smith, *Supramol. Chem.*, 2012, **24**, 14–22.

206 K. Jobe, Queen Mary University of London, 2013.

207 M. J. MacLachlan, a. Rose and T. M. Swager, *J. Am. Chem. Soc.*, 2001, **123**, 9180–9181.

208 P. H. Kwan and T. M. Swager, *J. Am. Chem. Soc.*, 2005, **127**, 5902–5909.

209 R. D. Shannon, *Acta Crystallogr. Sect. A*, 1976, **32**, 751–767.

210 Y. Zhou, K. Liu, J. Y. Li, Y. Fang, T. C. Zhao and C. Yao, *Org. Lett.*, 2011, **13**, 1290–1293.

211 P. M. Levine, K. Imberg, M. J. Garabedian and K. Kirshenbaum, *J. Am. Chem. Soc.*, 2012, **134**, 6912–6915.

212 M. Hu, J. Li and S. Q. Yao, *Org. Lett.*, 2008, **10**, 5529–5531.

213 F. Cuevas, A. I. Oliva and M. a. Pericàs, *Synlett*, 2010, **2010**, 1873–1877.

214 J. T. Fletcher and J. E. Reilly, *Tetrahedron Lett.*, 2011, **52**, 5512–5515.